Gas-Phase Ion and Radical Chemistry of CO2 Adducts with Possible Relevance in the Atmosphere of Mars

Héloïse Soldi-Lose

Gas-Phase Ion and Radical Chemistry of CO_2 Adducts with Possible Relevance in the Atmosphere of Mars

vorgelegt von
Dipl.-Chem. Héloïse Soldi-Lose
aus Châtenay-Malabry (Frankreich)

von der Fakultät II - Mathematik und Naturwissenschaften
der Technischen Universität Berlin
zur Erlangung des akademischen Grades

Doktor der Naturwissenschaften
− Dr. rer. nat. −

genehmigte Dissertation

Promotionsausschuss:

Vorsitzender:	Prof. Dr. Andreas Grohmann
Berichter:	Prof. Dr. rer. nat. Drs. h. c. Helmut Schwarz
	Dr. Odile Dutuit
	Dr. habil Detlef Schröder

Tag der wissenschaftlichen Aussprache: 23. April 2008

Berlin 2008

D83

In honorem matris prudentia ac sapientia praeditae

“Le fait est, on dirait, que tout ce qu’on peut espérer c’est d’être un peu moins, à la fin, celui qu’on était au commencement.”

“The fact is, it seems, that the most you can hope is to be a little less, in the end, the creature you were in the beginning.”

Samuel Beckett

Molloy

Abstract

Soldi-Lose Héloïse: **Gas-Phase Ion and Radical Chemistry of CO_2 Adducts with Possible Relevance in the Atmosphere of Mars**

In the Mars atmosphere, reactivity of trace components is as relevant as that of the major compounds if formation of complex molecules is considered. These are of great importance concerning the existence of a past or future life on Mars. In this context, the gas-phase chemistry of alkylcarbonate and alkyloxalate ions and radicals, $ROCOO^{-/\bullet}$ and $ROCOCOO^{-/\bullet}$, is investigated for different alkyl substituents R (H, CH_3, C_2H_5, *i*-C_3H_7, and *t*-C_4H_9). This study describes the structures, stability, and unimolecular dissociation behavior of these species and is achieved by means of mass spectrometric methods and *ab initio* calculations. Standard heats of formation of the ions and radicals are determined via computational methods, using atomization energies and bond-separation reactions.

Vertical charge-transfer experiments are performed to provide evidence for the existence of the radicals under study and the NIDD (ion and neutral decomposition difference) method is employed to determine their reactivity. Typical processes observed involve direct bond cleavages leading to elimination of carbon dioxide.

Concerning anionic compounds, classical metastable ion (MI) and collisional activation (CA) experiments enable the determination of their gas-phase behavior. This, in contrast to radicals, is not only constituted by direct bond cleavages, but also by hydride-transfer reaction or carbon monoxide expulsion involving formation of ion-neutral complexes as intermediates.

Translational energy loss spectra are also employed to gain more insights concerning the dissociation energetics of $CH_3OCOO^{\bullet}$ and CH_3OCOO^{+} formed by vertical charge-transfer of methylcarbonate. This rather unusual method for such study implies a careful evaluation of the error caused by the instrument which may otherwise generate dramatic deviations of the results compared to theory.

Zusammenfassung:

Soldi-Lose, Héloïse: **Gasphasenchemie ionischer und radikalischer Addukte von Kohlendioxid mit möglicher Relevanz für die Marsatmosphäre**

In Bezug auf die Bildung komplexerer Moleküle in der Marsatmosphäre ist die Reaktivität von Spurenbestandteilen ebenso wichtig wie die der Hauptkomponenten. Die Existenz komplexer Moleküle in der Marsatmosphäre spielt eine wichtige Rolle bei der Fragestellung nach vorherigem, gegenwärtigem oder zukünftigem Leben auf dem Mars. In der vorliegenden Arbeit wird die Gasphasenchemie von Alkylkarbonat- und Alkyloxalat-Ionen und Radikalen, $ROCOO^{-/\bullet}$ und $ROCOCOO^{-/\bullet}$, mit verschiedenen Alkylsubstituenten R (R = H, CH_3, C_2H_5, *i*-C_3H_7 und *t*-C_4H_9) untersucht. Dazu werden die Strukturen, die Stabilitäten und das unimolekulare Dissoziationsverhalten dieser Verbindungen mit massenspektrometrischen Methoden und *ab initio* Rechnungen untersucht. Standardbindungsenthalpien der Ionen und Radikale werden über rechnerische Methoden mit Hilfe von Atomisierungsenergien und Bindungstrennung-Reaktionen bestimmt.

Experimentell werden die $ROCOO^-$- und $ROCOCOO^-$-Ionen einem vertikalen Ladungstransfer unterworfen, um zu untersuchen, ob die entsprechenden neutralen Radikale in der Gasphase existieren können. Das unimolekulare Dissoziationsverhalten der Radikale wird mit Hilfe der NIDD-Methode (NIDD = Neutral and ion decomposition difference) studiert. Typisch beobachtete Prozesse sind direkte Bindungsspaltungen unter Verlust von Kohlendioxid. In Bezug auf die anionischen Spezies erlauben klassische metastabile Ionen-Spektren (metastable ion, MI) und Stoßaktivierungsexperimente (collisional activation, CA) das Studium des Gasphasenverhaltens dieser Verbindungsklasse. Hierbei werden nicht nur direkte Bindungsbrüche, sondern auch Hydridübertragungs-Reaktionen oder der Verlust von Kohlenmonoxid beobachtet, wobei viele dieser Prozesse die intermediäre Ausbildung von Ion-Neutral Komplex involvieren. Weitere Informationen über das Dissoziationsverhalten der durch vertikalen Elektronentransfer aus Methylkarbonat gebildeten transienten Spezies $CH_3OCOO^\bullet$ und CH_3OCOO^+ können aus Translationsenergieverlust-Spektren erhalten werden. Der Vergleich mit den theoretisch erwarteten Energiedefiziten zeigt auf, dass diese selten angewandte Methode mit beträchtlichen experimentellen Fehlern behaftet ist, so dass hinsichtlich der Redoxenergetik nur grobe Abschätzungen möglich sind.

Acknowledgments

The present work has been made possible thanks to many persons due to their help, support, and encouragements. I am pleased now to take the opportunity to express my gratitude to all of them.

The first person I would like to thank is my supervisor Prof. Dr. Drs. h.c. Helmut Schwarz who gave me the chance to carry out my Ph.D. in his group.

My sincere thanks go to Dr. Odile Dutuit for kindly accepting to officiate as second examiner.

I am very grateful to Dr. Detlef Schröder who, even far away, kept an eye on the progress of my work and was always available when I needed scientific advices and who accepted to officiate as examiner.

My thanks also go to Dr. Thomas Weiske for his essential assistance concerning the experimental part of my work, and to Waltraud Zummack who synthesized for me many compounds. Moreover, I cannot fail to mention Andrea Beck who is the most efficient secretary I ever met.

I thank my colleagues who are or have been present in the group and who contributed to a so pleasant working atmosphere, particularly Dipl. Chem. Sandra Feyel with whom I enjoyed a lot my time spent in Berlin.

More personally, I warmly express my gratitude to Ms Warnke, Pöschel and Tröger who made my life in Berlin much nicer, to Christel for her patience and to Mouhcine for his continuous encouragements and his inestimable help for the numerous corrections in this manuscript.

At last, I am extremely grateful to my family to have always support me with love and understanding. In particular, my mother receives my deepest thanks for everything she did for me. Thanks also to Didier, Elisa, Tamara, Charlotte, Mina, Lili and my grandparents for their continuous encouragements.

Table of Contents

I. Introduction 17

References 20

II. Methodological Overview 23

II.1. Important Concepts in Mass Spectrometry 23

II.1.1. Theory of Unimolecular Decay 23

II.1.2. Ion-Neutral Complexes 25

II.2. Ion-Beam Mass Spectrometry 26

II.2.1. Inlet System and Ion Generation 28

II.2.2. Physical Basis of a Sector Mass Spectrometer 29

II.2.3. Metastable Ion Decay (MI) 31

II.2.4. Collisional Activation (CA) 32

II.2.5. Charge-Reversal Experiments (CR) 33

II.2.6. Neutralization-Reionization Experiments (NR) 34

II.2.7. Neutral and Ion Decomposition Difference (NIDD) 35

II.2.8. Translational Energy Spectra 37

II.3. Computational Methods 39

II.3.1. The Hartree-Fock Theory 41

II.3.2. Møller-Plesset Perturbation Theory 44

II.3.3. Basis Sets 45

II.3.4. Computational Details 47

II.4. Thermochemistry 48

II.4.1. Complete Basis Set 48

II.4.2. Standard Heats of Formation 49

II.5. References and Notes 55

III. Gas-Phase Chemistry of Alkylcarbonate Ions and Radicals 63

III.1. Introduction 63

III.2. Structures and Energetics 64

III.2.1. Alkylcarbonate Ions and Radicals 64

III.2.2. Comparison with the Structures of Cations 67

III.3. Thermochemistry 69

III.4. Unimolecular Reactivity of Alkylcarbonate Ions 71

III.5. NIDD Study of Alkylcarbonate Radicals 77

III.6. Conclusions 86

III.7. References 87

IV. Translational Energy Spectra of $CO_2^{\bullet+}$ formed by Charge Reversal and Neutralization Reionization of Methylcarbonate 91

IV.1. Introduction 91

IV.2. Experimental Error due to Charge-Transfer Processes 93

IV.3. Experimental Results 103

IV.3.1. $CO_2^{\bullet+}$ Peak Shape 103

IV.3.2. Evaluation of $IE_v(CH_3OCOO^{\bullet})$, $EA_v(CH_3OCOO^{\bullet})$, $\Delta_rH°(CH_3O^{\bullet} + CO_2)$, and $\Delta_rH°(CH_3O^{\bullet} + CO_2^{\bullet+})$ 108

IV.3.3. Kinetic Energy Release 114

IV.4. Theoretical Approach 116

IV.5. Summary and Conclusions 121

IV.6. References and Notes 123

V. Gas-Phase Chemistry of Alkyloxalate Ions and Radicals 125

V.1. Introduction 125

V.2. Structures and Energetics 126

V.2.1. Alkyloxalate Ions 126

V.2.2. Alkyloxalate Radicals 134

V.2.3. Comparison with the Structures of Cations 140

V.3. Thermochemistry 144

V.4. Unimolecular Reactivity of Alkyloxalate Ions 146

V.5. NIDD Study of Alkyloxalate Radicals..... 154

V.6. Conclusions..... 163

V.7. References and Notes..... 165

VI. Conclusions and Perspectives 169

References and Notes..... 173

List of Abbreviations

ΔH_{298K}	heat capacity at 298 K
$\Delta H°_{atom,298K}$	atomization energy at 298 K
$\Delta_f H°_{298K}$	standard heat (enthalpy) of formation at 298 K
$\Delta_r H°_{298K}$	heat of reaction at 298 K
B1, B2	magnetic sector nr. 1, 2
BEBE	geometry of the instrument: B1/E1/B2/E2
BDE	bond-dissociation energy
BS	bond separation
C1, C2, .., C6	collision cell nr. 1, 2,.., 6
CA	collisional activation
CG	collision gas
CI	chemical ionization
CBS-Q	complete basis set quadratic
CR	charge reversal
D1,.., D4	detector nr. 1, …, 4
DFL1, DFL2	deflector electrodes nr.1, 2
E1, E2	electric sector nr. 1, 2
E_{el}	electronic energy
E_{kin}	kinetic energy
E_r	reverse energy
E_{rel}	relative energy
E_{tot}	total energy ($E_{tot} = E_{el}$ + ZPE)
EA	electron affinity
EC	electron convention
EI	electron ionization
FWHH	full width at half height
IC	ion convention
IE	ionization energy
IKE	ion kinetic energy
INC	ion-neutral complex
KER	kinetic energy release

MS	mass spectrometry
MI	metastable ion
MIKE	mass-analyzed ion kinetic energy
MP2	Møller-Plesset perturbation theory 2nd order
NICI	negative ion chemical ionization
NIDD	neutral and ion decomposition difference
NR	neutralization reionization
NRMS	neutralization-reionization mass spectrometry
PES	potential-energy surface
$Q_{min,CR}$	translational kinetic energy loss in the course of a CR experiment
$Q_{min,NR}$	translational kinetic energy loss in the course of a NR experiment
T	transmission
TE	translational energy
TS(s)	transition state(s) or structure(s)
VG	vacuum generator
ZAB/HF/AMD	zero-alpha-beta / high frequency / Advanced Micro Devices
ZPE	zero point energy
ZPVE	zero point vibrational energy

I. Introduction

The existence of life outside the Earth has always been a subject of dreams and of intensive search. This topic is closely related to the understanding of the origins of life in our planet and, in this context, one of the most widely accepted theory consists of the assumption that living systems have arisen from non-living ones.[1,2] This process, which involves the evolution of a simple initial system to states of greater and greater complexity, is nevertheless not fundamentally understood as yet. Plausible rationalizations of such an evolutionary process were formulated by Oparin[3,4] in 1924 and by Haldane[5] in 1928. Working independently, both authors postulated that life originates from a primitive reducing atmosphere in which simple organic compounds were synthesized. These organics accumulated in the surface of the ocean and formed a "primordial soup", from which life could have emerged in its most elementary form. On the nature of that prehistoric atmosphere, Haldane and Oparin disagreed. Haldane indeed favored a combination of ammonia, carbon dioxide, water vapor, and little or no oxygen, whereas Oparin's atmosphere consisted of methane, ammonia, water vapor, and hydrogen. These theories have later been supported by the experimental work of Miller and coworkers who obtained, by electric discharge, several amino acids from a mixture of methane, ammonia, water vapor, and hydrogen,[6-8] and formaldehyde and hydrogen cyanide from a mixture of methane, ammonia, carbon monoxide, and carbon dioxide.[9]

During the last eighty years, the so-called Haldane-Oparin theory has been modified and extended, but its essential features are still forming nowadays the basis for the accepted explanation of the origin and early evolution of life,[10-12] and are also largely taken into account in the search for extraterrestrial life. In this context, the planet Mars is of particular interest. Early Mars is indeed assumed to have presented many similarities with early Earth: a dense atmosphere allowing liquid water to persist at the surface and a steady influx of organic compounds brought from comets, asteroids, and dust. Moreover, both planets have probably possessed the same type of atmospheres, composed of a mixture of carbon dioxide, carbon monoxide, nitrogen, and water.[13] Since the detection in 2004 of methane in the Martian

atmosphere,[14-19] the search for a past or future life on this planet has never been so enthusiastic and so pertinent,[20-22] methane indeed being, referring to the Haldane-Oparin theory, a key component for the formation of prebiotic molecules.

As the present atmosphere of Mars consists of up to 95 % of carbon dioxide (Table I.1), this species might serve as a carbon source for the eventual formation of complex organic molecules. Moreover, due to the relatively high chemical inertness of carbon dioxide, trace components present in the Mars atmosphere are also expected to be significant contributors to the generation of new species. In this context, ionic species are of particular interest. Indeed, even though they are quite obviously several orders of magnitude lower in abundance than the neutral counterparts, they are generally known to show a pronounced reactivity and their role has been revealed decisive for instance in the chemistry of interstellar clouds.[23]

Table I-1

Identified gases in the homosphere[a] of Mars and their abundance, as given by Atreya[24] and Moroz.[25]

Constituent	Abundance	First detection
CO_2	95.37 %	1947[26]
N_2	2.7 %	1977[27]
Ar	1.6 %	1977[27]
O_2	0.13 %	1972[28,29]
CO	0.07 %	1969[30]
H_2O	0.02 %	1963[31]
Ne	2.5 ppm	1977[27]
He	1.1 ppm	1996[32]
Kr	0.3 ppm	1977[27]
Xe	0.08 ppm	1977[27]
O_3	0.01-0.8 ppm	1971[33]
CH_2O	0.5 ppm	1993[34]
CH_4	10 ppb	2003[15,35,36]

[a] The homosphere is the atmosphere layer located between 0 and 85 km of the surface.

Formation of new bonds in the Mars atmosphere can thus be envisaged as originating from charged or neutral species and these two possibilities need to be taken into account.

Initiated by these concepts, the present work intends to shed more light on some of the fundamental processes which could be at the origin of the formation of complex molecules in the atmosphere of Mars. In this context, this work has focused on two particular systems, the [R + CO_3] and [R + CO_2 + CO_2] families of compounds (R = alkyl). The former one is of interest because it contains a carbon trioxide neutral unit which is known to be a long-lived species and which is already considered as an important reaction intermediate in the atmosphere of Mars.[37-39] The second system consists in part of the association of two carbon dioxide units and its formation in the Mars atmosphere seems thus rather likely.[40]

In the neutral or in the ionic state, very little is known about these two systems concerning their structures, stability and reactivity. This thesis has thus been in part devoted to the study of the gas-phase behavior of these species in the anionic and neutral stage. To this end, mass spectrometric experiments performed with a four-sector mass spectrometer[41] were considered as ideal, because they allow the investigation of ionic as well as neutral transients by means of neutralization-reionization mass spectrometry (NRMS)[42] and related techniques. In this context, the NIDD method (NIDD = neutral and ion decomposition difference)[43] was of particular importance because it permitted the elucidation of the chemistry of transient neutral molecules generated by vertical electron-transfer processes from mass-selected ionic precursors. Furthermore, the experimental work has been complemented by theoretical studies at adequate levels of theory.

In the following sections, an introduction into mass spectrometry and some computational methods is first given as far as they contribute to this investigation. The first project of this thesis consists of the investigation of the gas-phase chemistry of alkylcarbonates ions and neutrals $ROCOO^{-/\bullet}$ with R = H, CH_3, C_2H_5, *i*-C_3H_7, and *t*-C_4H_9, including their structures, thermochemistry, and dissociation behavior. Some difficulties to understand the vertical electron-transfers processes performed on alkylcarbonate ions prompted the second project of this thesis, which is dedicated to the experimental determination of the dissociation energetics of methoxycarboxyl species formed by vertical charge transfer of methylcarbonate. This could be achieved using a particular technique available on the instrument which enables to access the translational kinetic energies of the species. In a third project, the gas-phase chemistry of alkyloxalate ions and neutrals has been probed in a similar manner to that for alkylcarbonates.

References

1. Brack, A., *Adv. Space Res.* **1999**, *24*, 417.
2. Gaidos, E.; Selsis, F., *From Protoplanets to Protolife: The Emergence and Maintenance of Life*, Protostars and Planets V Conference, Hawaii, **2006**.
3. Oparin, A. I., *Proiskhozhdenic Zhizny*; Izd. Moskovski Rabochii: Moscow, 1924.
4. Oparin, A. I., *The Origin of Life*; Macmillan: New York, 1938.
5. Haldane, J. B. S., *Possible Worlds*; Hugh & Bros: New York, 1928.
6. Miller, S. L., *Science* **1953**, *117*, 528.
7. Miller, S. L., *Biochim. Biophys. Acta* **1957**, *23*, 480.
8. Miller, S. L.; Urey, H. C., *Science* **1959**, *130*, 245.
9. Miller, S. L.; Schlesinger, G., *Origins Life Evol. Biospheres* **1984**, *V14*, 83.
10. Woese, C. R., *J. Mol. Evol.* **1979**, *13*, 95.
11. Fry, I., *Endeavour* **2006**, *30*, 24.
12. Ruse, M., *J. Theor. Biol.* **1997**, *187*, 473.
13. Pollack, J. B.; Kasting, J. F.; Richardson, S. M.; Poliakoff, K., *Icarus* **1987**, *71*, 203.
14. Kendrick, M. G.; Kral, T. A., *Astrobiology* **2006**, *6*, 546.
15. Krasnopolsky, V. A.; Maillard, J. P.; Owen, T. C., *Icarus* **2004**, *172*, 537.
16. Moran, M.; Miller, J. D.; Kral, T.; Scott, D., *Icarus* **2005**, *178*, 277.
17. Encrenaz, T., *Adv. Space Res.* **2007**, *In Press, Corrected Proof*.
18. Chastain, B. K.; Chevrier, V., *Planet. Space Sci.* **2007**, *55*, 1246.
19. Atreya, S. K.; Mahaffy, P. R.; Wong, A.-S., *Planet. Space Sci.* **2007**, *55*, 358.
20. Bada, J. L.; Sephton, M. A.; Ehrenfreund, P.; Mathies, R. A.; Skelley, A. M.; Grunthaner, F. J.; Zent, A. P.; Quinn, R. C.; Josset, J.-L.; Robert, F.; Botta, O.; Glavin, D. P., *Astron. Geophys.* **2005**, *46*, 6.26.
21. Report from the ESA Exobiology Team Study, *Exobiology in the Solar System and The Search for Life on Mars*, Wilson, A., ESA Publications Division: ESTEC, Noordwijk, 1997-1998.
22. Ponnamperuma, C.; Navarro-Gonzalez, R.; Honda, Y., *Adv. Space Res.* **1995**, *15*, 177.
23. Williams, D. A., *Chem. Eur. J.* **1997**, *3*, 1929.

24. Atreya, S. K.; Gu, Z. G., *Adv. Space Res.* **1995**, *16*, 57.

25. Moroz, V. I., *Adv. Space Res.* **1998**, *22*, 449.

26. Kuiper, G. P.; Wilson, W.; Cashmau, R. J., *Astrophys. J.* **1947**, *106*, 243.

27. Owen, T.; Biemann, K.; Rushneck, D. R.; Biller, J. E.; Howarth, D. W.; Lafleur, A. L., *J. Geophys. Res.* **1977**, *82*, 4635

28. Carleton, N. P.; Traub, W. A., *Science* **1972**, *177*, 988.

29. Barker, E. S., *Nature* **1972**, *238*, 447.

30. Kaplan, L. D.; Connes, J.; Cannes, P., *Astrophys. J.* **1969**, *157*, LI87.

31. Spinrad, H.; Munch, G.; Kaplan, L. D., *Astrophys. J.* **1963**, *13*, 1319.

32. Krasnopolsky, V. A.; Gladstone, G. R., *J. Geophys. Res.* **1996**, *98*, 15061.

33. Barth, C. A.; Hord, C. W., *Science* **1971**, *4*, 173.

34. Korablev, O.; Ackerman, M.; Krasnopolsky, V. A.; Moroz, V. I.; Müller, C.; Rodin, A. V.; Atreya Sushil, K., *Planet. Space Sci.* **1993**, *41*, 441.

35. Formisano, V.; Atreya, S.; Encrenez, T.; Ignatiev, N.; Giuranna, M., *Science* **2004**, *306*, 1758.

36. Mumma, M. J.; Novak, R. E.; DiSanti, M. A.; Bonev, B. P.; Dello Russo, N., *Bull. Am. Astron. Soc.* **2004**, *36*, 26.02.

37. Jamieson, C. S.; Mebel, A. M.; Kaiser, R. I., *ChemPhysChem* **2006**, *7*, 2508.

38. Mebel, A. M.; Hayashi, M.; Kislov, V. V.; Lin, S. H., *J. Phys. Chem. A* **2004**, *108*, 7983.

39. Perri, M. J.; VanWyngarden, A. L.; Lin, J. J.; Lee, Y. T.; Boering, K. A., *J. Phys. Chem. A* **2004**, *108*, 7995.

40. Smith, D., *Int. J. Mass Spectrom. Ion Processes* **1993**, *129*, 1.

41. Schalley, C. A.; Schröder, D.; Schwarz, H., *Int. J. Mass Spectrom. Ion Processes* **1996**, *153*, 173.

42. Schalley, C. A.; Hornung, G.; Schröder, D.; Schwarz, H., *Chem. Soc. Rev.* **1998**, *27*, 91.

43. Schalley, C. A.; Hornung, G.; Schröder, D.; Schwarz, H., *Int. J. Mass Spectrom. Ion Processes* **1998**, *172/173*, 181.

II. Methodological Overview

The understanding of the unimolecular dissociation of ions and molecules is based upon a large theoretical background. Two concepts have been of prime importance for the analysis and understanding of the processes investigated in this work: the theory of unimolecular decay and the intermediacy of ion-neutral complexes. A brief description of these two concepts is given in the following section. Moreover as several complementary mass-spectrometric techniques and theoretical methods are employed in this work, a general introduction concerning these methods is given in this chapter, as well as the methodologies which have been applied.

II.1. Important Concepts in Mass Spectrometry

In this Thesis, unimolecular dissociation processes of several compounds are investigated. Many intrinsic and external parameters of the system studied (internal and kinetic energy of the system, ionization conditions, etc) play an important role to help in the understanding of such unimolecular processes. The theory of unimolecular decay described in this section consists of a simplistic but complete description of the system under study and enables the understanding of the processes involved in unimolecular dissociation. Furthermore, the analysis of decomposition processes requires taking into account the existence of ion-neutral complexes. This particular feature is described in the second part of this section.

II.1.1. Theory of Unimolecular Decay

When ions are generated via conventional ionization techniques under the ultra-high vacuum conditions (10^{-6} - 10^{-9} mbar) existing in a mass spectrometer, they are formed with a certain amount of internal energy. During the ionization process, transitions to various electronic, vibrational, and rotational states of the ion are possible, leading to a variety of ions characterized by different internal energies. This internal energy distribution may differ from the Maxwell-Boltzmann distribution and depends on the conditions of ionization as well as on

the nature of the molecular species. Among the various models[1-3] which have been developed to describe the energetics of unimolecular decay processes, the quasi-equilibrium theory[4] (QET) and the Rice-Ramsberger-Kassel-Marcus (RRKM) theory[5-9] are the most commonly used. Both are based on the activated complex theory (transition state theory, TST) which has been introduced by Eyring and Polanyi.[10,11] The main concept of this theory consists in considering the ions formed in the mass spectrometer as isolated systems and in assuming that the redistribution of the internal energy of the ion is much faster than any subsequent reaction or dissociation of the ion, leading then to a quasi-equilibrium between the possible energy states. Such systems exhibit a so-called ergodic behavior, which means that a statistical distribution of the internal energy over all degrees of freedom is achieved before any unimolecular reaction occurs.

The model used in the statistical treatment is schematically depicted in Figure II.1-1. Dissociation occurs if the amount of internal energy E_{int} accumulated in the reaction coordinate is sufficient to overcome the activation energy barrier E_0 of the activated complex.

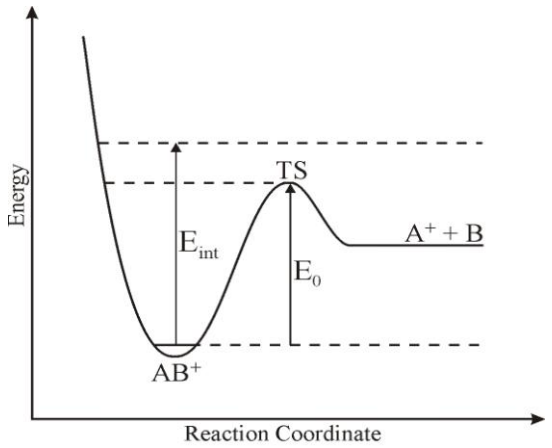

Figure II.1-1: Schematic potential-energy diagram for the unimolecular decomposition of an AB^+ ion.

According to both QET and RRKM theory, the rate of unimolecular dissociation of an isolated system AB^+ of internal energy E_{int} is given by Equation (II.1-1).[12]

$$k(E_{int}) = \frac{\sigma}{h} \cdot \frac{W^{\neq}(E_{int} - E_0)}{\rho(E_{int})} \qquad \text{(II.1-1)}$$

where h is Planck's constant, $W^{\neq}(E_{int} - E_0)$ is the number of vibrational and rotational states of the activated complex with energy < $E_{int} - E_0$, $\rho(E_{int})$ is the density of states of the reactant ion with an energy E_{int}, and σ is a symmetry factor for the number of identical reactions.

The rate constant $k(E_{int})$ of unimolecular decay is a function of the internal energy E_{int} but depends also on the geometry of the activated complex. Consequently, a distinction is made between loose and tight transition structures (TSs). In general, unimolecular processes can be divided in two groups: direct bond-cleavages and rearrangements (involving the formation of new bonds). The formers proceed via loose TSs which are characterized by a large number of low-lying rovibronic states and are, thus, entropically favored. In contrast, rearrangements, for which a specific geometrical arrangement is required, involve tight TSs (possessing a small number of low-lying states) and are in general thermodynamically favored. The case of a system which can dissociate along two dissociation paths, one characterized by a loose TS and the other by a tight one, is depicted in Figure II.1-2.

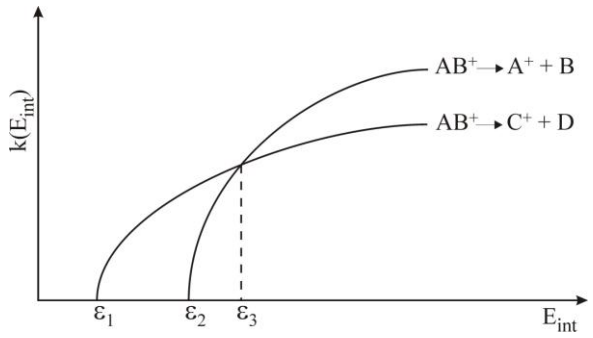

Figure II.1-2: Schematic representation of the energy dependence of $k(E_{int})$ for competing rearrangement and direct bond cleavage reactions.

The dissociative rearrangement of AB^+ to $(C^+ + D)$ proceeds with the lowest activation energy and the tightest transition state and will be observed for energies ranging between ε_1 and ε_2. If the internal energy is increased above ε_2, the direct bond cleavage (higher activation energy and looser transition state) leading to $(A^+ + B)$ will start to compete with the rearrangement. If the internal energy exceeds ε_3, the direct bond cleavage will dominate the reactivity.

II.1.2. Ion-Neutral Complexes

Experimental and theoretical studies have established the existence in the gas phase of simple organic ions with unusual structures consisting of an ionic part bound non-covalently to a neutral one.[13-23] Such ions are termed ion-neutral complexes or ion-dipole complexes since both parts are held together by electrostatic interaction. It is not always possible to distinguish an ion-dipole complex from its covalent analogue by mass spectrometric techni-

ques,[24] but (i) such complexes are easily characterized by theoretical calculations and (ii) the behavior of unconventional ions can sometimes only be understood from ion-dipole properties. The main feature of an ion-neutral complex is indeed that, as it is composed of two parts, the ion can undergo internal rearrangements independently from the rest of the complex. As it will be seen in the following chapters, the concept of ion-neutral complex is very important in the case of the systems studied in this Thesis. Chart II.1-1 shows the example of an ion-dipole complex involved in the dissociation of methyl oxalate. Throughout this work, such species will be presented in brackets in order to distinguish them from two separated neutral or ionic entities.

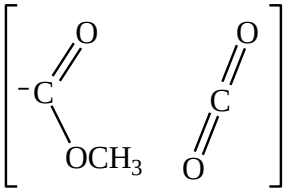

Chart II.1-1: The ion-neutral complex [CH_3O^- CO_2] involved in the decomposition of methyloxalate (Chapter V).

II.2. Ion-Beam Mass Spectrometry

The following chapter gives a brief overview of the instrumentation and of some experimental details which are necessary for the understanding of the present study. All the experiments presented in this work have been carried out using a modified VG ZAB/HF/AMD 604 four-sector mass spectrometer that has been built by the companies Vacuum Generator and AMD Intectra.[25-27]

Sector field instruments are often employed to monitor the unimolecular or collision-induced dissociation decay of ions having been accelerated to kinetic energies in the order of keV.[28-31] The Berlin instrument is depicted schematically in Figure II.2-1. After generation in the ion source, the ions of interest are usually accelerated to 8000 eV kinetic energy. Two magnetic (B1 and B2) and two electrostatic (E1 and E2) sectors are combined to a BEBE configuration, and are then used to separate and analyze the ions; the latter can be detected by any of the four electron multipliers (D1 to D4, Figure II.2-1) located behind each sector. The time needed for an ion to travel from the source to the detectors is within µs. Furthermore, MS^n experiments are possible, with up to n = 5, even though the absolute intensity of the ions usually restricts the performance of such experiments. In this work, the upper limit was at n = 2 or 3.

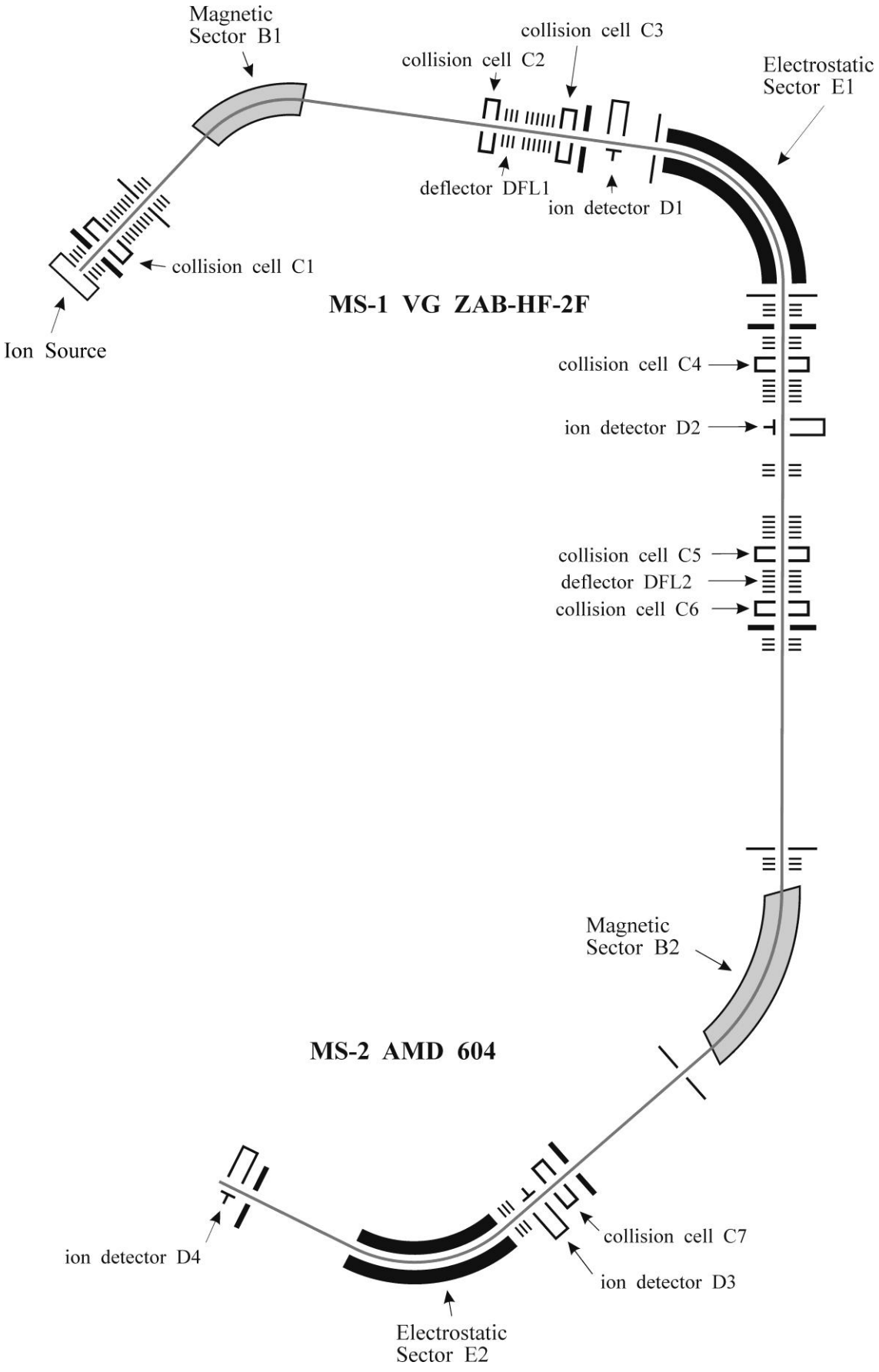

Figure II.2-1: Scheme of the Berlin VG ZAB-2F-HF/AMD 604 mass spectrometer.[25-27]

In the five field-free regions, seven differentially pumped collision cells allow to perform different types of collision experiments, as charge reversal or collisional activation. Furthermore, two deflector electrodes (DFL1 and DFL2) enable the study of the structure and the reactivity of neutral species by neutralization-reionization methods. All types of experiments which have been used in this work are discussed below in detail after a short description of some technical features of the ion-beam instrument. All mass spectra were recorded with the AMD-Intectra data system, and usually 10 to 80 scans were accumulated to improve the signal-to-noise ratio.

II.2.1. Inlet System and Ion Generation

Three commercial standard inlet systems have been used for the introduction of the precursor molecules in the ion source: (i) a gas inlet consisting of a thin quartz capillary for pressure reduction (ii) a heatable septum inlet system for the introduction of liquids and gases (ca. 20 - 300 °C) and (ii) a heatable (ca. 40 - 700 °C) direct inlet system for solid probes.

To ionize the precursor molecules, three ionization methods[32] are available on the instrument: electron ionization (EI),[33-35] chemical ionization (CI)[34,36-40] and fast-atom bombardment (FAB).[41] In this study, all cations were produced by electron ionization (EI) with an electron beam having energy of 70 eV and the repeller voltage sets to ca. 20 V; the generation of anions was achieved by negative ion chemical ionization (NICI).[42-44] The latter method is derived from the chemical ionization technique. A suitable reagent gas, which is present in large quantity compared to sample molecules, is ionized by a beam of electrons with energies up to 300 eV. A charge transfer is then occurring between the ionized reagent ions and the precursor molecules. An example is given in Scheme II.2-1 in the case of the NICI of methylcarbonate.

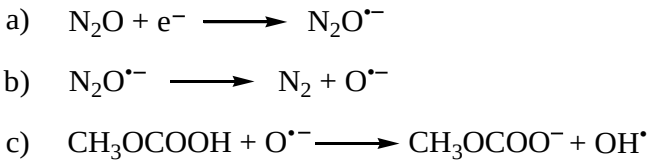

Scheme II.2-1: The three steps of the NICI of methylcarbonate with N_2O as reagent gas.

In our experiments, the NICI technique was used with N_2O present in excess (100 : 1) as a reagent gas.[42] To this end, ca. 3 µl of the precursor were introduced to the source. The neutrals were then converted to anions at a repeller voltage of ca. 0 V.

II.2.2. Physical Basis of a Sector Mass Spectrometer

Before being transferred into the analyzing sectors, the ions are accelerated through a voltage U (here 8000 eV) in the source. They acquire thus a kinetic energy E_{kin} which corresponds to zeU, where e is the charge of the electron and z that of the ion, m is the mass of the ion and v its velocity.

$$E_{kin} = \frac{1}{2} mv^2 = zeU \tag{II.2-1}$$

The velocity of each ion is accordingly expressed by:

$$v = \sqrt{\frac{2\,zeU}{m}} \tag{II.2-2}$$

Magnetic Sector

In a magnetic sector, the ions pass a magnetic field of strength B, perpendicular to their initial trajectory. They thus experience a force $Bzev$, producing an acceleration of v^2/r_B toward the center of a circular path of radius r_B. Consequently, from Newton's second law of motion,

$$Bzev = \frac{mv^2}{r_B} \tag{II.2-3}$$

the velocity v of the ions can then be written:

$$v = \frac{r_B zeB}{m} \tag{II.2-4}$$

Combining Equations (II.2-2) and (II.2-4) finally leads to the basic mass-spectrometer equation (Equations (II.2-5)).

$$\frac{m}{z} = \frac{r_B{}^2 B^2 e}{2U} \tag{II.2-5}$$

In the magnetic sector, only ions having a circular trajectory of radius R will be transmitted through the magnetic field to reach the collector plate (Figure II.2-2). Thus, by varying B

or *U*, ions of different *m*/*z* can be transmitted. The selection of the ions is accordingly made only with the magnetic field *B* (all the ions experience the same acceleration *U*). Further, Equation (II.2-3) shows that *B* is directly proportional to the momentum of the ion ($p = mv$), demonstrating the fact that a magnetic sector acts as a momentum analyzer rather than a mass analyzer as often anticipated.

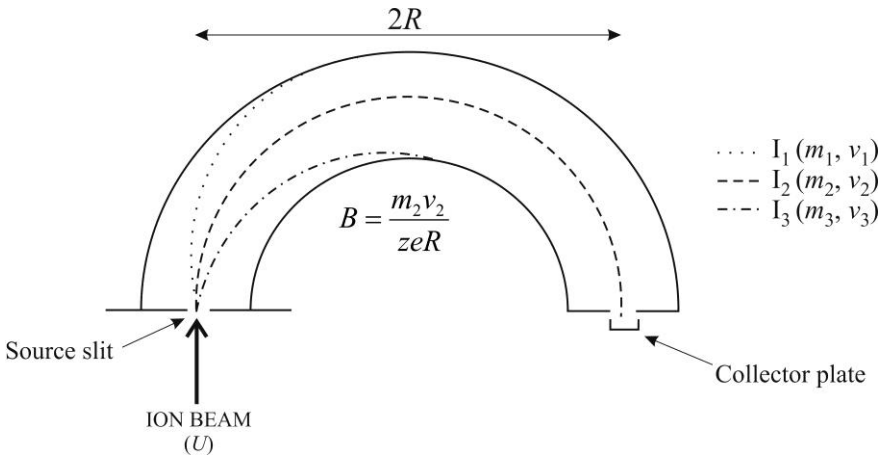

Figure II.2-2: Illustration of ion selection in a magnetic sector. The ion beam is constituted in this example of three ions I_1 (m_1, v_1), I_2 (m_2, v_2) and I_3 (m_3, v_3) of charge *z*. In the conditions of the experiment (accelerating voltage *U*, magnetic field *B*), only I_2 has a circular trajectory of radius *R* which is the radius of the magnetic sector and is transmitted to the collector plate. The radii of the trajectories of I_1 and I_3 are too large or too small, respectively, and these ions are not transmitted further.

Electrostatic Sector

In an electrostatic sector, ions are subjected to an electric field of strength *E* and accordingly to a force *zeE*. This force produces an acceleration of v^2/r_E towards the center of a circular path of radius r_E. According to Newton's second law of motion, this can be written as follow:

$$zeE = \frac{mv^2}{r_E} \tag{II.2-6}$$

An expression for the radius r_E can then be derived:

$$r_E = \frac{2E_{kin}}{zeE} \tag{II.2-7}$$

Equation (II.2-7) shows that the circular path of radius r_E followed by an ion submitted to an electrostatic field E is directly proportional to its kinetic energy. The electrostatic sector can therefore be termed as kinetic-energy analyzer.

Velocity Dispersion

As ions are not generated exactly at the same spatial position in the source, they do not experience exactly the same acceleration. A dispersion v' of the velocity has to be taken into account. The velocity of an ion is then written as $v \pm v'$. This effect avoids an exact selection of the ion of interest with the magnetic sector only as the selection is made in this sector with the momentum p of the ion.[45] Two ions of different velocities and different masses may indeed possess the same momentum. The use of the second sector (E) largely improves resolution.[29,31] Any ions having the same kinetic energy and the same momentum possess indeed the same mass (Equation (II.2-8)) and the same velocity (Equation (II.2-9)).

$$v_1 = \frac{m_1 v_1^{\,2}}{m_1 v_1} = \frac{2\mathrm{E}_{\mathrm{kin}\,1}}{p_1} = \frac{2\mathrm{E}_{\mathrm{kin}\,2}}{p_2} = \frac{m_2 v_2^{\,2}}{m_2 v_2} = v_2 \qquad \text{(II.2-8)}$$

$$m_1 = \frac{m_1^{\,2} v_1^{\,2}}{m_1 v_1^{\,2}} = \frac{p_1^{\,2}}{2\mathrm{E}_{\mathrm{kin}\,1}} = \frac{p_2^{\,2}}{2\mathrm{E}_{\mathrm{kin}\,2}} = \frac{m_2^{\,2} v_2^{\,2}}{m_2 v_2^{\,2}} = m_2 \qquad \text{(II.2-9)}$$

Practically, the cations studied in this work have been mass selected by two sectors, B1 and E1 as well as the anions submitted to charge-transfer experiments. In contrast, unimolecular decay of anions was investigated using only one sector for mass selection. These species are in general difficult to generate and the utilization of one sector for the mass selection reduces the time scale of the experiment, and facilitates thus the study of such ions.[43,46]

In the case of an ion selection with two sectors, the fragmentation occurring in the field free region between E1 and B2 was monitored by scanning B2, whereas when the ion was selected only with B1, the sector E1 was scanned to record the fragmentation occurring in the field free region between B1 and E1.

II.2.3. Metastable Ion Decay (MI)

The ionization of a sample molecule in the ion source can result in the transfer of a wide range of energies to the sample molecule. Highly excited ions will usually undergo one or more fragmentation processes within the ion source, whereas ions with lower internal energies

may not dissociate until they reach the detector. However, for some of these ions, the transfer of a small amount of energy can lead to the formation of ions which do not dissociate in the source, but which will fragment unimolecularly within the μs time scale of the ion-beam experiment. These ions are termed metastable ions (MI).[47] Decomposition of such ions allows investigation of energetically low-lying processes like rearrangements. It is important to note that a metastable peak may not be characteristic of the ground state structure but may arise from an excited state or from a different reacting configuration produced by rearrangement of the original ion. Although the range of energies involved for a metastable ion is quite small, the ions have indeed relative high internal energies and it is in general possible that prior to the fragmentation, the metastable ion rearranges to another structure.[48]

In addition, the kinetic energy release related to a dissociation process can be determined from the peak shape of a metastable decomposition. This particular feature is described in more details in section II.2.8.

In the spectra obtained in this work, the experimental error of the signal intensities does not exceed ± 5 %.

II.2.4. Collisional Activation (CA)

Collisional activation (CA) spectra[49-52] are obtained by colliding the accelerated ion beam with a neutral target gas. In these high-energy collisions, part of the kinetic energy of the ion is converted into internal energy. This excess energy leads either to an immediate decay of the ions in the ps time scale or to delayed decompositions within the ns to the μs time scale. For this reason, CA mass spectra are dominated by direct bond cleavages, whereas products due to rearrangements are less pronounced. The observed fragmentations provide a fingerprint spectrum, which is often structurally characteristic. Nevertheless, CA mass spectra will always be the result of a superposition of unimolecular and collision-induced decomposition processes.

In this study, CA experiments were performed by admitting helium as a neutral target gas to one of the collision chambers between E1 and B2 for the cations and between B1 and E1 for the anions. The pressure of the target gas was adjusted so that the ion beam intensity was reduced to 80 % transmission (80 % T), which corresponds to near single-collision conditions (each ion collides on average 1.1 to 1.2 times with the target gas).[53] The reproducibility of the fragment ion intensities is not as good as for MI spectra, and the experimental errors of the CA mass spectra range between ± 5 % and ± 10 %.[54]

II.2.5. Charge-Reversal Experiments (CR)

Charge reversal (CR) experiments have been introduced by Bowie and Blumenthal in 1975.[49,55-57] They are carried out by colliding the ion beam with a stationary collision gas under single collision conditions.[53] A fraction of the ions undergoes a double electron transfer. Since the time of interaction between the ions and the target gas is typically < to 10^{-15} s and as the frequency of a molecular vibration is generally > to 10^{-14} s, the Born-Oppenheimer[58] approximation is valid and the charge-transfer reactions represent vertical processes governed by the Franck-Condon factors.[59] One important consequence of the Born-Oppenheimer approximation is that changes in geometry are negligible. The ion produced from a vertical double electron transfer has the same geometry than its precursor ion.

Two types of CR experiments are possible: the generation of a cation from an anion ($^{-}CR^{+}$) and the generation of an anion from a cation ($^{+}CR^{-}$).[60] These experiments are in general quite useful for the structure determination of anions and the generation and investigation of unusual cations, which are difficult to generate by other means.[61,62] Figure II.2-3 shows the schematic setup of a CR experiment.

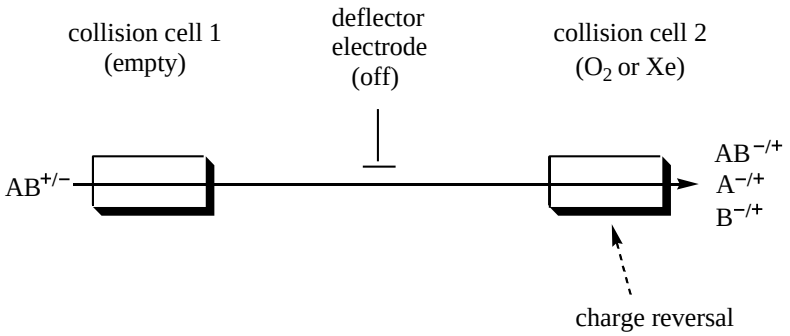

Figure II.2-3: Schematic representation of a charge-reversal (CR) experiment in a tandem collision cell equipped for NR experiments.

In this work, the $^{-}CR^{+}$ technique has been employed to study the unimolecular reactivity of neutral intermediates in combination with the NIDD method (section II.2.7) and the structural characterization of some anions which was not possible by traditional MI and CA experiments.

$^{-}CR^{+}$ mass spectra were achieved by selecting the negatively charged ions with B1/E1 and by colliding them with oxygen (80 % T) located in one of the collision cells located between E1 and B2. B2 was further scanned to monitor the spectra. $^{+}CR^{-}$ mass spectra were obtained

by mass selection with B1 and charge inversion with xenon as a target gas in one of the collision cells located between B1 and E1 while scanning E1.

II.2.6. Neutralization-Reionization Experiments (NR)

The investigation of the structure and reactivity of transient neutral species in the gas phase is made possible using the neutralization-reionization mass spectrometry (NRMS) technique.[49,57,60,63-69] A NR mass spectrum (Figure II.2-4) is usually obtained from fast moving particles which are subjected to two sequential events, in both of which electron transfers occur. The first charge transfer leads to the partial neutralization of the ion beam, yielding a mixture of ions and neutrals in the beam. Ions are then removed by a deflector electrode and the pure beam of neutrals is reionized by a second collision event in a second collision cell. For the same reasons as those given for the CR experiments, the charge transfers occurring are vertical and thus governed by the Franck-Condon factors. The Born-Oppenheimer approximation implies also that no geometry change takes place during the charge transfers, which means that the neutral initially obtained has the same geometry as its anionic or cationic precursor. As for other collision experiments, the pressure of the target gases are adjusted so that both collisions occur under near-single-collision conditions.[53]

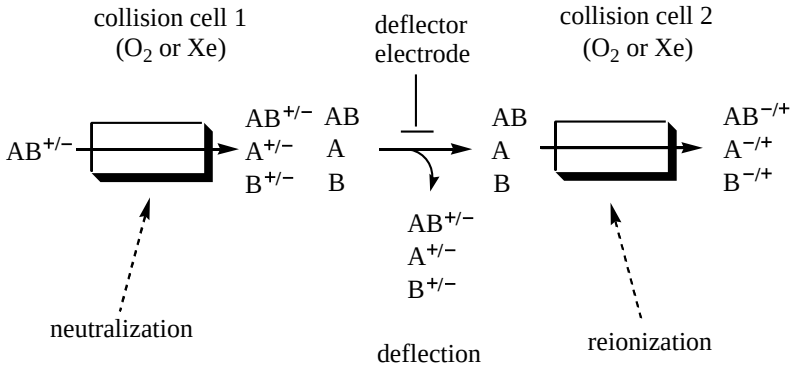

Figure II.2-4: Schematic representation of a neutralization-reionization (NR) experiment.

NR experiments exist in four variants: anions can be neutralized and neutrals then reionized to cations ($^{-}NR^{+}$) or to anions ($^{-}NR^{-}$) and vice versa, cations can be neutralized and the resulting neutrals are reionized to anions ($^{+}NR^{-}$) or to cations ($^{+}NR^{+}$). In this work, only the $^{-}NR^{+}$ and $^{-}NR^{-}$ techniques were employed. Neutralization of the anions was performed using oxygen as target gas (80 % T) and reionization of neutrals to cations or to anions was brought about with oxygen (80 % T) or xenon (80 % T).[70,71] $^{-}NR^{+}$ mass spectra were recorded by

scanning B2, while mass selection was made with B1/E1, the charge transfers with O_2 in C5 and C6, and the deflector electrode DFL2 used. Only two sectors were used for $^{-}NR^{-}$ experiments: B1 for the mass selection and E1 for the scan. The collision cells C2 (O_2) and C3 (Xe) served for the charge transfer processes together with DFL1 for the ion deflection.

The NRMS technique may provide valuable information concerning the existence or the structure of the neutralized species as well as its precursor ion, but very often its role is restricted to the observation of a recovery signal, which enables to show that the neutral of interest has a lifetime in the μs time scale of the experiment. Dissociation of the neutralized species is very often accompanied by that of the ionic ones, and thus it becomes difficult to assign unambiguously fragmentation features. Further, as the intensity of the recovery signal is very weak for the systems investigated in this work, no further NR/CA experiment, which could have provided more information concerning the neutrals, was possible. Several techniques have therefore been developed to study neutrals species by means of mass spectrometry and the following section presents the one used in this work.

II.2.7. Neutral and Ion Decomposition Difference (NIDD)

As underlined in the previous section, the question of probing the reactivity of neutral species or revealing their intramolecular rearrangements cannot generally be achieved by the conventional NRMS technique. Indeed, a clear-cut assignment of the spectra to the exclusive contribution of the neutral molecules to the total fragmentations in NR experiments is often difficult if not impossible, because the fragmentations of the neutral are superimposed by those of projectiles or recovery ions. To get around this difficulty, a new approach has been developed in 1998 by Schalley *et al.*[72] An identification of the reactions of neutral intermediates is possible by subtracting the CR from the NR mass spectra after applying an appropriate normalization procedure. This method is called the NIDD method: Neutral and Ion Decomposition Difference and exists in two variants: Anions can be oxidized into cations ($^{-}NIDD^{+}$) or cations can be reduced into anions ($^{+}NIDD^{-}$). Furthermore, to be applied, this approach needs some specific conditions to be met:

(i) Upon neutralization, the neutral of interest has to constitute a major component of the particle beam. This condition is usually easy to fulfill for electron detachment from anions ($^{-}NIDD^{+}$), but is more problematic in the neutralization of cations ($^{+}NIDD^{-}$), which is often associated with a sizable amount of fragmentation. To estimate the contribution of the desired

neutrals to the particle beam, a conventional NR technique can be used and the intensities of the reionized parents may serve as qualitative indicators.

(ii) The systems under study should not be very sensitive to the pressure of target gases used in the collision chambers, because only a single collision occurs in the CR experiment while the NR experiments require two collisions. If the species are sensitive to the collision conditions, artefacts may then arise in the spectra difference. To test this, the CR experiments should be conducted not only under single-collision procedure, but also under the conditions of the NR procedure (this is easily achieved by switching off the deflector electrode and performing a CR experiment under typical NR conditions).

(iii) The CR and NR spectra are normalized to the sum of all ions including the recovery signal. Subsequently, the NIDD spectrum is obtained by subtracting the normalized CR intensities *I*(CR) from the normalized NR intensities *I*(NR):

$$I_i(\mathrm{NIDD}) = \frac{I_i(\mathrm{NR})}{\sum_i I_i(\mathrm{NR})} - \frac{I_i(\mathrm{CR})}{\sum_i I_i(\mathrm{CR})} \qquad \text{(II.2-10)}$$

Signals with positive intensities can be traced back to the reactions of the neutral intermediate, while fragments formed from the ions either before neutralization or after reionization show up as negative peaks. Furthermore, due to essential differences between the CR and NR processes, some particular features appear in the NIDD spectra and have to be underlined:

(iv) The NR signals are generally broader compared to the CR spectra.

(v) Fragmentation is often more extensive in NR than in CR processes.

(vi) A slight shift of the apparent mass is observed between both spectra due to the kinetic energy loss in the collisionally-driven electron-transfer processes.

For these reasons, only NIDD intensities higher than |0.02| are assumed to be significant, and only peak heights at unit mass resolution are considered, which result in the fact that the NIDD spectra are usually presented as block diagrams,[66] even though discrete spectra may also be used.[73,74]

In this work, only $^{-}$NIDD^{+} schemes have been applied. They result from the difference between $^{-}$NR^{+} and $^{-}$CR^{+} experiments performed by scanning B2 while mass selection was achieved with B1/E1. To validate the conditions required for the NIDD method, $^{-}$CR^{+} spectra were recorded with one or two collision cells filled to make sure that the system studied was not too sensitive to the pressure of the target gases.

II.2.8. Translational Energy Spectra

In order to obtain information concerning ion-fragmentation energetics from an electric sector, it is possible to carry out mass separation of the beam of ions according to their translational energies. The ion kinetic energy spectra obtained in this way are referred to as IKE (ion kinetic energy) and as MIKE (mass analyzed ion kinetic energy) if a mass selection with the magnetic sector precedes the analysis.[47]

As underlined in section II.2.3, some features associated with the dissociation of an ion can be obtained from the analysis of the peak shape of the MI signal. This holds particularly true in the case of a release of kinetic energy in the course of the dissociation. The kinetic energy, *T*, released in the unimolecular decay of a metastable ion can arise from two different sources: (i) the excess energy, $\varepsilon^{\#}$, of the activated complex which is available for partioning between the internal energies of the products and translational energy of their separation, and (ii) the reverse activation energy, ε_0^{r}, which is partitioned as rovibrational excitation of the neutral and ionic products in the one hand and their translational energy on the other hand (Figure II.2-5).[75-77] Hence, the kinetic energy released (KER) *T* may be written as:

$$T = T^{e} + T^{\#} \tag{II.2-11}$$

where T^{e} is the contribution to the kinetic energy released from the reverse activation energy and $T^{\#}$ is that from the excess energy of the activated complex. T^{e} depends upon the detailed energetics and dynamics of the reaction and is intrinsic to the particular process; $T^{\#}$ varies with the internal energy of the reactant ion and has no fundamental significance.[47] The relationships between the different terms involved in the course of the unimolecular decay of a metastable ion are summarized in Figure II.2-5.

The release of kinetic energy in the course of the dissociation of an ion results in an isotropic gain of kinetic energy for the dissociation products. This feature is observable experimentally by a signal broadening and a variation of the shape of the peak, which are both directly related to the amount of KER. The different shapes of the metastable peak which can be obtained according to the value of KER are shown in Figure II.2-6. No further details will be given here to explain these shapes, as they are already well described in the literature.[47,75-77]

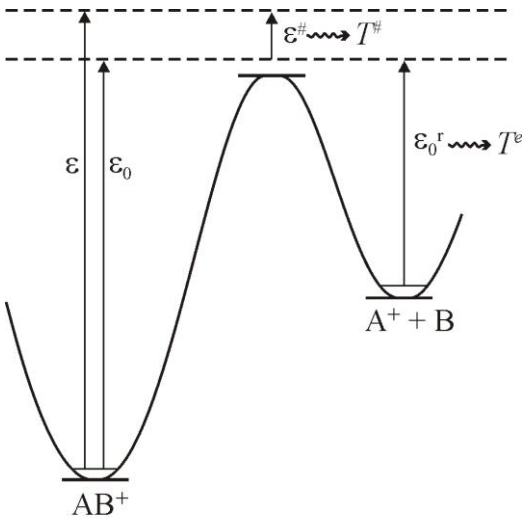

Figure II.2-5: Energy diagram for the dissociation of AB^+ into A^+ and B. ε_0 and ε_0^r are the activation energies for the forward and reverse reaction and $\varepsilon^\#$ is the excess energy of the activated complex, also termed "non-fixed" energy.[78,79] A portion of ε_0^r and $\varepsilon^\#$ appears as kinetic energies T^e and as $T^\#$.[49]

Cooks and coworkers[47,80] have shown that the kinetic energy released in the dissociation of a singly charged ion is connected to the full width at half height (FWHH) of the fragment ion by the following relation:

$$T = \frac{m_P{}^2 \cdot e \cdot U}{16 \cdot m_D \cdot m_N} \left(\frac{\Delta E}{E_0} \right)^2 \qquad \text{(II.2-12)}$$

where T stands for the KER (in eV), m_P, m_D, and m_N are the masses of the parent ion, the daughter ion, and the neutral fragment, respectively. E_0 is the electric sector voltage value corresponding to the center of the parent ion peak and ΔE is the range of values of electric sector voltage over which the daughter ion peak is observed (FWHH).

The experimental peak width ΔE must be corrected for instrumental broadening. If both the parent and product peaks are Gaussian-like the following correction is applied:[76]

$$\Delta E = \sqrt{\Delta E_D^2 - \Delta E_P^2} \qquad \text{(II.2-13)}$$

where ΔE_D and ΔE_P are the metastable and the parent peak widths (FWHH).

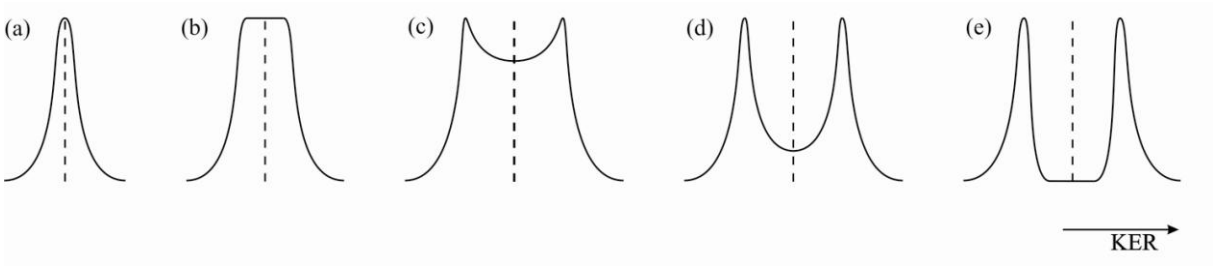

Figure II.2-6: Variation of the peak shapes of metastable ions as a function of the KER. The dashed lines represent the center of the peak which corresponds to the mass m_D^2/m_P^{81} and stays fixed. No KER is represented by the Gaussian-type shape (a). Increase of KER leads first to a flat-topped shape (b), then to dished-topped shapes (c) and (d). A very large KER (shape (e)) leads to a complete discrimination of the ions having a direction perpendicular to the main beam.

Translational energy spectra of fragment and parent ions give then easily access to the KER of a decomposition process. In this Thesis, such a technique has been employed to investigate the energetics of the bond-cleavage process of methylcarbonate cation and radical obtained by vertical electron transfer from methylcarbonate and leading to $CO_2^{\bullet+}$ and $CH_3O^{\bullet}$ and to CO_2 and $CH_3O^{\bullet}$. This investigation is somewhat unusual because the process investigated corresponds to metastable dissociation of ions produced by charge transfer and gives then rise to two types of results. First, the peak shape of the ions gives access to the KER of the process. Then, the position of the peak allows also the investigation of the energetic cost of the charge transfer and the dissociation processes. When no charge transfer takes place, the daughter ion of masse m_D will indeed be positioned at the electric voltage E_D defined as:

$$E_D = \frac{m_D}{m_P} \cdot E_P \qquad \text{(II.2-14)}$$

where E_P is the electric voltage selecting the parent ion. If the parent ion is subjected, prior to fragmentation, to a charge transfer, part of its translational energy will be converted into internal energy required in this charge transfer.[49] The resulting ion will have accordingly a smaller kinetic energy than the parent. The position of the dissociation fragments will therefore be connected to this ion and not to the initial parent. Experimentally, the positions of the initial parent ion and of the fragments are accessible, which enables to gain information concerning the energetics of the charge-transfer reaction.

II.3. Computational Methods

Quantum chemistry being applied in the present context of gas-phase experiments aims at the characterization of a given molecular system in terms of geometries, relative energies, and electronic states of reactants, intermediates, transition structures, and products formed in the course of a reaction. While the geometries of ground and transition states already reveal valuable information about the reaction mechanism, the determination of the relative energies allows a more quantitative description of the reaction mechanisms, i.e. the thermochemistry of a reaction and the location of reaction barriers.

According to the classical formulation of quantum mechanics, the wavefunction Ψ contains all information needed for the complete description of a system.[82,83] This wavefunction is described by the Schrödinger equation:[84]

$$\hat{H}\Psi = E\Psi \tag{II.3-1}$$

where $\hat{H}$ is the Hamiltonian operator and E the energy. The wavefunction $\Psi(x,R,t)$ depends on the spatial and spin coordinates x of the electrons, the spatial coordinates of the nuclei R, and the time t.

An analytical solution of Equation (II.3-1) is only accessible for one-electron systems. In the case of many-particles systems, it is necessary to employ approximations. A first assumption is the reduction of the time-dependent system into a time-independent one described by $\Psi(x,R)$. For most chemical processes, this reduction is an appropriate simplification if the system does not experience any time-dependent external forces. The second and most important approximation is the so-called Born-Oppenheimer (BO) approximation,[58] which assumes that the electrons, due to their lower mass, move considerably faster than the atomic nuclei. This assumption enables one to considerably simplify the Hamiltonian because the term describing the kinetic energy of the nuclei can be neglected and the term for the nuclei potential energy can be considered as constant.

Due to the electron-electron interaction in the Schrödinger equation, a further simplification by separation of the multi-particles problem into one-particle problems is impossible. As an approximation, the Hartree-Fock (HF) method uses one-electron operators in order to generate a Slater determinant of molecular orbitals. This method is described in details in the next section, followed by a brief description of the theoretical models used in this work, the

Møller-Plesset (MP) perturbation method. Finally, an overview of the basis sets used is also given, as well as the practical details of the computations performed.

II.3.1. The Hartree-Fock Theory

The Hartree-Fock theory is a variational[85] procedure in quantum mechanics, in which the n-electron wavefunction of a molecular system is represented as a single determinant wavefunction.[83,84] The variational concept is used to optimize the orbitals in Hartree-Fock wavefunctions. An individual molecular orbital (MO) Ψ_i can be expressed as a linear combination of a finite set of N one-electron functions known as basis functions, φ_1, φ_2, …, φ_N. When atomic orbitals of the constituent atoms are used as basis functions, one speaks of a linear combination of atomic orbital (LCAO). The individual orbitals Ψ_i are then written as:

$$\Psi_i = \sum_{\mu=1}^{N} c_{\mu i} \cdot \varphi_\mu \qquad \text{(II.3-2)}$$

where the MO expansion coefficients $c_{\mu i}$ are adjusted to minimize the expectation value of the total energy E. The final value of E will be as close to the exact energy as possible within the limitations of the Hartree-Fock theory, namely the limitations of a single determinant wavefunction and of the particular basis set chosen (see section II.3.3.).

The variational conditions lead to a set of algebraic equations for the $c_{\mu i}$, which were derived independently for closed-shell wavefunctions by Roothaan and Hall.[86,87] These Roothaan-Hall equations are:

$$\sum_{\nu=1}^{N} (F_{\mu\nu} - \varepsilon_i S_{\mu\nu}) \cdot c_{\mu i} = 0 \quad \mu = 1,2,...N \qquad \text{(II.3-3)}$$

where ε_i is the one-electron energy (or orbital energy) of molecular orbital Ψ_i, $S_{\mu\nu}$ are the elements of an N x N matrix, termed the overlap matrix, and $F_{\mu\nu}$ are the elements of another N x N matrix, the Fock matrix.

Since the Fock matrix $F_{\mu\nu}$ itself depends on the molecular orbital coefficients, a solution can only be achieved by an iterative process. The resulting molecular orbitals are derived from their own effective potential, and the method is therefore frequently called the self-consistent field (SCF) method.

For open-shell systems, the Roothaan-Hall equations need to be modified, which can be done in two ways. The first is described as spin restricted Hartree-Fock (RHF) theory.[88,89] In this approach, a single set of molecular orbitals is used, some of them being doubly occupied and some being singly occupied with electrons of either all α spin or all β spin. The corresponding n-electron wavefunction is a single determinant wavefunction, representing a pure doublet, triplet, and so on, spin state, that is, it is an eigenfunction of the spin operator S^2. This is an advantage since the exact wavefunctions are also pure spin states. On the other hand, the RHF method shows in some cases bad convergence and, as it requires electrons to remain paired, this method fails in cases where the electrons necessarily uncouple, such as bond breaking processes. A variant of RHF, ROHF (O stands for open-shell) has been developed to cope with this effect. The ROHF method utilizes indeed restricted type orbitals for doubly occupied orbitals but allows (for singly occupied orbitals) to have different spatial functions.

The second type of molecular orbital theory in common use for open-shell systems is the spin unrestricted Hartree-Fock (UHF) theory.[90] In this approach, the orbitals associated with α and β are treated independently. The two sets of molecular orbitals are defined by:

$$\Psi_i^{\alpha} = \sum_{\mu=1}^{N} c_{\mu i}^{\alpha} \cdot \varphi_{\mu}$$

$$\Psi_i^{\beta} = \sum_{\mu=1}^{N} c_{\mu i}^{\beta} \cdot \varphi_{\mu} \qquad \text{(II.3-4)}$$

The coefficients $c_{\mu i}$ are varied independently, leading to the UHF generalization of the Roothaan-Hall equations, the Pople-Nesbet equations:[90]

$$\sum_{\nu=1}^{N} (F_{\mu\nu}^{\alpha} - \varepsilon_i^{\alpha} S_{\mu\nu}) \cdot c_{\mu i}^{\alpha} = 0$$

$$\sum_{\nu=1}^{N} (F_{\mu\nu}^{\beta} - \varepsilon_i^{\beta} S_{\mu\nu}) \cdot c_{\mu i}^{\beta} = 0 \quad \mu = 1,2,...N \qquad \text{(II.3-5)}$$

The advantages of the UHF method are that it is capable of providing a qualitatively correct description of bond dissociation, and in practice, it converges more easily than the RHF method. However, the principal drawback is that the resulting wavefunction is no longer spin pure. An UHF calculation on a system with one extra α electron might lead to a

wavefunction that is a mixture of a doublet and a quartet, or higher components, rather than a pure doublet. The amount of spin contamination is reflected in the expectation value of the S^2 operator, $<S^2>$. For a pure doublet wavefunction, this amounts to 0.75 a.u., but it will be greater than 0.75 a.u. when quartet states are involved. If values of $<S^2>$ are much greater than 0.75 a.u., the result will be at least suspect. As a criterion for the acceptability of an UHF wavefunction, it has been proposed that the $<S^2>$ deviation should be less than 10 % or, better, below 5 %.[83,91,92] Whether these deviations are of the right order of magnitude or not is hard to say and this point is rarely discussed in literature.

The choice of the methods to be used depends on the open shell system under study. RHF is better defined theoretically, but UHF has a better convergence behavior, which makes it more useful in some cases.

The primary deficiency of Hartree-Fock theory is the inadequate treatment of the correlation between the motions of the electrons. While correlation of the motions of electrons with the same spin is partially taken into account by virtue of the determinant form of the wavefunctions, single configuration wavefunctions do not take into account the correlation between electrons with opposite spin. This means that the calculated HF energies will be greater than the exact values. By convention, the difference between the HF and exact (non relativistic, Born-Oppenheimer approximated) energies is called the correlation energy:

$$E(\text{exact}) = E(\text{Hartree-Fock}) + E(\text{correlation}) \qquad \text{(II.3-6)}$$

The neglect of correlation between electrons of opposite spins leads to a number of qualitative deficiencies in the description of electronic structures. One important consequence is that the closed-shell Hartree-Fock function often does not describe correctly molecular dissociation and the near degeneracy of two different states of the same symmetry.

Most of the different models[93] which incorporate electron correlation have a very high computational expense and are either non-variational or not size-consistent.[94] Among the most used ones are: full configuration interaction (CI),[38] limited configuration interaction (DCI and SDCI),[95-98] coupled pair theory (CCD),[99,100] multi-configuration SCF (MCSCF)[101] and complete active space SCF (CASSCF).[102] A different approach to the correlation problem is the Møller-Plesset (MP) perturbation theory, closely related to the many-body perturbation theory (MBPT). A brief description of this method, which has been used in this Thesis, is given in the following section.

II.3.2. Møller-Plesset Perturbation Theory

In perturbation theory,[103,104] the electronic Hamiltonian is divided into a zero order $\hat{H}_0$ and a perturbation $\hat{v}$, according to:

$$\hat{H} = \hat{H}_0 + \lambda\hat{V} \tag{II.3-7}$$

where λ is a dimensionless parameter that can take on values ranging continuously from 0 (no perturbation) to 1 (the full perturbation).

The assumption that $\hat{v}$ is a small perturbation to $\hat{H}_0$ suggests that the perturbed wave-function and energy can be expressed as a power series in $\hat{V}$. The usual way to do so is in terms of the parameter λ:

$$\begin{aligned} \Psi &= \Psi^{(0)} + \lambda\Psi^{(1)} + \lambda^2\Psi^{(2)} + \lambda^3\Psi^{(3)} + \ldots \\ E &= E^{(0)} + \lambda E^{(1)} + \lambda^2 E^{(2)} + \lambda^3 E^{(3)} + \ldots \end{aligned} \tag{II.3-8}$$

If the model system closely resembles the wavefunction of the system of interest, only a small amount of distortion is needed, but when the difference between the model system and the system of interest is large, higher order perturbation will be required.

Perturbation theory assumes that the reference wavefunction is close to the exact wavefunction determined from Hartree-Fock. Thus, if the HF wavefunction is not a suitable reference wavefunction, then MP calculations will break down and become unreliable.

The MP perturbation includes the sum of Fock operators as a starting point to calculate correlation energy, and thus the zero-order energy is simply the sum of the MOs. MP methods are labeled MP*n*, where *n* is the order of perturbation.

$$E(\text{MP0}) = E^{(0)} = \sum_{i}^{\text{occ.}} \varepsilon_i \tag{II.3-9}$$

The first-order wavefunction is the Hartree-Fock determinant, from which the first-order energy is simply the Hartree-Fock energy. The lowest order of perturbation that includes electron correlation is second order. That is, electron correlation only begins to be included at second order. The correlated energy is determined from exciting two electrons from occupied to virtual orbitals.

$$E(MP1) = E(MP0) + E^{(1)} = E(HF) \tag{II.3-10}$$

$$E(MP2) = E(MP0) + E^{(1)} + E^{(2)} \tag{II.3-11}$$

The MP3 method, which contains corrections to the energy to third order, may similarly be obtained from the first-order correction to the wavefunction. Fourth order (MP4) includes determinants that are singly, doubly, triply, and quadruply (SDTQ) excited.

MP2 calculations can be done reasonably rapidly because Equation (II.3-11) can be efficiently evaluated. The scaling behavior of the MP2 method is roughly N^5, where N is the number of basis functions. Analytical gradients and second derivatives are available for this level of theory, so it can conveniently be used to explore potential-energy surfaces. MP2, and indeed all orders of MP_n, are size-consistent, which is a particularly desirable feature.

II.3.3. Basis Sets

The basis sets are a set of mathematical functions from which the wavefunction is constructed. In the basis set limit (infinite expansion of basis functions), no restriction is made on the form of the MOs. In a practical way, *ab initio* methods require the introduction of finite basis sets. The accuracy of calculated properties is largely determined by the "quality" of the basis set as well as the type and number of basis functions.

To provide a basis set that is well defined for any nuclear configuration, it is convenient to define a particular set of basis functions associated with each nucleus, depending only on the charge of that nucleus. Such functions may have the symmetry properties of atomic orbitals, and may be classified as s, p, d, f, .. types according to their angular properties. The two types of atomic basis functions which are the most frequently used are the Slater-type orbitals (STOs) [105,106] and the cartesian Gaussian-type orbital (GTOs):[107,108]

$$\varphi_\mu^{STO} = N_S \cdot r^{n_S - 1} \cdot e^{-\xi r}$$

$$\varphi_\mu^{GTO} = N_g \cdot x^m \cdot y^n \cdot z^o \cdot e^{-\alpha r^2} \tag{II.3-12}$$

where ξ and α are constants determining the size of the orbitals, that is, the radial extent of the function.

In order to combine the best features of GTOs with those of STOs, a third possibility consists in using GTOs as building blocks to approximate STOs, which means that the basis functions are not individual GTOs, but linear combinations of GTOs fit to reproduce as accurately as possible a STO. Basis functions of this type are called contracted Gaussians.

Table II.3-1

The two basis sets used in this study and their description.

Basis	Type[a]	Scaling factor[b] (Method)
6-311++G(d)[109-111]	TSV d-polarization on heavy atoms diffuse functions on all atoms	0.9496[112] (MP2)
6-311++G(3df,3pd)[111,113]	TSV 1f- and 3d-polarization on heavy atoms 1d- and 3p-polarization on hydrogen atoms diffuse functions on all atoms	

[a] TSV (triple split-valence) indicates that the valence orbitals are split in three contracted basis functions. *n*d (or *n*f)-polarization on heavy atoms means the addition of *n* d (or *n* f) functions to polarize the p functions in 6-31G; *n*p (or *n*d)-polarization on hydrogen (and helium) atoms means the addition of *n* p or (*n* d) functions to polarize the s functions in 6-31G. "Diffuse functions on all atoms" (++) indicate that heavy atoms have been augmented with additional s and p functions having small exponents and hydrogen (and helium) atoms with additional s functions.

[b] The scaling factors is only indicated for the basis sets which has been used to perform frequency calculations.

Several contracted basis sets have been developed particularly by Pople and coworkers[114,115] (and are referred to as "Pople-style" basis sets). One of the most popular comes from Hehre, Stewart, and Pople[116] and is the STO-MG (for "Slater-Type Orbital approximated by M Gaussians) basis set, where M is the number of Gaussians used in the linear combination. It was discovered that the optimum combination of speed and accuracy (compared to calculations using GTOs or STOs) is achieved for M = 3. This STO-3G basis set is designed as a minimal basis set because there is only one basis function defined for each atomic orbital in an occupied shell (e.g. 1s or 2s or $2p_{x,y,z}$). It is far away from the basis set limit and some modifications of the basis can be achieved in order to improve it.[92] First, an expansion of the basis set can be performed by doubling all the basis functions, producing a double zeta (DZ) basis set. This expansion may be extended to triple zeta (TZ), quadruple zeta (QZ), etc. More-

over, a distinction can be made between core and valence orbitals as in general valence orbitals play a more intensive role from a chemical point of view. The core orbitals continue to be represented by a single contracted basis function, whereas valence orbitals are split into several ones. These basis sets are called split-valence (SV) basis sets. In addition, diffuse functions, which have very small orbital coefficients and thus are extended very far from the nucleus, may be added to basis functions (and are particularly indicated for calculations involving anions) as well as polarization functions, which possess a higher angular momentum than the valence orbitals (i.e. they have small orbital exponents). In this Thesis, three "Pople-style" basis sets have been employed and their features are given in Table II.3-1.

II.3.4. Computational Details

Quantum chemistry has been used in this work in parallel to experiment in order to shed more light on the gas-phase behavior of the species under study. This section summarizes the different theoretical approaches used and gives some computational details.

Several topics have been investigated in this Thesis, but they can roughly be divided into two groups according to the nature of the studied species: the investigation of the unimolecular reactivity of anions and that of neutrals. As underlined above, the accuracy of the calculations performed is partly related to the basis set chosen and the need for each system studied may vary. Anions, for instance, require the inclusion of polarization functions. Furthermore, it is also important to find a good balance between accuracy and time of calculation. Three types of calculations have been conducted: geometry optimizations, vibrational frequency analyses and single point energies. Geometry optimizations attempt to locate minima on the potential-energy surface, thereby predicting equilibrium structures of molecular systems. It also enables the localization of transition structures. To characterize these structures, vibrational frequencies are calculated and the number of imaginary frequencies is considered: zero corresponds to a minimum and one to a transition structure. Zero-point vibrational energy (ZPVE) corrections are also obtained from vibrational frequency calculations. The ZPVE values have to be scaled and each scaling factor (see Table II.3-1) was taken in literature according to the basis set used for the calculation.[117] Furthermore, single points energy (SPE) calculations have also been required for the investigation of the CR and NR processes. As it was underlined in the experiment part of this chapter, charge-transfer processes in keV collisions are vertical processes which conserve the geometry of the ionic precursor. The optimized geometries of this precursor were then used to obtain the energies of the corresponding ion and neutral.

All calculations presented in this work have been carried out using the GAUSSIAN 03 program package.[118] Calculations have been performed at the MP2/6-311++G(3df,3pd)//MP2/6-311++G(d) level of theory. This particular notation means that two different levels of theory have been used for the system and has to be read in the following manner: SPE//(geometry + frequency). It has indeed been shown that even quite small basis sets can give very good results for structure optimization.[92] A larger basis is then not necessary and saves computational time. As frequency calculations characterize the optimized structure, they have to be done at the same level of theory.

II.4. Thermochemistry

In gas-phase ion chemistry, thermochemical data are often important criteria for the analysis of the unimolecular decay of metastable ions. They may also enable a better understanding of the reactions taking, for instance, place in atmospheres. Thermochemistry of the organic compounds studied in this Thesis is often not known, but may be relevant in the context of this study. Thus, the heats of formation of anions and radicals investigated in this work have been evaluated by theory. The theoretical prediction of thermochemical quantities requires a very high accuracy of the energies obtained. For this reason, the CBS-Q model has been used. This method is described in this section as well as the different approaches employed to access standard heats of formation.

II.4.1. Complete Basis Set

A large variety of compound methods have been developed in an attempt to accurately model thermochemical quantities. The goal of these methods is to achieve high accuracy by combining the results of several different calculations as an approximation to a single, very high level computation which is much too expensive to be practical. In this Thesis, the CBS-Q method, which shows in general results in very good agreement with experiment,[119,120] has been used to compute heats of formation. A brief description of this method is made in this section.

The Complete Basis Set (CBS) methods were developed in 1996 by Ochterski, Petersson and Montgomery.[121] The name of these methods reflects the fundamental observation underlying these methods: the largest errors in *ab initio* thermochemical calculations result from

basis set truncations. The aim of these methods is to include a component which extrapolates from calculations using a finite basis set to the estimated complete basis set limit.

The extrapolation to the complete basis set limit is based upon the Møller-Plesset expansion (Equation (II.3-8)). Petersson and coworkers have extended the two-electron formulation of asymptotic convergence from Schwartz[122] to many-electrons atoms. They note that the second-order Møller-Plesset correlation energy for a many-electron system may be written as a sum of pair energies, each one describing the energetic effect of the electron correlation between that pair of electrons.[123-126] The total energy is computed from the results of a series of calculations. The component calculations are defined on the basis of the following principle. The successive contributions to the total energy decrease with order of perturbation theory, while the computational expense increases rapidly. The CBS models take advantage of these complementary trends by using smaller basis sets as the level of theory increases.

Different types of CBS methods exist according to the level of theory employed. In this work, the CBS-Q (Q stands for quadratic) method has been used to derivate thermochemical properties of anions, radicals and cations.

The CBS-Q model starts with a geometry optimization at the MP2 level of theory. The zero-point energy is computed at the HF level. An MP2 calculation with a large basis set (6-311+G(3d,2f,2df,2p)) is then performed as well as a CBS extrapolation to correct the energy through second order. Two additional calculations are used to approximate higher order contributions: MP4(SDQ)/6-31+G(d,p) (for the higher order correlation effects), and QCISD(T)/6-31+G(d')[127] for still higher order effects. This model also has empirical corrections for spin contamination and a size-consistent higher order correction. The zero-point energy obtained is scaled by a factor 0.91844.

As it will be outlined in the next section, standard heats of formation of ions and neutrals can be obtained via different theoretical methods. All those require nevertheless the same data which are the electronic energy at 0 K, the unscaled ZPE and the so-called term "thermal correction to enthalpy". All these data are available in the CBS-Q output file.

II.4.2. Standard Heats of Formation

Three principal methods can be used to determine the standard enthalpies of formation of a molecule. They proceed via formation reactions, atomization reactions, or isodesmic reactions. In this work, only the two latter methods have been used and a comparison of the results obtained is made for each studied systems.

Atomization Energies

The atomization energy $\Delta H°_{atom.,T}$ of a molecule M constituted, for instance, by three different types of atoms (A1, A2 and A3, with x_1, x_2 and x_3, respectively, for stoichiometric coefficients), is defined as the heat of reaction of the following reaction in the gas phase at a temperature T:

$$x_1A1 + x_2A2 + x_3A3 \xrightarrow{\Delta H°_{atom.,T}} M \qquad \text{(II.4-1)}$$

This atomization energy can be related either to the total electronic energies of the molecule M (including ZPE) and its constituting isolated atoms or to their heats of formation $\Delta_f H°_T$ through the two following equations:[128]

$$\Delta H°_{atom.,T}(M) = E_{tot,T}(M) - \sum_i x_i \cdot E_{tot,T}(Ai)$$
$$\Delta H°_{atom.,T}(M) = \Delta_f H°_T(M) - \sum_i x_i \cdot \Delta_f H°_T(Ai) \qquad \text{(II.4-2)}$$

where $E_{tot,T}(M)$ is the total energy of the molecule M at the temperature T and $E_{tot,T}(Ai)$ that of one of its constituting atom Ai (having the stoichiometric coefficient x_i).

In this Thesis, the molecules of interest are composed exclusively of hydrogen, carbon and oxygen. As the experimental enthalpies of formation of these atoms at 0 K are very accurately known (Table II.4-1), the enthalpy of formation of the molecule M at 0 K can therefore be deduced from Equations (II.4-2).

Furthermore, the total electronic energy $E_{el,T}$ of a compound M at a temperature T is related to its total electronic energy at 0 K by:

$$E_{el,T}(M) = E_{el,0K}(M) + \Delta H_T(M) \qquad \text{(II.4-3)}$$

where $\Delta H_T(M)$ is the heat capacity correction at the temperature T of the molecule M and corresponds to the difference between the enthalpy of the compound M at the temperature T and at 0 K ($H_T - H_{0K}$).

Combining Equations (II.4-2) and (II.4-3) for T = 298 K leads to the following expression of the heat of formation of the molecule M:

$$\Delta_f H^\circ_{298K}(\mathrm{M}) = \Delta_f H^\circ_{0K}(\mathrm{M}) + \Delta H_{298K}(\mathrm{M}) - \sum_i x_i \cdot \Delta H_T(\mathrm{Ai}) \qquad \text{(II.4-4)}$$

where ΔH_T(Ai) is the heat capacity correction at the temperature T of the atom Ai in its standard state and taken directly from literature (see Table II.4-1).

Table II.4-1

Enthalpies of formation $\Delta_f H^\circ_{0K}$ at 0 K for isolated gaseous atoms and ΔH_{298K} values of the elements in their standard states from experiment (in kcal/mol).[a]

	$\Delta_f H^\circ_{0K}$ (kcal/mol)	ΔH_{298K} (kcal/mol)
H	51.63 ± 0.001	1.01
C	169.98 ± 0.1	0.25
O	58.99 ± 0.02	1.04

[a] Values are taken from the JANAF tables.[129]

The common way to treat the heat capacity ΔH_T(M) of a molecule M at a temperature T consists in separating the partition function into a product of translational, rotational, vibrational, and electronic components. It can then be calculated by adding the different contributions of each parameter: vibrational frequencies for the vibrations in the harmonic approximation,[130] 3⁄2 RT for the translation, and 3⁄2 RT for the rotation (non linear molecules) in the classical approximation, and an additional RT term to convert energy to enthalpy. Since the expression of the electronic partition function does not contain a temperature-dependent term, the heat capacity correction due to electronic motion is zero.[130]

Practically, the heat capacity corrections at 298 K are obtained from the "thermal correction" term, appearing in the output file of a frequency calculation, from which the unscaled ZPE is subtracted.

If this method is used to obtain the heat of formation of an ion at a temperature different than 0 K, the electron which is involved in the reaction has to be taken into account.[131] In this context, two different postulates exist: the Ion Convention (IC) which ignores the thermochemistry of the electron and the Electron Convention (EC) which does not. The relation be-

tween the heats of formation of an anion M^- or a cation M^+, calculated with both conventions, is given in Equation (II.4-3).

$$\Delta_f H°_T(M^-)_{IC} = \Delta_f H°_T(M^-)_{EC} + \frac{5}{2}RT$$
$$\Delta_f H°_T(M^+)_{IC} = \Delta_f H°_T(M^+)_{EC} - \frac{5}{2}RT \qquad \text{(II.4-5)}$$

where 5/2RT refers to the heat capacity of an electron at 298 K, corresponding to that of an ideal gas following Boltzmann statistic.

Even though the use of the Electron Convention is more correct as it includes the thermochemistry of the electron, a large majority of the community dealing with such thermochemical quantities uses IC.[132] To avoid any confusion, the thermochemical properties of ions are accordingly given in the Ion Convention.

Bond-Separation Reactions

Bond separation (BS) reactions have been defined for the first time in 1970 by Hehre et *al.*[133] as: "the reaction in which all formal bonds between heavy (non hydrogen) atoms are separated into the simplest (or parent) molecules with the same type of bonds". Since reactants and products possess the same number and type of bonds, this type of reaction can be termed isodesmic. It is assumed that the similarity of bonding environment in both sides of an isodesmic reaction leads to the cancellation of the systematic errors in the *ab initio* MO calculations.[92,117,134] For this purpose, bond-separation reactions attract interest for the determination of accurate standard heats of formation.[135] Previous work has shown that thermochemical data derived from BS reactions are in very good agreement with experiment in the case of radicals (see, for instance, the work of Yu *et al.*[136] concerning the thermochemistry of the radicals of formic and acetic acids).[137] Figure II.4-1 gives the example of the BS reaction used to obtain the heat of formation of the methylcarbonate radical (Chapter III).

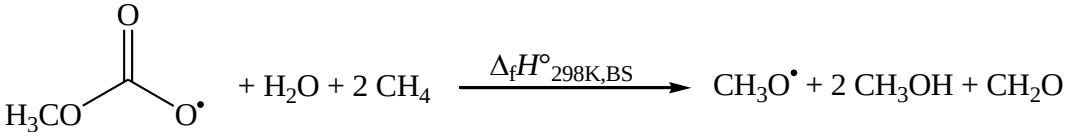

Figure II.4-1: The bond separation reaction used to calculate the standard heat of formation of the methylcarbonate radical (Chapter III).

The heat of reaction $\Delta_r H°_{298K,BS}$ of a BS reaction can be calculated using the total electronic energies (at 298 K and including ZPE) of the reactants and products of the reaction or using their standard heats of formation. Therefore, the heat of formation $\Delta_f H°_{298K,BS}$ of a neutral radical $M^{\bullet}$ can easily be deduced from the calculated total electronic energies of the species involved in the reaction and from the well defined experimental standard heats of formation of the other molecules taking part to the reaction. Those molecules are listed in Table II.4-2 as well as their thermochemical quantities.

From the heats of formation of radicals, those of anions are obtained, using the following reaction:

$$M^{\bullet} + e^{-} \xrightarrow{EA(M^{\bullet})} M^{-} \qquad \text{(II.4-6)}$$

where $EA(M^{\bullet})$ is the adiabatic electronic affinity of the radical $M^{\bullet}$ at 0 K.

Table II.4-2

Theoretical and experimental data of the molecules involved in the BS reactions used in this work.

	$E(CBS\text{-}Q)_{0K}$ (H)	ZPE (H)[a]	Thermal Correction to Enthalpy (H)	$\Delta_f H°_{298K,exp}$[b] (kcal/mol)
CH_4	-40.409587	0.047506	0.051303	-17.8 ± 0.1
C_2H_6	-79.629747	0.079346	0.083695	-20.1 ± 0.2
H_2O	-76.336506	0.023058	0.026835	-57.8 ± 0.1[c]
CH_3OH	-115.53829	0.055148	0.059342	-48.0 ± 0.1
$CH_3O^{\bullet}$	-114.872223	0.040044	0.043946	3.1 ± 1.0
CH_2O	-114.342754	0.029001	0.032799	-26.0 ± 0.1

[a] ZPE unscaled.

[b] If not stated otherwise, taken from Gurvich *et al.*[138]

[c] Taken from Cox *et al.* [139]

The electron affinity of the neutral $M^{\bullet}$ is obtained from the difference between the total electronic energies of $M^{\bullet}$ and M^{-} at 0 K. Using the heat capacities corrections $\Delta H°_{298K}$ of $M^{\bullet}$ and M^{-}, and the heat of formation of the $M^{\bullet}$ obtained by the BS reaction, the standard heat of formation of the anion is derived in kcal/mol using Equation (II.4-7).

$$\Delta_f H^\circ_{298K}(M^-) = \Delta_f H^\circ_{298K}(M^\bullet) + \Delta H_{298K}(M^\bullet) - \Delta H_{298K}(M^-) + EA(M^\bullet) \qquad \text{(II.4-7)}$$

The deviation between experimental thermochemical values and those determined by BS method is mostly due to the uncertainty of the experimental enthalpies of formation used. The error bar is within 0.5 kcal/mol for all species unless for the $CH_3O^\bullet$ radical, whose heat of formation is known with 1 kcal/mol uncertainty (Table II.4-2). The reliability of the heats of formation obtained with this method will be discussed further and the values will be compared to those obtained by the atomization energy method.

II.5. References and Notes

1. Forst, W., *Theory of Unimolecular Reactions*; Academic Press: New York, 1973.

2. Steinfeld, J. I.; Francisco, J. S.; Hase, W. L., *Chemical Kinetics and Dynamics*; Prentice Hall: New Jersey, 1989.

3. Lorquet, J. C., *Mass Spectrom. Rev.* **1994**, *13*, 233.

4. Rosenstock, H. M.; Wallenstein, M. B.; Wahrhaftig, A. L.; Eyring, H., *Proc. Nat. Acad. Sci.* **1952**, *38*, 667.

5. Rice, O. K.; Ramsberger, H. C., *J. Am. Chem. Soc.* **1927**, *49*, 1617.

6. Rice, O. K.; Ramsberger, H. C., *J. Am. Chem. Soc.* **1928**, *50*, 617.

7. Kassel, L. S., *J. Phys. Chem.* **1928**, *32*, 225.

8. Marcus, R. A.; Rice, O. K., *J. Phys. Colloid Chem.* **1951**, *55*, 894.

9. Marcus, R. A., *J. Chem. Phys.* **1952**, *20*, 359.

10. Evans, M. G.; Polanyi, M., *Trans. Faraday Soc.* **1935**, *31*, 875.

11. Eyring, H., *J. Chem. Phys.* **1935**, *3*, 107.

12. Baer, T.; Mayer, P. M., *J. Am. Chem. Soc.* **1997**, *8*, 103.

13. Tajima, S.; Sekiguchi, O., *J. Mass Spectrom. Soc. Jap.* **1996**, *44*, 133.

14. Aschi, M.; Attina, M.; D'Arcangelo, G., *Chem. Phys. Lett.* **1998**, *283*, 307.

15. Audier, H. E., *Analusis* **1993**, *21*, 15S.

16. Bowen, R. D., *Acc. Chem. Res.* **1991**, *24*, 364.

17. Hammerum, S., *J. Chem. Soc., Chem. Commun.* **1988**, 858.

18. Holmes, J. L.; Lossing, F. P.; Terlouw, J. K.; Burgers, P. C., *J. Am. Chem. Soc.* **1982**, *104*, 2931.

19. Longevialle, P., *Mass Spectrom. Rev.* **1992**, *11*, 157.

20. Longevialle, P., *Adv. Mass Spectrom.* **1995**, *13*, 347.

21. McAdoo, D. J., *Mass Spectrom. Rev.* **1988**, *7*, 363.

22. Terlouw, J. K.; Heerma, W.; Dijkstra, G.; Holmes, J. L.; Burgers, P. C., *Int. J. Mass Spectrom. Ion Phys.* **1983**, *47*, 147.

23. Heinrich, N.; Schwarz, H. in *Ion and Cluster-Ion Spectroscopy and Structure*; Maier, J. P., Ed.; Elsevier: Amsterdam, 1989, p. 329.

24. Among numerous experimental works leading to the observation of ion-neutral complexes, one can cite: (a) Grandinetti, F.; Hrušák, J.; Schröder, D.; Karrass, S.; Schwarz, H., *J. Am. Chem. Soc.* **1992**, *114*, 2806. (b) Halim, H.; Ciommer, B.; Schwarz, H., *Angew. Chem.* **1982**, *94*, 547. (c) Hudson, C. E.; McAdoo, D. J., *J. Am. Soc. Mass Spectrom.* **2007**, *18*, 270.

25. Srinivas, R.; Sülzle, D.; Weiske, T.; Schwarz, H., *Int. J. Mass Spectrom. Ion Processes* **1991**, *107*, 368.

26. Srinivas, R.; Sülzle, D.; Koch, W.; DePuy, C. H.; Schwarz, H., *J. Am. Chem. Soc.* **1991**, *113*, 5970.

27. Schalley, C. A.; Schröder, D.; Schwarz, H., *Int. J. Mass Spectrom. Ion Processes* **1996**, *153*, 173.

28. Levsen, K., *Fundamental Aspects of Organic Mass Spectrometry*; VCH Publishers: Weinheim, 1978.

29. McLafferty, F. W., *Tandem Mass Spectrometry*; Wiley: New York, 1983.

30. McLuckey, S. A.; Wells, J. M., *Chem. Rev.* **2001**, *101*, 571.

31. Busch, K. L.; Glish, G. L.; McLuckey, S. A., *Mass Spectrometry/Mass Spectrometry: Techniques and Applications of Tandem Mass Spectrometry*; VCH Publishers: New York, 1988.

32. Vestal, M. L., *Chem. Rev.* **2001**, *101*, 361.

33. Kumar, A.; Roy, B. N., *Phys. Lett. A* **1978**, *66*, 362.

34. Chapman, J. R., *Practical Organic Mass Spectrometry*; Wiley: New York, 1985.

35. McDowell, C. A.; Warren, J. W., *Discuss. Faraday Soc.* **1951**, *10*, 53.

36. Forbes, R. A.; Tews, E. C.; Freiser, B. S.; Wise, M. B.; Perone, S. P., *Anal. Chem.* **1986**, *58*, 684.

37. Forbes, R. A.; Tews, E. C.; Huang, Y.; Freiser, B. S.; Perone, S. P., *Anal. Chem.* **1987**, *59*, 1937.

38. Harrison, R. J.; Handy, N. C., *Chem. Phys. Lett.* **1983**, *95*, 386.

39. Munson, M. S. B.; Field, F. H., *J. Am. Chem. Soc.* **1966**, *88*, 2621.

40. Richter, W. J.; Schwarz, H., *Angew. Chem., Int. Ed. Engl.* **1978**, *17*, 424.

41. Fenselau, C.; Cotter, R. J., *Chem. Rev.* **1987**, *87*, 501.

42. Froelicher, S. W.; Freiser, B. S.; Squires, R. R., *J. Am. Chem. Soc.* **1986**, *108*, 2853.

43. Graul, S. T.; Squires, R. R., *J. Am. Chem. Soc.* **1988**, *110*, 607.

44. Ingólfsson, O.; Weik, F.; Illenberger, E., *Int. J. Mass Spectrom. Ion Processes* **1996**, *155*, 1.

45. Schröder, D.; Schwarz, H., *Int. J. Mass Spectrom. Ion Processes* **1995**, *146/147*, 183.

46. Hunt, D. F.; Stafford, G. C.; Crow, F. W.; Russel, J. W., *Anal. Chem.* **1976**, *48*, 2098.

47. Cooks, R. G.; Beynon, J. H.; Caprioli, R. M.; Lester, G. R., *Metastable Ions*; Elsevier: Amsterdam, 1973.

48. Postma, R., Ph. D. Thesis, Rijksuniversiteit, Utrecht (NL), 1985.

49. Cooks, R. G., *Collision Spectroscopy*; Plenum Press: New York, 1978.

50. Levsen, K.; Schwarz, H., *Mass Spectrom. Rev.* **1983**, *2*, 77.

51. Shukla, A. K.; Futrell, J. H., *J. Mass Spectrom.* **2000**, *35*, 1069.

52. Cooks, R. G., *J. Mass Spectrom.* **1995**, *30*, 1215.

53. Holmes, J. L., *Org. Mass Spectrom.* **1985**, *20*, 169.

54. Proctor, C. J.; McLafferty, F. W., *Org. Mass Spectrom.* **1983**, *18*, 193.

55. Bowie, J. H.; Blumenthal, T., *J. Am. Chem. Soc.* **1975**, *97*, 2959.

56. Bowie, J. H.; Blumenthal, T., *Aust. J. Chem.* **1976**, *29*, 115.

57. Villeneuve, S.; Burgers, P. C., *Org. Mass Spectrom.* **1986**, *21*, 733.

58. Born, M.; Oppenheimer, J. R., *Ann. Phys.* **1927**, *84*, 457.

59. On the contrary, an adiabatic charge transfer is controlled by thermodynamics, which means that the process is not vertical but leads to the most favorable structure of the resulting species from a thermodynamic point of view. A large difference in geometry between the precursor and the resulting ion may thus be observed.

60. McMahon, A. W.; Chowdhury, S. K.; Harrison, A. G., *Org. Mass Spectrom.* **1989**, *24*, 620.

61. Bowie, J. H.; Blumenthal, T., *J. Am. Chem. Soc.* **1975**, *97*, 2959.

62. Bursey, M. M.; Harvan, D. J.; Parker, C. E.; Pedersen, L. G.; Hass, J. R., *J. Am. Chem. Soc.* **1979**, *101*, 5489.

63. Holmes, J. L., *Mass Spectrom. Rev.* **1989**, *8*, 513.

64. McLafferty, F. W., *Science* **1990**, *247*, 925.

65. Polce, M. J.; Beranová, Š.; Nold, M. J.; Wesdemiotis, C., *J. Mass Spectrom.* **1996**, *31*, 1073.

66. Schalley, C. A.; Hornung, G.; Schröder, D.; Schwarz, H., *Chem. Soc. Rev.* **1998**, *27*, 91.

67. Terlouw, J. K.; Schwarz, H., *Angew. Chem., Int. Ed. Engl.* **1987**, *26*, 805.

68. Zagorevskii, D. V.; Holmes, J. L., *Mass Spectrom. Rev.* **1994**, *13*, 133.

69. Tureček, F. in *Modern Mass Spectrometry*; Schalley, C. A., Ed.; Springer Berlin/Heidelberg, 2003; Vol. 225, p. 77.

70. Danis, P. O.; Feng, R.; McLafferty, F. W., *Anal. Chem.* **1986**, *58*, 348.

71. Danis, P. O.; Feng, R.; McLafferty, F. W., *Anal. Chem.* **1986**, *58*, 355.

72. Schalley, C. A.; Hornung, G.; Schröder, D.; Schwarz, H., *Int. J. Mass Spectrom. Ion Processes* **1998**, *172/173*, 181.

73. Roithová, J.; Schröder, D.; Schwarz, H., *Angew. Chem., Int. Ed. Engl.* **2005**, *44*, 3092.

74. Schröder, D. in *Encyclopedia of Mass Spectrometry*; Armentrout, P. B., Ed.; Elsevier: Amsterdam, 2003; Vol. 1, p. 521.

75. Bowen, R. D.; Williams, D. H.; Schwarz, H., *Angew. Chem., Int. Ed. Engl.* **1979**, *18*, 451.

76. Holmes, J. L.; Terlouw, J. K., *Org. Mass Spectrom.* **1980**, *15*, 383.

77. Laskin, J.; Lifshitz, C., *J. Mass Spectrom.* **2001**, *36*, 459.

78. Brenton, A. G.; Morgan, R. P.; Beynon, J. H., *Ann. Rev. Phys. Chem.* **1979**, *30*, 51.

79. Boyd, R. K.; Beynon, J. H., *Int. J. Mass Spectrom. Ion Phys.* **1977**, *23*, 163.

80. Terwilliger, D. T.; Beynon, J. H.; Cooks, R. G., *Proc. R. Soc. London, Ser. A* **1974**, *341*, 135.

81. Hipple, J. A.; Fox, R. E.; Condon, E. U., *Phys. Rev.* **1946**, *69*, 347.

82. Atkins, P. W., *Molecular Quantum Mechanics*; Oxford University Press: New York, 1983.

83. Levine, I. N., *Quantum Chemistry*; Prentice Hall: New York, 1991.

84. Schrödinger, E., *Ann. Phys.* **1926**, *79*, 361.

85. The electronic energy related to a variational theory corresponds to an upper bound value of the exact energy as derived from the exact solution of the Schrödinger equation. Variational methods have the great advantage of having a criterion from which the quality of the theoretical model can be judged.

86. Roothaan, C. C., *Rev. Mod. Phys.* **1951**, *23*, 69.

87. Hall, G. G., *Proc. R. Soc. London, Ser. A* **1951**, *A205*, 541.

88. Binkley, J. S.; Pople, J. A.; Dobosh, P. A., *Mol. Phys.* **1974**, *28*, 1423.

89. Roothaan, C. C., *Rev. Mod. Phys.* **1960**, *32*, 179.

90. Pople, J. A.; Nesbet, R. K., *J. Chem. Phys.* **1954**, *22*, 571.

91. Cramer, C. J., *Essentials of Computational Chemistry*; John Wiley & Sons Ltd: Chichester, 2002.

92. Hehre, W. J.; Radom, L.; Schleyer, P. v. R.; Pople, J. A., *Ab lnitio Molecular Orbital Theory*; Wiley: New York, 1986.

93. Schleyer, P. v. R.; Allinger, N. L.; Clark, T.; Gasteiger, J.; Kollmann, P. A.; Schafer III, H. F.; Schreiner, P. R., *The Encyclopedia of Computational Chemistry*; Wiley and Sons Ltd: Chichester, 1998.

94. A size consistent method gives additive results when applied to an assembly of isolated molecules. If the model is not size consistent, comparison of properties or energies of molecules of different sizes is inadequate.

95. Davidson, E. R.; Silver, D. W., *Chem. Phys. Lett.* **1977**, *52*, 403.

96. Langhoff, S. R.; Davidson, E. R., *Int. J. Quantum Chem.* **1974**, *8*, 61.

97. Pople, J. A.; Seeger, R.; Krishnan, R., *Int. J. Quantum Chem.* **1977**, *11*, 149.

98. Siegbahn, P. E. M., *Chem. Phys. Lett.* **1978**, *55*, 386.

99. Sinanoglu, O., *J. Chem. Phys.* **1962**, *36*, 706.

100. Sinanoglu, O., *Adv. Chem. Phys.* **1969**, *14*, 237.

101. Wahl, A. C.; Das, G., *Adv. Quantum Chem.* **1970**, *5*, 261.

102. Siegbahn, P. E. M.; Almlöf, J.; Heiberg, A.; Roos, B. O., *J. Chem. Phys.* **1981**, *74*, 2384.

103. Møller, C.; Plesset, M. S., *Phys. Rev.* **1934**, *46*, 618.

104. Pople, J. A.; Krishnan, R.; Schlegel, H. B.; Binkley, J. S., *Int. J. Quantum Chem.* **1979**, *325*.

105. Slater, J. C., *Phys. Rev.* **1929**, *34*, 1293.

106. Slater, J. C., *Phys. Rev.* **1930**, *36*, 57.

107. Boys, S. F., *Proc. R. Soc. London, Ser. A* **1942**, *A200*, 542.

108. Shavitt, I. in *Methods in Computational Physics*; Alder, B., Fernbach, S., Rotenberg, M., Eds.; Academic Press: New York, 1963; Vol. 2, p. 1.

109. Hariharan, P. C.; Pople, J. A., *Theor. Chim. Acta* **1973**, *28*, 213.

110. Krishnan, R.; Binkley, J. S.; Seeger, R.; Pople, J. A., *J. Chem. Phys.* **1980**, *72*, 650.

111. Clark, T.; Chandrasekhar, J.; Spitznagel, G. W.; Schleyer, P. v. R., *J. Comput. Chem.* **1983**, *4*, 294.

112. Scott, A. P.; Radom, L., *J. Phys. Chem.* **1996**, *100*, 16502.

113. Frisch, M. J.; Pople, J. A.; Binkley, J. S., *J. Chem. Phys.* **1984**, *80*, 3269.

114. Binkley, J. S.; Pople, J. A.; Hehre, W. J., *J. Am. Chem. Soc.* **1980**, *102*, 939.

115. Hehre, W. J.; Ditchfield, R.; Pople, J. A., *J. Chem. Phys.* **1972**, *56*, 2257.

116. Hehre, W. J.; Stewart, R. F.; Pople, J. A., *J. Chem. Phys.* **1969**, *51*, 2657.

117. Foresman, J. B.; Frisch, A., *Exploring Chemistry with Electronic Structure Methods*; Second Edition; Gaussian Inc.: Pittsburgh, 1996.

118. GAUSSIAN 03, Revision C.02: Frisch, M. J.; Trucks, G. W.; Schlegel, H. B.; Scuseria, G. E.; Robb, M. A.; Cheeseman, J. R.; Montgomery, J., J. A. ; Vreven, T.; Kudin, K. N. B., J. C. ; Millam, J. M.; Iyengar, S. S.; Tomasi, J.; Barone, V.; Mennucci, B.; Cossi, M.; Scalmani, G.; Rega, N.; Petersson, G. A.; Nakatsuji, H.; Hada, M.; Ehara, M.; Toyota, K.; Fukuda, R.; Hasegawa, J.; Ishida, M.; Nakajima, T.; Honda, Y.; Kitao, O.; Nakai, H.; Klene, M.; Li, X.; Knox, J. E.; Hratchian, H. P.; Cross, J. B.; Bakken, V.; Adamo, C.; Jaramillo, J.; Gomperts, R.; Stratmann, R. E.; Yazyev, O.; Austin, A. J.; Cammi, R.; Pomelli, C.; Ochterski, J. W.; Ayala, P. Y.; Morokuma, K.; Voth, G. A.; Salvador, P.; Dannenberg, J. J.; Zakrzewski, V. G.; Dapprich, S.; Daniels, A. D.; Strain, M. C.; Farkas, O.; Malick, D. K.; Rabuck, A. D.; Raghavachari, K.; Foresman, J. B.; Ortiz, J. V.; Cui, Q.; Baboul, A. G.; Clifford, S.; Cioslowski, J.; Stefanov, B. B.; Liu, G.; Liashenko, A.; Piskorz, P.; Komaromi, I.; Martin, R. L.; Fox, D. J.; Keith, T.; Al-Laham, M. A.; Peng, C. Y.; Nanayakkara, A.; Challacombe, M.; Gill, P. M. W.; Johnson, B.; Chen, W.; Wong, M. W.; Gonzalez, C.; Pople, J. A., GAUSSIAN Inc.: Wallingford CT, 2004.

119. Curtiss, L. A.; Raghavachari, K.; Redfern, P. C.; Stefanov, B. B., *J. Chem. Phys.* **1998**, *108*, 692.

120. Harvey, Z., Ph. D. Thesis, La Trobe University, Bundoora (AU), 2006.

121. Ochterski, J. W.; Petersson, G. A.; Montgomery, J. J. A., *J. Chem. Phys.* **1996**, *104*, 2598.

122. Schwartz, C., *Phys. Rev.* **1962**, *126*, 1025.

123. Nyden, M. R.; Petersson, G. A., *J. Chem. Phys.* **1981**, *75*, 1843.

124. Petersson, G. A.; Al-Laham, M. A., *J. Chem. Phys.* **1991**, *94*, 6081.

125. Petersson, G. A.; Nyden, M. R., *J. Chem. Phys.* **1981**, *75*, 3423.

126. Petersson, G. A.; Yee, A. K.; Bennet, A., *J. Chem. Phys.* **1985**, *83*, 5105.

127. Petersson, G. A.; Tensfeldt, T. G.; Montgomery, J. J. A., *J. Chem. Phys.* **1991**, *94*, 6091.

128. Pople, J. A.; Luke, B. T.; Frisch, M. J.; Binkley, J. S., *J. Phys. Chem.* **1985**, *89*, 2198.

129. Chase, M. W. J.; Davies, C. A.; Downey Jr., J. R.; Frurip, D. J.; MacDonald, R. A.; Syverud, A. N., *J. Phys. Chem. Ref. Data* **1985**, *No 1*, (Suppl.14).

130. Lewis, G. N.; Randall, M., *Thermodynamics*; Second Edition, revised by K. S. Pitzer and L. Brewer; Mc Graw-Hill: New York, 1961.

131. Ervin, K. M., *Chem. Rev.* **2001**, *101*, 391.

132. Linstrom, P. J.; Mallard, W. G., Eds., NIST Chemistry WebBook, National Institute of Standards and Technology, Gaithersburg MD, 20899, June 2005 (http://webbook.nist.gov).

133. Hehre, W. J.; Ditchfield, R.; Radom, L.; Pople, J. A., *J. Am. Chem. Soc.* **1970**, *92*, 4796.

134. Ponomarev, D. A.; Takhistov, V. V., *J. Chem. Educ.* **1997**, *74*, 201.

135. Raghavachari, K.; Stefanov, B. B.; Curtiss, L. A., *J. Chem. Phys.* **1997**, *106*, 6754.

136. Yu, D.; Rauk, A.; Armstrong, D. A., *J. Chem. Soc., Perkin Trans. 2* **1994**, 2207.

137. Henry, D. J.; Radom, L. in *Quantum-Mechanical Prediction of Thermochemical Data.*; Cioslowski, J., Ed.; Kluwer Academic: Dordrecht, 2001, p. 161.

138. Gurvich, L. V.; Veyts, I. V.; Alcock, C. B., *Thermodynamic Properties of Individual Substances*; Fouth Edition; Hemisphere Pub. Co.: New York, 1989.

139. Cox, J. D.; Wagman, D. D.; Medvedev, V. A., *CODATA Key Values for Thermodynamics.*; Hemisphere: New York, 1989.

III. Gas-Phase Chemistry of Alkylcarbonate Ions and Radicals

III.1. Introduction

The first project presented in this Thesis concerns the gas-phase behavior of anionic and neutral alkylcarbonate species $ROCOO^{-/\bullet}$ with R = H, CH_3, C_2H_5, *i*-C_3H_7, and *t*-C_4H_9 (Chart III.1-1). The stability and the dissociation behavior of these species have not been explored in detail so far, and only few experimental studies of their gas-phase chemistry have been reported.[1,2] These species may nevertheless be of some relevance in the context of the study of Mars as their presence has been recently detected in martian dust.[3]

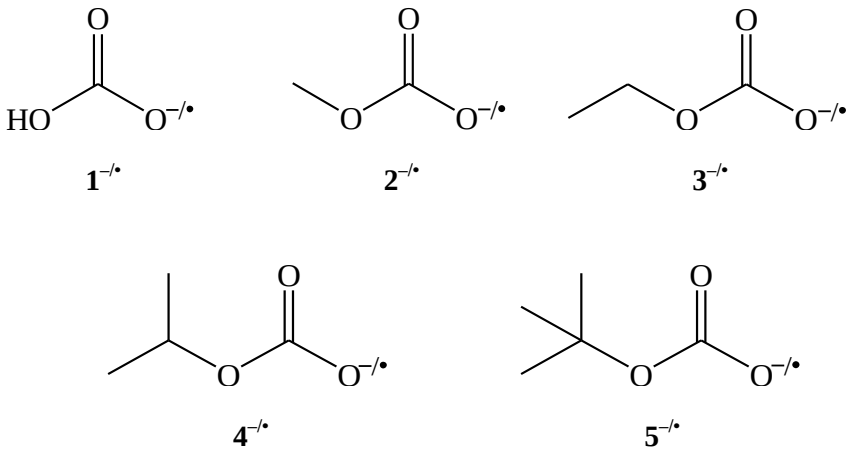

1$^{-/\bullet}$ **2**$^{-/\bullet}$ **3**$^{-/\bullet}$

4$^{-/\bullet}$ **5**$^{-/\bullet}$

Chart III.1-1

The alkylcarbonate anions $ROCOO^-$ were generated by chemical ionization and the mass-selected ions were investigated by metastable ion (MI) and collisional activation (CA) experiments. The chemistry of the neutral radicals $ROCOO^{\bullet}$ was studied by different variants of mass spectrometric techniques involving electron-transfer from the corresponding anions, i.e. charge-reversal (CR), neutralization-reionization (NR), and the neutral and ion decomposition difference (NIDD) method.[4] Further, the geometries, relative energies, and standard heats of

formation of the $ROCOO^{-/\bullet}$ compounds have been determined by appropriate *ab initio* methods for R = H, CH_3, C_2H_5, *i*-C_3H_7, and *t*-C_4H_9.

III.2. Structures and Energetics

III.2.1. Alkylcarbonate Anions and Radicals

With regard to the structures of the $ROCOO^{-/\bullet}$ compounds in the charge states considered, we decided to perform geometry optimizations at a level of theory which can describe the anions as well as neutral radicals reasonably well. This particularly requires the inclusion of diffuse functions in the basis-set for the description of anions. As the systems are not too demanding in calculation time, the basis set 6-311++G(d) was chosen in combination with the MP2 method.

Not unexpectedly, some larger structural differences exist between the corresponding pairs of alkylcarbonate anions and radicals. Thus, while the $O_{(1)}$-$C_{(1)}$ and $O_{(2)}$-$C_{(1)}$ bonds are of similar length for all $ROCOO^-$ ions (the differences are in the order of 0.01 Å), the $O_{(1)}$-$C_{(1)}$ bond is clearly longer than the $O_{(2)}$-$C_{(1)}$ bond for $ROCOO^\bullet$ neutrals (by more than 0.1 Å for all R substituents). The symmetry of the carboxyl group of the anions can easily be explained by the delocalization of the negative charge on the whole carboxyl group, which induces a slight increase of both bond lengths ($O_{(1)}$-$C_{(1)}$ and $O_{(2)}$-$C_{(1)}$) compared for instance to those of monoalkylcarbonates.[8] In contrast, when the unpaired electron of the radicals is localized at the $O_{(1)}$ atom, only the $O_{(1)}$-$C_{(1)}$ bond length is elongated, whereas the $O_{(2)}$-$C_{(1)}$ one has a length typical of that of a double bond.[9] Further, the $O_{(3)}$-$C_{(1)}$ bond length also differs by more than 0.1 Å between alkylcarbonate anions and radicals, i.e. about 1.33 Å for the radicals compared to ca. 1.47 Å for the anions. We attribute this elongation to the negatively charged carboxyl group directly bonded to the atom $O_{(3)}$ and which may induce a repulsive effect on the other part of the anions. Concerning the angles of anions and radicals, the carboxyl group of the anions is on average 12 ° more opened ($O_{(2)}C_{(1)}O_{(1)}$ angle, ca. 133 °) as compared with the radicals (ca. 121 °); this is again attributed to the charge delocalization in the anions. Consistent with this line of reasoning, except for R = H, the $RO_{(3)}C_{(1)}$ angle is found to vary very little between alkylcarbonate anions and radicals (ca. 1 °).

The substituent effects on the geometries of alkylcarbonate radicals and anions are not very much pronounced but some small, expected differences can nevertheless be observed in the immediate vicinity of the substituent. Thus, differences of a few thousandths of Å are observed for the $O_{(1)}C_{(1)}$, $O_{(2)}C_{(1)}$, and $O_{(3)}C_{(1)}$ bond lengths of both the anions and radicals for

all systems studied. Not surprisingly, the $O_{(3)}$-R bond length is much smaller for R = H compared to the alkyl substituents and then smoothly increases with the size of the substituent, i.e. from 0.966 Å for $HOCOO^{\bullet}$ to 1.444 Å for $CH_3OCOO^{\bullet}$ and 1.481 Å for $t\text{-}C_4H_9OCOO^{\bullet}$ in the case of the radicals and from 0.964 Å for $HOCOO^{-}$ to 1.410 Å for CH_3OCOO^{-} and 1.427 Å for $t\text{-}C_4H_9OCOO^{-}$ for the anions.

Table III.2-1

Selected bond lengths (in Å) and bond angles (in degree) of $ROCOO^{-/\bullet}$ species (R = H - $t\text{-}C_4H_9$) according to MP2/6-311++G(d) calculations.

	Calculated structural parameters (Å and °)						
	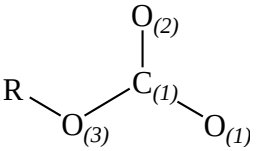						
	$O_{(1)}C_{(1)}$	$O_{(2)}C_{(1)}$	$O_{(3)}C_{(1)}$	$O_{(3)}R$	$O_{(2)}C_{(1)}O_{(1)}$	$O_{(3)}C_{(1)}O_{(2)}$	$RO_{(3)}C_{(1)}$
Neutral Radicals							
1$^{\bullet}$	1.331	1.204	1.337	0.966	121.9	128.4	107.6
2$^{\bullet}$	1.337	1.206	1.330	1.444	121.6	128.9	113.9
3$^{\bullet}$	1.338	1.206	1.329	1.455	121.4	129.1	114.3
4$^{\bullet}$	1.341	1.207	1.326	1.470	120.7	130.6	118.3
5$^{\bullet}$	1.342	1.207	1.326	1.481	120.5	131.0	119.6
Anions							
1^{-}[a]	1.255	1.237	1.448	0.964	132.8	113.4	102.9
2^{-}	1.248	1.239	1.460	1.410	133.2	115.0	114.3
3^{-}	1.248	1.237	1.468	1.413	133.3	115.2	115.4
4^{-}	1.247	1.237	1.471	1.416	133.4	115.2	116.1
5^{-}	1.247	1.236	1.474	1.427	133.2	116.1	120.5

[a] The geometry of the hydrogencarbonate ion has already been the subject of several works, see for instance Squires[5] and Alexeev.[6,7]

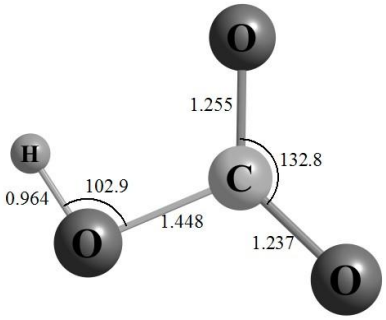
O
1.255
H
132.8
C
0.964
102.9
1.448
1.237
O
O

1⁻

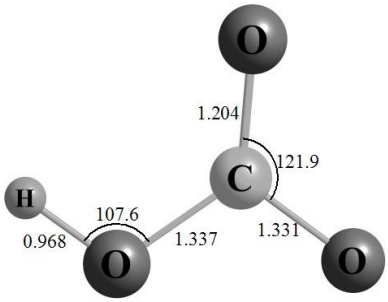
O
1.204
121.9
C
H
107.6
0.968
1.337
1.331
O
O

1•

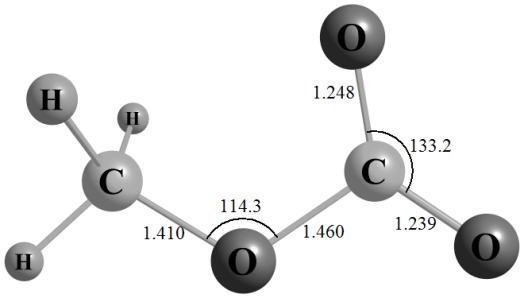
O
1.248
H
H
133.2
C
C
H
114.3
1.410
1.460
1.239
H
O
O

2⁻

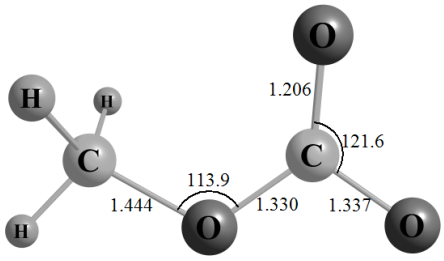
O
1.206
H
H
C
121.6
C
113.9
1.444
1.330
1.337
H
O
O

2•

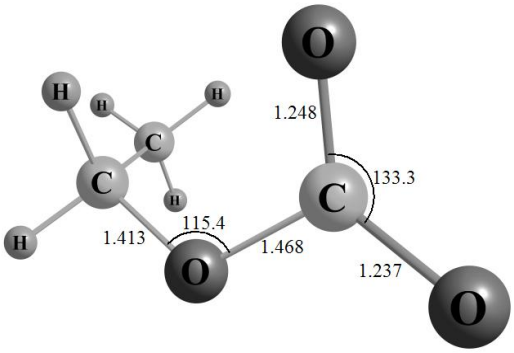
O
H
1.248
H
H
C
133.3
C
C
H
115.4
1.413
1.468
1.237
H
O
O

3⁻

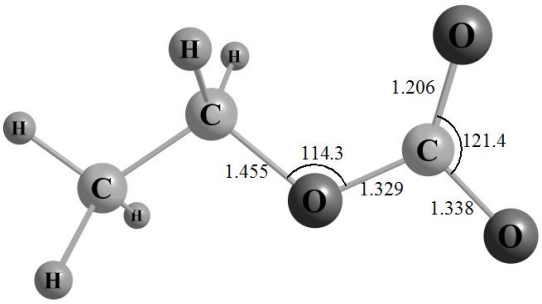
O
H
H
1.206
C
H
121.4
C
114.3
1.455
1.329
C
1.338
H
O
O

3•

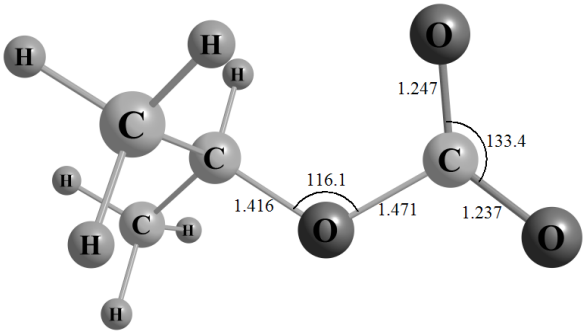
O
H
H
1.247
H
C
133.4
C
C
H
116.1
1.416
1.471
1.237
C
H
O
O
H

4⁻

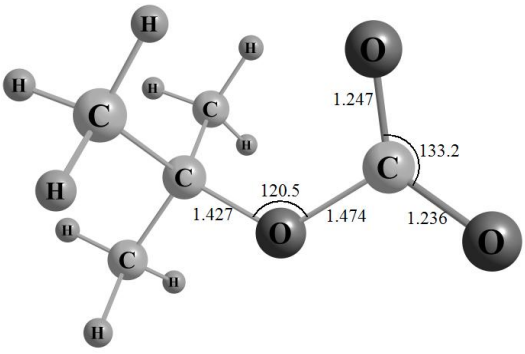
H
O
H
1.247
C
H
C
H
133.2
C
C
H
120.5
1.427
1.474
1.236
C
H
O
O
H

4•

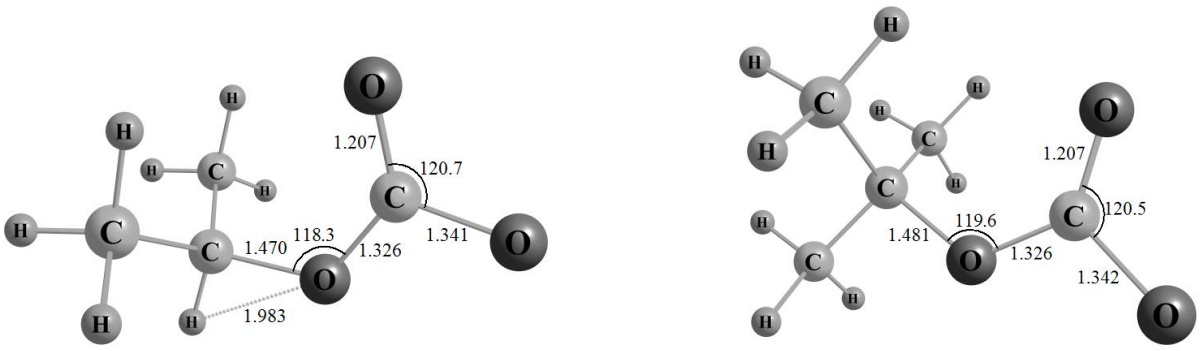

$\mathbf{5}^-$ $\mathbf{5}^{\bullet}$

Chart III.2-1: Optimized geometries of alkyloxalate ions and radicals $\mathbf{1}^{-/\bullet}$ to $\mathbf{5}^{-/\bullet}$ obtained at the MP2/6-311++G(d) level of theory.

III.2.2. Comparison with the Structures of Cations

The optimized geometries of the $ROCOO^+$ cations do not correspond to the most stable structures on the singlet potential-energy surface (for example, for $R \neq H$, structures having at least one O-H bond are much more stable), but for the sake of comparison, they correspond to the most stable structure having the same connectivity as the respective anions and radicals. The structural parameters obtained differ, nevertheless, quite largely from those of the anions and radicals (Charts III-2.1 and III.2-2). For instance, the $O_{(2)}C_{(1)}O_{(1)}$ angle has an average value of 81.0 ° for all substituents which is much smaller than for the anions or radicals. These structure can almost be considered as "ring-like" between the $C_{(1)}$, $O_{(1)}$, and $O_{(2)}$ atoms (the $O_{(1)}$-$O_{(2)}$ bond has a length of 1.700 Å in average for all R) and would hence correspond to 1,2-dioxiranyl cations. At first sight, this proposal may seem curious but previous examples in the literature show that such a structure has already been envisaged (see Reetz and Maier[10,11] for the acyloxy cation and Schröder et *al.*[12] for the O – O cyclization of acetolactone).

Apart from this particular feature of alkoxycarboxyl cations, some of their bond lengths are also very different from those of anions and neutrals. The $O_{(3)}$-$C_{(1)}$ bond, which slightly decreases with the size of the substituent, is shorter by ca. 0.1 Å compared to the radicals and by more than 0.2 Å compared to the anions (Charts III-2.1 and III.2-2). On the other side, the $O_{(3)}$-R bond varies much more according to the size of the R substituent ($O_{(3)}R$ = 0.981 Å for R = H and 1.745 Å for R = *t*-C_4H_9) and is much longer as for anions and neutrals (ca. + 0.01 Å for R = H to ca. + 0.3 Å for R = *t*-C_4H_9). The vicinity of this "short" $O_{(3)}$-$C_{(1)}$ bond with this "long" $O_{(3)}$-R one induces clearly more a structure of ion-neutral complex for alkoxycarboxyl

cation than the traditional covalent one which is obtained for anions and neutrals.[13-17] This conjecture is supported by an analysis of the Mulliken's charges of the cations which shows that the positive charge is carried by the alkyl group, thus revealing a [R^+ CO_3] structure for alkoxycarboxyl cations (R = H to *t*-C_4H_9).

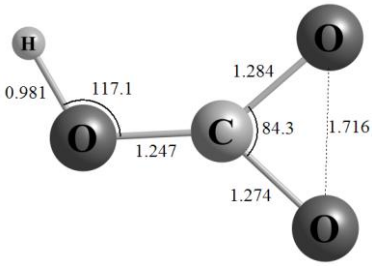

1$^+$

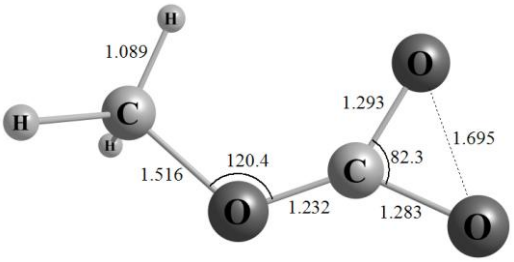

2$^+$

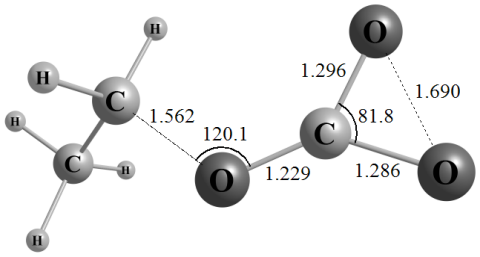

3$^+$

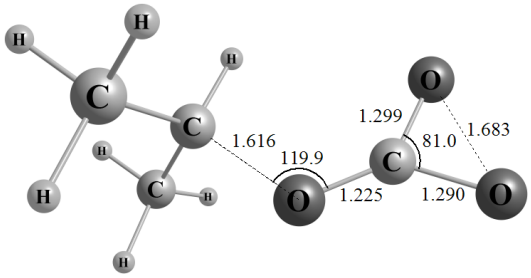

4$^+$

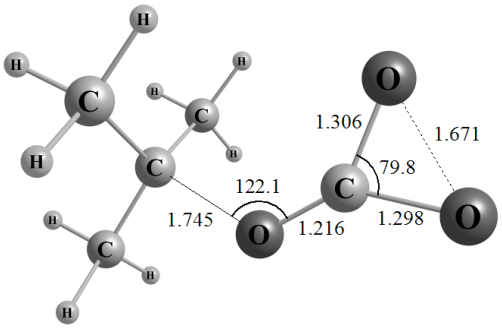

5$^+$

Chart III.2-2: Optimized geometries of alkoxycarboxyl cations **1**$^+$ to **5**$^+$ obtained at the MP2/6-311++G(d) level of theory.

Table III.2-2

Selected bond lengths (in Å) and bond angles (in degree) of $ROCOO^+$ ions (R = H - *t*-C_4H_9) according to MP2/6-311++G(d) calculations.

	Calculated structural parameters (Å and °)					
	$O_{(1)}C_{(1)}$	$O_{(2)}C_{(1)}$	$O_{(3)}C_{(1)}$	$O_{(3)}R$	$O_{(2)}C_{(1)}O_{(1)}$	$RO_{(3)}C_{(1)}$
$\mathbf{1}^+$	1.274	1.284	1.247	0.981	84.3	117.1
$\mathbf{2}^+$	1.283	1.293	1.232	1.516	82.3	120.4
$\mathbf{3}^+$	1.286	1.296	1.229	1.562	79.8	120.1
$\mathbf{4}^+$	1.290	1.299	1.225	1.616	81.0	119.9
$\mathbf{5}^+$	1.294	1.303	1.216	1.686	79.8	122.1

III.3. Thermochemistry

Standard heats of formation of alkylcarbonate anions and radicals have been determined using the bond-separation (BS) reactions and atomization energies. The BS reactions which have been used are given in Scheme III.3-1.

(a)

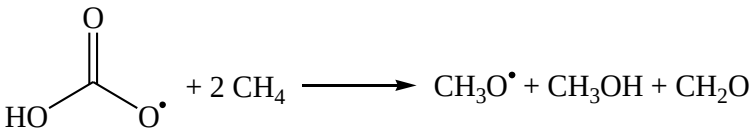

(b)

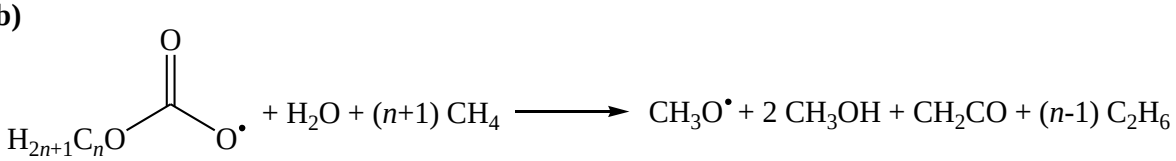

Scheme III.3-1: Bond-separation reactions used for the determination of the standard heats of formation of (a) hydrogencarbonate radical $\mathbf{1}^\bullet$ and (b) alkylcarbonate radicals $\mathbf{2}^\bullet$ to $\mathbf{5}^\bullet$ (n = 1 to 4).

The formation enthalpies obtained with the two methods are in rather good agreement for alkylcarbonate radicals $ROCOO^\bullet$, with difference in general lower than 1 kcal/mol (Table

III.3-1). The deviation is slightly higher for the anions $ROCOO^-$ (between 1.0 and 1.4 kcal/mol for R = H, CH_3, and C_2H_5, less for R = *i*-C_3H_7 and *t*-C_4H_9). This difference is attributed to the fact that two steps are required in the application of the BS method for the anion because their heats of formation are deduced from those of the radicals, accumulating thus errors due to the uncertainties of the experimental data used.

Table III.3-1

Total electronic energies $E_{CBS-,0K}$ (in Hartrees, H), electron affinities *EA* (in eV), heat capacities ΔH_{298K} (in kcal/mol), heats of formation $\Delta_f H°_{298K,atom.}$ and $\Delta_f H°_{298K,BS}$ (in kcal/mol) calculated from atomization energies and bond-separation reactions, respectively, for alkyloxalate anions and radicals $\mathbf{1}^{-/\bullet}$ to $\mathbf{5}^{-/\bullet}$.

		$E_{CBS-Q,0K}$ (H)	*EA* (eV)	ΔH_{298K} (kcal/mol)	$\Delta_f H°_{298K,atom.}$ (kcal/mol)	$\Delta_f H°_{298K,BS}$ (kcal/mol)
1	Anion	-264.159396		2.7	-176.2	-176.5
	Radical	-264.012368	3.9	2.7	-86.1	-86.0
2	Anion	-303.367279		3.6	-169.8	-169.8
	Radical	-303.222788	3.8	3.6	-82.3	-82.0
3	Anion	-342.597974		4.3	-178.0	-178.2
	Radical	-342.452499	3.8	4.4	-90.6	-90.7
4	Anion	-381.830987		5.1	-187.5	-188.3
	Radical	-381.691816	3.8	5.2	-100.0	-100.6
5	Anion	-421.061749		5.8	-195.6	-196.7
	Radical	-420.914745	3.8	5.8	-108.9	-109.9

Heats of formation obtained for alkylcarbonate anions $ROCOO^-$ range from ca. -176 to -196 kcal/mol for R = H to *t*-C_4H_9 (Table III.3-1). Standard formation enthalpy of hydrogencarbonate has already been the subject of two previous works. Thus, in a combined experimental and theoretical study, Squires[5] estimated it as -177.8 ± 2.5 kcal/mol and in a theoretical work, Armstrong *et al.*[18,19] have reported a theoretical value of -175.9 kcal/mol. Both of these values are in accordance with the heats of formation that have been determined in this work (-176.2 (atom.) and -176.5 (BS) kcal/mol). Furthermore, comparison the formation enthalpies of alkylcarbonates with those, for instance, of alkylcarboxylates $RCOO^-$, shows that alkylcarbonates are expected to be very stable compounds ($\Delta_f H°_{298K}(RCOO^-)$ = -120.4 to

-140.1 kcal/mol, for R = H to *t*-C_4H_9).[20] This high intrinsic stability is also reflected in their high electronic affinities which range between 3.8 and 3.9 eV (Table III.3-1).

For alkylcarbonate radicals ROCOO$^{\bullet}$, the heats of formation which have been determined are comprised between about -86 and -109 kcal/mol for R = H to *t*-C_4H_9 (Table III.3-1). Our two theoretical values of -86.1 kcal/mol (atom.) and -86.0 kcal/mol (BS) for hydrogen-carbonate radical agree well with the value of -86.2. given by Armstrong *et al.*[18,19] Comparing the heats of formation of alkylcarbonate radicals with those of compounds with the same formula (e.g. alkylperoxylates RC(O)OO$^{\bullet}$ or peroxyesters ROO(O)C$^{\bullet}$) reveals that, like the anions, the enthalpies of formation of the radicals are very low, showing the high stability of these species ($\Delta_f H°_{298K}$(RC(O)OO$^{\bullet}$) = -21 to -52 kcal/mol and $\Delta_f H°_{298K}$(ROO(O)C$^{\bullet}$) = -20 to -45 kcal/mol for R = H to *t*-C_4H_9).[21]

III.4. Unimolecular Reactivity of Alkylcarbonate Ions

Alkylcarbonates ROCOO$^-$ have been submitted to MI and CA experiments. Whereas MI processes can be attributed to the low-energy fragmentation pathways of an ion, CA experiments open up pathways which require more energy, either due to a barrier or due to a higher endothermicity.[22] The fragments observed in both spectra are given in Table III.4-1.

The analysis of the fragments observed in the MI spectra of alkylcarbonate anions shows that few decomposition pathways are involved in the unimolecular decomposition of all the anions. Hence, a fragment corresponding to alkoxide ions RO$^-$ is present in all spectra. These fragments largely dominate the spectra except for methylcarbonate (see below) and are obtained from a direct bond cleavage concomitant with the expulsion of neutral carbon dioxide (Δm = 44). In the case of ethylcarbonate, the fragment at *m/z* = 45 may also be attributed to a CO_2H^- ion instead of the isobaric ethoxide ion $C_2H_5O^-$, as discussed in more details below. The MI spectra of hydrogen-, methyl-, ethyl-, and *i*-propylcarbonates exhibit also a fragment whose mass corresponds to carbon trioxide anion $CO_3^{\bullet -}$ (*m/z* = 60)[23] concomitant with an expulsion of the corresponding alkyl radical. The $CO_3^{\bullet -}$ fragment ion is not observed for *t*-butylcarbonate which may, however, be due to the low signal-to-noise ration of this particular spectrum. In the MI spectrum of methylcarbonate, an additional fragment at *m/*z = 45 is observed to which we return in more details further below.

In the corresponding CA spectra of the alkylcarbonate ions, a few additional features appear. First, decarboxylation becomes the dominant decomposition process for all substituents

R. Then, the $CO_3^{\bullet -}$ fragment shows up in the spectrum of *t*-butylcarbonate and in general its intensity increases in all CA spectra relative to the MI experiments. Further, fragments at *m/z* = 43 and *m/z* = 57 appear in the CA spectra of ethyl-, *i*-propyl-, and *t*-butylcarbonate which are attributed to CH_2CHO^- (*m/z* = 43) and to $CH_3C(CH_2)O^-$ (*m/z* = 57); they are formed in the structurally characteristic high energy dissociation of alkoxide ions having a primary (1,2 elimination of H_2), secondary (1,2 elimination of H_2 and loss of CH_4), and tertiary alkyl substituent (loss of CH_4).[24]

Table III.4-1

Intensities[a] of observed fragments in MI and CA[b] spectra of mass-selected[c] alkylcarbonates $ROCOO^-$ (**1**$^-$ to **5**$^-$ for R = H to *t*-C_4H_9).

R (*m/z*)[d]	*m/z* (I)
H (61)	MI: 17 (100), 60 (34) CA: 17 (100), 60 (82)
CH_3 (75)	MI: 31 (12), 45 (100) CA: 31 (100), 45 (51), 60 (49)
C_2H_5 (89)	MI: 45 (100), 60 (9) CA: 43 (11), 45 (100), 60 (12)
i-C_3H_7 (103)	MI: 59 (100), 60 (4) CA: 43 (4), 57 (7), 59 (100), 60 (3)
t-C_4H_9 (117)	MI: 73 (100) CA: 57 (23), 60 (21), 73 (100)

[a] Intensity relative to the base peak (= 100); peaks < 1 are neglected.

[b] CA obtained with He (80% T) in C3 (Figure II.2-1).

[c] Mass selection was made using B1 while E1 was scanned.

[d] Mass-to-charge ratio of precursor anion in amu.

In Table III.4-2, the calculated heats of reaction of the observed dissociation pathways of alkylcarbonates $ROCOO^-$ (R = H to *t*-C_4H_9) are compiled. All heats of reaction are positive, which identifies these as endothermic processes. While the fragment ion at *m/z* = 45, observed in the MI and CA spectra of methyl- and ethylcarbonate, may correspond either to $HCOO^-$ or

to $HOCO^-$ (and in the case of ethylcarbonate also to $C_2H_5O^-$, see below), the computed heats of reaction (Table III.4-2) reveal that the hydrogen-atom transfer leading to the formate ion, $HCOO^-$, and the corresponding carbonyl compound is by far (ca. 28 kcal/mol) the thermodynamically most favorable fragmentation. This process has only been calculated for methyl-, ethyl-, and *i*-propylcarbonates due to the particular mechanisms of this hydrogen transfer, as will be explained below. Further, the two direct bond cleavages observed in the spectra corresponding to losses of CO_2 and $R^\bullet$, respectively, require about 35 and 90 kcal/mol. These computed reaction enthalpies are consistent with the relative intensities of the corresponding fragments in the MI and CA spectra, i.e. the intensities of the RO^- anions resulting from decarboxylation are always much higher than those of $CO_3^{\bullet-}$ obtained upon loss of $R^\bullet$.

Table III.4-2

Total electronic energies E_{tot}[a] of alkylcarbonates **1**$^-$ to **5**$^-$ (in Hartrees, H) and heats of reaction at 298 K (in kcal/mol) of their observed dissociation processes according to MP2/6-311++G(3df,3pd)// MP2/6-311++G(d) calculations.

	E_{tot}[a] (H)	$\Delta_r H_{298K}$ (kcal/mol)[a]			
		$-CO_2$	$-R^\bullet$	$HCOO^-$	$HOCO^-$
1$^-$	-264.0523306	42.5[b]	106.3		
2$^-$	-303.2267746	37.8	85.5	27.6	64.1
3$^-$	-342.4273903	35.1	89.3	23.1	59.7
4$^-$	-381.6302516	33.4	90.8	20.9	57.5
5$^-$	-420.8300958	30.2	91.9		

[a] Obtained at the MP2/6-311++G(3df,3pd)//MP2/6-311++G(d) level of theory; ZPE included and scaled.

[b] This value is in acceptable agreement with a value of 45 kcal/mol given in a recent theoretical work of Leung *et al.*[25]

Hayes *et al.*[1] have already investigated the unimolecular dissociation of the methylcarbonate ion by means of CA experiments. Their results agree with the data presented in Table III.4-1 with only small differences in relative intensities. In their work, the fragment ion at *m/z* = 45 has been shown to correspond to the HCO_2^- anion and not to the isomeric $HOCO^-$ form; this assignment is further supported by the heats of reaction shown in Table III.4-2. The suggested mechanism of the dissociation leading to HCO_2^- (Scheme III.4-1) involves the

formation of an ion-neutral complex [CH_3O^- CO_2] followed by an intracomplex hydride transfer to the electrophilic carbon atom of CO_2.

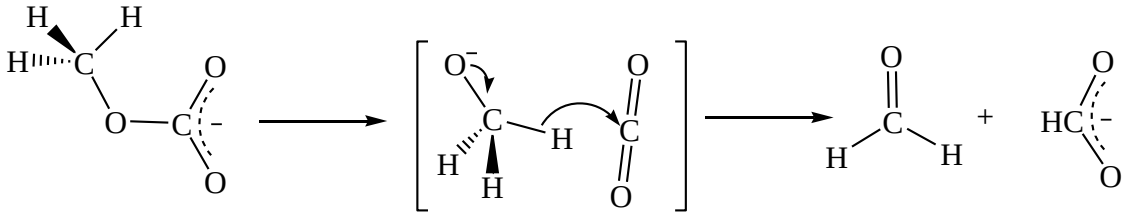

Scheme III.4-1: The hydride transfer reaction of CH_3OCOO^- as proposed by Hayes *et al*.[1]

An interesting point concerns the occurrence of this type of hydride-transfer reaction for the other alkylcarbonate ions, ethyl- and *i*-propylcarbonates in particular. In the case of ethylcarbonate, an ion at *m/z* = 45 is indeed observed but, in addition to HCO_2^-, this ion may also correspond to $C_2H_5O^-$ resulting from the loss of neutral carbon dioxide rather than of acetaldehyde. In order to further characterize this particular fragment ion, we have accordingly recorded a CA/CA spectrum of the *m/z* = 45 fragment generated from ethylcarbonate (Figure III.4-1).

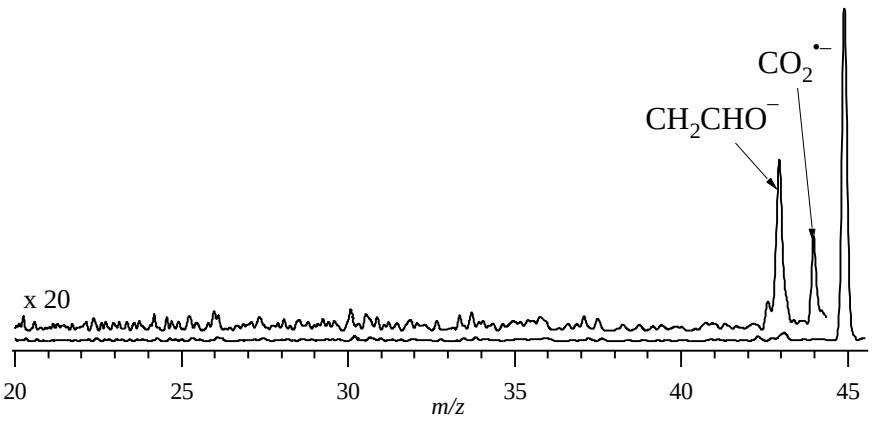

Figure III.4-1: CA/CA spectrum of the *m/z* = 45 ion generated from $C_2H_5OCOO^-$.

In the CA/CA spectrum of the *m/z* = 45 ion from $C_2H_5OCOO^-$, fragments corresponding to $CO_2^{\bullet-}$ (*m/z* = 44) and $C_2H_3O^-$ (*m/z* = 43) are observed. The latter is assigned to the CH_2CHO^- ion resulting from the decomposition of $C_2H_5O^-$.[24] The *m/z* = 45 fragment of $C_2H_5OCOO^-$ is hence in part composed of the ethoxide ion, obtained by decarboxylation, and in part arises from the loss of acetaldehyde leading to HCO_2^- (or, less likely, to $HOCO^-$).[26] For *i*-propylcarbonate, this particular dissociation process does not take place, as neither in the

MI nor in the CA spectrum a fragment at *m/z* = 45 is observed. Thermochemistry predicts yet that loss of acetone is the most favorable dissociation process for *i*-propylcarbonate, requiring only 20.9 kcal/mol (Table III.4-2). In order to understand this feature, the ion-neutral complexes [RO^- CO_2] and transition structures TS_{HT} associated with the hydride-transfer reaction (analogous to Scheme III.4-1) have been calculated for $ROCOO^-$ ions with R = CH_3, C_2H_5, and *i*-C_3H_7 (Chart III.4-1 and Table III.4-3).

Table III.4-3

Total and relative energies E_{tot}[a] and E_{rel}[b] (in Hartrees, H and in kcal/mol, respectively) of the ion-neutral complexes [RO^- CO_2] (R = CH_3, C_2H_5, and *i*-C_3H_7) and the transitions structures TS_{HT} for H^- transfer analogous to Scheme III.4-1 according to MP2/6-311++G(3df,3pd)//MP2/6-311++G(d) calculations.

	E_{tot}[a] (H)	E_{rel}[b] (kcal/mol)
[CH_3O^- CO_2]	-303.1738650	33.2
TS_{HT}(CH_3OCOO^-)	-303.1688287	36.4
[$C_2H_5O^-$ CO_2]	-342.3783041	30.8
TS_{HT}($C_2H_5OCOO^-$)	-342.3742294	33.4
[*i*-$C_3H_7O^-$ CO_2]	-381.5831204	29.6
TS_{HT}(*i*-$C_3H_7OCOO^-$)	-381.5793109	32.0

[a] ZPE scaled and included.

[b] Energies are given relative to those of the corresponding alkylcarbonate (Table III.4-2).

The energetics obtained for the ion-neutral complexes [RO^- CO_2] (R = CH_3, C_2H_5, and *i*-C_3H_7) and the transitions structures TS_{TH} show a slight decrease of the energy demand of the hydride transfer when the size of the substituent increases (Table III.4-3). Thus, this reaction is as favorable for the *i*-propylcarbonate ion as for methyl- and ethylcarbonates, even though it is not observed for the ion with R = *i*-C_3H_7 (Table III.4-1). There are (at least) three possibilities to account for the deviating behavior of the isopropylcarbonate anion. (i) In the competition between the barrierless loss of CO_2 to generate *i*-$C_3H_7O^-$ and the energetics of the transition state for hydrogen transfer to produce $(CH_3)_3CO$ and HCO_2^- according to Scheme III.4-1, the calculated energy difference of 3.8 kcal/mol may be unrealistic. (ii) While CO_2 eli-

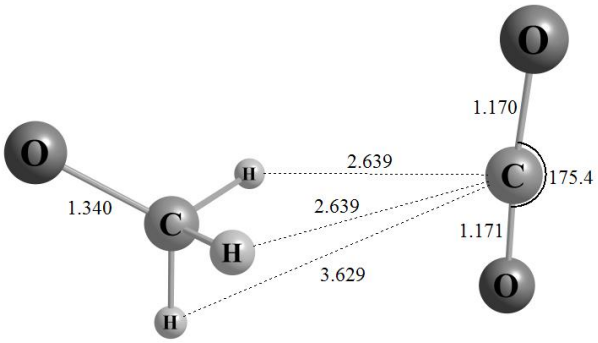

$[CH_3O^- \; CO_2]$

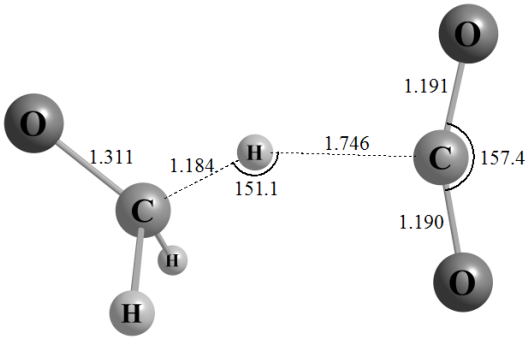

$TS_{HT}(CH_3OCOO^-)$

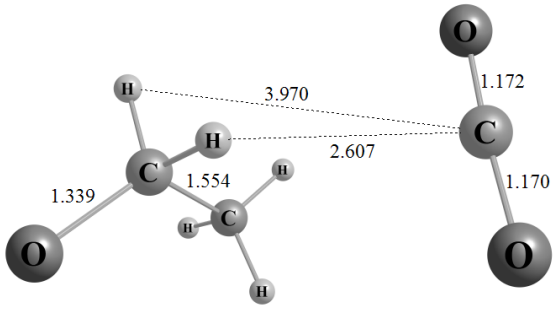

$[C_2H_5O^- \; CO_2]$

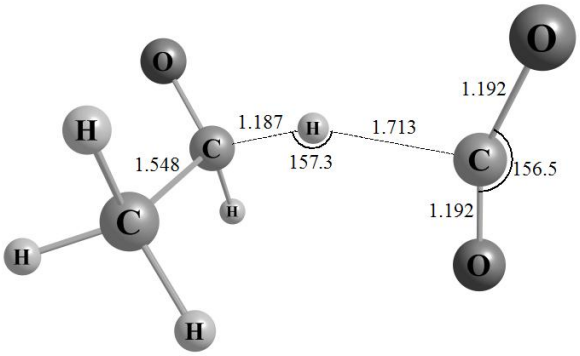

$TS_{HT}(C_2H_5OCOO^-)$

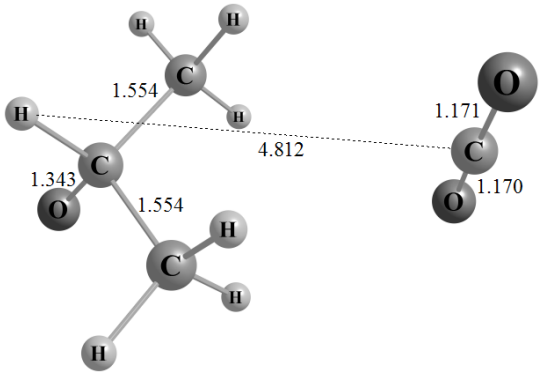

$[i\text{-}C_3H_7O^- \; CO_2]$

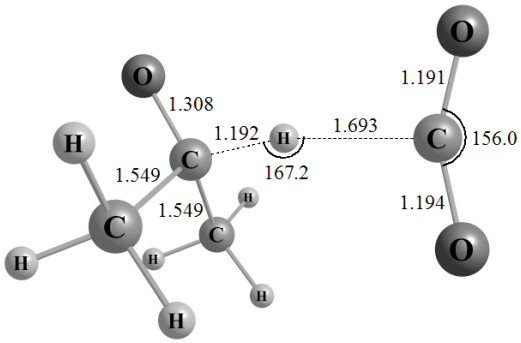

$TS_{HT}(i\text{-}C_3H_7OCOO^-)$

Chart III.4-1: Optimized structures of the ion-neutral complexes $[RO^- \; CO_2]$ and the transition states TS_{HT} for methyl-, ethyl, and *i*-propylcarbonates (R = CH_3, C_2H_5, and *i*-C_3H_7) (bond lengths in Å, angles in degree).

mination is entropically favored, the rearrangement-elimination to produce HCO_2^- from *i*-$C_3H_7OCOO^-$ is aggrevated by a statistical disadvantage in that only one hydrogen is available as compared to two and three for the lighter homologues with R = C_2H_5 and CH_3, respectively. For all three anions, the energetic differences for direct CO_2 loss vs HCO_2^- formation are comparable. (iii) There is a significant structural difference in the geometric details of the transition state for hydrogen migration as indicated in Chart III.4-1. For the anions with R = CH_3 and C_2H_5, the [RO^- CO_2] complexes need much less reorganization to reach the transition state for a hydride transfer to the electrophilic carbon atom of CO_2. In contrast, for R = *i*-C_3H_7, the migrating hydrogen is as much as 4.812 Å away from the accepting carbon atom, and major structural adjustment is necessary to complete the rearrangement.

In summary, the fragmentation behavior of alkylcarbonates follows rather established rules in that the MI dissociation processes are preferentially controlled by thermochemistry, whereas the CA processes are more subject of a kinetic control. Hence, for methyl- and ethylcarbonates, the most thermodynamically favored process corresponds to a hydride transfer leading to HCO_2^- and the neutral RCHO (R = H, CH_3). This reaction dominates the MI spectra of these two ions, but the relative intensity of the corresponding fragments decreases in the CA spectra. This effect is clearly due to kinetic reasons which favor direct bond cleavages, compared to processes requiring the passage through entropically demanding transition structures. For the other alkylcarbonates, the MI as well as the CA processes are dominated by decarboxylation. Another minor decomposition process, leading to $CO_3^{\bullet -}$ and $R^\bullet$ is also observed in the MI and CA spectra with a higher relative intensity in the CA spectra. While this direct bond cleavage is not favorable thermochemically, it has an entropic advantage and thus gains in importance under CA conditions.

III.5. NIDD Study of Alkylcarbonate Radicals

In order to probe the chemistry of alkylcarbonate radicals, the corresponding anions $ROCOO^-$ (R = H, CH_3, C_2H_5, *i*-C_3H_7, and *t*-C_4H_9) have been submitted to $^-CR^+$ and $^-NR^+$ experiments. While charge-reversal experiments with negative ions can provide structural information about both negative ions and the cations formed therefrom,[27] neutralization-reionization experiments provide information about the chemistry of the neutral counterparts.[28] However, the interpretation of the corresponding NR spectra is made difficult due to the superposition of fragmentations related to the chemistry of the neutral species and those

arising from ionic dissociation. In order to simplify the analysis, the neutral and ion decomposition difference (NIDD) method had been developed,[4] which - in essence - consists in subtracting the normalized intensities of the CR from those of the NR spectra. A NIDD spectrum is thus composed of signals with negative and positive intensities that can be related to the respective chemistry of the ionic and neutral species.

Table III.5-1

Intensities[a] of selected[b] fragments in the $^{-}CR^{+c}$ and $^{-}NR^{+c}$ spectra of mass-selected[d] alkylcarbonates $ROCOO^{-}$ (**1**$^{-}$ to **5**$^{-}$ for R = H to *t*-C_4H_9).

R (*m/z*)[e]
H (61)
CR: 16 (6), 17 (9), 28 (37), 29 (14), 44 (100), 45 (84), 61 (2)
NR: 16 (16), 17 (9), 28 (70), 29 (5), 44 (100), 45 (26), 61 (6)
CH_3 (75)
CR: 28 (18), 29 (50), 30 (12), 43 (3), 44 (100), 45 (17), 56 (2), 59 (4)
NR: 28 (71), 29 (69), 30 (30), 43 (5), 44 (100), 45 (6), 59 (1)
C_2H_5 (89)
CR: 28 (24), 29 (98), 30 (24), 43 (26), 44 (100), 45 (19), 56 (3)
NR: 28 (67), 29 (76), 30 (42) , 43 (39), 44 (100), 45 (19), 56 (1)
i-C_3H_7 (103)
CR: 28 (12), 29 (26), 39 (19), 40 (5), 41 (23), 43 (100), 44 (59), 45 (10), 56 (2), 59 (2)
NR: 28 (40), 29 (51), 39 (20), 40 (6), 41 (18), 43 (100), 44 (86), 45 (6), 56 (2), 59 (6)
t-C_4H_9 (117)
CR: 28 (11), 29 (16) , 40 (11), 41 (36), 43 (100), 44 (29), 45 (11), 56 (7), 57 (25), 58 (9)
NR: 28 (31), 29 (21) , 40 (17), 41 (33), 43 (100), 44 (35), 45 (5), 56 (12), 57 (10), 58 (4)

[a] Intensity relative to the base peak (= 100) into brackets.

[b] Due to the large number of fragments present in the $^{-}CR^{+}$ and $^{-}NR^{+}$ spectra of alkyloxalates, only the major signals and those considered the most relevant ones are presented.

[c] CR obtained with O_2 (80 % T) in C5 and NR with O_2 (80 % T) in C5 and C6.

[d] The mass selection was made with B1/E1 while B2 was scanned.

[e] Mass-to-charge ratio in amu.

Prior to the analysis of the NIDD spectra of the alkylcarbonates, some comments about the $^{-}CR^{+}$ and $^{-}NR^{+}$ spectra are indicated (Table III.5-1). First, the signals obtained in the two spectra differ in intensities but not in their types. Hence, except for the *m/z* = 56 fragment of methylcarbonate which is present in the CR but not in the NR spectrum, all fragments observed in the CR spectra are also observed upon NR. Furthermore, except for $HOCOO^{-}$, recovery signals are observed neither in the CR nor in the NR spectra. This feature combined with massive fragmentations observed in both spectra indicate significant differences in geometry between the anions (or the radicals) and the cations. If the structures of the cations differ largely from those of anions or radicals, vertical electron transfer will indeed lead to the formation of highly vibrationally excited cations which will dissociate at very short timescales. The computed geometries of anions, radicals and cations confirm this conjecture (Tables III.2-1 and III.2-2). Hence, even though alkylcarbonate anions and radicals can exist as long-lived species, no recovery signals are observed in the corresponding NR and CR spectra. As a lifetime of the order of microseconds for the radical intermediates is required to apply the NIDD method,[4] another variant of NR experiment has been applied. McMahon *et al.* have shown that $^{-}NR^{-}$ experiments can provide information on the stability of neutrals that are not accessible in other charge mutation NR experiments.[29] We have accordingly recorded the $^{-}NR^{-}$ spectra of the five alkylcarbonates under study. As an example, the $^{-}NR^{-}$ spectrum of the ethylcarbonate ion is shown in Figure III.5-1.

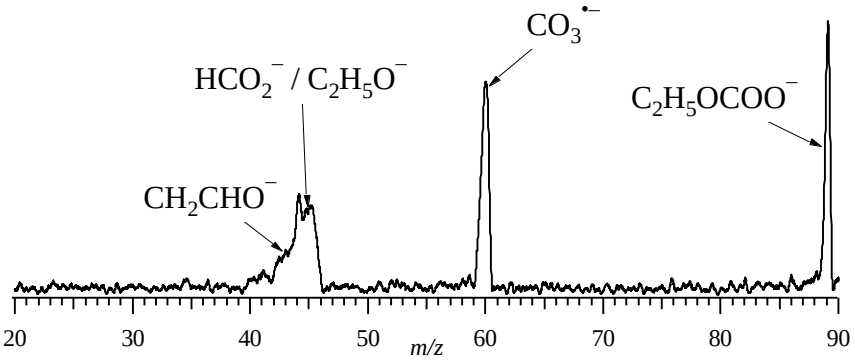

Figure III.5-1: $^{-}NR^{-}$ spectrum of B1-mass selected $C_2H_5OCOO^{-}$ **3**$^{-}$ (*m/z* = 89) using O_2 (C2, 80 % T) and Xe (C3, 80 % T).

The $^{-}NR^{-}$ spectrum of $C_2H_5OCOO^{-}$ is composed of signals at *m/z* = 43, 45, 60, and 89 (Figure III.5-1). As all charged species are deflected after the ion beam is passed through the collision cell where neutralization takes place, the signal at *m/z* = 89 can clearly be attributed

to the reionized $C_2H_5OCOO^{\bullet}$ radical. The ions at *m/z* = 43, 45, and 60 originate either from the dissociation of $C_2H_5OCOO^{\bullet}$ or from decomposition of reionized $C_2H_5OCOO^-$ and are attributed to CH_2CHO^-, HCO_2^- and/or $C_2H_5O^-$, and $CO_3^{\bullet-}$, respectively, which correspond, though with different relative intensities, to the fragments obtained upon CA of $C_2H_5OCOO^-$ (Table III.4-1). Further, the peak for *m/z* = 45 in the $^-NR^-$ spectrum of $C_2H_5OCOO^-$ shows a notable broadening, which indicates that decarboxylation is associated with a considerable kinetic energy release.[30-32]

Notwithstanding these fragmentations, the observation of a pronounced recovery signal in the $^-NR^-$ spectrum of ethylcarbonate establishes the existence of the neutral $C_2H_5OCOO^{\bullet}$ in the time scale of the experiment. Similarly, recovery signals are observed in the $^-NR^-$ spectra of the other $ROCOO^-$ ions with R = H,[29] CH_3, *i*-C_3H_7, and *t*-C_4H_9.

From the relative intensities of the fragments observed in $^-CR^+$ and $^-NR^+$ spectra of alkylcarbonates (Table III.5-1), some general features concerning the dissociation of the cationic species emerge. Hence, the *m/z* = 45 fragment is present in both spectra, but as its intensity is much more abundant in CR than in NR (about twice as high), its origin is attributed to the dissociation of alkoxycarboxyl cations formed from vertical electron transfer (in the case of ethylcarbonate, a mass overlap with the isobaric $C_2H_5O^+$ ion excludes this conclusion). This cationic fragment ion corresponds to $HOCO^+$ and thus demonstrates the occurrence of a rearrangement at the cationic stage, except for hydrogencarbonate for which this ion is accessible by direct C – O bond cleavage. Further, a weak signal at *m/z* = 56 is observed in the spectra for all R, expect R = H (for R = *t*-C_4H_9, there exists an overlap with $C_4H_8^+$). This fragment ion corresponds most likely to ionized ethylene dione, $C_2O_2^{\bullet+}$.[33] The difference in the relative intensities of this ion in the CR and NR spectra is so small, however, that it does not allow to unambiguously tracing back the origin of this ion to a particular ionic or neutral species. Nevertheless, as the relative lifetime of neutral C_2O_2 has been found to be < 10^{-9} s,[33] the $C_2O_2^{\bullet+}$ ion observed can be exclusively related to the cation chemistry. Finally, it remains to be reiterated that the precursor ions submitted to a NR process undergo two collisions, whereas only one collision is required for CR. Accordingly, fragmentation is more excessive in a NR process than in a CR one, which is also reflected in the data of the alkylcarbonates (Table III.5-1) in that the fragments with smaller *m/z* ratios are larger in the NR than in the CR spectra, e.g. $CO^{\bullet+}$ (*m/z* = 28), HCO^+ (*m/z* = 29).

The normalized differences in the $^{-}CR^{+}$ and $^{-}NR^{+}$ spectra are further used to deduce information about the unimolecular chemistry of the radicals by means of the NIDD scheme. The resulting spectra are presented in Figure III.5-2.

The $^{-}NIDD^{+}$ spectrum of $HOCOO^{-}$ (Figure III.5-2a) is dominated by positive signals for the ionic fragments O^{+}, $CO^{\bullet+}$, and $CO_2^{\bullet+}$ which is consistent with reionization of neutral CO_2 formed upon decarboxylation of the neutral radical as suggested earlier;[34] the corresponding counterpart HO^{+} is not formed in significant amounts, most likely due to inefficient reionization cross section of this light fragment. The negative part of the NIDD spectrum is dominated by signals corresponding to the cation $HOCO^{+}$ and its dissociation product HCO^{+},[35] as a result of direct bond cleavages in the ion states.

The NIDD spectra of the other alkylcarbonates studied provide less direct information about the chemistry of the corresponding neutral radicals. This is mostly due to the presence of mass overlaps in the spectra and due to the massive fragmentation processes observed in the CR and NR spectra which give rise to NIDD spectra whose most significant ions are related to consecutive fragmentations which cannot be clearly traced back to a particular precursor. The two dominant positive signals in the NIDD spectrum of CH_3OCOO^{-} (Figure III.5-2b) correspond to $CH_2O^{\bullet+}$ (*m/z* = 30) and $CO^{\bullet+}$ (*m/z* = 28). If the hypothesis of a rearrangement at the neutral stage leading to the dissociation products $CO/CH_3O_2^{\bullet}$ or $CH_2O/HOCO^{\bullet}$ is excluded, these two ions may originate then only from the reionization of the neutral dissociation products $CH_3O^{\bullet}/CO_2$ or $CH_3OCO^{\bullet}/O$. As no other relevant positive signals are present in the NIDD spectrum of CH_3OCOO^{-}, no further conclusions about the chemistry of $CH_3OCOO^{\bullet}$ can be made. However, negative NIDD signals reveal two interesting features about the ionic chemistry. First, the ion at *m/z* = 43 originates from a loss of molecular oxygen and corresponds to CH_3CO^{+} or to the isomeric, however much less stable, CH_3OC^{+} cation.[36] Secondly, as already deduced by comparing the CR and NR spectra, a negative NIDD signal at *m/z* = 45 is observed which is assigned to a hydrogen migration from the methyl group to one of the oxygen atoms in the transient CH_3OCOO^{+} cation followed by expulsion of formaldehyde. A last point to be addressed concerns the $CO_2^{\bullet+}$ ion which gives rise to an intense negative signal in the NIDD spectrum. Instead, the NIDD signal for $CO_2^{\bullet+}$ would have expected to be positive because, according to the Stevenson's rule,[37] dissociation of the CH_3OCOO^{+} cation leads preferentially to the CH_3O^{+}/CO_2 products rather than $CH_3O^{\bullet}/CO_2^{\bullet+}$, given the ionization energies of $CH_3O^{\bullet}$ (10.7 eV) and of CO_2 (13.8 eV).[38] However, if $CH_3OCOO^{\bullet}$ serves as a precursor, the reionization of the $CH_3O^{\bullet}$ and CO_2 fragments should lead to both CH_3O^{+} and $CO_2^{\bullet+}$ ions with positive signal intensities in the NIDD spectrum, which is not the case.

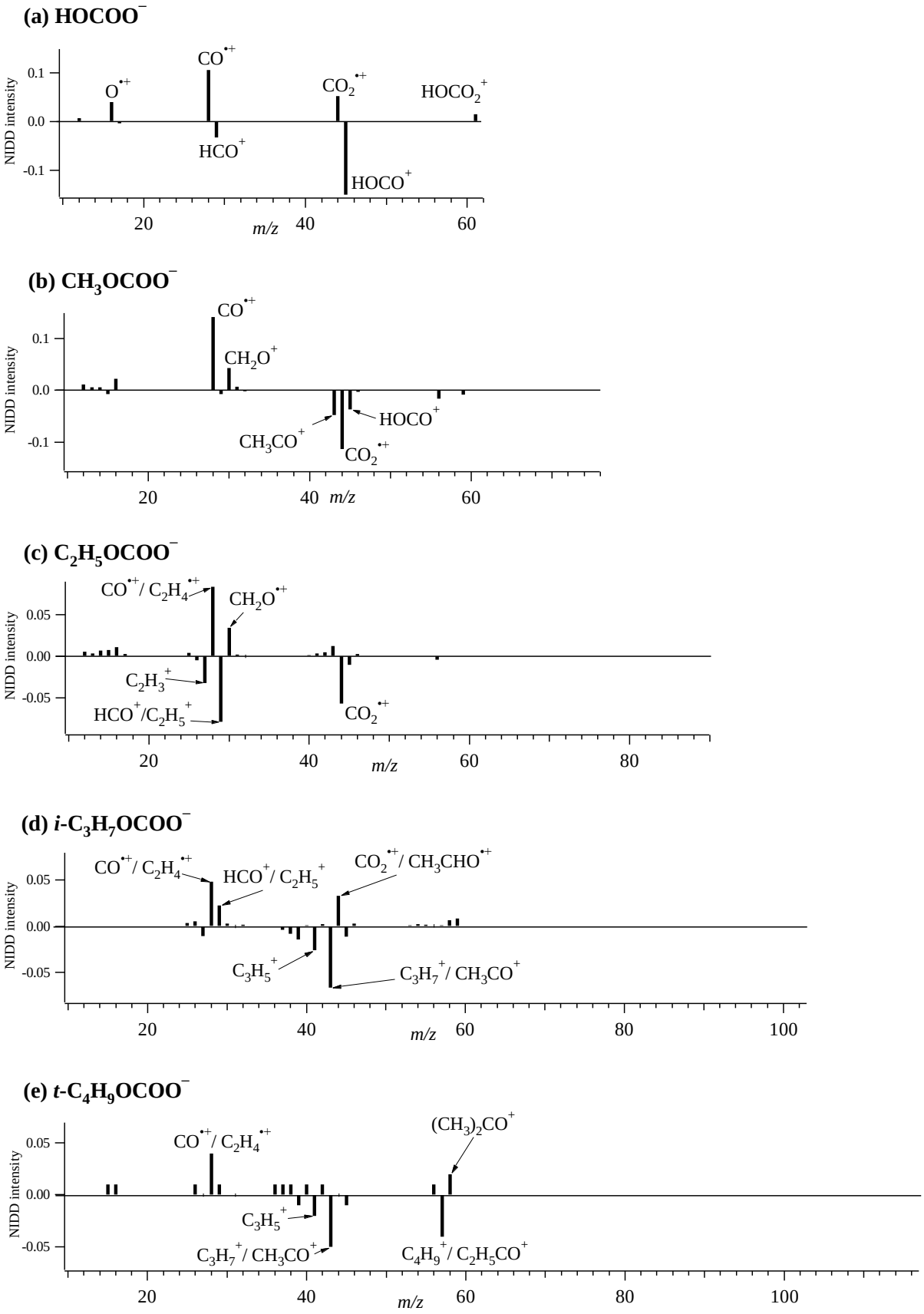

Figure III.5-2: $^{-}$NIDD^{+} spectra of the five alkylcarbonates under study. Only signals with intensity higher than |0.02| are assigned.

We have considered various scenarios to resolve this problem. For example, assuming that $CO_2^{\bullet+}$ originates from dissociation of $CH_3OCO_2^+$ and not from reionization of neutral CO_2 implies that the neutral radical precursor $CH_3OCO_2^\bullet$ hardly undergoes cleavages of the methoxy-carbon bond. This assumption is neither supported by experimental[39] nor by computational findings (Table III.5-2). For example, rupture of the $CH_3O^\bullet$ – CO_2 bond is 15.6 kcal/mol exothermic, whereas other conceivable bond cleavages are endothermic by > 70 kcal/mol. More likely, excessive fragmentation in a NR process, as compared to CR, may be operative,[40] although we do not conceal the fact that we are facing a problem which is not yet really and fully understood.

A closer inspection of the NIDD spectrum of CH_3OCOO^- further shows that the information contained in the spectrum cannot simply and directly be associated with the chemistry of the ionic or neutral species. As shown above, a negative NIDD signal for $CO_2^{\bullet+}$ does not relate this ion to the chemistry of its precursor ion and reionization of the neutral fragments does not provide an explanation either. Fundamental differences between the CR and NR processes have to be taken into account to give a coherent interpretation of the spectrum. For alkylcarbonates with larger substituents, the analysis becomes even more complex due to the occurrence of many mass overlaps between the fragments. We did not perform any complementary experiments with labeled alkylcarbonates because most of the fragmentation patterns are associated with consecutive dissociations which are difficult to trace back to a particular origin.

The NIDD spectrum of $C_2H_5OCOO^-$ (Figure III.5-2c) exhibits only two relevant positive fragments, which are the same as for CH_3OCOO^-, i.e. the ions at *m/z* = 28 and 30. The latter corresponds to $CH_2O^{\bullet+}$, whereas a mass overlap between $CO^{\bullet+}$ or $C_2H_4^{\bullet+}$ prevents an unambiguous assignment of the ion at *m/z* = 28. Again, $CO_2^{\bullet+}$ shows up with a pronounced negative NIDD peak which can be interpreted in the same manner as above. Two other ions with significant negative intensities are $C_2H_3^+$ at *m/z* = 27 and HCO^+ and/or $C_2H_5^+$ at *m/z* = 29. The latter mass overlap at *m/z* = 29 prevents any definitive proof of a rearrangement of the $C_2H_5OCOO^+$ cation formed from double electron transfer and leading to the $HOCO^+$ ion, as observed for $HOCOO^+$ and CH_3OCOO^+. Concerning the predicted thermochemistry, the $C_2H_5O^\bullet$ – CO_2 bond cleavage is also strongly preferred (13.2 kcal/mol exothermic), whereas other bond ruptures are endothermic by more than 70 kcal/mol (Table III.5-2).

The complexity due to possibly isobaric species is, of course, even more pronounced in the $^-NIDD^+$ spectra of *i*-$C_3H_7OCOO^-$ and *t*-$C_4H_9OCOO^-$ (Figures III.5-2d and III.5-2e). The major positive signals in the NIDD spectrum of *i*-$C_3H_7OCOO^-$ may tentatively be attributed

to $CO^{\bullet+}/C_2H_4^{\bullet+}$ for *m/z* = 28, $HCO^+/C_2H_5^+$ for *m/z* = 29, and $CO_2^{\bullet+}/CH_3CHO^{\bullet+}$ for *m/z* = 44. In the case of *t*-$C_4H_9OCOO^-$, only the formation of the ion $(CH_3)_2CO^+$ can be attributed to the chemistry of the neutral radical. Again, the ion at *m/z* = 28 cannot be assigned unambiguously and the other ions do not have a significant NIDD intensity. Likewise, the negative parts of NIDD spectra of *i*-$C_3H_7OCOO^-$ and *t*-$C_4H_9OCOO^-$ are subject to mass overlaps: $C_3H_7^+/CH_3CO^+$ (*m/z* = 43) in both of the spectra and $C_4H_9^+/C_2H_5CO^+$ (*m/z* = 57) in the spectrum of *t*-$C_4H_9OCOO^-$. The thermochemistry of dissociation of *i*-$C_3H_7OCOO^\bullet$ and *t*-$C_4H_9OCOO^\bullet$ is similar to that of the other alkoxycarboxy radicals studied. The $RO^\bullet - CO_2$ bond cleavage is exothermic while other direct dissociations are endothermic by more than 70 kcal/mol.

Table III.5-2

Total electronic energies E_{tot}[a] of alkylcarbonates $ROCOO^\bullet$ (**2**$^\bullet$ to **5**$^\bullet$, for R = H - *t*-C_4H_9) and heats of reaction at 298 K of their possible dissociation processes (in Hartrees, H, and in kcal/mol, respectively) according to MP2/6-311++G(3df,3pd)//MP2/6-311++G(d) calculations.

R	E_{tot}[a] (H)	$\Delta_r H°_{298K}$ (kcal/mol)[a]		
		$RO^\bullet + CO_2$	$R^\bullet + CO_3$	$ROCO^\bullet + O$
H	-263.8997798	-8.3	87.4	98.0
CH_3	-303.0782731	-15.6	69.1	99.5
C_2H_5	-342.2785890	-13.2	72.8	99.5
i-C_3H_7	-381.4781208	-13.0	73.2	98.7
t-C_4H_9	-420.6820272	-12.4	75.8	98.1

[a] ZPE included and scaled.

While it appears that $RO^\bullet - CO_2$ bond cleavage seems the most plausible dissociation process at the neutral stage, the NIDD spectra provide no clear evidence of such processes. However, a previous NIDD study by Hornung *et al.*[41] about neutral alkoxy radicals may help to resolve the dilemma. From their study, they derived a general behavior of transient alkoxy radicals under the conditions of $^-NR^+$ experiments (Scheme III.5-1). Hence, if $RO^\bullet$ species are produced upon dissociation of neutral $ROCOO^\bullet$ radicals, characteristic fragments should occur in the positive parts of the NIDD spectra. Such signals are indeed observed in the spectra of the $ROCOO^-$ species and correspond to $CH_2O^{\bullet+}$ (*m/z* = 30) for R = CH_3 and C_2H_5 as well as $CH_3CHO^{\bullet+}$ (*m/z* = 44) and $(CH_3)_2CO^{\bullet+}$ (*m/z* = 58) for R = *i*-C_3H_7 and *t*-C_4H_9. These posi-

tive signals are fully consistent with the anticipated presence of transient $RO^{\bullet}$ species at the neutral stage.

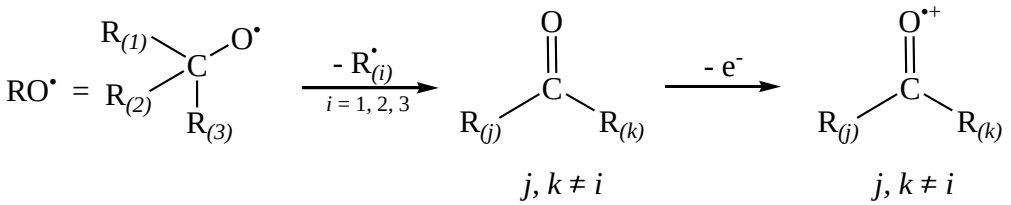

Scheme III.5-1: Fragmentation occurring for an alkoxy radical $RO^{\bullet}$ (with side chains bearing three or less carbon atoms) and the fragments obtained after reionization to cation according to Hornung.[41]

A final point to be clarified concerns the large negative $CO_2^{\bullet+}$ signals in all NIDD spectra. As explained above, the $ROCOO^+$ cation formed from vertical electron transfer is expected to dissociate mostly into $RO^+ + CO_2$ instead of the charge-permuted product couple $RO^{\bullet} + CO_2^{\bullet+}$. Above, the intense negative signal of $CO_2^{\bullet+}$ in almost all NIDD spectra has been attributed to the larger amount of fragmentation in the NR process, but nothing was said concerning the dominance of $CO_2^{\bullet+}$ compared to RO^+ in the CR processes. This point is all but obvious, because the ionization energies of the $RO^{\bullet}$ species range from ca. 9 to 10.7 eV for the various alkyl substituents (13 eV for R = H), whereas $IE(CO_2)$ is as large as 13.77 eV.[38] The dissociation of the transient alkoxycarboxy cations obtained upon vertical detachment of two electrons from the anion should accordingly lead to RO^+ ions, which is in contradiction with the experimental observation in the CR spectra obtained.[42] In this respect, it has first to be recalled that the ionization energies given here correspond to adiabatic values. As a vertical electron transfer may populate excited electronic stated of the cations, their dissociation can also lead to electronically excited products. The mere comparison of the adiabatic ionization energies of $RO^{\bullet}$ and CO_2 is thus not anymore appropriate for the prediction of the preferred decomposition process. Moreover, the conservation of the overall spin multiplicity of the system has to be taken into account as well.[43] As the anionic alkylcarbonate precursors bear singlet ground states and charge transfer is likely to conserve the overall spin multiplicity of the system,[44] the transient alkylcarbonate cations are likely to be also formed in singlet states. Dissociation of these cations following the spin-conservation rule should hence lead to alkoxy cations in the singlet state because the associated fragment CO_2 also has a singlet ground state.[45] It is known, however, that alkoxy cations do not exist in the singlet state and instead undergo rearrangement via hydrogen- or alkyl migrations.[46,47] Hence, the preferential formation of $RO^{\bullet}/CO_2^{\bullet+}$ compared to that of RO^+/CO_2 in the course of dissociation of alkylcarbo-

nate cations may be rationalized if one assumes a dissociation that is controlled by kinetic rather than thermodynamic factors in conjunction with pronounced Franck-Condon effects.

III.6. Conclusions

The structures and energetics of $ROCOO^{\bullet/-}$ anions and neutrals (R = H, CH_3, C_2H_5, *i*-C_3H_7, and *t*-C_4H_9) in the gas phase are investigated theoretically. The results point out the structural differences between the anions and the radicals, which nevertheless enable to show experimentally that both of the species are intrinsically stable in the gas phase. Bond-separation reactions and atomization energies are used to determine the standard heats of formation of alkylcarbonate anions and radicals. The comparison of the two methods shows a good agreement as a deviation of less than 1 kcal/mol is obtained between the enthalpies of formation.

The unimolecular reactivity of metastable alkylcarbonate ions is mostly controlled by thermochemistry, which favors hydrogen transfer for R = CH_3 and C_2H_5, and decarboxylation for R =H, *i*-C_3H_7, and *t*-C_4H_9. At larger energies, decarboxylation becomes the main dissociation process for all $ROCOO^-$ anions, which is interpreted in terms of a kinetically controlled dissociation. Comparison of the $^-NR^+$ and the $^-CR^+$ spectra of the alkylcarbonate anions leads to the identification of only one dissociation process for the neutral radicals $ROCOO^{\bullet}$, which corresponds to C – O bond cleavage leading to the fragments $RO^{\bullet}$ and CO_2. The investigation of other dissociation channels is hindered by the extensive fragmentations observed in the experiments and the multiple mass overlaps, but even though the contribution of other decomposition pathways cannot be ruled out strictly, they appear unlikely from a thermochemical point of view.

III.7. References

1. Hayes, R. N.; Waugh, R. J.; Bowie, J. H., *Rapid Commun. Mass Spectrom.* **1989**, *3*, 338.

2. Iraqi, M.; Goldberg, N.; Schwarz, H., *Int. J. Mass Spectrom. Ion Processes* **1993**, *124*, R7.

3. Quinn, R.; Zent, A. P.; McKay, C. P., *Astrobiology* **2006**, *6*, 581.

4. Schalley, C. A.; Hornung, G.; Schröder, D.; Schwarz, H., *Chem. Soc. Rev.* **1998**, *27*, 91.

5. Squires, R. R., *Int. J. Mass Spectrom. Ion Processes* **1992**, *117*, 565.

6. Alexeev, Y.; Windus, T. L.; Zhan, C.-G.; Dixon, D. A., *Int. J. Quantum Chem.* **2005**, *102*, 775.

7. Alexeev, Y.; Windus, T. L.; Zhan, C.-G.; Dixon, D. A., *Int. J. Quantum Chem.* **2005**, *104*, 379.

8. George, P.; Bock, C. W.; Trachtman, M., *J. Comput. Chem.* **1982**, *3*, 283.

9. Johnson III, R. D., NIST Computational Chemistry Comparison and Benchmark Database, NIST Standard Reference Database Number 101, Release 12, Aug. 2005 (http://srdata.nist.gov/cccbdb).

10. Maier, W. F.; Reetz, M. T., *J. Am. Chem. Soc.* **1975**, *97*, 3687.

11. Reetz, M. T.; Maier, W. F., *Theor. Chim. Acta* **1974**, *35*, 163.

12. Schröder, D.; Goldberg, N.; Zummack, W.; Schwarz, H.; Poutsma, J. C.; Squires, R. R., *Int. J. Mass Spectrom. Ion Processes* **1997**, *165/166*, 71.

13. Tajima, S.; Sekiguchi, O., *J. Mass Spectrom. Soc. Jap.* **1996**, *44*, 133.

14. Audier, H. E., *Analusis* **1993**, *21*, 15S.

15. Bowen, R. D., *Acc. Chem. Res.* **1991**, *24*, 364.

16. Holmes, J. L.; Lossing, F. P.; Terlouw, J. K.; Burgers, P. C., *J. Am. Chem. Soc.* **1982**, *104*, 2931.

17. Terlouw, J. K.; Heerma, W.; Dijkstra, G.; Holmes, J. L.; Burgers, P. C., *Int. J. Mass Spectrom. Ion Phys.* **1983**, *47*, 147.

18. Armstrong, D. A.; Waltz, W. L.; Rauk, A., *Can. J. Chem.* **2006**, *84*, 1614.

19. Armstrong, D. A.; Waltz, W. L.; Rauk, A., *Can. J. Chem.* **2007**, *85*, 239.

20. Schröder, D.; Soldi-Lose, H.; Schwarz, H., *Aust. J. Chem.* **2003**, *56*, 443.

21. Benassi, R.; Taddei, F., *THEOCHEM* **1994**, *303*, 101.

22. Levsen, K.; Schwarz, H., *Mass Spectrom. Rev.* **1983**, *2*, 77.

23. Hunton, D. E.; Albertoni, C. R.; Märk, T. D.; Castleman, A. W., Jr., *Chem. Phys. Lett.* **1984**, *106*, 544.

24. Mercer, R. S.; Harrison, A. G., *Can. J. Chem.* **1988**, *66*, 2947.

25. Leung, K.; Nielsen, I. M. B.; Kurtz, I., *J. Phys. Chem. B* **2007**, *111*, 4453.

26. Sheldon, J. C.; Bowie, J. H., *J. Am. Chem. Soc.* **1990**, *112*, 2424.

27. Bowie, J. H.; Blumenthal, T., *J. Am. Chem. Soc.* **1975**, *97*, 2959.

28. Goldberg, N.; Schwarz, H., *Acc. Chem. Res.* **1994**, *27*, 347.

29. McMahon, A. W.; Chowdhury, S. K.; Harrison, A. G., *Org. Mass Spectrom.* **1989**, *24*, 620.

30. Bowen, R. D.; Williams, D. H.; Schwarz, H., *Angew. Chem., Int. Ed.* **1979**, *18*, 451.

31. Holmes, J. L.; Terlouw, J. K., *Org. Mass Spectrom.* **1980**, *15*, 383.

32. Laskin, J.; Lifshitz, C., *J. Mass Spectrom.* **2001**, *36*, 459.

33. Schröder, D.; Heinemann, C.; Schwarz, H.; Harvey, J. N.; Dua, S.; Blanksby, S. J.; Bowie, J. H., *Chem. Eur. J.* **1998**, *4*, 2550.

34. Iraqi, M.; Goldberg, N.; Schwarz, H., *Int. J. Mass Spectrom. Ion Processes* **1993**, *124*, R7.

35. Burgers, P. C.; Holmes, J. L.; Mommers, A. A., *Int. J. Mass Spectrom. Ion Processes* **1983**, *54*, 283.

36. van Baar, B.; Burgers, P. C.; Terlouw, J. K.; Schwarz, H., *J. Chem. Soc., Chem. Commun.* **1986**, 1607.

37. Stevenson, D. P., *Discuss. Faraday Soc.* **1951**, *10*, 35.

38. Linstrom, P. J.; Mallard, W. G., (Eds.), NIST Chemistry WebBook, NIST Standard Reference Database Number 69, National Institute of Standards and Technology, Gaithersburg MD, 20899, June 2005 (http://webbook.nist.gov).

39. Schröder, D.; Soldi-Lose, H.; Schwarz, H., *Aust. J. Chem.* **2003**, *56*, 443.

40. Schröder, D.; Schalley, C. A.; Harvey, J. N.; Schwarz, H., *Int. J. Mass Spectrom.* **1999**, *185/186/187*, 25.

41. Hornung, G.; Schalley, C. A.; Dieterle, M.; Schröder, D.; Schwarz, H., *Chem. Eur. J.* **1997**, *3*, 1866.

42. Stevenson, D. P., *Discuss. Faraday Soc.* **1951**, *10*, 35.

43. Schwarz, H., *Int. J. Mass Spectrom.* **2004**, *237*, 75.

44. Enos, C. S.; Brenton, A. G.; Lee, A. R., *Int. J. Mass Spectrom. Ion Processes* **1992**, *122*, 361.

45. Herzberg, G., *Molecular Spectra and Molecular Structure. Volume III- Electronic Spectra and Electronic Structure of Polyatomic Molecules*; Van Nostrand: Princeton, 1950.

46. Aschi, M.; Harvey, J. N.; Schalley, C. A.; Schröder, D.; Schwarz, H., *Chem. Commun.* **1998**, 531.

47. Lossing, F. P., *J. Am. Chem. Soc.* **1977**, *99*, 7526.

IV. Translational Energy Spectra of $CO_2^{\bullet+}$ formed by Charge Reversal and Neutralization Reionization of Methylcarbonate

IV.1. Introduction

As for the other alkylcarbonates investigated, the $^{-}$NIDD^{+} study of methylcarbonate (section III.5) has shown that the $CO_2^{\bullet+}$ fragment bears a negative intensity in the NIDD spectrum, which was quite surprising. The CH_3OCOO^+ ion formed from vertical charge transfer from methylcarbonate is instead expected to dissociate mostly into CH_3O^+ and CO_2 rather than into $CH_3O^{\bullet}$ and $CO_2^{\bullet+}$.[1,2] Concerning the $CH_3OCOO^{\bullet}$ radical, a $CH_3O^{\bullet} - CO_2$ bond cleavage leads to the fragments $CH_3O^{\bullet}$ and CO_2 which further undergo reionization into CH_3O^+ and $CO_2^{\bullet+}$.[3] The $CO_2^{\bullet+}$ ion is thus expected to be more present in processes related to the neutral chemistry as in processes related to the cation one. Nevertheless, the $CO_2^{\bullet+}$ signal is negative in the NIDD spectrum of methylcarbonate (Figure III.5-2b). In Chapter III, it was concluded that this feature could be explained assuming that dissociation of the CH_3OCOO^+ ion formed by vertical charge transfer from the corresponding anion is controlled by kinetic rather than by thermodynamic factors and that pronounced Franck-Condon effects are operative which favors formation of the ionic fragment $CO_2^{\bullet+}$ instead of CH_3O^+. As this assumption was not probed any further, the present chapter is dedicated to the study of the energetics associated with the formation of the $CO_2^{\bullet+}$ ion obtained from charge-reversal (CR) and neutralization-reionization (NR) experiments of methylcarbonate. The aim of this investigation is to achieve more insight about the mechanisms of formation of $CO_2^{\bullet+}$ from these two processes and to try to understand why formation of $CO_2^{\bullet+}$ is more favored at the cationic than at the neutral stage. To this end, the translational energies of $CO_2^{\bullet+}$ formed from CR and NR experiments of CH_3OCOO^- have been determined and compared to that of the parent ion CH_3OCOO^-, using high resolution translational energy loss spectroscopy (HRTELS). This comparison enables to

determine the translational energy of $CO_2^{\bullet+}$ which has been lost and hence to evaluate the energetics associated with the formation of this ion.

The processes investigated in this study consist of charge-transfer reactions which are induced by collisions with molecular oxygen and are followed by dissociation. In order to obtain information from the corresponding translational energy spectra, the processes investigated have been simplified according to the following well-known postulates.

(i) The system under study is considered as isolated, i.e. no interactions with its environment can occur and the total (kinetic and potential) energy remains constant. The energy required for the charge-transfer and dissociation processes may thus only originate from the energy available in the system. As the system is constituted initially of the parent ion and the neutral target which is at rest, the energy required is exclusively obtained from the kinetic energy of the parent which is converted into internal energy by collision. Measurement of the kinetic energy loss in the course of the experiment enables therefore to access the energetics of the charge-transfer and dissociation processes.

(ii) Charge transfer and dissociation processes are considered using the two-step model developed by Los and Govers.[4] Initially, this model was proposed in the collision-activated decomposition (CAD) study of diatomic ions and has been extended to larger systems and to dissociative charge-transfer (DCT) processes.[5] It consists to consider the CAD or DCT process to occur in two steps. The first step is the collision between the ion and the neutral target; the second is the dissociation of the molecule (see Scheme IV.1-1 for the example of a dissociative charge-reversal process).

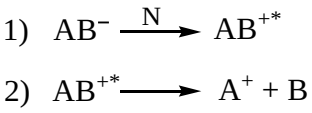

Scheme IV.1-1: The two reactions that constitute the two steps model.

The validity of the two-step model only concerns collisions performed in the keV regime and is based on a theoretical argument comparing the collision time with the molecular vibration. Using this model enables a significant simplification of the processes under study: in the first-step, only the electronic excitation of the parent ion is considered to occur whereas in the second step, its dissociation is the only process taking place.[6]

(iii) The neutral collision gas is treated as a passive target and its role is in helping in the expulsion of one (or more) electron(s) from the parent ion. This assumption has the advantage

to enable considering that the collision gas, which is initially at rest, does not undergo any electronic excitation in the course of the collision and, thus, that the kinetic energy of the ions which is converted into internal energy is exclusively imparted to the ionic beam. This hypothesis has been justified by Cooks *et al.*[7] which have shown mathematically that the kinetic energy transferred to the neutral target is negligible compared to that transferred to the ions.

This chapter consists of four parts. The first part is dedicated to the determination of the experimental error which is due to the charge-transfer processes and which is unknown for our instrument. The second part presents the experimental results including the measurements of the kinetic energy losses associated with the processes investigated. As theory was of great interest in this work to help in the understanding of the experimental results, some *ab initio* calculations have been performed and are presented in the third part of this chapter. Finally, in the fourth part, a comparison between experiment and theory is made as well as an analysis of the results is given.

IV.2. Experimental Error due to Charge-Transfer Processes

The aim of this study is to use energy-resolved collision experiments to access more insights into the dissociation mechanisms of $CH_3OCOO^{\bullet}$ and CH_3OCOO^{+} into $CH_3O^{\bullet}$ and CO_2 and $CH_3O^{\bullet}$ and $CO_2^{\bullet+}$, respectively, when these species are formed by vertical charge transfer (CT) from the corresponding anion. Such a study involves two types of processes, charge transfer and dissociation, and requires a good knowledge of the experimental errors which may result when these processes take place. This holds particularly true for vertical charge transfers for which the reliability of the results obtained with our instrument was unknown. Determination of vertical ionization energies or electron affinities using energy-resolved collision experiments is a method already well-known in literature and results are generally in accordance with those obtained by other methods.[8,9] A correction factor related to an intrinsic error of the instrument may nevertheless need to be applied,[5] which has thus to be verified and determined prior to any further investigation.

Monoatomic ions are relevant systems to determine the experimental errors obtained for CT processes. As no rovibrational excitation is occurring, the energy lost during the CT process can indeed be directly related to the ionization energy and/or electron affinity of these atoms. The thermodynamic quantities of common monoatomic ions are moreover accurately known which thus allows a precise determination of the error due to the instrument.

Experimentally, minimum translational energies losses are accessible. For a charge-transfer process ($^{-}CR^{+}$ or $^{-}NR^{+}$), these are defined for atomic ions $X^{\bullet}$ as follow:

$$Q_{min,CR,exp.}(X^{+}) = IE(X^{\bullet}) + EA(X^{\bullet}) + \delta_{CR}(X^{\bullet}) \qquad \text{(IV.2-1)}$$

$$Q_{min,NR,exp.}(X^{+}) = IE(X^{\bullet}) + EA(X^{\bullet}) + \delta_{NR}(X^{\bullet}) \qquad \text{(IV.2-2)}$$

where $Q_{min,CR,exp.}(X^{+})$ and $Q_{min,NR,exp.}(X^{+})$ are the kinetic energies lost in the course of a $^{-}CR^{+}$ or of a $^{-}NR^{+}$ process performed on an atomic ion and $\delta_{CR}(X^{+})$ and $\delta_{NR}(X^{+})$ correspond to the experimental deviations due to the instrument in the CR and in the NR processes of an atomic ion X^{-}, respectively. $IE(X^{\bullet})$ and $EA(X^{\bullet})$ are the ionization energy and the electron affinity of the atom $X^{\bullet}$.

In order to quantify the deviation terms δ_{CR} and δ_{NR}, and further determine the correction factor which has to be applied, the experimental kinetic energy losses $Q_{min,CR,exp.}$ and $Q_{min,NR,exp.}(X^{+})$ have to be compared to the theoretical energy losses $Q_{min,CR,theory}$ or $Q_{min,NR,theory}(X^{+})$ defined by Equations (IV.2-1) and (IV.2-2), respectively, when $\delta_{CR}(X^{\bullet})$ and $\delta_{NR}(X^{\bullet})$ are equal to 0.

One has to note that a rigorous treatment would require to consider that the minimum translational energy loss is not only constituted by *IE* and *EA*, but that other terms as the translational and excitation energy imparted to the collision gas and the energy of the ejected electrons must also be taken into account. However, it has been shown by Ast[10] and Cooks[7] that these terms can be neglected. Furthermore, the energy loss represents a minimal value because the population of excited electronic states of the ions leads to larger energy defects.

In this study, four monoatomic ions have been investigated: O, $Cl^{\bullet}$, $Br^{\bullet}$, and $I^{\bullet}$. These atoms differ by their *m/z* ratios, *IE*s, and *EA*s (Table IV.2-1) which can thus enable to determine if some intrinsic factors of the ions submitted to experiment may influence the resulting experimental error.

For these atomic ions, kinetic-energy resolved experiments have been recorded following a strict procedure. As the aim of these experiments consists in the determination of the kinetic energy losses during CT processes (CR or NR) of monoatomic ions, two types of translational energy (TE) had thus to be compared, those before and those after the charge transfer. The former ones correspond to the TE of ions X^{-} which do not experience any collision and the latter ones, to the TE of the ions X^{+} obtained from X^{-} by charge reversal or neutralization reionization. Consequently, the experimental conditions (instrument optimization, etc.) have

to be the same to allow for a relevant comparison between these two TEs values. Furthermore, as the ESA voltage may undergo some temporal variation, the spectra to be compared have to be recorded one after the other. One "complete" experiment has therefore consisted of the record of the spectra of X^-, X^+ (CR) and X^+ (NR), X^-. Any unwanted variation of the ESA voltage could thus easily be detected and the corresponding experiment discarded. An example of the TE spectra obtained for the four monoatomic ions investigated is given in Figure IV.2-1.

Table IV.2-1

Ionization energies, electron affinities and *m/z* ratios of the atomic species investigated.

	IE[a] (eV)	*EA*[b] (eV)	*m/z*
^{16}O	13.62	1.46	16.0
$^{35}Cl^{\bullet}$	12.97	3.61	35.5
$^{79}Br^{\bullet}$	11.81	3.36	79.9
$^{127}I^{\bullet}$	10.45	3.06	126.9

[a] Obtained from NIST.[11]

[b] Obtained from the following references: O,[12] Cl,[13] Br,[14] and I.[15]

For each monoatomic ion studied, the TEs of X^+ obtained by CR are shifted towards smaller values compared to those of X^+ obtained by NR. The corresponding kinetic energies losses are accordingly larger for X^+ (CR) than for X^+ (NR) and the experimental deviation is thus different according to the process considered because the energy required to perform the charge transfer is in theory the same (i.e. *IE* + *EA*).

Furthermore, the TE signals of X^+ obtained from CR and NR do not have a Gaussian-type shape like the TE signal of X^-, but are enlarged for smaller TE values (Figures IV.2-1 and IV.2-2a). This effect is attributed to the population of excited electronic states of X^+ which are accessible when a sufficient amount of TE of the ion is converted into internal energy.[5] The experimental peaks can thus be represented by a sum of several Gaussian curves, each of them representing the population of an electronic level of X^+, as schematized in Figure IV.2-2b.

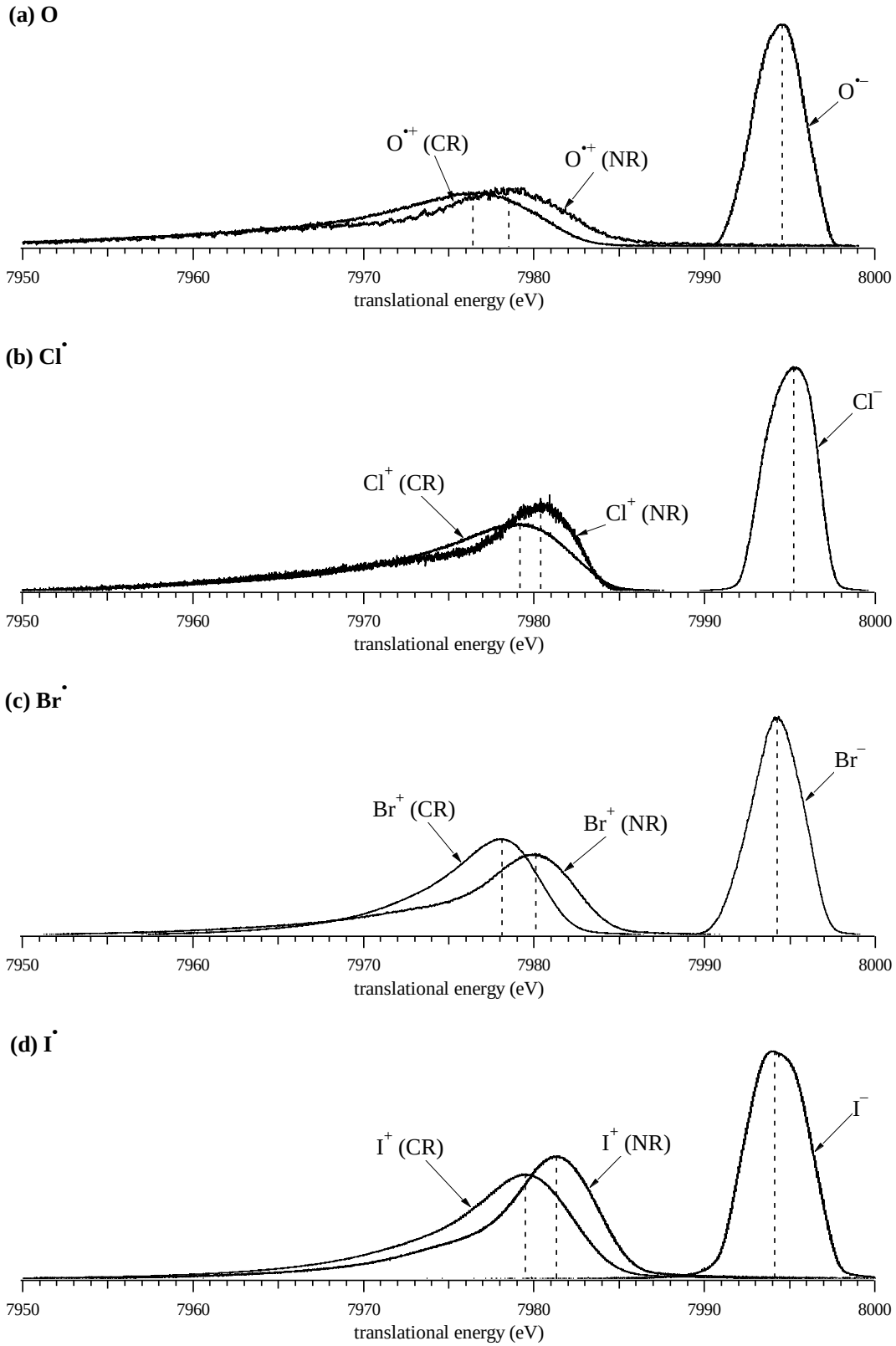

Figure IV.2-1: Translational energy spectra of the ions X^- and X^+ formed by CR and NR of X^- for the atomic gases (a) O, (b) $Cl^•$, (c) $Br^•$, and (d) $I^•$ (Each graph corresponds to the superposition of three spectra). The CR and NR experiments were performed using B1 for mass selection while E1 was scanning; the collision gas used was O_2 (CR: C2, 80 % T; NR: C2/C3, 80 %).

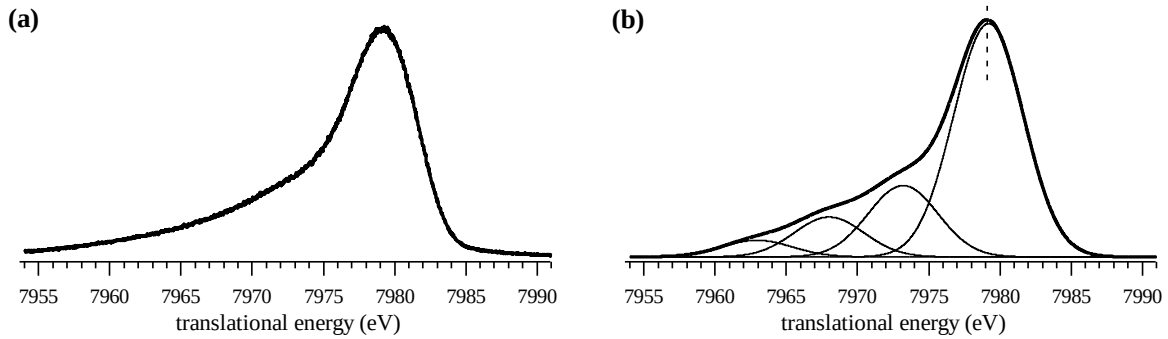

Figure IV.2-2: (a) Experimental and (b) simulated translational energy spectra of Br^+ obtained from NR of Br^-. The spectrum (b) is composed of four Gaussians curves (thin line), each of them representing an electronic energy level of Br^+ and whose sum is the bold shape. It has to be noted that the peak (b) is a schematization of the peak (a), i.e. the Gaussians curves shown do not represent the real electronic levels of Br^+.

It would be also plausible to consider that the parent ions X^- are formed in the source in different electronic states. The formation of a mixture of electronically excited states is in fact much more likely to occur than that of ions only in the ground electronic state.[5,16,17] The chemical ionization (CI) method used in this work is a soft method which reduces the excitation of the ions formed,[18] but which cannot completely avoid it.[19] Nevertheless, as we are dealing here with monoatomic ions and as only electronic excitation of the ions take place (no rovibrational excitation), it seems thus quite justified to consider that the mass-selected beam of parent ions is constituted almost exclusively by ions in a ground electronic state.[5,7]

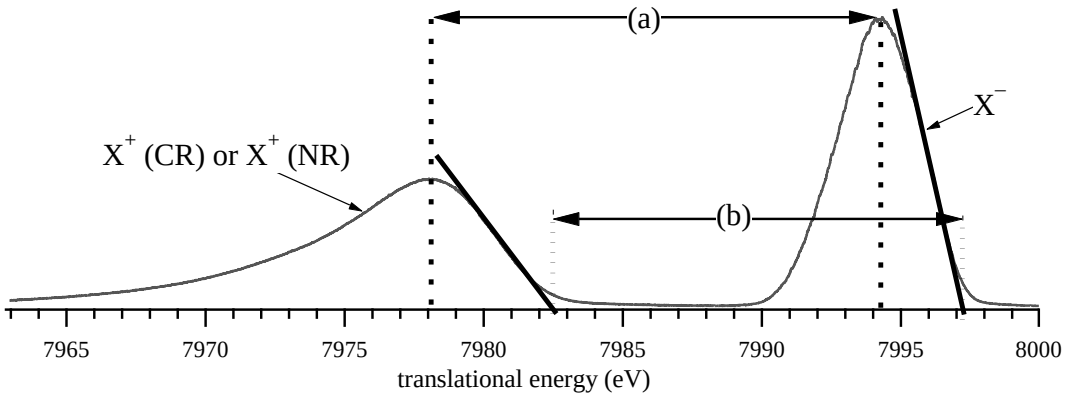

Figure IV.2-3: The two methods to measure the translational energy losses $Q_{min,CR,exp.}$ or $Q_{min,NR,exp.}(X^+)$. The translational energies of the parent and fragment ions are obtained from (a) the top of the peaks or (b) by the extrapolation of the high-energy onset of the ion signals to the baseline.

Moreover, the quantities $Q_{min,CR,exp.}$ and $Q_{min,NR,exp.}(X^+)$, as defined in Equations (IV.2-1) and (IV.2-2) are obtained by subtracting the TE of the ion X^+ obtained by CR or NR to the TE of the initial ion X^-. To measure these two TEs, two possibilities exist, they can either be measured directly at the top of the peak,[8] or obtained by extrapolating the high-energy onset of the ion signals to the baseline (Figure IV.2-3).

The two methods to measure the TEs have been applied to the spectra of the atomic ions and also to the spectra of methylcarbonate and of $CO_2^{\bullet+}$ formed by CR or NR from CH_3OCOO^- (section IV.3). Particularly for the $CO_2^{\bullet+}$ ion, the reproducibility of the results obtained by the measurement of the TEs from the onsets was not satisfying. In this case, the standard deviation associated with the results obtained is indeed as large as 8.3 eV , whereas it is only ca. 1.5 eV for the TEs measured at the top of the peaks (Figure IV.2-4). As the reproducibility was an important criterion in this work to ensure the best evaluation of the energetic values searched, TEs have accordingly been measured only from the top of the ion peaks for all the systems investigated (the atomic ions, methylcarbonate and $CO_2^{\bullet+}$). For each monoatomic gas, the experiments have been performed several times (between three and nine). All the data collected are presented in Figure IV.2-5.

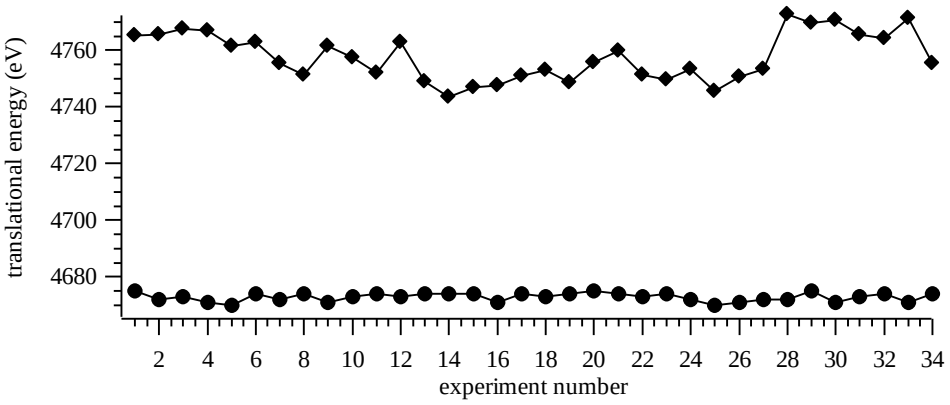

Figure IV.2-4: All TEs obtained for $CO_2^{\bullet+}$ formed by CR of CH_3OCOO^- when the TE is measured at the top of the peak (●) or obtained by extrapolation of the onset (♦). The standard deviations associated with these values are of 1.5 and 8.3 eV respectively. Each circle and diamond is related to particular experimental conditions (optimization, etc.). Accordingly, comparison of all data obtained enables one to show the degree of reproducibility of the results.

The results provided by all the experiments show a good reproducibility for each gas. The difference between the TEs of X^- and X^+ (CR or NR) is indeed rather constant (Figure IV.2-5). For each experiment, the kinetic energy losses $Q_{min,CR,exp.}$ and $Q_{min,NR,exp.}(X^+)$ have been

calculated and the results show that the standard deviations for the values obtained are in general smaller than 0.5 eV, which is rather satisfying and thus allow to use averages TE values for the ions considered (Table IV.2-2).

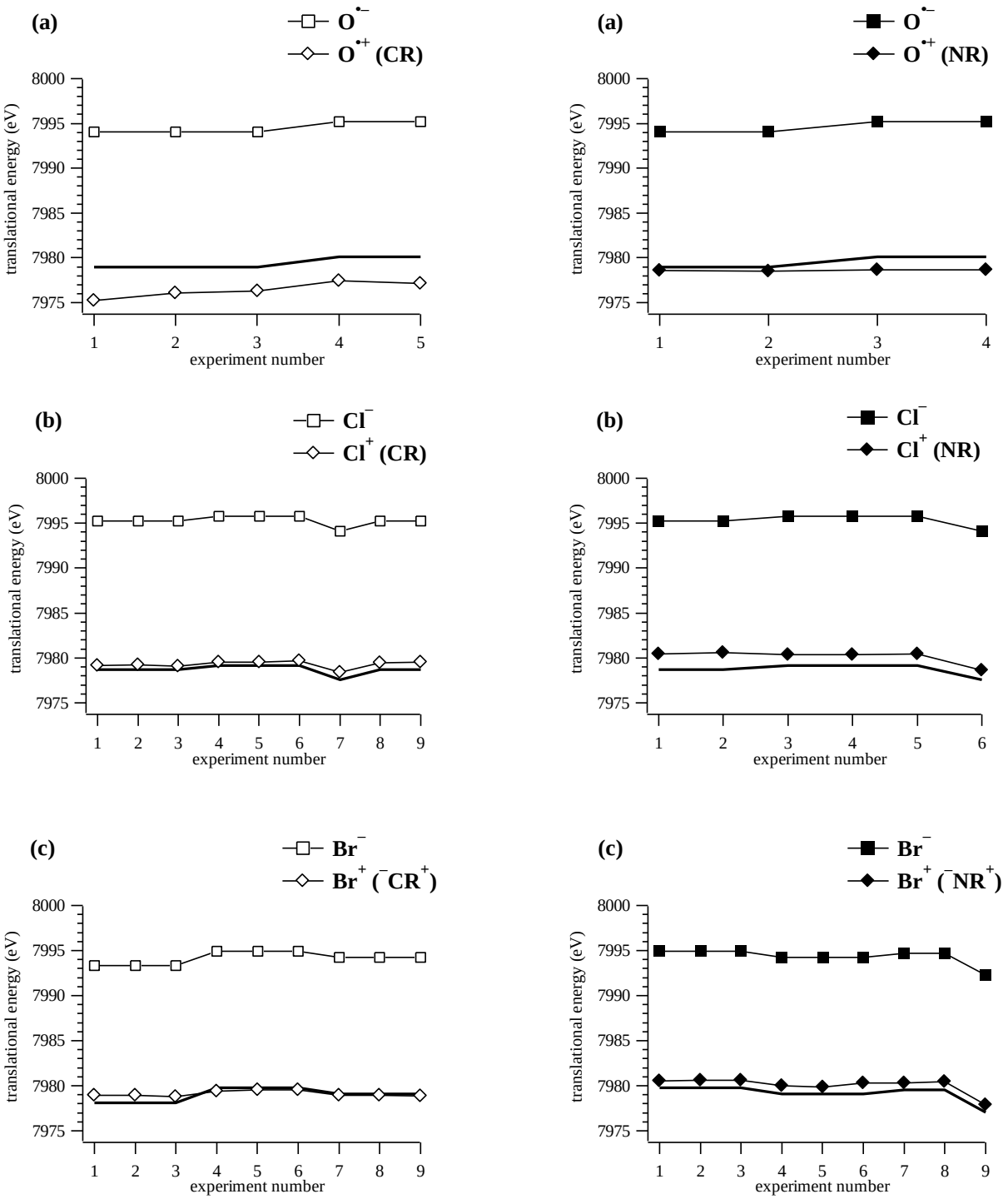

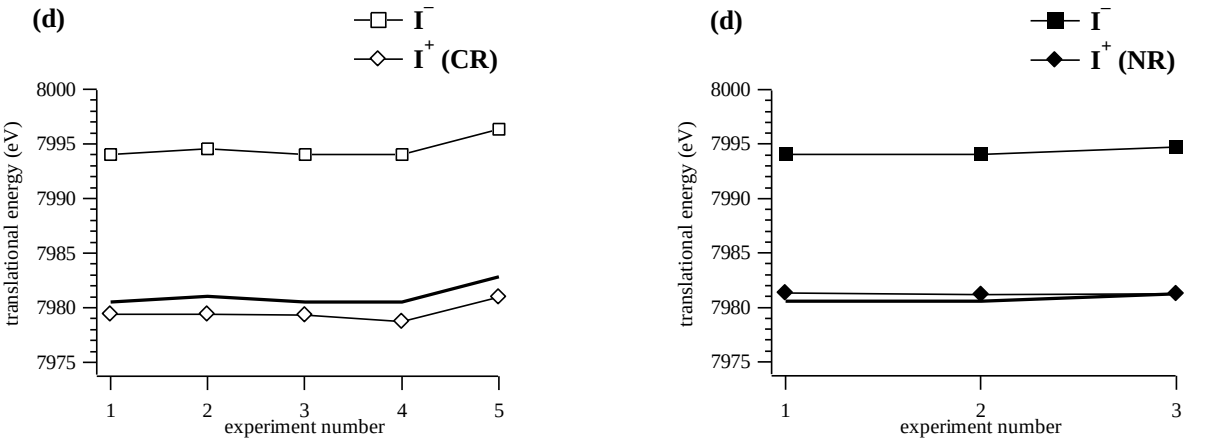

Figure IV.2-5: All TE values obtained for X^- and X^+ (formed by CR or NR of X^-) for the atomic gases (a) O, (b) $Cl^{\bullet}$, (c) $Br^{\bullet}$, and (d) $I^{\bullet}$. One experiment (termed 1,2,..) consists in the recording of the TE spectrum of the ion X^- followed by that of X^+ (CR or NR) (see text). Each experiment number is related to a square and a diamond of the same color (□/◊ or ■/♦) which correspond to average TEs of X^- and of X^+ (CR, white or NR, black). Further, in each graph, a bold line indicates the expected TE of X^+ (CR or NR), obtained by subtracting ($IE(X^{\bullet})$ - $EA(X^{\bullet})$) to the TE of X^-. As discussed above, these TEs values are measured on the tops of the peaks.

The experimental data obtained have further been compared to theory by determining the corresponding relative error. The general expression of the relative error χ used throughout this work is the following:

$$\chi = \frac{Q_{min,theory}(X^+) - Q_{min,exp.}(X^+)}{Q_{min,theory}(X^+)} \qquad \text{(IV.2-3)}$$

Using Equations (IV.2-1) and (IV.2-2), the relative errors $\chi_{CR}(X^+)$ and $\chi_{NR}(X^+)$ related to the CR and NR processes performed on the monoatomic ions X^- are thus defined as:

$$\chi_{CR}(X^{\bullet}) = \frac{-\delta_{CR}(X^+)}{IE(X^{\bullet}) + EA(X^{\bullet})}$$

$$\chi_{NR}(X^{\bullet}) = \frac{-\delta_{NR}(X^+)}{IE(X^{\bullet}) + EA(X^{\bullet})} \qquad \text{(IV.2-4)}$$

Table IV.2-2

Average and theoretical minimum translational energy losses, $Q_{min,CR,exp.}$, $Q_{min,NR,exp}$, $Q_{min,CR,theory}$ and $Q_{min,NR,theory}$ (X^+) (in eV), corresponding deviations to theory $\delta_{CR}(X^+)$ and $\delta_{NR}(X^+)$ (in eV) and relative errors $\chi_{CR}(X^+)$ and $\chi_{NR}(X^+)$ for $X^\bullet$ = O, $Cl^\bullet$, $Br^\bullet$ and $I^\bullet$.

		$Q_{min,CR,exp.}(X^+)^a$ or $Q_{min,NR,exp.}(X^+)^a$ (eV)	$Q_{min,CR,theory}(X^+)^b$ or $Q_{min,NR,theory}(X^+)^b$ (eV)	$\delta_{CR}(X^+)^c$ or $\delta_{NR}(X^+)^c$ (eV)	$\chi_{CR}(X^+)$ or $\chi_{NR}(X^+)$
O	CR	18.3 (0.5)	15.1	-1.2	8.0 %
	NR	16.0 (0.6)		-0.9	6.2 %
$Cl^\bullet$	CR	16.0 (0.2)	16.6	-0.6	3.4 %
	NR	15.2 (0.3)		-1.4	8.4 %
$Br^\bullet$	CR	15.1 (0.5)	15.2	0.9	-5.9 %
	NR	14.2 (0.1)		-1.0	6.5 %
$I^\bullet$	CR	14.9 (0.4)	13.5	1.4	-10.6 %
	NR	12.8 (0.1)		-0.7	5.3 %

[a] Average obtained using all TEs given in Figure IV.2-5. Standard deviation is indicated in brackets (eV).

[b] Corresponds to ($IE(X^\bullet)$ - $EA(X^\bullet)$) (Equations (IV.2-1) and (IV.2-2) with $\delta_{CR} = \delta_{NR} = 0$).

[c] Obtained by subtracting $Q_{min,CR,exp.}$ to $Q_{min,CR,theory}$ and $Q_{min,NR,exp.}$ to $Q_{min,NR,theory}$.

The relative errors χ_{CR} and χ_{NR} obtained for the reference gases are not constant. Considering the CR process, it varies from -10.6 % for $Br^\bullet$ to 8.0 % for O, and for the NR process, from 5.3 % for $I^\bullet$ to 8.4 % for O (Table IV.2-2). This shows that the deviation of the results compared to theory depends on some intrinsic parameters of the systems under study, because otherwise the relative error would have been expected to be constant. Among possible parameters which are expected to play a role, the mass of the system, the electron affinity and the ionization energy seem to be the most plausible because the processes involved consist in collision(s) leading to charge transfer. A the mass of the system, different expressions may be considered: the *m/z* ratio, the reduced mass μ, or the relative mass m_{rel} defined by:

$$\mu = \frac{m_{ion} \cdot m_T}{m_{ion} + m_T} \quad \text{and} \quad m_{rel} = \frac{m_{ion}}{m_{ion} + m_T} \tag{IV.2-5}$$

where m_{ion} and m_T are the masses of the ion X^- and of the target respectively.

The relations between the relative errors and the parameters cited above have been tested considering various combinations like *IE* • *EA*, *IE* + *EA*, *IE* • *EA* • m_{rel}, *IE* • *EA* / μ, etc. Among all combinations envisaged, the most satisfying results have been obtained with m_{rel} / (*IE* + *EA*) for the CR process and m_{rel} / (*EA*) for NR, showing a linear relation with correlation coefficients of 0.993 and 0.998 respectively (Figure IV.2-6).

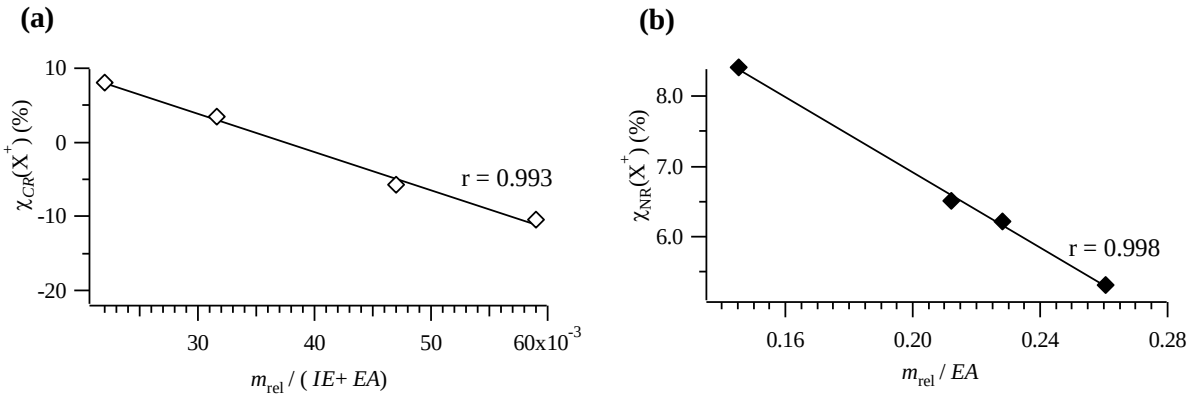

Figure IV.2-6: Variation of (a) the relative error $\chi_{CR}(X^+)$ as a function of m_{rel} / (*IE*+*EA*) and of (b) $\chi_{NR}(X^+)$ as a function of m_{rel} / *EA*. The values of $\chi_{CR}(X^+)$ and $\chi_{NR}(X^+)$ are taken from Table IV.2-2 and correspond to the deviation of the experimental kinetic energies losses for the atomic ions submitted to $^{-}CR^+$ (◊) and $^{-}NR^+$ (♦) experiments compared to theory. Linear fits (full line) are indicated for each type of experiments as well as the resulting correlation coefficients r.[20]

The best fits obtained show that the values for translational energies of the atomic ions depend on the relative mass of the system and on *IE* + *EA* and *EA* for CR and NR experiments, respectively. The fact that different terms influence the TEs measured for the CR and NR processes can be in part understood by considering the processes occurring. In the CR process, only one collision takes place, in which, at least, an amount (*IE* + *EA*) of kinetic energy is converted into internal energy. For the NR process, two collisions takes place, the first one leading to the conversion of at least an amount *EA* of kinetic energy into internal energy and the second one, to at least an amount *IE*. Thus, the energy converted in the course of the first collision in the NR process and of the unique collision in the CR one plays a role in the instrumental deviation. This effect is rather difficult to understand particularly for the NR process for which both of the collisions occurring would have been expected to play a role. Nevertheless, despite the fact that we are not able to completely understand and explain the effect observed, Equations (IV.2-6) and (IV.2-7) derived from the fits in Figure IV.2-6 will be further used to obtain an evaluation of the instrumental error which arises from charge

transfer processes. It is nevertheless important to remind that these equations do not pretend to describe exactly the deviation of the experiment, but that they only represent the best relation that has been found between the errors observed in the experimental results and the intrinsic parameters of the systems investigated.

$$\chi_{CT,\,CR}(\mathrm{X}^+) = 19.4 - 517.1 \cdot \frac{m_{\mathrm{rel}}}{IE + EA} \qquad \text{(IV.2-6)}$$

$$\chi_{CT,\,NR}(\mathrm{X}^+) = 12.3 - 26.8 \cdot \frac{m_{\mathrm{rel}}}{EA} \qquad \text{(IV.2-7)}$$

IV.3. Experimental Results

Following the procedure given in the previous section for monoatomic gases, the TE spectra of CH_3OCOO^- and $CO_2^{\bullet+}$ formed by charge reversal and neutralization reionization of CH_3OCOO^- have been recorded. An illustration of the spectra obtained is given in Figure IV.3-1. Some comments are made in the following section to explain the particular shape of the $CO_2^{\bullet+}$ peaks.

IV.3.1. $CO_2^{\bullet+}$ Peak Shape

As the peak shape of the CH_3OCOO^- ion corresponds to a Gaussian distribution (Figure IV.3-1a), ions obtained by simple processes like charge transfer or bond cleavage from CH_3OCOO^- are also expected to possess a Gaussian-like shape, except in three cases, which are the following:

(i) The signal is constituted by ions (in this case $CO_2^{\bullet+}$) formed by different processes.[5,9] The peak obtained thus results from the superposition of different signals.

(ii) Neighbor ions are also present in the signal.

(iii) $CO_2^{\bullet+}$ is formed by a process which releases kinetic energy. In such cases, the peak shape may not be Gaussian-like (See Chapter II, section II.2.8).[7]

Considering the CR process leading to the $CO_2^{\bullet+}$ ion, only a double charge transfer of CH_3OCOO^- followed by dissociation of the CH_3OCOO^+ ion is conceivable. Other possibilities like dissociation of CH_3OCOO^- into CO_2 and CH_3O^- followed by CT to CO_2 leading to $CO_2^{\bullet+}$ have been shown by Szulejko *et al.*[21] not to occur. The shape of the $CO_2^{\bullet+}$ (*m/z* = 44) peak observed (Figure IV.3-1b) can therefore only be explained by the presence of

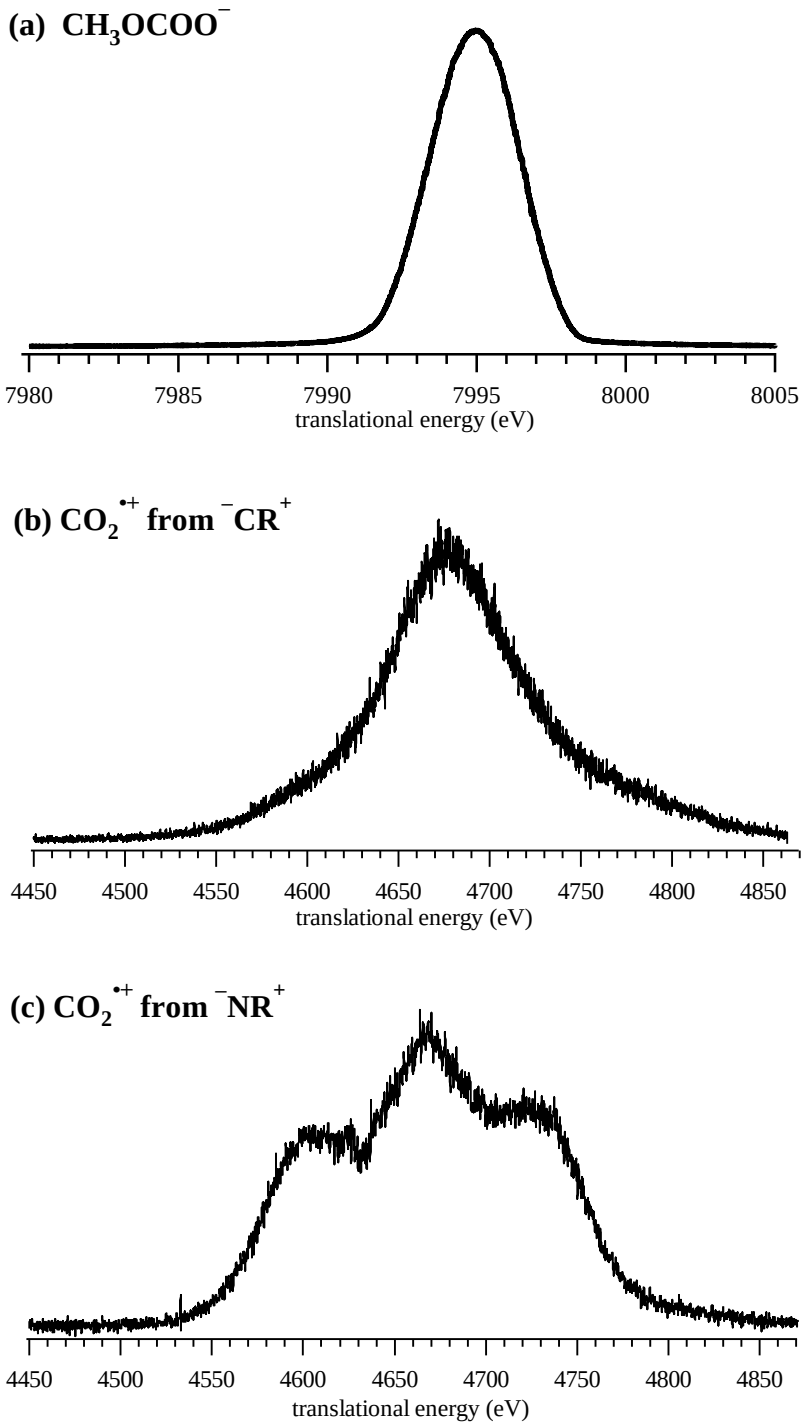

Figure IV.3-1: Translational energy spectra of (a) CH_3OCOO^- and $CO_2^{\bullet+}$ obtained from (b) $^-CR^+$ and (c) $^-NR^+$ of CH_3OCOO^-. CR and NR experiments were performed using B1 for mass selection while E1 was scanning; the collision gas used was O_2 (CR: C2, 80 % T; NR: C2/C3, 80 %).

neighbor ions, CO_2H^+ at *m/z* = 45 and CH_3CO^+ at *m/z* = 43 (or CH_3OC^+,[22] see Chapter III, section III.5). These two ions appear indeed in the $^-CR^+$ spectrum of CH_3OCOO^- (Table III.3-1) with an intensity relative to $CO_2^{\bullet+}$ of 3 and 17, respectively, and should accordingly be

present in the recorded TE spectrum of this process. The signal shown in Figure IV.3-1b can therefore be considered as the sum of three Gaussians-like signals, which correspond to $CO_2^{\bullet+}$, CO_2H^+ and CH_3CO^+ formed from dissociation of CH_3OCOO^+ obtained by vertical double charge transfer of CH_3OCOO^-. The general expression of a Gaussian curve is the following:

$$G(x) = A \cdot \exp(-(x - x_0)^2 / b) \qquad \text{(IV.3-1)}$$

where A, x_0, and b are the peak height, the position of the center of the peak, and a constant (> 0), respectively.

We have thus tried to model the signal observed in Figure IV.3-1b by three Gaussian curves. An example of one of the best fits obtained is given in Figure IV.3-2.

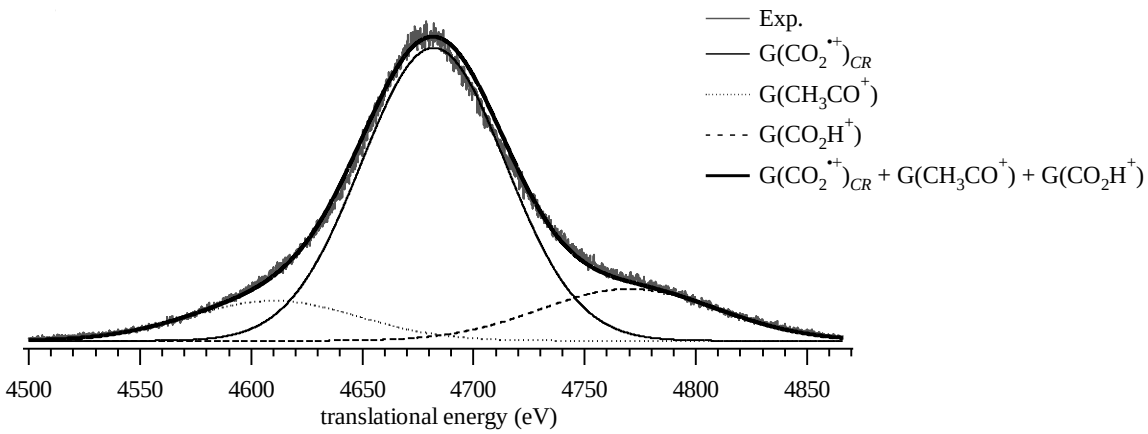

Figure IV.3-2: Fit of the TE signal of $CO_2^{\bullet+}$, CH_3CO^+, and CO_2H^+ formed from dissociation of CH_3OCOO^+ obtained by CR from CH_3OCOO^-.

Concerning the signal resulting from the NR process (Figure IV.3-1c), the signal shape is more complex to analyze because (i) it originates from different mechanisms of formation of $CO_2^{\bullet+}$ and (ii) among these processes, one is releasing kinetic energy.[23-25] This process most likely corresponds to dissociation of neutral $CH_3OCOO^{\bullet}$ and results in an ion discrimination along the z axis accompanied with a broadening of the signal. The two "tops on the extremities" of the signal in Figure IV.3-1c are attributed to this process, i.e. formation of $CO_2^{\bullet+}$ by vertical ionization of CO_2 (second collision cell) which is a dissociation product of $CH_3OCOO^{\bullet}$ formed by vertical charge transfer from the corresponding anion (first collision cell). Furthermore, as mentioned in Chapter II, the investigation of the dissociation of neutral

species in NRMS spectra is often obscured by competitive dissociations of the ionic species which are also formed in the course of this process. This feature appears in the signal in Figure IV.3-1c, and leads to the central peak which is attributed to fragmentation of transient CH_3OCOO^+ obtained by NR of CH_3OCOO^-. Neutralization of CH_3OCOO^- in the collision cell C2 (Figure II.2-1) leads indeed to transient $CH_3OCOO^\bullet$ which either dissociate or survive until they reach the collision cell C3 and then undergo reionization into CH_3OCOO^+. The latter can further give rise to $CO_2^{\bullet+}$ and $CH_3O^\bullet$, as observed in the CR experiment (see above). $CO_2^{\bullet+}$ is therefore formed from dissociation of $CH_3OCOO^\bullet$ or of CH_3OCOO^+. The signal in Figure IV.3-1c can thus be modeled by two curves, one associated to the formation of $CO_2^{\bullet+}$ from neutral methylcarbonate and the other one to the formation of $CO_2^{\bullet+}$ from methoxy-carboxy cation. The latter has a Gaussian-type shape (by reference to the CR process, Figure IV.3-2) whereas the former is the multiplication product of a positive Gaussian curve, $G(CO_2^{\bullet+})_{NR}$ and of a negative one, $G(CO_2^{\bullet+})_{NR,lost}$, which represent the ions $CO_2^{\bullet+}$ formed from dissociation of $CH_3OCOO^\bullet$ followed by reionization and those lost due to the kinetic energy released and the resulting discrimination along the z-axis (Figure IV.3-3). The negative Gaussian, $G(CO_2^{\bullet+})_{NR,lost}$, is defined according to the general equation:

$$G(x)_{lost} = 1 - A \cdot \exp(-(x - x_0)^2 / b) \qquad \text{(IV.3-2)}$$

where A, x_0, and b are defined as in Equation (IV.3-1).

In contrast to the signal modeled in Figure IV.3-2, the neighbor ions of $CO_2^{\bullet+}$, i.e. CH_3CO^+ and CO_2H^+, have not been included in the fit of the NR signal even though these ions also appear in the $^-NR^+$ spectrum of methylcarbonate (Table III.3-1). Inclusion of these two ions in the model could indeed not lead to satisfying results, mostly because the signal is already constituted by several Gaussian curves and the further inclusion of new parameters would make the modeling rather complex, if not meaningless.

The example of one of the fits obtained in Figure IV.3-3 is not as good as the fits of the CR signal (Figure IV.3-2). The bold curve does not completely match the signal experimentally observed, but its shape is in general rather similar. The full-line curve represents the ions $CO_2^{\bullet+}$ formed from dissociation of transient CH_3OCOO^- followed by reionization and, as already mentioned, is the multiplication product of the ions formed ($G(CO_2^{\bullet+})_{NR}$) by the ions lost ($G(CO_2^{\bullet+})_{NR,lost}$).

The best parameters of the Gaussian curves used to model the $CO_2^{\bullet+}$ signals are given in Table IV.3-1. Rather little information concerning the elementary processes occurring can be

deduced from these parameters as they only correspond to models and do not match perfectly the experimental shape, but as shown below, they will be helpful for the extraction of values of translational energies from the experimental signals.

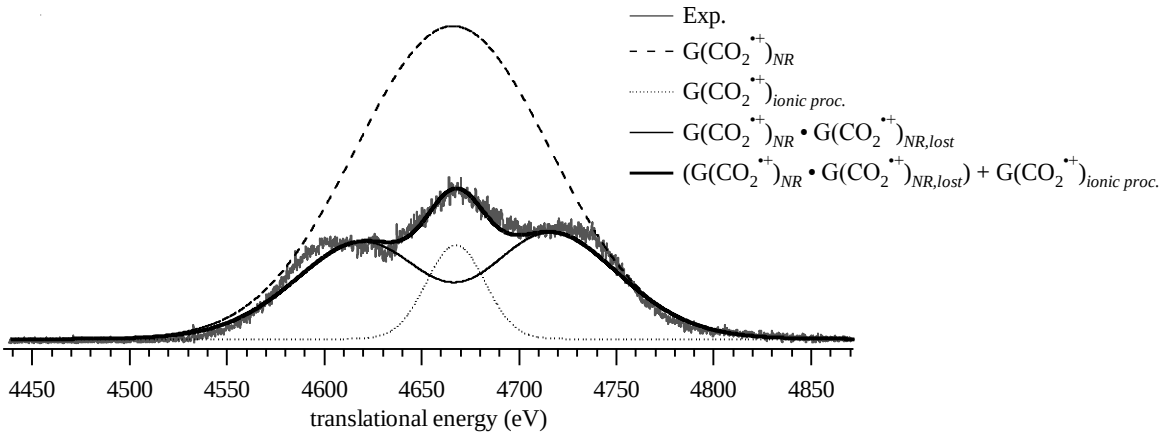

Figure IV.3-3: Fit of the TE signal of $CO_2^{\bullet+}$ formed from dissociation of CH_3OCOO^+ obtained by NR from CH_3OCOO^-.

Table IV.3-1

Height A, position of the center of the peak x_0 (eV), and constant b of the Gaussians functions[a] used to model the peaks in Figure IV.3-1. These values correspond to the curves shown in Figures IV.3-2 and IV.3-3. The peak height A is given for normalized spectra.

		A	x_0[c] (eV)	b
G	$(CO_2^{\bullet+})_{CR}$	$3.9 \bullet 10^{-4}$	4682	2100
	$(CO_2^{\bullet+})_{NR}$	$6.5 \bullet 10^{-4}$	4667	5000
	$(CO_2^{\bullet+})_{NR,lost}$[b]	1 - 0.8	4667	3700
	$(CO_2^{\bullet+})_{ionic\ proc.}$	$1.95 \bullet 10^{-4}$	4667	450
	(m/z = 43)	$2.6 \bullet 10^{-4}$	4610	4300
	(m/z = 45)	$2.73 \bullet 10^{-4}$	4775	12600

[a] If not state otherwise, the Gaussian curve have the form expressed in Equation (IV.3-1).

[a] The Gaussian curve has the expression given in Equation (IV.3-2).

[c] x_0 represents the position of the top of the corresponding Gaussian.

IV.3.2. Evaluation of $IE_v(CH_3OCOO^{\bullet})$, $EA_v(CH_3OCOO^{\bullet})$, $\Delta_r H°(CH_3O^{\bullet} + CO_2)$, and $\Delta_r H°(CH_3O^{\bullet} + CO_2^{\bullet+})$

Charge Reversal

Charge-transfer experiments take place when a sufficient amount of kinetic energy of the parent ion is converted into internal energy through collision. In Figure IV.3-4, the dominant mechanism of a CR experiment leading to $CO_2^{\bullet+}$ is presented. Once the cation is formed by CR of methylcarbonate, two scenarios are possible: either it dissociates directly or dissociation takes place after vibrational relaxation. Both scenarios may occur simultaneously and their presence mostly depends on the structures of the cation and of its precursor. If the geometries of the anion and of the cation obtained by vertical CT are similar, CR will lead to the formation of a cation with rather little rovibrational excitation. In contrast, if the geometries are different, the cation can be highly rovibrationally excited or even formed in a dissociative state.[26]

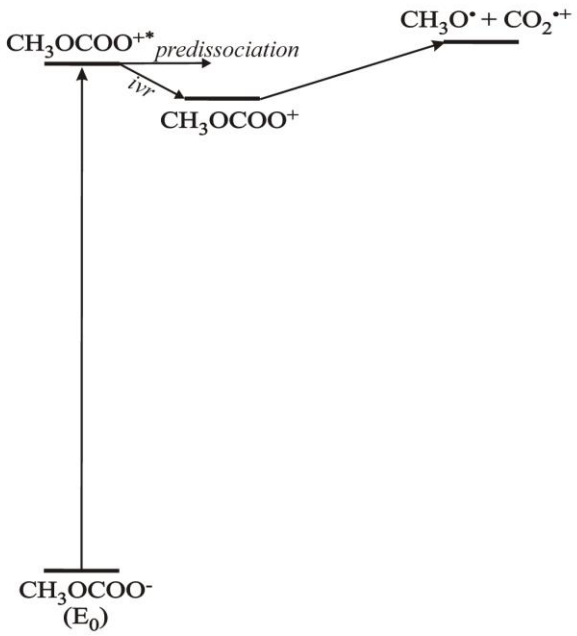

Figure IV.3-4: Illustration of the main process occurring upon the charge-reversal experiment of CH_3OCOO^-. The CH_3OCOO^{+*} formed by CR of methylcarbonate may dissociate directly or first undergo intramolecular vibrational relaxation (*ivr*).

In the case of the methylcarbonate system, the geometries of the CH_3OCOO^- and CH_3OCOO^+ ions have been compared in Chapter III and the results reveal rather large differences in geometry (section III.1.2). Moreover, the $^-CR^+$ experiment performed on

CH_3OCOO^- (Table III.3-1) has also shown that no recovery signal was present. The hypothesis of a direct dissociation of the cation formed seems thus the most likely (see below).

The minimum amount of energy required for a non dissociative $^-CR^+$ process corresponds to $IE_v + EA_v$ which is the energy difference between the cation and the anion, when the cation is formed by vertical CT from the anion (IE_v and EA_v are the vertical ionization energy and vertical electron affinity of $CH_3OCOO^\bullet$, respectively).[9,26,27] Furthermore, when the cation dissociates, the minimum energy required is related to the heat of the dissociation reaction, $\Delta_r H°_{298K}(CH_3O^\bullet/\ CO_2^{\bullet+})_{v,A/C}$. Here, a distinction is made between the heat of dissociation of the CH_3OCOO^+ ion in its ground state ($\Delta_r H°_{298K}(CH_3O^\bullet/CO_2^{\bullet+})$) and that of the CH_3OCOO^+ ion formed by vertical charge transfer from the anion ($\Delta_r H°_{298K}(CH_3O^\bullet/CO_2^{\bullet+})_{v,A/C}$; v stands for vertical and A/C for anion/cation).

The corresponding maximum translational energy of $CO_2^{\bullet+}$, $E_{kin,max}(CO_2^{\bullet+})_{CR}$, when formed by dissociative CR of methylcarbonate can be expressed as follow:

$$E_{kin,\,max}(CO_2^{\bullet+})_{CR} = \left[E_0 - (IE_v + EA_v + \delta_{CR} + \Delta_r H°_{298K}(CH_3O^\bullet/CO_2^{\bullet+})_{v,A/C}\right] \cdot \frac{m_{CO_2}}{m_{CH_3OCOO}} \quad \text{(IV.3-3)}$$

where E_0 is the initial TE of the parent ion and δ_{CR} the experimental deviation due to the charge transfer which takes place in the CR process.

Neutralization Reionization

The neutralization-reionization process of CH_3OCOO^- comprises two collision events, the first one leading to transient $CH_3OCOO^\bullet$. As mentioned in the previous section, this neutral may dissociate or survive during the time scale between the two collision cells employed. In this case, its reionization leads to CH_3OCOO^+ which further dissociates in part into $CO_2^{\bullet+}$ and $CH_3O^\bullet$. This process occurs in parallel to the main NR process, which consists, after formation of $CH_3OCOO^\bullet$ from CH_3OCOO^-, in the dissociation of the radical into $CH_3O^\bullet$ and CO_2 followed by the reionization of these products (Figure IV.3-5). The minimum energy required to drive this process is (i) EA_v for the first collision,[28] (ii) $\Delta_r H°_{298K}(CH_3O^\bullet/CO_2)_{v,A/R}$ for dissociation of $CH_3OCOO^\bullet$ formed by vertical CT of methyl-carbonate into $CH_3O^\bullet$ and CO_2 (A/R stands for anion/radical) and (iii) $IE_v(CO_2)$ for vertical reionization of CO_2 (with $IE_v(CO_2)$ = 13.78 eV).[29] For the process involving the passage through CH_3OCOO^+ (this process is termed as "ionic process"), the minimum energy required is (i) EA_v for the first col-

lision, (ii) IE_v for the second collision, and (iii) $\Delta_r H°_{298K}(CH_3O^{\bullet}/CO_2^{\bullet+})_{v,R/C}$ for dissociation of CH_3OCOO^+ formed by vertical CT of $CH_3OCOO^{\bullet}$ (R/C stands for radical/cation).

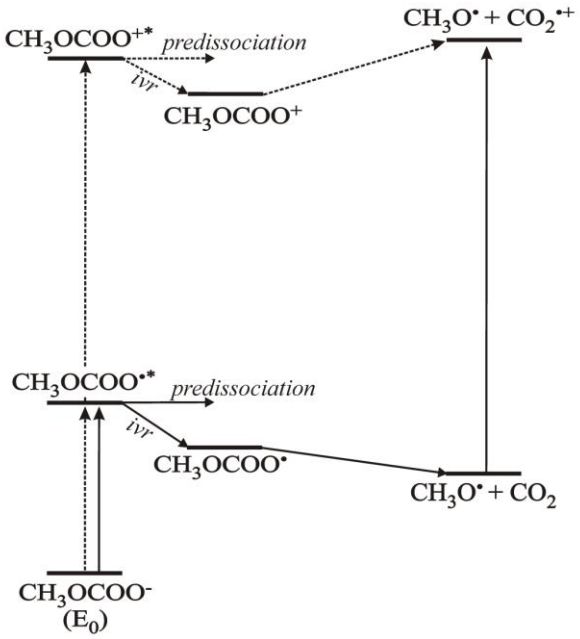

Figure IV.3-5: Illustration of the neutral (full line) and ionic (dotted line) processes occurring during the neutralization-reionization of CH_3OCOO^-. For each ion, the corresponding translational energy is indicated in brackets. *ivr* stands for intramolecular vibrational relaxation (for the sake of clarity, no activation energy is shown for dissociation of methylcarbonate neutral, even though this feature is present (see next section)).

The maximum translational energies of $CO_2^{\bullet+}$ acquired in the NR experiment following the ionic and the main pathways are thus expressed as:

$$\mathrm{E}_{\mathrm{kin,\,max}}(\mathrm{CO_2}^{\bullet+})_{NR,ionic\ proc.} = \left[\mathrm{E}_0 - (IE_v + EA_v + \delta_{NR} + \Delta_r H°(\mathrm{CH_3O^{\bullet}/CO_2}^{\bullet+})_{v,A/R})\right] \cdot \frac{m_{\mathrm{CO_2}}}{m_{\mathrm{CH_3OCOO}}} \tag{IV.3-4}$$

$$\mathrm{E}_{\mathrm{kin,\,max}}(\mathrm{CO_2}^{\bullet+})_{NR} = \left[\mathrm{E}_0 - (EA_v + \delta_{NR} + \Delta_r H°(\mathrm{CH_3O^{\bullet}/CO_2})_{v,R/C})\right] \cdot \frac{m_{\mathrm{CO_2}}}{m_{\mathrm{CH_3OCOO}}} - IE_v(\mathrm{CO_2}) \tag{IV.3-5}$$

where E_0 is the initial TE of the parent ion and δ_{NR} is the experimental deviation due to the charge transfers which are occurring in the NR process.

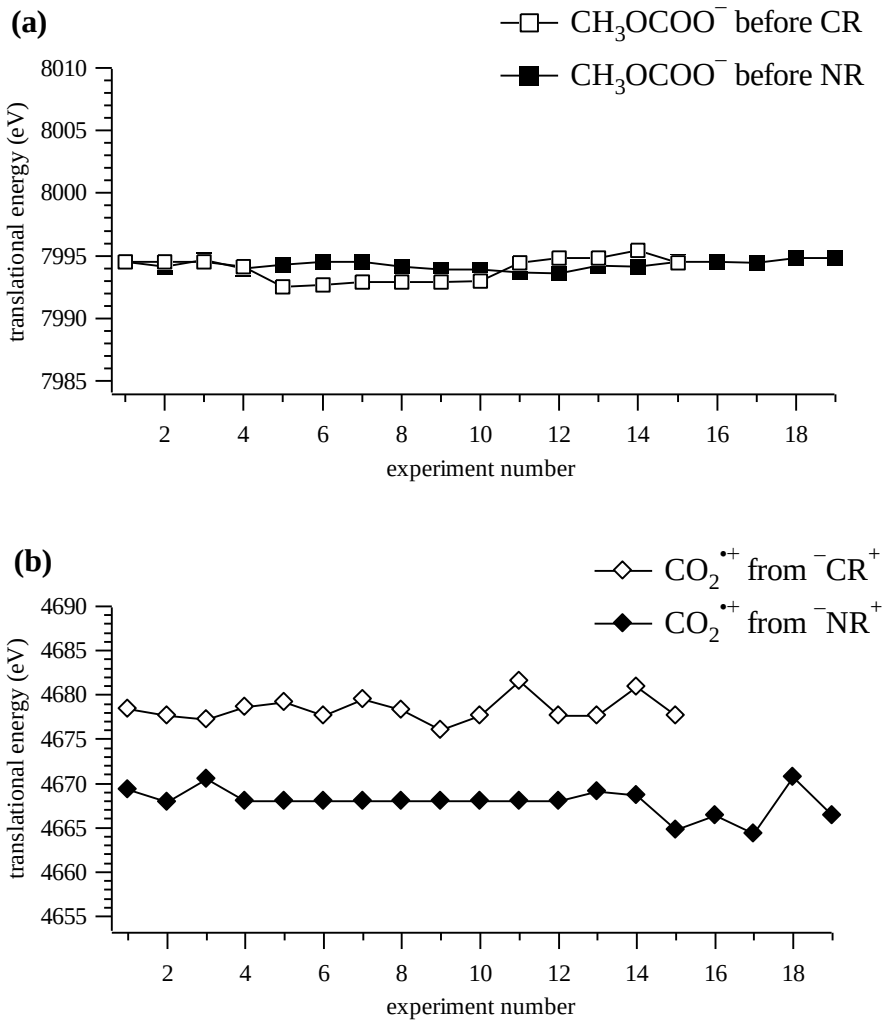

Figure IV.3-6: TE values (measured at the top of the peaks) obtained for (a) CH_3OCOO^- and (b) the CO_2^{+} fragment obtained from $^-CR^+$ (◊) or $^-NR^+$ (♦) experiments of CH_3OCOO^-. The CH_3OCOO^- experiment in graph (a) is either related to a $^-CR^+$ (□) or to a $^-NR^+$ experiment (■) in graph (b). The procedure followed for the recording of the spectra was similar to that described for the reference gases (Section IV-2); one experiment (termed 1, 2,3, ...) has consisted in the recording of the following TE spectra: CH_3OCOO^- / $CO_2^{\bullet+}$ (CR) and $CO_2^{\bullet+}$ (NR) / CH_3OCOO^-, at least three times. The TE value given for one experiment corresponds thus to the average of min. three spectra. When a large deviation was observed between TEs obtained at different steps, the whole experiment was discarded.

Equations (IV.3-3), (IV.3-4), and (IV.3-5) enable one to gain information concerning EA_v, IE_v, $\Delta_rH°_{298K}(CH_3O^{\bullet}/CO_2^{\bullet+})_{v,A/C}$, $\Delta_rH°_{298K}(CH_3O^{\bullet}/CO_2)_{v,A/R}$, and $\Delta_rH°_{298K}(CH_3O^{\bullet}/CO_2)_{v,R/C}$ if E_0, $E_{kin,max}(CO_2^{\bullet+})_{CR}$, $E_{kin,max}(CO_2^{\bullet+})_{NR}$, and $E_{kin,max}(CO_2^{\bullet+})_{NR,ionic\ proc.}$ are known. These TEs are available from the experimental data and correspond to the TEs related to the top of the peaks.[8] In this case, $E_{kin,max}(CO_2^{\bullet+})_{NR}$ and $E_{kin,max}(CO_2^{\bullet+})_{NR,ionic\ proc.}$ have the same value, because, as shown in the previous section, the center of the signals related to both of these TEs

have the same position (Figure IV.3-3 and Table IV.3-1). As for the monoatomic gases which have been investigated in section IV.2, the experiments have been carried out several times to verify the reproducibility of the results (Figure IV.3-6).

Like for the atomic ions (section IV.2), the reproducibility of the experiments is quite satisfactory. The TEs obtained for $CO_2^{\bullet+}$ are more subject to variations as those obtained for the parent ion CH_3OCOO^- (standard deviations of ca. 1.5 eV vs ca. 0.5 eV, Table IV.3-2), Table IV.3-2); this is mostly because the measurement of TEs for signals which do not have a Gaussian-type shape is not as easy as for Gaussian-like signals. The first comment which can be made concerning the values obtained is that the NR signal is shifted compared to the CR one in the other direction than found for the monoatomic ions. This means that formation of $CO_2^{\bullet+}$ requires more energy in the NR than in the CR processes. This point is of interest, because the NIDD study of alkylcarbonate neutrals (Chapter III) has revealed that the $CO_2^{\bullet+}$ ion appears with a negative NIDD intensity, implying thus the formation of this ion at the ionic stage (Figure III.5-2b). This feature is not well understood because formation of $CO_2^{\bullet+}$ should be more favored in the NR process (dissociation of the neutral, followed by reionization). In the CR process, dissociation of $ROCOO^+$ ions (R = H to *t*-C_4H_9) is expected to lead preferentially to RO^+ and CO_2 instead of $RO^\bullet$ and $CO_2^{\bullet+}$, according to Stevenson's rule.[2] The occurrence of a negative NIDD signal for $CO_2^{\bullet+}$ was thus somewhat surprising and could not be simply understood. The fact that the experiments presented here reveal that formation of $CO_2^{\bullet+}$ requires less energy in the CR than in the NR process points towards a first step in the understanding of this unexpected feature.

Table IV.3-2

Average maximum translational energies $E_{kin,max}$ (in eV) of CH_3OCOO^- recorded before CR or NR experiment and of $CO_2^{\bullet+}$ obtained $^-CR^+$ or $^-NR^+$ experiments of methylcarbonate. Corresponding standard deviations are indicated into brackets.

	$E_{kin,max}$ (eV)	
CH_3OCOO^- before CR	7993.9 (0.6)	
$CO_2^{\bullet+}$ (CR)		4678.4 (1.5)
CH_3OCOO^- before NR	7994.3 (0.4)	
$CO_2^{\bullet+}$ (NR)		4667.9 (1.6)

The TE data of Figure IV.3-6 have been averaged (Table IV.3-2) and their combination to Equations (IV.3-3), (IV.3-4), and (IV.3-5) leads to the following equations:

$$IE_v + EA_v + \Delta_r H°(CH_3O^{\bullet}/CO_2^{\bullet+})_{v,A/C} + \delta_{CR} = 16.5 \text{ eV} \quad \text{(IV.3-6)}$$

$$EA_v + \Delta_r H°(CH_3O^{\bullet}/CO_2)_{v,A/R} + \delta_{NR} = 6.6 \text{ eV} \quad \text{(IV.3-7)}$$

$$IE_v + EA_v + \Delta_r H°(CH_3O^{\bullet}/CO_2^{\bullet+})_{v,R/C} + \delta_{NR} = 20.4 \text{ eV} \quad \text{(IV.3-8)}$$

Equations (IV.3-6) to (IV.3-8) cannot be entirely solved because they contain too many unknown parameters. Nevertheless, as the energy range of IE_v and EA_v can be estimated, some comments can be made about these equations. The vertical ionization energy and the electron affinity of $CH_3OCOO^{\bullet}$ are expected to be in the order of 11 and 4 eV respectively. Concerning EA_v, this approximation is made referring to the adiabatic electron affinity of methylcarbonate neutral which has been estimated to be 3.8 eV (Chapter III, Table III.3-1). As the geometries of the methylcarbonate anion and its neutral counterpart are rather similar, EA_v can be expected to be only slightly higher than EA_a, i.e. in the order of 4 eV. For IE_v, the value of 11 eV is estimated considering systems like $RO^{\bullet}$ and $RCOO^{\bullet}$ (R = CH_3) for which the ionization energies are in general comprised between 10 and 11 eV (no better suited system has been found for this estimation but, as shown below, the value of 11 eV is relevant).[11] As the energy range of IE_v and EA_v is known, δ_{CR} and δ_{NR} can thus also be approximated; they are about 0.7 and -1.1 eV (Equation (IV.2-6) with m_{rel} = 0.70). Consequently, $\Delta_r H°_{298K}(CH_3O^{\bullet}/CO_2^{\bullet+})_{v,A/C}$, $\Delta_r H°_{298K}(CH_3O^{\bullet}/CO_2)_{v,A/R}$, and $\Delta_r H°_{298K}(CH_3O^{\bullet}/CO_2^{\bullet+})_{v,R/C}$ can be evaluated as 0.8, 3.7, and 6.5 eV, respectively. Even though these values need first to be compared to theory in order to discuss their relevance, some comments can be already made. First, all three values are found positive, which means that the dissociation processes that they describe are endothermic. This feature was not expected for transient methylcarbonate, for which an exothermicity of -0.7 eV was found in Chapter III (Table III.5-2). Concerning CH_3OCOO^+, an endothermicity of dissociation is also expected, but the value of 6.5 eV found for $\Delta_r H°_{298K}(CH_3O^{\bullet}/CO_2^{\bullet+})_{v,R/C}$ seems extremely large. In contrast, the value obtained for $\Delta_r H°_{298K}(CH_3O^{\bullet}/CO_2^{\bullet+})_{v,A/C}$ is rather small, which was also not really expected, because dissociation of CH_3OCOO^+ into $CH_3O^{\bullet}$ and $CO_2^{\bullet+}$ is not supposed to be a thermodynamically favorable dissociation process as formation of the $CO_2^{\bullet+}$ ion is rather demanding in energy.[1,30]

IV.3.3. Kinetic Energy Release

The kinetic energy release (KER) is one of the most important characteristics of a fragmentation process, giving valuable experimental information about the potential-energy surface.[23,24,31] Part of the KER may originate from the excess energy of a reaction. This is distributed among the vibrational degrees of freedom and the reaction coordinate. The KER originating from the excess energy is in general relatively small, rarely exceeding 50 meV.[24] Higher KER values, especially those > to 100 meV, usually have a different origin. When the reverse reaction has a critical energy (reverse critical energy, RCE), a significant part of it may be converted into KER in addition to that discussed above. The combined application of detailed molecular orbital and molecular dynamic calculations can estimate the partitioning ratio, but this is possible only for very small systems.[32] Generally, the ratio between the part of RCE released as KER and that converted into internal energy is not well known. Nevertheless, an average value of KER is accessible through the full width at half height (FWHH) of the peak of the product ion (see Chapter II, Equations (II.2-12) and (II.2-13)).[7]

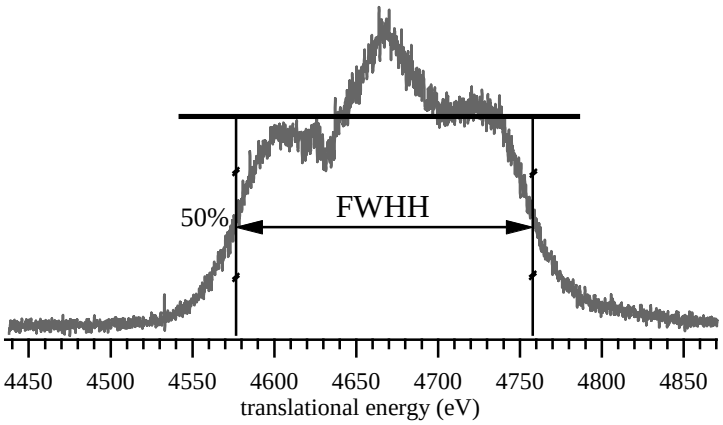

Figure IV.3-7: Method used to measure the FWHH associated to the $CO_2^{\bullet+}$ signal obtained by dissociation of transient $CH_3OCOO^{\bullet}$ and which gives access to the kinetic energy released in the course of this process.

Therefore, the FWHHs of the $CO_2^{\bullet+}$ signals obtained by CR and NR experiment of CH_3OCOO^- have been measured in order to determine the KER associated with dissociation of CH_3OCOO^+ and $CH_3OCOO^{\bullet}$ formed by vertical CT from methylcarbonate. This could be made easily for the signals obtained from the CR experiment as they have an almost Gaussian-type shape and further as the top of the peak corresponds to the process of interest (dissociation of CH_3OCOO^+, section IV.3), but for those arising from NR, one had to be careful

in the determination of the FWHH. It has thus been shown that these signals are composed by ions formed from two different processes, the main and the ionic one. The two "tops on the extremities" are attributed to dissociation of transient $CH_3OCOO^{\bullet}$ while the top in the middle corresponds to the ionic process (section IV.3-1). Consequently, determination of the KER associated with the process of dissociation of $CH_3OCOO^{\bullet}$ had to be made considering the "tops on the extremities" (Figure IV.3-7).[33]

The FWHHs of the signals have been measured in all spectra and the resulting KER were determined using Equations (II.2-11) and (II.2-12). Figure IV.3-8 gives an overview of the results. The reproducibility obtained is rather satisfying as both KERs determined vary only by ± 0.01 eV.

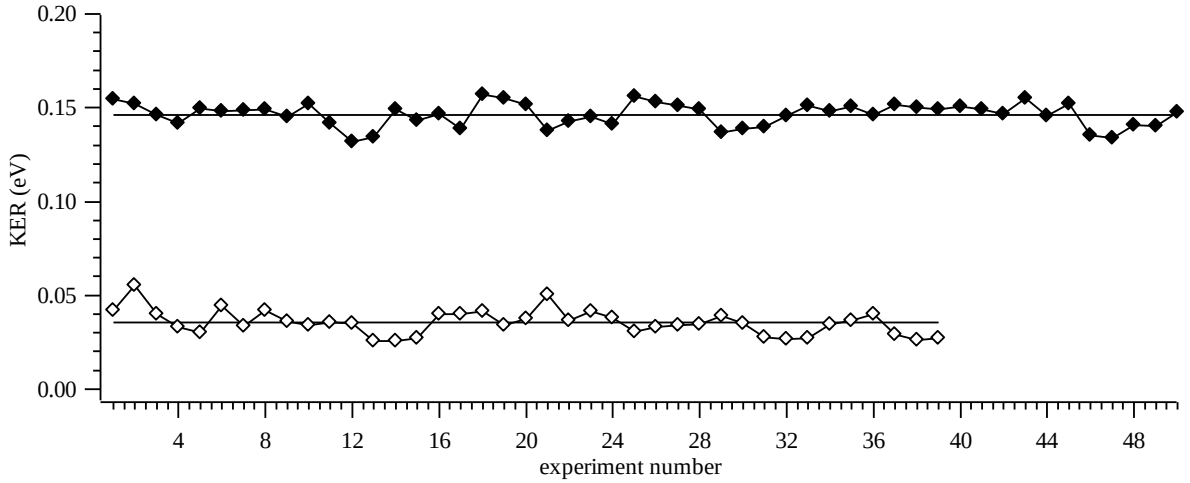

Figure IV.3-8: All KER values (eV) obtained from the $CO_2^{\bullet+}$ signal formed from CR (◊) or NR (♦) experiments of CH_3OCOO^-.

Table IV.3-3

Average kinetic energy release of $CO_2^{\bullet+}$ (in meV) formed from $^-CR^+$ or $^-NR^+$ experiments. Standard deviations are indicated in brackets.

	KER (meV)
$CO_2^{\bullet+}$ from CR	36.0 (2)
$CO_2^{\bullet+}$ from NR	139.8 (4)

Dissociation of CH_3OCOO^+ is associated with an average KER of 36 meV whereas decomposition of $CH_3OCOO^{\bullet}$ releases ca. 139.8 meV (Table IV.3-3). The kinetic energy re-

leased by dissociation of methylcarbonate radical is thus rather large; this generally indicates the presence of a barrier in the course of the dissociation. An interpretation of these KER values is made in section IV.5.

IV.4. Theoretical Approach

Dissociation of $CH_3OCOO^{\bullet}$ and CH_3OCOO^{+} Formed by Vertical CT of Methylcarbonate

In the context of this study, a computational evaluation of IE_v, EA_v, and the dissociation energetics of CH_3OCOO^+ and $CH_3OCOO^{\bullet}$ is relevant to help to understand the experimental results. The $[C_2H_3O_3]^{-/\bullet/+}$ potential-energy surfaces have thus been explored at the MP2/6-311++G(3df,3pd)//MP2/6-311++G(d) level of theory. As the dissociation process investigated is the bond cleavage $CH_3O - CO_2^{\bullet/+}$, the PESs have been projected on the r(CH_3O-CO_2) coordinate (Figure IV.4-1).

Results of the calculations reveal that dissociations of CH_3OCOO^- and of CH_3OCOO^+ into CH_3O^- and CO_2 and into $CH_3O^{\bullet}$ and $CO_2^{\bullet+}$ are endothermic processes, by 1.6 and 3.6 eV, respectively, whereas the $CH_3O^{\bullet} - CO_2$ bond cleavage leading to $CH_3O^{\bullet}$ and CO_2 is exothermic by -0.6 eV (Table IV.4-1). Furthermore, the energetics required for charge transfers between the different charged species could also have been determined. The adiabatic and vertical electron affinities of methylcarbonate neutral are found to be 3.8 eV (Table IV.4-1) and are in agreement with the value determined with the CBS-Q method (3.8 eV, Table III.3-1). The energy required to form $CH_3OCOO^{\bullet}$ from vertical or adiabatic charge transfer of methylcarbonate is thus the same, showing again how close are the equilibrium geometries of the anion and radical. In contrast, the adiabatic and vertical ionization energies of methylcarbonate radical differ by more than 1 eV (11.7 and 10.5 eV respectively, Table IV.4-1), underlining the large geometry difference between the cation and the radical. The energy difference between the anion and the cation having the geometry of anion is also much larger than the sum of IE_a and EA_a (16.9 vs 14.5 eV, Table IV.4-1), showing thus that the cation obtained by vertical CT from the anion is formed in a highly rovibrationally excited state.

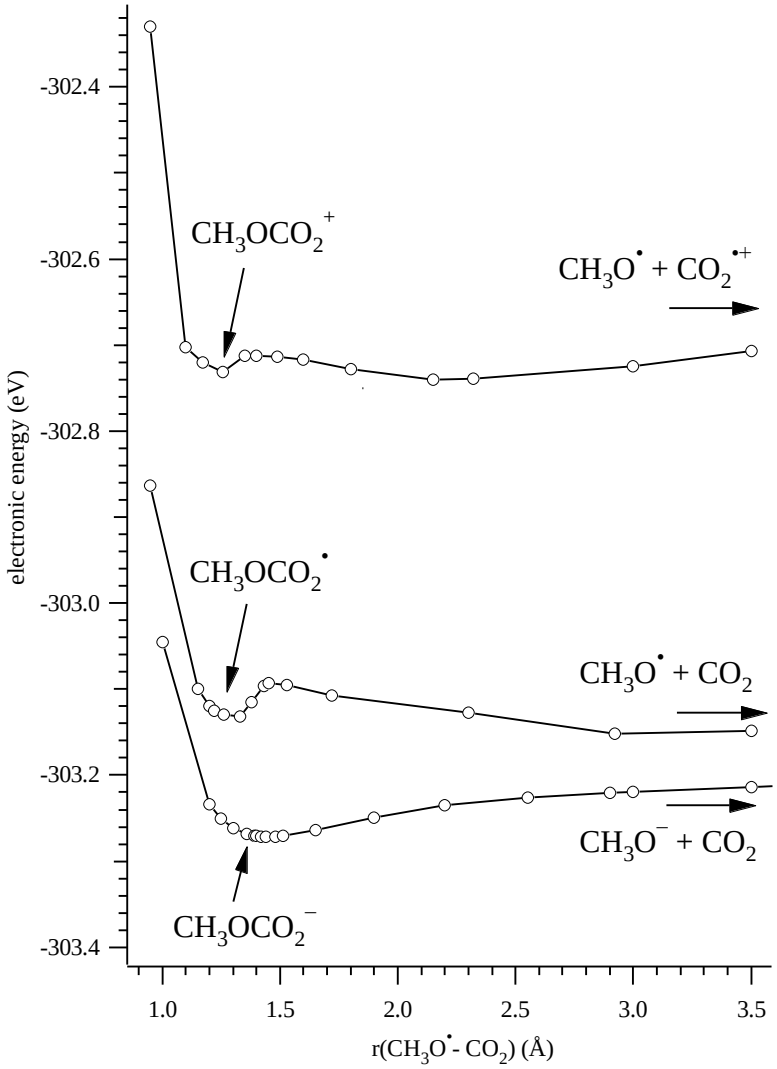

Figure IV.4-1: Projection of the $[C_2H_3O_3]^{-/\bullet/+}$ potential-energy surfaces on the r($CH_3O^\bullet$ – CO_2) coordinate as determined by single point energy calculations (MP2/6-311++G(3df,3pd)//MP2/6-311++G(d)). Here, the $CH_3O^\bullet$ - CO_2 bond was kept frozen, while all other parameters of the species were fully optimized. The PESs have been extrapolated from several optimized structures of anion, radical and cation, indicated by a circle (○).

The quantities $\Delta_r H°_{298K}(CO_2^{\bullet+})_{v,A/C}$, $\Delta_r H°_{298K}(CO_2)_{v,A/R}$ and $\Delta_r H°_{298K}(CO_2^{\bullet+})_{v,R/C}$ are evaluated as 1.3, -0.5, and 2.3 eV respectively (Table IV.4-1). Comparing these values with those obtained experimentally (section IV.3.2) shows that: (i) for the radical, the energy difference is quite large as theory predicts an exothermicity of the dissociation of 0.5 eV whereas dissociation was experimentally found endothermic by 3.7 eV. (ii) For the methoxycarboxyl cation formed by vertical CT from methylcarbonate, the results are closer between theory and experiment, 1.3 vs 0.8 eV, respectively. (iii) An endothermicity of 2.3 eV is predicted theo-

retically for dissociation of CH_3OCOO^+ formed by vertical CT of $CH_3OCOO^\bullet$, whereas it is experimentally evaluated as 6.5 eV.

Table IV.4-1

Total energies E_{tot} (in Hartrees, H) of $CH_3OCOO^{-/\bullet/+}$ and their dissociation products, electronic energies E_{el} (in Hartrees, H) of $CH_3OCOO^{\bullet/+}$ obtained by vertical electron transfer of the corresponding anion or radical, and derived properties (eV), obtained at the MP2/6-311++G(3df,3pd)//MP2/6-311++G(d) level of theory.

	E_{el} (H)	E_{tot} (H)	Derived properties (eV)
CH_3OCOO^-		-303.2268921	
$CH_3OCOO^\bullet$		-303.0883935	EA_a = 3.8 eV
CH_3OCOO^+		-302.6915434	IE_a = 10.5 eV
$CO_2 + CH_3O^-$		-303.1670722	$\Delta_r H°_{298K}(CH_3O^-/CO_2)$ = 1.6 eV[d]
$CO_2 + CH_3O^\bullet$		-303.0961903	$\Delta_r H°_{298K}(CH_3O^\bullet/CO_2)$ = -0.6 eV[e]
$CO_2^{\bullet+} + CH_3O^\bullet$		-302.5618090	$\Delta_r H°_{298K}(CH_3O^\bullet/CO_2^{\bullet+})$ = 3.6 eV[f]
$CH_3OCOO^\bullet{}_v$[b]	-303.0869996		EA_v = 3.8 eV $\Delta_r H°_{298K}(CO_2)_{v,A/R}$ = -0.5 eV[g]
$CH_3OCOO^+{}_{v,anion}$[b]	-302.6069989		$IE_v + EA_v$ = 16.9 eV $\Delta_r H°_{298K}(CO_2^{\bullet+})_{v,A/C}$ = 1.3 eV[h]
$CH_3OCOO^+{}_{v,radical}$[c]	-302.6471831		IE_v = 11.7 eV $\Delta_r H°_{298K}(CO_2^{\bullet+})_{v,R/C}$ = 2.3 eV[i]

[a] ZPE included and uniformly scaled (0.9496).

[b] Electronic energies of the radical and cation with the geometry of the anion.

[c] Electronic energy of the cation with the geometry of the radical.

[d] Heat of reaction for dissociation of CH_3OCOO^- into CO_2 and CH_3O^-.

[e] Heat of reaction for dissociation of $CH_3OCOO^\bullet$ into CO_2 and $CH_3O^\bullet$.

[f] Heat of reaction for dissociation of CH_3OCOO^+ into $CH_3O^\bullet$ and $CO_2^{\bullet+}$.

[g] Heat of reaction for dissociation of $CH_3OCOO^\bullet$ into $CH_3O^\bullet$ and CO_2, when the neutral is formed by vertical CT from the anion (A/R stands for anion/radical).

[h] Heat of reaction for dissociation of CH_3OCOO^+ into $CH_3O^\bullet$ and $CO_2^{\bullet+}$, when the cation is formed by vertical CT from the anion (A/C stands for anion/cation).

[i] Heat of reaction for dissociation of CH_3OCOO^+ into $CH_3O^\bullet$ and $CO_2^{\bullet+}$ when the cation is formed by vertical CT from the radical (R/C stands for radical/cation).

Kinetic Energy Release

As shown in Figure IV.4-1, the dissociation of a methylcarbonate radical requires some activation energy. A more detailed representation of the mechanism involved is given in Figure IV.4-2. The $CH_3OCOO^{\bullet}$ radical has an equilibrium geometry which corresponds to the structure **A** (Figure IV.4-2). The dissociation process starts first with an elongation of the $C_{(1)}$-$O_{(1)}$ bond and an increase of the $O_{(1)}$-$C_{(1)}$-$O_{(2)}$ angle (structure **B**). The energy maximum is reached, in the course of dissociation, with the structure **C** which has, in comparison with **A**, the bond lengths $C_{(1)}$-$O_{(1)}$, $C_{(1)}$-$O_{(3)}$, and $O_{(3)}$-$C_{(3)}$ much more elongated (by 0.126, 0.135, and 0.056 Å, respectively). Once the barrier is passed, the major change in the $CH_3OCOO^{\bullet}$ structure concerns the $O_{(1)}$-$C_{(1)}$-$O_{(2)}$ angle which increases considerably until the $O_{(1)}C_{(1)}O_{(2)}$ group becomes planar (structures **D** and **E**). The reverse activation energy of the dissociation is the energy difference between the structures **E** and **C** and has a value of 1.31 eV.[34] One part of this reverse activation energy is liberated as kinetic energy and the other part is contained as internal energy of the products.

Concerning the CH_3OCOO^{+} cation formed from vertical charge transfer from the anion, a value of 36.0 meV has been determined experimentally (Table IV.3-3). Such values, which are < 50 mV, do generally not correspond to processes accompanied with a barrier, but are associated with a spread of the ion beam resulting in a broadening of the signal.[5] The theoretical exploration of the $[C_3H_3O_3]^{+}$ PES reveals indeed that dissociation of the CH_3OCOO^{+} ion into $CO_2^{\bullet+}$ and $CH_3O^{\bullet}$ does not require an activation energy, even though the increase of the $CH_3O - CO_2^{+}$ bond length first lead to a slight decrease of the total energy of the system (formation of the $[CH_3O^{\bullet}\ CO_2^{\bullet+}]$ complex, Chart IV.4-1), followed by the separation of the products $CH_3O^{\bullet}$ and $CO_2^{\bullet+}$ (Figure IV.4-1), giving an overall exothermicity of the reaction of 3.6 eV (Table IV.4-1).

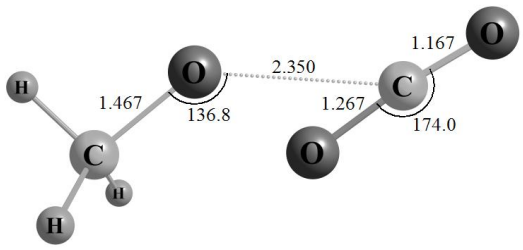

Chart IV.4-1: Optimized geometry of the $[CH_3O^{\bullet}\ CO_2^{\bullet+}]$ ion-neutral complex with a CH_3O-CO_2 bond length of 2.350 Å, obtained at the MP2/6-311++G(3df,3pd)//MP2/6-311++G(d) level of theory. All bond lengths are given in Å.

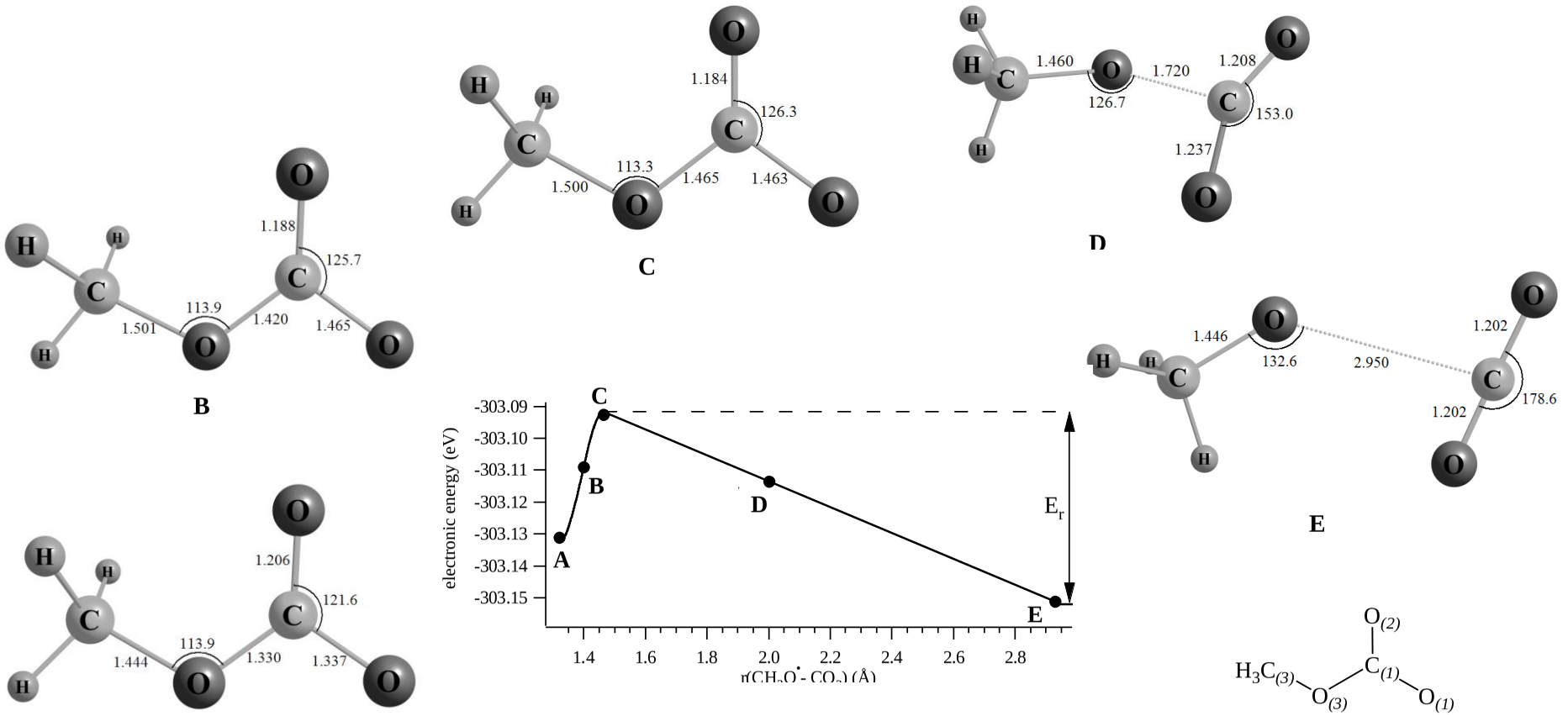

Figure IV.4-2: Projection of the $[C_3H_3O_3]^{\bullet}$ potential energy surface on the r($CH_3O^{\bullet}$ – CO_2) coordinate between 1.3 and 3 Å (MP2/6-311++G(3df,3pd)/MP2/6-311++G(d) level of theory). Energies are given in Hartrees (H) and bond lengths in Å. The letters **A**, **B**, **C**, **D**, and **E** given on the graph are related to the optimized structures shown all around, and for which the CH_3O – $CO_2^{\bullet}$ bond has a length of 1.330, 1.420, 1.465, 1.720, and 2.950 Å respectively. The structure **A** corresponds to the energetic minimum of methylcarbonate neutral, the structure **C** to the energy maximum reached in the course of the CH_3O-$CO_2^{\bullet}$ bond cleavage, and the structure **E** to the energetic minimum of the dissociation complex [$CH_3O^{\bullet}$ CO_2]. The associated reverse activation energy, E_r, is indicated on the graph.

IV.5. Summary and Conclusions

Dissociation of $CH_3OCOO^{\bullet}$ and CH_3OCOO^{+} formed by CT from Methylcarbonate

Experimental results have provided information about the energetics of the $[CH_3O - CO_2]^{+/\bullet}$ bond cleavage of CH_3OCOO^{+} and $CH_3OCOO^{\bullet}$ formed by vertical charge transfer of the corresponding anion. These results have been compared to theoretical predictions and show a good agreement for the quantity derived from the CR process, with an error of 0.5 eV, but larger differences for those obtained from the NR experiment (error > 4 eV).

Nevertheless, all the experimental heats of dissociation have been determined using approximate values of EA_v and IE_v. From the theoretical predictions of IE_v and EA_v (Table IV.4-1), δ_{CR} and δ_{NR} can be evaluated as 0.3 and -1.2 eV. Hence, $\Delta_r H°_{298K}(CH_3O^{\bullet}/CO_2^{\bullet+})_{v,A/C}$, $\Delta_r H°_{298K}(CH_3O^{\bullet}/CO_2)_{v,A/R}$, and $\Delta_r H°_{298K}(CH_3O^{\bullet}/CO_2^{\bullet+})_{v,R/C}$ are changed resp. in -0.7, 4.0, and 4.7 eV, which have to be compared to the corresponding theoretical values of 1.3, -0.5, and 2.3 eV, respectively (Table IV.4-1). Thus, the difference between experiment and theory remains very large for $\Delta_r H°_{298K}(CH_3O^{\bullet}/ CO_2)_{v,A/R}$ and $\Delta_r H°_{298K}(CH_3O^{\bullet}/CO_2^{\bullet+})_{v,R/C}$, (4.5 and 2.4 eV, respectively), and is increased for $\Delta_r H°_{298K}(CH_3O^{\bullet}/CO_2^{\bullet+})_{v,A/C}$ (from 0.5 to 2.0 eV).

This work was performed to gain more insights into the dissociation energetics of the methoxycarboxyl radical and its cation formed by vertical charge-transfer processes of CH_3OCOO^{-}. This could be achieved only if the experimental method used was able to provide results with a good accuracy. As already discussed, this was not the case as a difference larger than 2 eV is observed between the experimental and theoretical results. A general insufficiency of the experimental accuracy is evoked to explain these large differences, but the problem also lies in the evaluation of the instrumental deviation. We have indeed used, in this study, an approximate value to correct the error due to the instrument. This value was determined by extrapolating results obtained for atomic ions. A linear relation between the error observed and the intrinsic parameters of the ions (*IE*, *EA*, and m_{rel}) was indeed found and further used for the study of dissociation of $CH_3OCOO^{\bullet/+}$ species. Nevertheless, this model, even simple, could not be understood mostly because it shows that the instrumental error is only depending on the first collision occurring (as, for the NR process, only *EA* was found to affect the error). A better comprehension of the origin of the instrumental deviation and of the parameters influencing it is thus first necessary in order to obtain results as accurate as possible. Furthermore, as mentioned in the introduction, determination of dissociation energetics using energy-resolved collision experiment has not been performed so

far. This work was also achieved to determine if this method is adequate or not. Therefore, even a better evaluation of the instrumental error could lead to the conclusion that it is not.

Kinetic Energy Release

The experimental value of KER associated with dissociation of methylcarbonate radical and cation is 139.8 and 36 meV respectively (Table IV.3-3). These KERs originate in part from the excess energy of the activated complex, $\varepsilon^{\#}(CH_3OCOO^{\bullet})$ and $\varepsilon^{\#}(CH_3OCOO^{+})$, and in part from the associated reverse reaction, $\varepsilon_0^{r}(CH_3OCOO^{\bullet})$ and $\varepsilon_0^{r}(CH_3OCOO^{+})$ (Chapter II, section II.2-8). The partitioning of these energies into kinetic energy release is not accessible experimentally, but Cooks *et al.*[7] have shown that when the kinetic energy release measured is large (> 0.1 eV), it can then be related only to the associated reverse activation energy $\varepsilon_0^{r}(CH_3OCOO^{\bullet})$ because the contribution from the non-fixed energy of the activated complex is negligible. Thus, the KER obtained for dissociation of methylcarbonate radical can exclusively be related to the energy $\varepsilon_0^{r}(CH_3OCOO^{\bullet})$ which has been determined as 1.31 eV (section IV.4). From these 1.31 eV, in average 139.8 meV are thus released. For dissociation of CH_3OCOO^{+}, the approximation cannot be made as the value obtained for the KER is < 0.1 eV, but as shown in the previous section, the process is not accompanied with a barrier. The kinetic energy released observed was thus attributed to a spread of the ion beam resulting in a broadening of the signal.

IV.6. References and Notes

1. The CH_3O^+ ion does not exist within this structure in the singlet multiplicity, but has a CH_2OH^+ structure (see for instance: Aschi, M.; Harvey, J. N.; Schalley, C. A.; Schröder, D.; Schwarz, H., *Chem. Commun.* **1998**, 531.).

2. Stevenson, D. P., *Discuss. Faraday Soc.* **1951**, *10*, 35.

3. In this case, the cation may be formed in the triplet or in the singlet states and has either a $^3CH_3O^+$ or a $^1CH_2OH^+$ structure.

4. Los, J.; Gover.T.R. in *Collision Spectroscopy*; Cooks, R. G., Ed.; Plenum: New York, 1978, Chapt. 6.

5. Cooks, R. G., *Collision Spectroscopy*; Plenum Press: New York, 1978.

6. Kim, M. S., *Org. Mass Spectrom.* **1991**, *26*, 565.

7. Cooks, R. G.; Beynon, J. H.; Caprioli, R. M.; Lester, G. R., *Metastable Ions*; Elsevier: Amsterdam, 1973.

8. Howe, I.; Bowie, J. H.; Szulejko, J. E.; Beynon, J. H., *J. Chem. Soc., Chem. Commun.* **1979**, 983.

9. Levsen, K.; Schwarz, H., *Mass Spectrom. Rev.* **1983**, *2*, 77.

10. Ast, T.; Porter, C. J.; Proctor, C. J.; Beynon, J. H., *Bull. Soc. Chim. Beograd* **1981**, *46*, 135.

11. Linstrom, P. J.; Mallard, W. G., (Eds.), NIST Chemistry WebBook, NIST Standard Reference Database Number 69, National Institute of Standards and Technology, Gaithersburg MD, 20899, June 2005 (http://webbook.nist.gov).

12. Valli, C.; Blondel, C.; Delsart, C., *Phys. Rev. A* **1999**, *59*, 3809.

13. Martin, J. D. D.; Hepburn, J. W., *J. Chem. Phys.* **1998**, *109*, 8139.

14. Blondel, C.; Cacciani, P.; Delsart, C.; Trainham, R., *Phys. Rev. A* **1989**, *40*, 3698.

15. Hanstorp, D.; Gustafsson, M., *J. Phys. B: At., Mol. Opt. Phys.* **1992**, *25*, 1773.

16. Amme, R. C.; Hayden, H. C., *J. Chem. Phys.* **1965**, *42*, 2011.

17. Barnett, C. F.; Stier, P. M., *Phys. Rev.* **1958**, *109*, 385.

18. Fales, H. M.; Mihe, G. W. A.; Vestal, M. L., *J. Am. Chem. Soc.* **1969**, *91*, 3682.

19. Grabowy, J. A. D.; Mayer, P. M., *Eur. J. Mass Spectrom.* **2004**, *10*, 899.

20. Pearson, K., *Philos. Trans. R. Soc. London* **1896**, *187*, 253.

21. Szulejko, J., E.; Bowie, J. H.; Howe, I.; Beynon, J. H., *Int. J. Mass Spectrom. Ion Phys.* **1980**, *34*, 99.

22. van Baar, B.; Burgers, P. C.; Terlouw, J. K.; Schwarz, H., *J. Chem. Soc., Chem. Commun.* **1986**, 1607.

23. Bowen, R. D.; Williams, D. H.; Schwarz, H., *Angew. Chem., Int. Ed. Engl.* **1979**, *18*, 451.

24. Holmes, J. L.; Terlouw, J. K., *Org. Mass Spectrom.* **1980**, *15*, 383.

25. Laskin, J.; Lifshitz, C., *J. Mass Spectrom.* **2001**, *36*, 459.

26. Bowie, J. H.; Blumenthal, T., *J. Am. Chem. Soc.* **1975**, *97*, 2959.

27. Szulejko, J. E.; Howe, I.; Beynon, J. H., *Int. J. Mass Spectrom. Ion Phys.* **1981**, *37*, 27.

28. EA_v is the energy difference between $CH_3OCOO^{\bullet}$ and CH_3OCOO^{-} when the neutral is formed by vertical CT of the anion.

29. Benoit, F. M.; Harrison, A. G., *J. Am. Chem. Soc.* **1977**, 3980.

30. Wang, L.; Reutt, J. E.; Lee, Y. T.; Shirley, D. A., *J. Electron Spectrosc. Relat. Phenom.* **1988**, *47*, 167.

31. Laskin, J.; Lifshitz, C., *J. Mass Spectrom.* **2001**, *36*, 459.

32. Uggerund, E.; Helgaker, T., *J. Am. Chem. Soc.* **1992**, *114*, 465.

33. Vékey, K.; Pócsfalvi, G., *Org. Mass Spectrom.* **1992**, *27*, 1203.

34. Obtained with E_{tot}(**C**) = -303.0931011 H and E_{tot}(**E**) = -303.1411102 H.

V. Gas-Phase Chemistry of Alkyloxalate Ions and Radicals

V.1. Introduction

In this chapter, our attention will focus on the alkyloxalate ions and neutrals $ROCOCOO^{-/\bullet}$ with R = H, CH_3, C_2H_5, *i*-C_3H_7, and *t*-C_4H_9 (Chart V.1-1). These species are of particular interest in the context of this Thesis because they are in part constituted by two CO_2 units and can thus potentially be formed in the atmosphere of Mars. Quite surprisingly, only very little is known about the structures as well as about the dissociation of metastable oxalate ions and radicals in the gas phase. Accordingly, a systematic study of the structures and of the dissociation behavior of some representative alkyloxalate ions and radicals has been performed and is presented in this chapter.

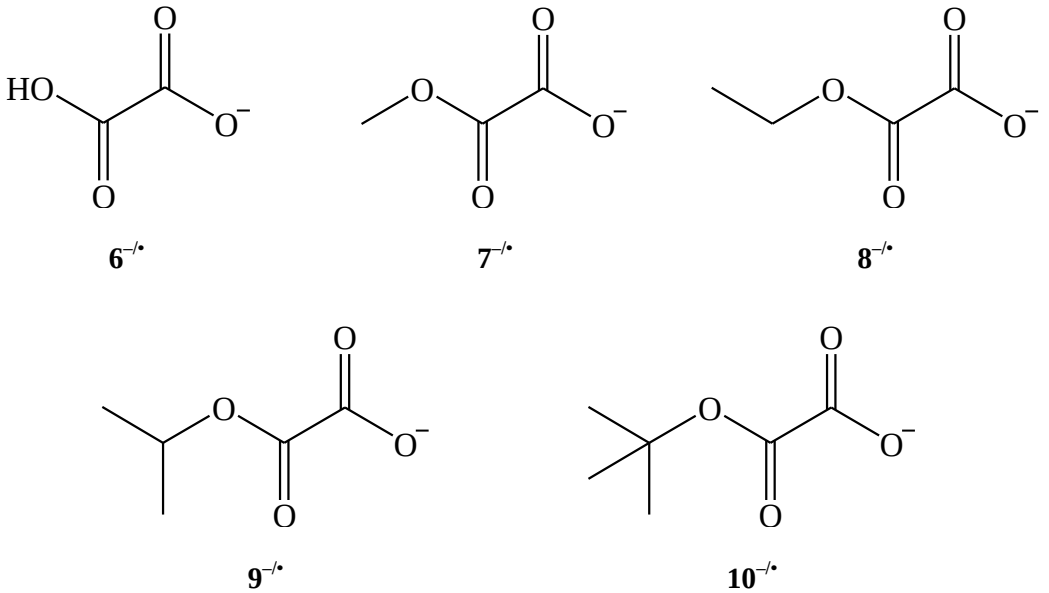

6$^{-/\bullet}$ **7**$^{-/\bullet}$ **8**$^{-/\bullet}$

9$^{-/\bullet}$ **10**$^{-/\bullet}$

Chart V.1-1

Theory and experiment have been combined to probe and understand the unimolecular dissociations of the $ROCOCOO^{-/\bullet}$ compounds of which structural minima have been

determined by *ab initio* methods. Because the species investigated possess several internal rotors, they may exist in different conformational structures. The structures and energetics of different conformers have accordingly been determined at the MP2/6-311++G(3df,3pd)// MP2/6-311++G(d) level of theory for the anions and radicals. Furthermore, alkyloxalate ions have been generated by negative ion chemical ionization (NICI) and the mass-selected ions have been submitted to metastable ion (MI) and collisional activation (CA) experiments. For the radicals, charge-reversal (CR) and neutralization-reionization (NR) experiments have been carried out in order to probe their unimolecular reactivity by means of the NIDD scheme.

V.2. Structures and Energetics

The structure of oxalic acid has already formed the subject of many investigations, particularly because it is one of the simplest examples of a molecule possessing three internal rotors.[1-6] It can indeed exhibit internal rotation around the central carbon-carbon bond connecting the two carbonyl groups and around the two C-OH bonds. In contrast, the structures of deprotonated oxalic acid, i.e. the hydrogen oxalate anion $\mathbf{6}^-$ and its corresponding radical $\mathbf{6}^\bullet$, as well as generally monoalkyloxalates $ROCOCOO^{-/\bullet}$, have been investigated in much less detail. These species may potentially exist in different conformations and the determination of the conformational minimum is not obvious as will be shown below. Thus, we have investigated the different conformational structures of alkyloxalates anions and radicals $ROCOCOO^{-/\bullet}$ for R = H, CH_3, C_2H_5, *i*-C_3H_7, and *t*-C_4H_9 and compared them with those of the corresponding cations. The thermochemistry of these species has also been determined and is presented in the last part of this section.

V.2.1. Alkyloxalate Ions

Alkyloxalate ions possess two internal rotors which can thus lead to numerous geometrical conformations of these anions. The four conformers corresponding to the limits of the two relevant dihedral angles are presented in Chart V.2-1. Here, the symbols *C* and *T* refer to the conformation of the dihedral angle $O_{(1)}C_{(1)}C_{(2)}O_{(4)}$, whereas the conformers involving rotations of the $C_{(2)}$-$O_{(4)}$ bond (i.e. the dihedral angle $O_{(3)}C_{(2)}O_{(4)}R$) are denoted by *c* and *t* (here, *c* and *C* stand for cis, *t* and *T* for trans, respectively).[3] The most relevant features of the optimized geometries of the alkyloxalates $\mathbf{6}^-$ to $\mathbf{10}^-$ in these four conformations are given in Table V.2-1.

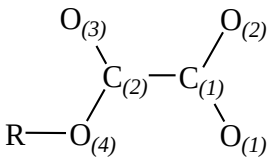

tC

$O_{(1)}C_{(1)}C_{(2)}O_{(4)}$ = 0 °

$O_{(3)}C_{(2)}O_{(4)}R$ = 0 °

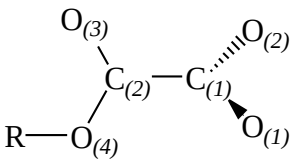

tT

$O_{(1)}C_{(1)}C_{(2)}O_{(4)}$ = 90 °

$O_{(3)}C_{(2)}O_{(4)}R$ = 0 °

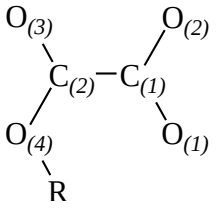

cC

$O_{(1)}C_{(1)}C_{(2)}O_{(4)}$ = 0 °

$O_{(3)}C_{(2)}O_{(4)}R$ = 180 °

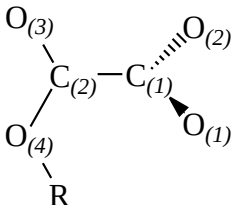

cT

$O_{(1)}C_{(1)}C_{(2)}O_{(4)}$ = 90 °

$O_{(3)}C_{(2)}O_{(4)}R$ = 180 °

Chart V.2-1: The four conformations of alkyloxalates anions ROCOCOO$^-$ (**6**$^-$ to **10**$^-$, R = H, CH_3, C_2H_5, *i*-C_3H_7, and *t*-C_4H_9) for limiting values of the dihedral angles $O_{(1)}C_{(1)}C_{(2)}O_{(4)}$ and $O_{(3)}C_{(2)}O_{(4)}R$.

The analysis of the optimized structural parameters presented in Table V.2-1 reveals changes of bond lengths and angles of alkyloxalates between the various conformations. Rotation around the central $C_{(1)}$-$C_{(2)}$ bond (conformers *C* and *T*) induces a minor decrease of the $C_{(1)}$-$O_{(2)}$ bond length when passing from the *T* to the *C* conformation. This difference is moderate for the small substituents R (ca. 0.01 Å for R = H and ca. 0.007 Å for R = CH_3) and decreases even further for larger ones (ca. 0.005 Å for R = C_2H_5, *i*-C_3H_7, and *t*-C_4H_9). In marked contrast, much more pronounced changes occur for the $C_{(1)}$-$C_{(2)}$ bond length, for which a passage from the *T* to the *C* conformation leads to bond elongations of about 0.045 Å. This increase may be explained by steric constraints due to the "planar" backbone structure of the *C* conformation. The same reasoning also explains the differences in the $O_{(4)}$-R bond lengths observed between the *cT* and *tT* conformers and between the *cC* and *tC* structures with an average elongation of 0.005 Å in the *c* conformers. The R groups of these conformers present indeed some proximity to the carbonyl group $O_{(1)}C_{(1)}O_{(2)}$, which may hinder it to be favorably positioned for small $O_{(4)}$-R bond lengths. Hence, an elongation of the $O_{(4)}$-R bond is observed to allow a good spatial organization of the R group. For another reason, this increase is particularly important for the hydrogen oxalate ion when passing from the *tC* to the *cC* conformation (+ 0.019 Å). This latter conformation is indeed strongly stabilized through an intra-

Table V.2-1

Selected bond lengths (in Å) and bond angles (in degree) of the alkyloxalates **6**$^-$ to **10**$^-$ in the four conformations investigated at the MP2/6-311++G(d) level of theory.

		Calculated structural parameters (Å and °)							
		$C_{(1)}O_{(1)}$	$C_{(1)}O_{(2)}$	$C_{(1)}C_{(2)}$	$C_{(2)}O_{(3)}$	$C_{(2)}O_{(4)}$	$O_{(4)}R$	$O_{(1)}C_{(1)}O_{(2)}$	$O_{(3)}C_{(2)}O_{(4)}$
6$^-$	*tT*	1.252	1.252	1.541	1.219	1.372	0.970	132.4	120.0
	cT	1.255	1.255	1.546	1.210	1.384	0.966	128.3	118.8
	cC	1.273	1.238	1.584	1.212	1.355	0.988	127.3	122.1
	tC	1.250	1.249	1.584	1.218	1.370	0.969	132.4	119.5
7$^-$	*tT*	1.253	1.253	1.540	1.218	1.373	1.424	132.2	121.1
	cT	1.255	1.253	1.546	1.213	1.380	1.431	131.7	117.7
	cC	1.257	1.243	1.597	1.212	1.380	1.430	131.4	115.4
	tC	1.251	1.250	1.584	1.217	1.370	1.422	132.1	120.6
8$^-$	*tT*	1.254	1.253	1.540	1.218	1.375	1.430	132.2	121.6
	cT	1.256	1.253	1.545	1.213	1.381	1.436	132.1	117.7
	cC	1.257	1.243	1.598	1.212	1.382	1.435	131.4	115.5
	tC	1.251	1.250	1.584	1.217	1.372	1.426	132.1	120.7
9$^-$	*tT*	1.254	1.254	1.540	1.219	1.372	1.441	132.1	122.5
	cT	1.257	1.251	1.546	1.215	1.381	1.446	131.2	116.4
	cC	1.256	1.244	1.593	1.211	1.390	1.444	131.3	116.1
	tC	1.251	1.250	1.586	1.217	1.369	1.439	132.0	121.9
10$^-$	*tT*	1.254	1.254	1.541	1.218	1.373	1.448	132.2	122.9
	cT	1.251	1.251	1.546	1.214	1.384	1.453	131.2	116.1
	cC	1.251	1.244	1.594	1.214	1.384	1.453	131.2	116.1
	tC	1.254	1.250	1.588	1.218	1.373	1.448	132.2	122.9

molecular hydrogen bond (see below) which implies an approach of the hydrogen to the $O_{(1)}$ atom. Furthermore, as for the $O_{(4)}$-R bond, a slight increase of the $C_{(1)}$-$O_{(1)}$ bond length is observed when changing from the *t* to the *c* conformation. The $C_{(2)}O_{(3)}$ and $C_{(2)}O_{(4)}$ distances are also influenced by a rotation around the $C_{(2)}$-$O_{(4)}$ axis. Again, both bonds are slightly longer in the *c* than in the *t* conformation. Concerning the angles, one notices that the $O_{(1)}C_{(1)}O_{(2)}$ angle remains almost unchanged for the various conformers, except for the hydrogen oxalate

Table V.2-2

Total and relative energies E_{tot}[a] and E_{rel}[b] (in Hartrees, H, and in kcal/mol, respectively) and number of imaginary frequencies of the four conformers of the alkyloxylates **6**$^-$ to **10**$^-$ according to MP2/6-311++G(3df,3pd)//MP2/6-311++G(d) calculations.

	Conformer	E_{tot}[a] (H)	E_{rel}[b] (kcal/mol)	Number of imaginary frequencies
6$^-$	*tT*	-377.1981850	8.9	0
	cT	-377.1968332	9.8	1
	cC	-377.212433	0.0	0
	tC	-377.1930629	12.2	1
7$^-$	*tT*	-416.3727241	0.3	0
	cT	-416.3732318	0.0	0
	cC	-416.3690674	2.6	1
	tC	-416.3645157	5.5	1
8$^-$	*tT*	-455.5723569	0.5	0
	cT	-455.5731566	0.0	0
	cC	-455.5688245	2.7	1
	tC	-455.5649954	5.1	1
9$^-$	*tT*	-494.7701893	0.0	0
	cT	-494.7693479	0.5	0
	cC	-494.7596878	6.6	1
	tC	-494.765386	3.0	1
10$^-$	*tT*	-533.9737309	0.0	0
	cT	-533.9731006	0.4	0
	cC	-533.9634608	6.4	1
	tC	-533.9700754	2.3	1

[a] ZPE included and uniformly scaled (0.9496).

[b] The energy is given relative to the most stable conformer for each alkyloxalate.

ion which presents a structure that is more "opened" by ca 4 ° in the *c* conformation compared to the *t* one. Slightly larger changes are observed for the $O_{(3)}C_{(2)}O_{(4)}$ angle which decreases by ca. 6 ° when passing from the *t* to the *c* configuration.

To summarize, comparison of the different conformational structures predicted by theory, shows that if the central backbone is planar (*C*), the structures of alkyloxalates are elongated along the $C_{(1)}$-$C_{(2)}$ axis. The most compact structure corresponds to the *cT* conformation and the loosest one to the *tT* conformation.

The total electronic and relative energies of alkyloxalates $\mathbf{6}^-$ to $\mathbf{10}^-$ calculated at the MP2/6-311++G(3df,3pd) level of theory for the four optimized conformational structures are given in Table V.2-2. The number of imaginary frequencies is also included as they allow the characterization of the conformers as minima or as transition structures.

A comparison of the energetics of the four conformers of the alkyloxalates $\mathbf{7}^-$ to $\mathbf{10}^-$ shows that the planar conformers *cC* and *tC* correspond to transition structures, whereas the non-planar structures *cT* and *tT* are minima. A more detailed discussion for each alkyloxalate will be presented after the examination of the particular case of the hydrogen oxalate ion $\mathbf{6}^-$. The ion with R = H differs from the other $ROCOCOO^-$ anions studied because the conformation *cC* possesses the option to form an intramolecular hydrogen bond between two oxygen atoms (Chart V.2-2). The resulting overall stabilization of this structure amounts to ca. 10 kcal/mol compared to the other conformers (Table V.2-2). Furthermore, frequency calculations characterize the *tT* conformer as a minimum and the *cT* and *tT* conformers as transition structures. The results concerning the relative energies of the conformers as well as their characterization as minima or saddle points are in complete agreement with the findings of Cheng and Shyu[7] in which the four conformations of the hydrogen oxalate ion were considered at various levels of theory.

Hydrogen Oxalate

As already mentioned, the conformations *cT* and *tC* correspond to transitions structures for $HOCOCOO^-$, and the normal modes associated with the imaginary frequency of each conformer are associated with torsions around both the $C_{(1)}$-$C_{(2)}$ and $C_{(2)}$-H axis. A schematic description showing the conformational connections between the relevant conformers of the hydrogen oxalate ion is presented in Figure V.2-1.

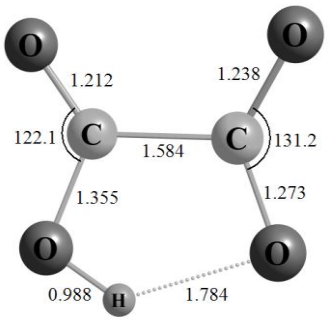

6^{-}(*cC*)

Chart V.2-2: Optimized structure of the most stable conformer of the hydrogen oxalate ion **6**$^{-}$ at the MP2/6-311++G(d) level of theory.

The conformational structures **6**$^{-}$(*cT*) and **6**$^{-}$ (*tT*) differ by only 0.9 kcal/mol, and Cheng and Shyu[7] even found the transition structure **6**$^{-}$ (*cT*) to be 0.4 kcal/mol lower in energy than the local minimum **6**$^{-}$ (*tT*). Nevertheless, the most favorable conformer **6**$^{-}$(*cC*) is clearly lower in energy than all other conformational structures investigated and is accordingly assumed as the most stable conformer of the ion **6**$^{-}$.

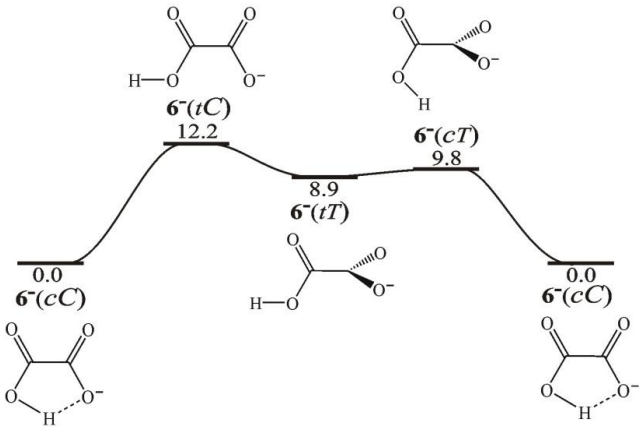

Figure V.2-1: Connections between the different conformers of the hydrogen oxalate ion **6**$^{-}$ according to MP2/6-311++G(3df,3pd)//MP2/6-311++G(d) calculations (energies in kcal/mol).

Alkyloxalates (R = CH_3, C_2H_5, i-C_3H_7, and t-C_4H_9)

Concerning the other four alkyloxalates investigated, energy calculations show that all conformers *cC* and *tC* correspond to transition structures, while the *tT* and *cT* conformers are minima. For methyl- and ethyloxalate ions, the most stable structure is the conformation *cT* whereas for *i*-propyl- and *t*-butyloxalate it is the conformation *tT* (Chart V.2-3).

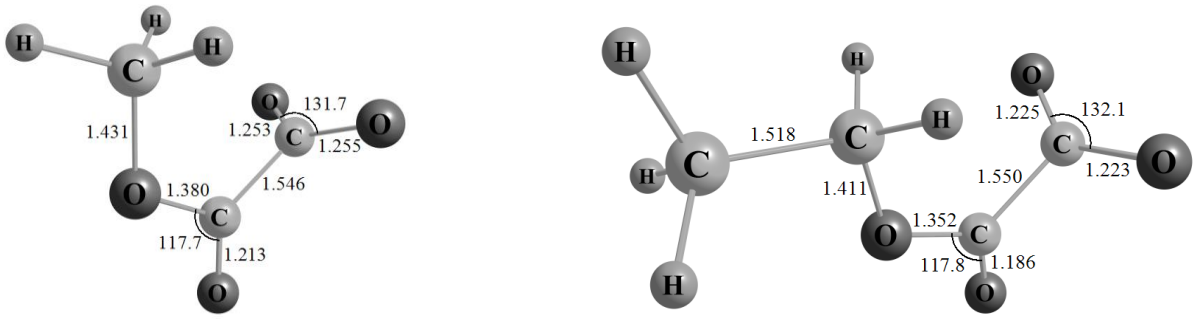

7^{-}(*cT*) **8**$^{-}$(*cT*)

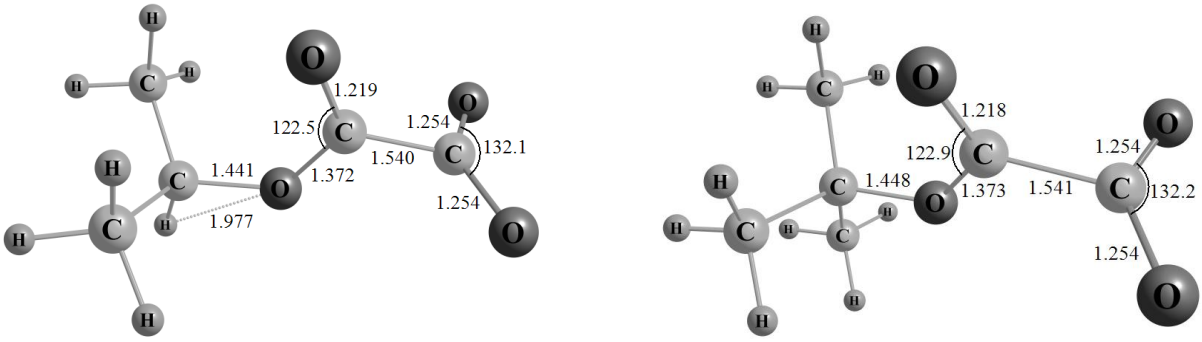

9^{-}(*tT*) **10**$^{-}$(*tT*)

Chart V.2-3: The most stable conformational minima of the alkyloxalates anions **7**$^{-}$ to **10**$^{-}$ obtained at the MP2/6-311++G(d) level of theory.

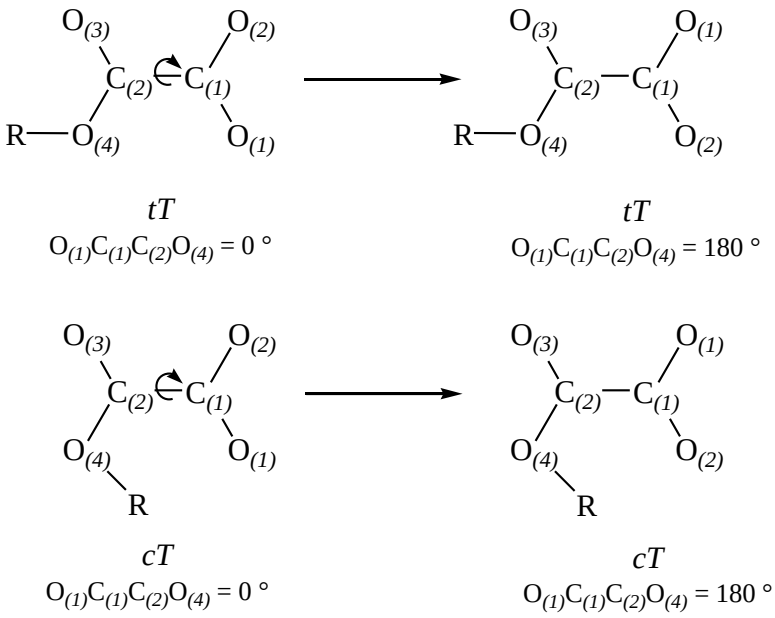

Scheme V.2-1: The conformational structure of alkyloxalates ROCOCOO^{-} (R = H, CH_3, C_2H_5, *i*-C_3H_7, and *t*-C_4H_9) is conserved by rotation of 180 ° around the $C_{(1)}$-$C_{(2)}$ axis due to the symmetry of the carboxylate group.

The connections between the various conformers of the alkyloxylates **7**$^-$ to **10**$^-$ are not as straightforward as in the case of **6**$^-$. An analysis of the normal mode associated with the imaginary frequency of the conformers *cC* and *tC* reveals that these transition structures correspond to rotations around the $C_{(1)}$-$C_{(2)}$ axis, changing the value of the dihedral angle $O_{(1)}C_{(1)}C_{(2)}O_{(4)}$ from 0 ° to 180 °. Due to the symmetry of the carboxylate group, these two values of the dihedral angle correspond to the same conformation (Scheme V.2-1).

The passage of the conformation *cT* to *tT* requires a rotation around the $C_{(2)}$-$O_{(4)}$ axis to change the dihedral angle $O_{(3)}C_{(2)}O_{(4)}R$ from 180 ° to 0 ° (R = CH_3, C_2H_5, *i*-C_3H_7, and *t*-C_4H_9). The transition structure TS(*cT*/*tT*) associated with this rotation has a T-shaped conformation and a dihedral angle $O_{(3)}C_{(2)}O_{(4)}R$ of 90 ° (R = CH_3, C_2H_5, *i*-C_3H_7, and *t*-C_4H_9). The optimized geometries of the transition structures TS(*cT*/*tT*) of the ion **7**$^-$ to **10**$^-$ are shown in Chart V.2-4, their relative energies are given in Table V.2-3 and a schematization of the conformational connections in Figure V.2-2.

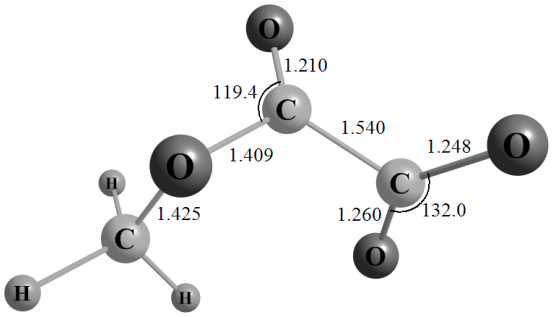

TS(*cT*/*tT*)(**7**$^-$)

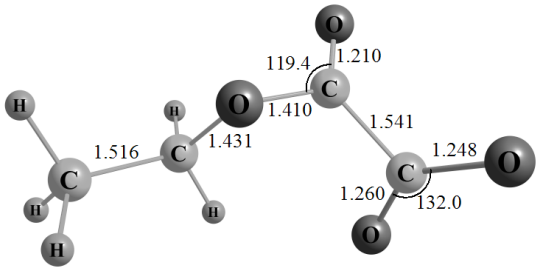

TS(*cT*/*tT*)(**8**$^-$)

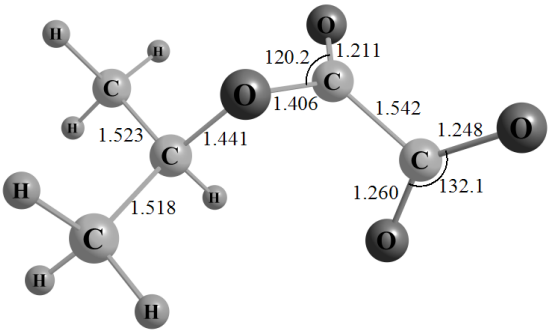

TS(*cT*/*tT*)(**9**$^-$)

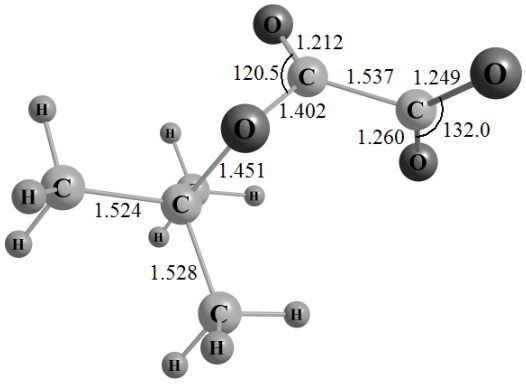

TS(*cT*/*tT*)(**10**$^-$)

Chart V.2-4: Optimized transition structures associated with the passage of the *cT* to the *tT* conformation for the ions **7**$^-$ to **10**$^-$ according to MP2/6-311++G(d) calculations.

Table V.2-3

Total and relatives energies E_{tot}[a] and E_{rel}[b] (in Hartrees, H, and in kcal/mol, respectively) of the transition structures TS(*cT*/*tT*) for the alkyloxalates **7**$^-$ to **10**$^-$ according to MP2/6-311++G(3df,3pd)//MP2/6-311++G(d) level of theory.

		E_{tot}[a] (H)	E_{rel}[b] (kcal/mol)
TS(*cT*/*tT*)	**7**$^-$	-416.3598209	8.4
	8$^-$	-455.5603955	8.0
	9$^-$	-494.7625286	4.8
	10$^-$	-533.9625372	5.3

[a] ZPE included and uniformly scaled (0.9496).

[b] Energies given relative to those of the corresponding alkyloxalates (Table V.2-2) in the most stable conformation (*cT* or *tT*).

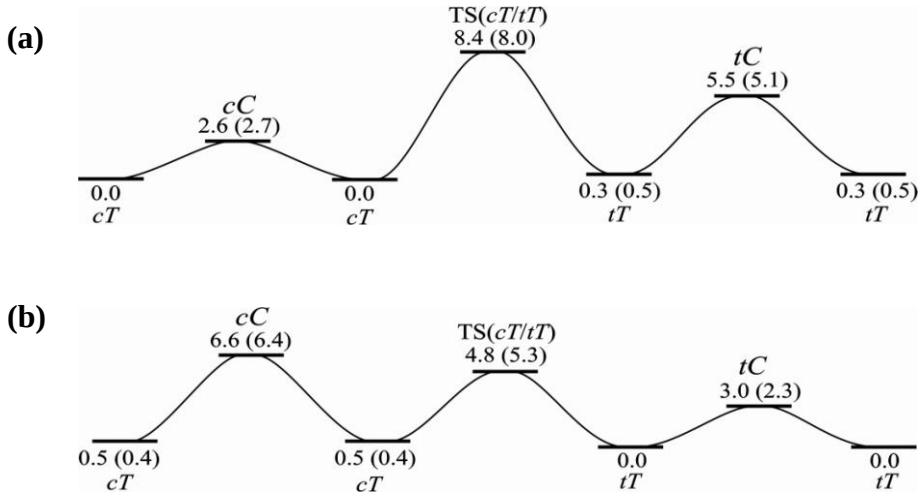

Figure V.2-2: Conformational interconversion of (a) methyloxalate ions (data for ethyloxalate in brackets) and (b) *i*-propyloxalate ions (data for *t*-butyloxalate in brackets). Energies are given relative to the conformer (a) *cT* of methyl- and ethyloxalate and (b) *tT* of *i*-propyl- and *t*-butyloxalate according to MP2/6-311++G(3df,3pd)//MP2/6-311++G(d) calculations (energies in kcal/mol).

V.2.2. Alkyloxalate Radicals

In contrast to alkyloxalate anions, the corresponding radicals do not have many stable conformational structures, even though they possess two internal rotors as well. Calculations reveal indeed that only two conformers, *tC* and *cT* (Chart V.2-5) can be defined as covalently bound, the others (*cC* and *tT*, Chart V.2-1) being found with a structure of an ion-neutral

complex. An example of the conformational structures *cC* and *tT* of **6**$^{\bullet}$ is depicted in Chart V.2.6.

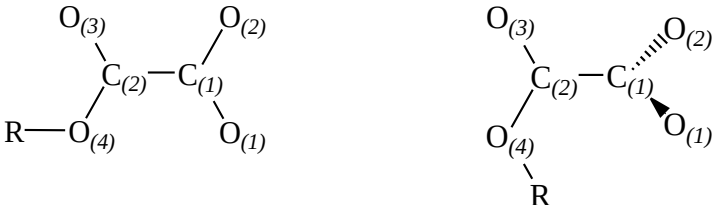

tC | *cT*

$O_{(1)}C_{(1)}C_{(2)}O_{(4)}$ = 0 ° | $O_{(1)}C_{(1)}C_{(2)}O_{(4)}$ = 90 °

$O_{(3)}C_{(2)}O_{(4)}R$ = 0 ° | $O_{(3)}C_{(2)}O_{(4)}R$ = 180 °

Chart V.2-5

The optimized geometries of **6**$^{\bullet}$(*cC*) and **6**$^{\bullet}$(*tT*) indicate clearly that these conformers have an ion-neutral complex structure of the form [$CH_3OCO^{\bullet}$ CO_2]. The bond lengths between the two carbon atoms of the carbonyl groups amount to 3.320 and 3.754 Å, respectively; this is much longer than any other bond of the radicals (Chart V.2.6). Similar geometries have been found for the conformers (*cC*) and (*tT*) of other alkyloxalates ROCOCOO$^{\bullet}$ (R = H, C_2H_5, *i*-C_3H_7, and *t*-C_4H_9) with a general structure of the form [$ROCO^{\bullet}$ CO_2].

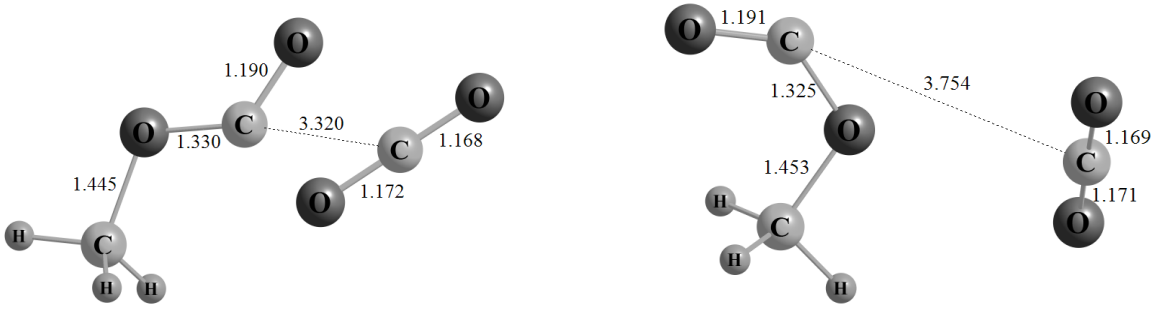

6$^{\bullet}$(*cC*) **6**$^{\bullet}$(*tT*)

Chart V.2-6: Optimized structures of the conformers *cC* and *tT* of methyloxalate **6**$^{\bullet}$ according to MP2/6-311++G(d) calculations.

In the context of this study, only covalently bound structures of alkyloxalate radicals are of interest, as they are the most likely to be stable with respect to dissociation. Therefore, only the conformations *tC* and *cT* of alkyloxalate radicals have been investigated in more details. Some structural parameters of these conformers are given in Table V.2-4 for the alkyloxalate neutrals under study.

Table V.2-4

Selected bond lengths (in Å) and bond angles (in degree) of the alkyloxalate radicals **6**$^{\bullet}$ to **10**$^{\bullet}$ in the *tC* and *cT* conformations obtained at the MP2/6-311++G(d) level of theory.

		Calculated structural parameters (Å and °)							
		$C_{(1)}O_{(1)}$	$C_{(1)}O_{(2)}$	$C_{(1)}C_{(2)}$	$C_{(2)}O_{(3)}$	$C_{(2)}O_{(4)}$	$O_{(4)}R$	$O_{(1)}C_{(1)}O_{(2)}$	$O_{(3)}C_{(2)}O_{(4)}$
6$^{\bullet}$	*tC*	1.328	1.204	1.547	1.201	1.342	0.970	123.6	126.9
	cT	1.325	1.208	1.549	1.203	1.339	0.972	123.4	125.9
7$^{\bullet}$	*tC*	1.329	1.205	1.547	1.204	1.335	1.444	123.2	127.3
	cT	1.326	1.208	1.549	1.206	1.332	1.457	123.8	123.4
8$^{\bullet}$	*tC*	1.329	1.205	1.547	1.205	1.334	1.454	123.2	127.5
	cT	1.326	1.209	1.550	1.206	1.332	1.457	124.3	123.4
9$^{\bullet}$	*tC*	1.330	1.205	1.547	1.205	1.334	1.466	123.1	128.0
	cT	1.321	1.209	1.555	1.205	1.332	1.469	125.9	123.8
10$^{\bullet}$	*tC*	1.330	1.206	1.550	1.205	1.332	1.481	123.0	129.3
	cT	1.321	1.209	1.558	1.205	1.331	1.488	126.2	124.1

For the *tC* and *cT* conformations, localization of the unpaired electron on one oxygen atom is revealed by a long $C_{(1)}$-$O_{(1)}$ bond length compared to the double bonds of $C_{(1)}$-$O_{(2)}$ and $C_{(2)}$-$O_{(3)}$; on average, they amount to 1.33 Å vs 1.205 Å (Table V.2-4). This feature differentiates the radicals from the anions for which a similar length was found for the $C_{(1)}$-$O_{(1)}$ and $C_{(1)}$-$O_{(2)}$ bonds indicating a delocalization of the negative charge over the atoms $O_{(1)}$, $O_{(2)}$, and $C_{(1)}$ (Table V.2-1).[8] This difference between anions and radicals is also reflected in the $O_{(3)}C_{(2)}O_{(4)}$ angle which is smaller by 8 ° for the radicals.

The conformations *tC* and *cT* show rather few differences in bond lengths and angles. The $C_{(1)}$-$O_{(1)}$ bond is shortened in the *cT* conformation compared with the *tC* one by 0.03 Å for the substituents H, CH_3, and C_2H_5 and by 0.09 Å for the larger ones, *i*-C_3H_7 and *t*-C_4H_9 (Table V.2-4). In contrast, the $C_{(1)}$-$O_{(2)}$ bond is longer by ca. 0.04 Å in this conformation than in the conformation *tC*. The presence of the R substituent in *cis* position in the *cT* conformation induces an increase of the $C_{(1)}$-$C_{(2)}$ and $O_{(4)}$-R bond lengths of about 0.05 Å compared with the *tT* conformation (for steric reason). Another noteworthy change between the conformations studied concerns the $O_{(3)}C_{(2)}O_{(4)}$ angle which is decreased by 4 ° on average when passing from the *cT* to the *tC* conformation. This decrease can also be attributed to a steric

hindrance of the R group: a higher value of the $O_{(3)}C_{(2)}O_{(4)}$ angle would lead to a shorter distance between the R and the $O_{(1)}C_{(1)}O_{(2)}$ groups, and disfavor a good spatial organization of R.

Table V.2-5

Total and relative energies E_{tot}[a] and E_{rel}[b] (in Hartrees, H, and in kcal/mol, respectively) of the conformers *tC* and *cT* of alkyloxalate radicals **6**• to **10**• according to MP2/6-311++G(3df,3pd)//MP2/6-311++G(d) calculations.

	Conformer	E_{tot}[a] (H)	E_{rel}[b] (kcal/mol)
6•	*tC*	-377.0292279	0.0
	cT	-377.0143191	9.4
7•	*tC*	-416.2098823	0.0
	cT	-416.1983418	7.2
8•	*tC*	-455.4103475	0.0
	cT	-455.4005186	6.2
9•	*tC*	-494.6130852	0.0
	cT	-494.6041546	5.6
10•	*tC*	-533.8139407	0.0
	cT	-533.805627	5.2

[a] ZPE included and uniformly scaled (0.9496).

[b] The energy is given relative to the conformer *tC* for each alkyloxalate.

Concerning variations of the structural parameters between the different substituents R, they prevail in particular for the *cT* conformation. When the size of R increases in this conformation, the lengths of the $C_{(1)}$-$C_{(2)}$ and $O_{(4)}$-R bonds increase as well (from 1.549 Å for R = H and 1.444 Å for R = CH_3, respectively, to 1.558 and 1.488 Å for R = *t*-C_4H_9). The angle $O_{(1)}C_{(1)}O_{(2)}$ is also affected of increases of 3 ° when the size of R increases. These changes in bond lengths and angles according to the size of the substituent R are due to steric constraints which require a "horizontal elongation" of the radical to enable the positioning of the R group. For the *tC* conformation, similar changes are observed, but they are less pronounced. The $C_{(1)}$-$C_{(2)}$ bond is increased by only 0.03 Å when passing from R = H to R = *t*-C_4H_9 and

the $O_{(4)}$-R bond undergoes a change of 0.31 Å between R = CH_3 and R = *t*-C_4H_9, which is slightly smaller than the corresponding change observed in the *cT* conformation (0.37 Å).

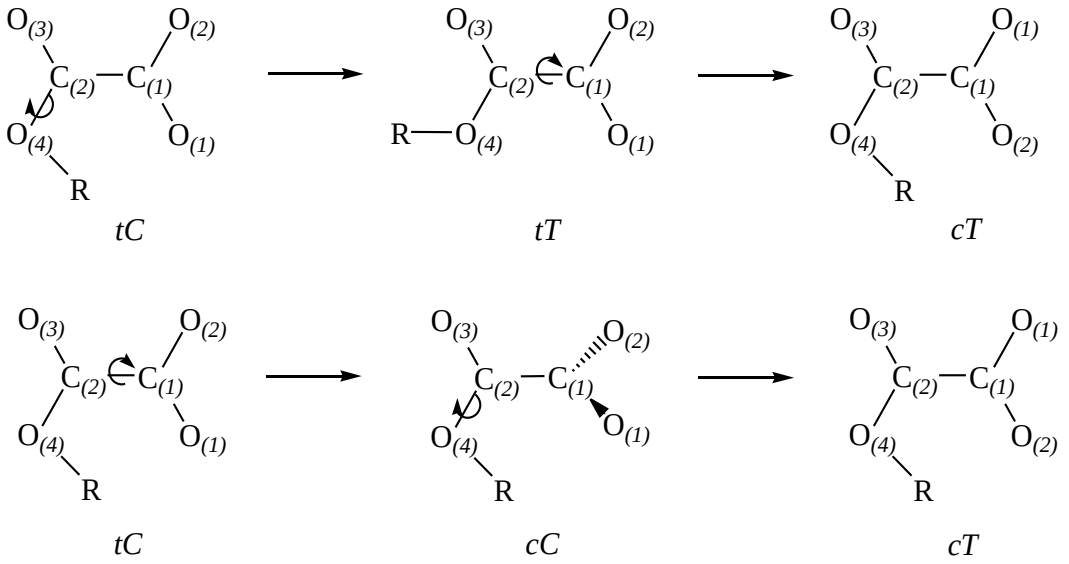

Scheme V.2-2: The two mechanisms for passage of the conformation *tC* to the conformation *cT* for alkyloxalate radicals ROCOCOO$^{\bullet}$ (R = H, CH_3, C_2H_5, *i*-C_3H_7, and *t*- C_4H_9).

Furthermore, the energies of conformers *tC* and *cT* have been determined and compared (Table V.2-5). These two conformations have been characterized as minima. For all substituents R, the conformation *tC* is more stable than *cT*. The difference between these two conformations varies according to the size of the substituents, and is larger for smaller substituents (from 5.2 kcal/mol for R = *t*-C_4H_9 to 9.4 kcal/mol for R = H). The optimized structures of alkyloxalate radicals in the *tC* conformation are shown in Chart V.2-7.

Interconnections between conformers *tC* and *cT* require two rotations, one around the $C_{(1)}$-$C_{(2)}$ axis and one around the $C_{(2)}$-$O_{(4)}$ axis. A change in conformation is therefore made through an intermediate structure, having the conformation *cC* or the *tT* (Scheme V.2-2). As already mentioned, the conformers *cC* and *tT* have a structure of ion-neutral complex (INC). For this reason, the passage of the conformation *tC* to *cT* (and vice versa) does not seem very likely as the initial and final conformations are covalently bound, whereas the intermediate is an INC. Morton[9] has indeed shown that an INC is usually not able to return to a covalently bound structure, particularly because dissociation is often the most favorable channel that INCs can follow from a kinetic and thermodynamic point of view.

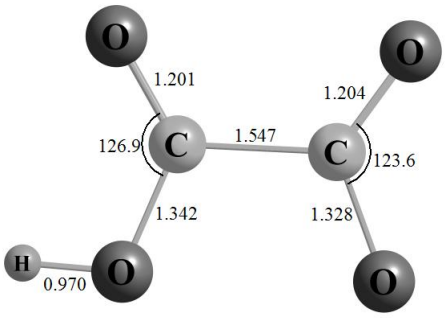

6$^{\bullet}$(*tC*)

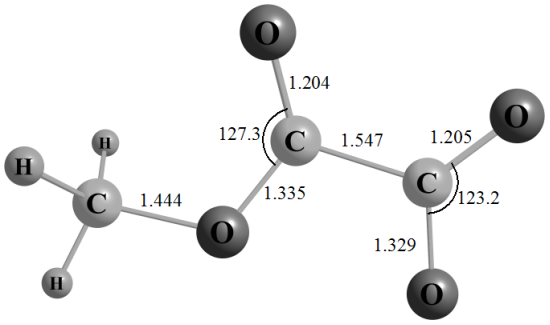

7$^{\bullet}$(*tC*)

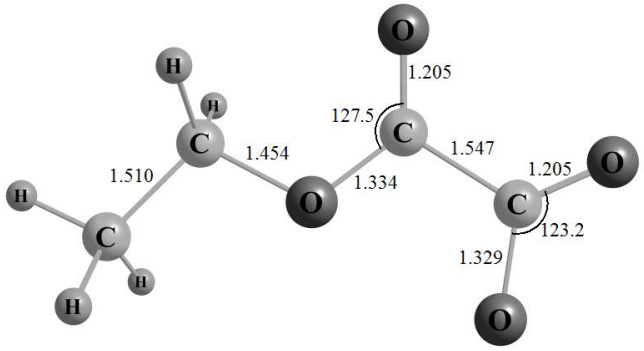

8$^{\bullet}$(*tC*)

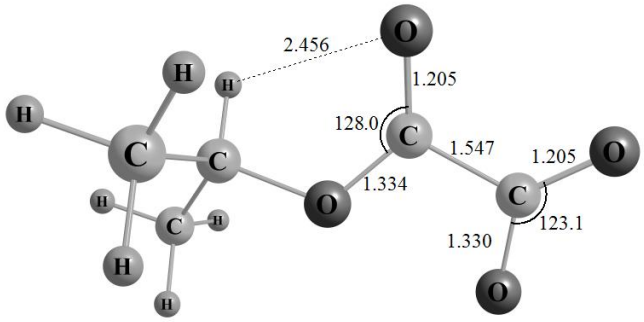

9$^{\bullet}$(*tC*)

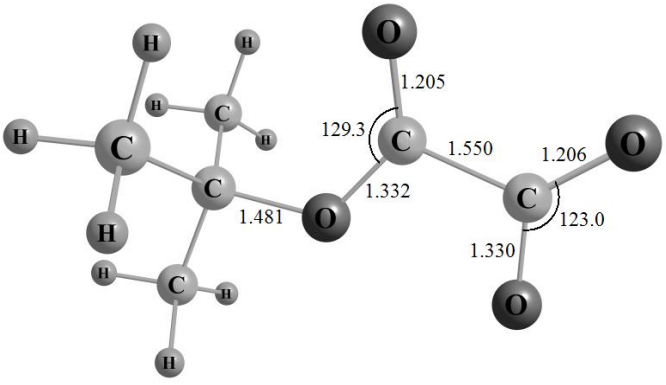

10$^{\bullet}$(*tC*)

Chart V.2-7: Optimized geometries of alkyloxalate radicals **6**$^{\bullet}$ to **10**$^{\bullet}$ in the *tC* conformation obtained at the MP2/6-311++G(d) level of theory.

V.2.3. Comparison with the Structures of Cations

To probe the gas-phase behavior of alkyloxalate radicals, charge-reversal (CR) and neutralization-reionization (NR) experiments have been used. These experiments consist in part of vertical charge-transfer processes leading to the detection of positively charged species. Determination of the structures of $ROCOCOO^+$ ions is thus important because it can help in the understanding of the signals observed. Comparison of these structures with those of anions and radicals is particularly relevant because it enables to explain the presence or absence of a recovery signal in the CR and NR spectra.

As for anions and radicals, the existence of the conformational structures *tT*, *cT*, *cC*, and *tC* (Chart V.2-1) has been probed for each (carboxyalkyl)carboxyl ions $ROCOCOO^+$ (R = H to *t*-C_4H_9). Selected structural parameters obtained are presented in Table V.2-6. It has to be noted that these ions which possess the same connectivity as the anions and radials do nevertheless not correspond to the most stable isomers of the $[RC_2O_4]^+$ potential-energy surfaces (R = H to *t*-C_4H_9).[10]

As alkoxycarboxyl cations $ROCOO^+$ (Chapter III), (carboxyalkyl)carboxyl ions possess an $O_{(1)}C_{(1)}O_{(2)}$ angle much smaller than that of corresponding anions and radicals, i.e. ca. 83 ° vs 130 ° and 124 °, respectively (Tables V.2-1, V.2-4, and V.2-6). This effect induces for the cations a $O_{(1)}$-$O_{(2)}$ bond length of ca. 1.7 Å, conferring them a quasi ring-like structure, as described for $ROCOO^+$ ions (Chapter III, section III.2.2). Furthermore, comparison of the structural parameters of $ROCOCOO^+$ for the different conformations investigated will not be made in details, as these structures have been computed mostly to enable their comparison with the structures of alkyloxalate anions and radicals.

The positive charge of (carboxyalkyl)carboxyl ions is delocalized on the atoms $O_{(1)}$, $O_{(2)}$, and $C_{(1)}$ as deduced by the similar lengths of the bonds $C_{(1)}$-$O_{(1)}$ and $C_{(1)}$-$O_{(2)}$. Extensive delocalization of the charge is also observed for the anions, but not for the radicals (Tables V.2-1 and V.2-4). Nevertheless, the $C_{(1)}$-$O_{(1)}$ and $C_{(1)}$-$O_{(2)}$ bonds of the anions are shorter than those of the cations: ca. 1.25 Å vs 1.28 Å. Concerning the $C_{(1)}$-$C_{(2)}$ bond, its lengths is similar for the cations and the radicals (about 1.55 Å) and longer for the anions (ca. 1.55 Å). No large differences are observed for the $C_{(2)}$-$O_{(3)}$ and $C_{(2)}$-$O_{(4)}$ bond lengths of anions, radicals and cations which have an average value of 1.2 and 1.3 Å respectively. The most pronounced change in geometry between (carboxyalkyl)carboxyl ions and alkyloxalate anions and radicals resides thus almost exclusively in the $O_{(1)}C_{(1)}O_{(2)}$ angle.

Table V.2-6

Selected bond lengths (in Å) and bond angles (in degree) of (carboxyalkyl)carboxyl ions $\mathbf{6}^+$ to $\mathbf{10}^+$ in the four conformations investigated[a] at the MP2/6-311++G(d) level of theory.

		Calculated structural parameters (Å and °)							
		$C_{(1)}O_{(1)}$	$C_{(1)}O_{(2)}$	$C_{(1)}C_{(2)}$	$C_{(2)}O_{(3)}$	$C_{(2)}O_{(4)}$	$O_{(4)}R$	$O_{(1)}C_{(1)}O_{(2)}$	$O_{(3)}C_{(2)}O_{(4)}$
$\mathbf{6}^+$	*tT*	1.276	1.276	1.540	1.195	1.304	0.977	84.1	135.7
	cT	1.280	1.278	1.542	1.198	1.297	0.972	83.7	130.1
	cC	1.280	1.266	1.559	1.195	1.301	0.971	85.9	129.9
	tC	1.272	1.270	1.536	1.199	1.308	0.977	86.6	135.5
$\mathbf{7}^+$	*tT*	1.277	1.277	1.540	1.200	1.292	1.483	83.6	135.8
	cT	1.283	1.281	1.550	1.202	1.286	1.467	83.0	132.0
	cC	1.279	1.269	1.567	1.200	1.291	1.462	86.0	131.4
	tC	1.273	1.271	1.534	1.201	1.297	1.480	86.1	135.5
$\mathbf{8}^+$	*tT*	1.278	1.278	1.541	1.202	1.289	1.505	83.4	136.3
	cT	1.283	1.281	1.552	1.203	1.284	1.483	83.0	132.6
	tC	1.274	1.272	1.539	1.204	1.291	1.529	85.9	137.2
$\mathbf{9}^+$	*tT*	1.279	1.278	1.542	1.203	1.286	1.529	83.2	136.6
	cT	1.284	1.282	1.550	1.205	1.281	1.503	82.5	133.1
	tC	1.274	1.272	1.540	1.205	1.290	1.554	85.8	137.6
$\mathbf{10}^+$	*tT*	1.280	1.280	1.547	1.204	1.283	1.559	83.0	138.0
	cT	1.285	1.283	1.528	1.214	1.275	1.535	82.4	131.8
	tC	1.274	1.272	1.540	1.205	1.290	1.554	85.8	137.6

[a] Structures of conformers *cC* for R = C_2H_5, *i*-C_3H_7, and *t*-C_4H_9 could not have been located.

The most stable conformation of the $ROCOCOO^+$ ions is the *cT* arrangement (see Table V.2-7) as is for radicals. One conformation, *tT*, has been found to correspond to a transition structure and is associated to a rotation of 180 ° around the $C_{(1)}$-$C_{(2)}$ axis, conserving the conformation *tC* (see Chart V.2-2). The conformers *cT* and *cC* are in general more than 9 kcal/mol less stable than the conformer *tT* (in the case of *cC*, results are given only for R = H and CH_3). The relations between the different conformers of $ROCOCOO^+$ are not shown as they are not relevant in this study. The optimized structures of (carboxyalkyl)carboxyl ions in the conformation *tC* are presented in Chart V.2-8.

Table V.2-7

Total energies E_{tot},[a] relative energies E_{rel}[b] (in Hartrees, H, and in kcal/mol, respectively) and number of imaginary frequencies of conformers of (carboxyalkyl)carboxyl ions **6**$^+$ to **10**$^+$ according to MP2/6-311++G(3df,3pd)//MP2/6-311++G(d) calculations.

	Conformer	E_{tot}[a] (Hartree)	E_{rel}[b] (kcal/mol)	Number of imaginary frequencies
6$^+$	*tT*	-376.6141604	2.0	1
	cT	-376.6015286	9.9	0
	cC	-376.602266	9.4	0
	tC	-376.6172766	0.0	0
7$^+$	*tT*	-415.8051271	2.1	1
	cT	-415.7912674	10.8	0
	cC	-415.7913418	10.8	0
	tC	-415.8085516	0.0	0
8$^+$	*tT*	-455.0094947	2.1	1
	cT	-454.9976043	9.6	0
	tC	-455.0128545	0.0	0
9$^+$	*tT*	-494.215814	2.1	1
	cT	-494.2043956	9.2	0
	tC	-494.2190831	0.0	0
10$^+$	*tT*	-533.4211112	1.7	1
	cT	-533.4093438	9.1	0
	tC	-533.4238179	0.0	0

[a] ZPE included and uniformly scaled (0.9496).

[b] The energy is given relative to the most stable conformer for each cation.

A comparison of the structures of the $ROCOCOO^+$ ions with the structures of the corresponding anions and radicals reveals large differences between the values of the $O_{(1)}C_{(1)}O_{(2)}$ angles, whereas the bond lengths are in general rather similar. As discussed in section V.4, charge-reversal $^-CR^+$ and neutralization-reionization $^-NR^+$ experiments do not lead to recovery signals (except for the $^-NR^+$ experiment of methyloxalate). The differences in

geometry between the cations, anions, and neutrals are considered as one of the major factors that causes this feature. Thus, on the one hand, bond lengths and angles of anions and radicals are roughly similar and present large differences with those of cations. On the other hand, the most stable conformations of the cations and radicals are the same, whereas those of the anions are different. A combination of these two features may therefore prevent forming transient, observable alkyloxalate radicals.

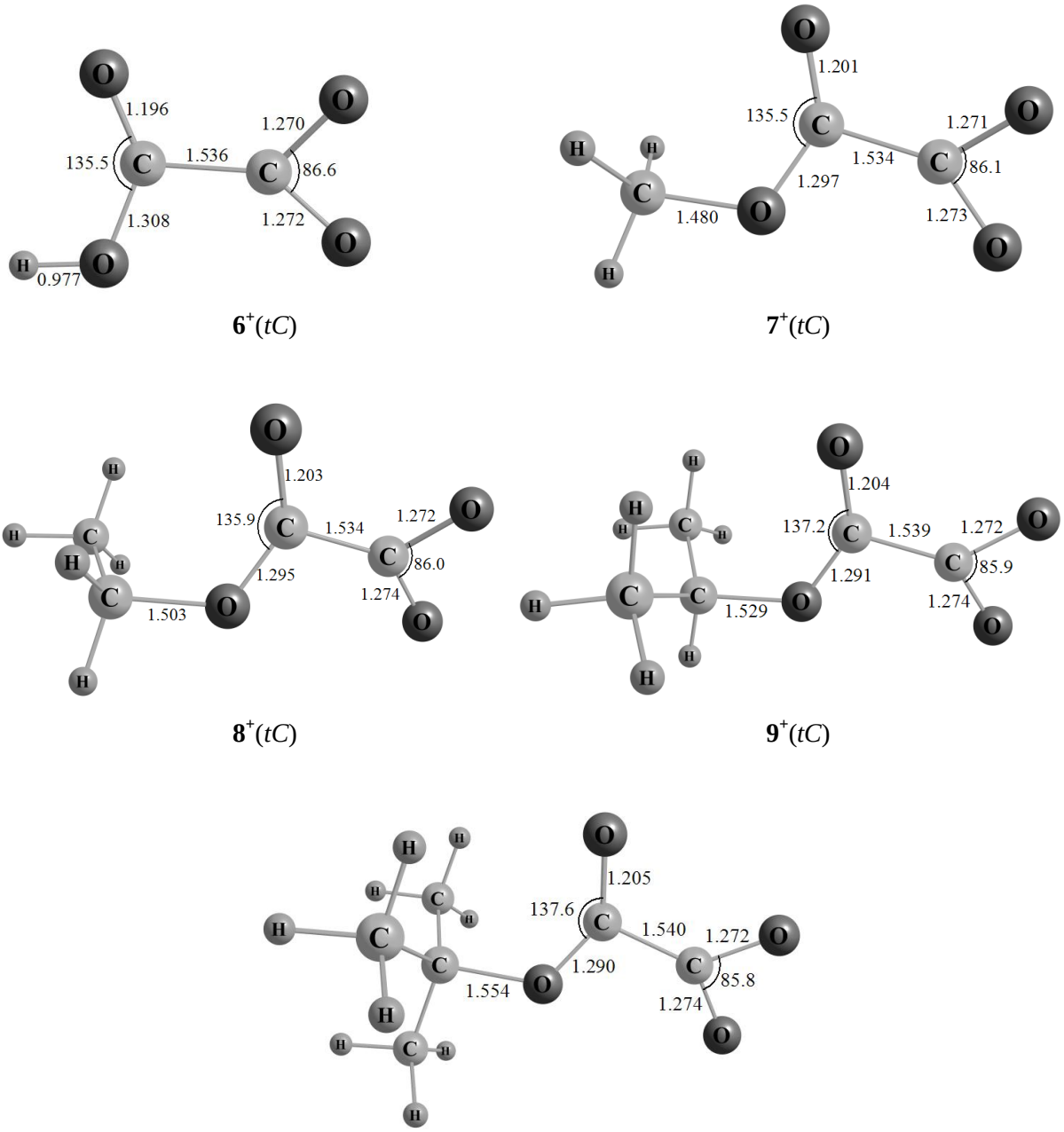

$\mathbf{6}^{+}(tC)$ $\mathbf{7}^{+}(tC)$

$\mathbf{8}^{+}(tC)$ $\mathbf{9}^{+}(tC)$

$\mathbf{10}^{+}(tC)$

Chart V.2-8: Optimized geometries of (carboxyalkyl)carboxyl ions $\mathbf{6}^{+}$ to $\mathbf{10}^{+}$ in the conformation *tC* obtained at the MP2/6-311++G(d) level of theory.

For hydrogen oxalate, the most stable structure has been found to correspond to a *cC* conformation for the anion (Table V.2-2), and to a *cT* one for the cations and radicals (Tables V.2-5 and V.2-7). Vertical ionization of $HOCOCOO^-$ leads therefore to radicals and cations with a structural conformation not very favorable, which in one case could not even be located on the potential energy surface (for $HOCOCOO^{\bullet}$). Furthermore, the two stable conformations found for $HOCOCOO^{\bullet}$, *tC* and *cT* (Table V.2-5) correspond to transition structures in the anionic state (Table V.2-2). These conformers thus cannot be reached by vertical charge transfer from the anion, and the experimental observation of this radical seems consequently compromised (see section V.5).

For the other alkyloxalates, the conformations corresponding to minima are *cT* and *tT* for the anions (Table V.2-2), and *tC* and *cT* for radicals and cations (and *cC* for $CH_3OCOCOO^+$, Tables V.2-5 and V.2-7). Consequently, one structural conformation is common to anions, radicals and cations and allows thus to envisage a successful experimental determination of the gas-phase behavior of alkyloxalate neutrals.

V.3. Thermochemistry

Standard heats of formation of the $ROCOCOO^{-/\bullet}$ species have been determined using the two methods described in Chapter II, i.e. atomization energies and bond-separation reactions. Cations have not been included even though their optimized structures have been computed because, as already mentioned, they do not correspond to the most stable isomers of the $[RC_2O_4]^+$ potential-energy surface and the calculation of their heats of formation is thus not particularly relevant.[10] The bond-separation (BS) reactions which have been used are given in Scheme V.3-1.

Heats of formation obtained for the $ROCOCOO^{-/\bullet}$ species are in rather good accordance for the different methods used (Table V.3-1). For the anions, the difference between the methods does not exceed 0.5 kcal/mol except for $HOCOCOO^-$ (0.8 kcal/mol), and for the radicals, it remains below 0.6 kcal/mol for all R.

Standard heats of formations of alkyloxalate $ROCOCOO^-$ obtained range from -206.0 (atom.) and -205.5 (BS) kcal/mol for R = CH_3 to -231.1 (atom.) and -231.7 (BS) kcal/mol for R = *t*-C_4H_9. These values are very low, compared, for instance, to those for the corresponding alkylcarboxylates $RCOO^-$ (from -120.8 to -140.1 kcal/mol for R = CH_3 to *t*-C_4H_9)[11] or alkylcarbonates ($\Delta_f H°_{298K}$ = -176 to -196 kcal/mol for R = H to *t*-C_4H_9, see Chapter III, section III.3), and they show therefore the high intrinsic stability of alkyloxalate ions. This

feature is confirmed by the high electron affinities which are obtained for the radicals and which range from 4.1 to 4.7 eV (Table V.3-1).

(a) 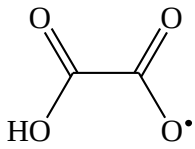

+ 4 CH_4 ⟶ $CH_3O^{\bullet}$ + CH_3OH + 2 CH_2O + C_2H_6

(b) 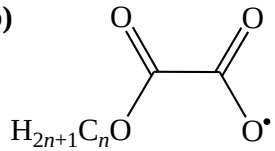

+ H_2O + (n + 3) CH_4 ⟶ $CH_3O^{\bullet}$ + 2 CH_3OH + 2 CH_2O + n C_2H_6

Scheme V.3-1: Bond-separation reactions used for the determination of the standard heats of formation of (a) hydrogen oxalate radical **6**$^{\bullet}$ and (b) alkyloxalate radicals **7**$^{\bullet}$ to **10**$^{\bullet}$ (for n = 1 to 4).

Table V.3-1

Total electronic energies $E_{CBS\text{-},0K}$ (in Hartrees, H) electron affinities *EA* (in eV), heat capacities ΔH_{298K} (in kcal/mol), heats of formation $\Delta_f H°_{298K,atom.}$ and $\Delta_f H°_{298K,BS}$ (in kcal/mol) calculated from atomization energies and bond-separation reactions, respectively, for alkyloxalate anions, and radicals **6**$^{-/\bullet}$ to **10**$^{-/\bullet}$.[a]

		$E_{CBS\text{-}Q,0K}$ (H)	*EA* (eV)	ΔH_{298K} (kcal/mol)	$\Delta_f H°_{298K,atom.}$ (kcal/mol)	$\Delta_f H°_{298K,BS}$ (kcal/mol)
6	Anion	-377.367957		3.6	-221.4	-220.6
	Radical	-377.193405	4.7	3.8	-111.6	-111.3
7	Anion	-416.562025		4.9	-206.0	-205.5
	Radical	-416.407415	4.2	4.8	-109.0	-108.5
8	Anion	-455.79342		5.7	-214.5	-214.4
	Radical	-455.638608	4.2	5.6	-117.4	-117.2
9	Anion	-495.021026		6.4	-220.7	-220.9
	Radical	-494.871674	4.1	6.4	-127.0	-127.2
10	Anion	-534.255404		7.2	-231.1	-231.7
	Radical	-534.103852	4.1	7.1	-136.0	-136.6

[a] Results given for the most stable conformers of anions and radicals which have been determined in the previous section.

For radicals, more data are available for comparison in the literature. Thus, the heats of formation obtained range on average from -111.5 kcal/mol for R = H to -136.5 kcal/mol for R = *t*-C_4H_9 (Table V.3-1), whereas for the same substituents R, heats of formation of the alkylcarboxylate neutrals $RCO_2^{\bullet}$ range from -49.6[12] to -65.1 kcal/mol,[11] for the alkylcarbonate radicals $ROCO_2^{\bullet}$ from -82.3 to -108.9 kcal/mol (Chapter III, section III.3), and for the alkylperoxyl radicals $RC(O)OO^{\bullet}$ from -22.1 to -51.2 kcal/mol.[13] All these values are much larger than those obtained for the alkyloxalate radicals, which thus imply a high intrinsic stability for these species.

V.4. Unimolecular Reactivity of Alkyloxalate Ions

To study the gas-phase behavior of the alkyloxalate ions $\mathbf{6}^-$ to $\mathbf{10}^-$, they have been submitted to MI and CA experiments. The results obtained are summarized in Table V.4-1 and reveal that, in general, the anions $\mathbf{6}^-$ to $\mathbf{10}^-$ show a rather similar behavior. Quite surprisingly, all spectra are largely dominated by a signal corresponding to the loss of neutral CO (Δm = 28). Two minor signals refer to the elimination of CO_2 (Δm = 44) and to the combined losses of CO_2 and CO (Δm = 72). The spectra are thus exclusively composed by signals corresponding to CO_x losses (x = 1, 2); no other eliminations are capable to compete with these processes. Furthermore, almost no drastic changes occur when the internal energy of the system is increased (CA experiment), in contrast to what is in general expected in comparing MI and CA processes.[14]

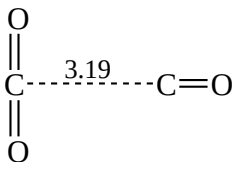

Chart V.4-1: Structure of most stable isomer of $^1C_2O_3$. The bond length (in Å) is taken from Peppe *et al.*[15]

The decomposition process corresponding to the combined loss of CO_2 and CO could consist of either a direct loss of one or a consecutive loss of two neutral molecules. As only small changes in intensity for this signal are observed between the MI and CA experiments, the second hypothesis seems less likely as an internal energy gain (by collision) of the system should accordingly lead to a higher intensity. While we attribute this reaction to the formation

of CO and CO_2, it has to be mentioned that, in principle, it could also correspond to the loss of a genuine neutral C_2O_3 unit. This molecule has already been extensively studied by both experiment and theory.[15-20] Peppe *et al.*[15] have shown that the most stable structure of neutral C_2O_3, in the singlet multiplicity, corresponds to a van der Waals complex (Chart V.4-1) which is stable with respect to dissociation to CO_2 and CO by only 1.2 kcal/mol (CCSD(T)/aug-cc-pVDZ//B3LYP/6-31G(d) level of theory). For this reason, we assume that if the neutral species with $\Delta m = 72$ corresponds to C_2O_3, it seems very likely that it dissociates immediately into CO and CO_2. In the following, we will hence assume that the mass difference of $\Delta m = 72$ corresponds to the combined formation of CO + CO_2, rather than genuine C_2O_3.[21]

Table V.4-1

Intensities[a] of fragments in MI and CA[b] spectra of mass-selected[c] alkyloxalates ROCOCOO$^-$ (**6**$^-$ to **10**$^-$ with R = H, CH_3, C_2H_5, *i*-C_3H_7, and *t*-C_4H_9).

R (*m/z*)[d]		– CO	– CO_2	– (CO + CO_2)
H (89)	MI	100	1	1
	CA	100	2	2
CH_3 (103)	MI	100	1	1
	CA	100	1	2
C_2H_5 (117)	MI	100	1	1
	CA	100	2	1
i-C_3H_7 (131)	MI	100	3	1
	CA	100	3	2
t-C_4H_9 (145)	MI	100	13	0
	CA	100	16	4

[a] Intensity relative to the base peak (= 100); peaks < 1 are neglected.

[b] CA obtained with He (80% T) in C3 (Figure II.2-1).

[c] Mass selection was made using B1 while E1 was scanned.

[d] Mass-to-charge ratio of precursor anion in amu.

The structure of the product ion and the mechanism by which decarbonylation ($\Delta m = 28$) occurs is not obvious because this fragment cannot be formed in a direct bond cleavage of the anions, as is the case for the decarboxylation or the combined elimination of CO_2 and CO.

Nevertheless, the nature of the product ions due to CO loss can be easily probed by MS/MS experiments because their intensities are high enough to allow consecutive mass selection of the alkyloxalates and of the subsequently formed fragment ions (Table V.4-2).

Table V.4-2

Intensities of observed fragments in the CA/CA spectra of $[C_{n+1}H_{2n+1}O_3]^-$ ions formed from mass-selected alkyloxalates $ROCOCO_2^-$ (R = C_nH_{2n+1}, n = 1 to 4).

R	Selection[b]	*m/z* (Intensity)[b,c]
H	89/61	17 (100), 60 (80)
CH_3	103/75	31 (100), 45 (48), 60 (20)
C_2H_5	117/89	43 (6), 45 (100), 60 (5)
i-C_3H_7	131/103	57 (4), 59 (100), 60 (2)
t-C_4H_9	145/117	57 (20), 60 (11), 73 (100)

[a] CA/CA obtained with He (80 % T) in C3 and C5 (Figure II.2-1, Chapter II).

[b] Mass-to-charge ratio in amu.

[c] Intensity relative to the base peak (= 100).

[d] The experiment consists in selecting the precursor ion alkyloxalate with B1 and the resulting charged fragments with E1 while B2 is scanned. The masses indicated correspond to the mass of the alkyloxalate parent and to the mass of the fragment selected with E1.

The loss of CO from the alkyloxalates $ROCOCOO^-$ formally leads to $[C_{n+1}H_{2n+1}O_3]^-$ ions with R = C_nH_{2n+1} and n = 1 to 4. The CA/CA mass spectra of these ions (Table V.4-2) are dominated by signals of the corresponding alkoxide ions RO^- (loss of neutral CO_2). A characteristic peak for the loss of alkyl radicals concomitant with the generation of the radical anion $CO_3^{\bullet -}$ (*m/z* = 60) is also present, which indicates that all three oxygen atoms are bound to the same carbon atom. Moreover, in the case of the $C_2H_3O_3^-$ ion, elimination of formaldehyde concomitant with formation of HCO_2^- also takes place. This CA/CA spectrum agrees thus well with the CA spectrum of methylcarbonate given by Hayes and coworkers,[22] as well as the other CA/CA data given in Table V.4-2, with CA experiments of genuine alkylcarbonate ions $ROCOO^-$ (Table III.3-1, Chapter III). O'Hair and coworkers[23] have also investigated the unimolecular reactivity of $HOCOCOO^-$ ions and observed a fragment at *m/z* = 61 which

they attributed to the hydrogencarbonate ion $HOCOO^-$. A consideration of the thermochemistry of the dissociation of the alkyloxalates **6**$^-$ - **10**$^-$ further reveals that the decomposition of alkyloxalate ions into alkylcarbonates and CO is quite favorable, as it is endothermic by only a few kcal/mol (Table V.4-3). In comparison, the direct bond cleavages leading to decarboxylation as well as decarboxylation combined with decarbonylation are more than 30 kcal/mol higher in energy. Decarboxylation leads to alkoxycarbonyl anions $ROCO^-$ which are well-known species in the gas phase,[24,25] and alkoxy anions RO^- are obtained by simultaneous loss of CO_2 and CO from alkyloxalates.[24,26]

Table V.4-3

Calculated heats of reaction[a] at 298 K (in kcal/mol) of the observed dissociation processes of alkyloxalates $ROCOCOO^-$ (**6**$^-$ to **10**$^-$ with R = H, CH_3, C_2H_5, *i*-C_3H_7, and *t*-C_4H_9) obtained at the MP2/6-311++G(3df,3pd)//MP2/6-311++G(d) level of theory.[b]

	$\Delta_rH°_{298K}$ (kcal/mol)[a]		
R	$ROCOO^- + CO$	$ROCO^- + CO_2$	$RO^- + CO + CO_2$
H	17.7	44.9	60.3
CH_3	9.2	35.5	47.0
C_2H_5	8.7	34.2	43.8
i-C_3H_7	5.1	32.5	38.5
t-C_4H_9	7.4	31.3	37.6

[a] ZPE included and uniformly scaled (0.9496).

[b] Total energies of alkyloxalates are obtained from the most stable conformation and taken from Table V.2-2.

The general dissociation scheme of alkyloxylates can accordingly be summarized by three competing pathways with decarbonylation as the by far major route (Scheme V.4-1).

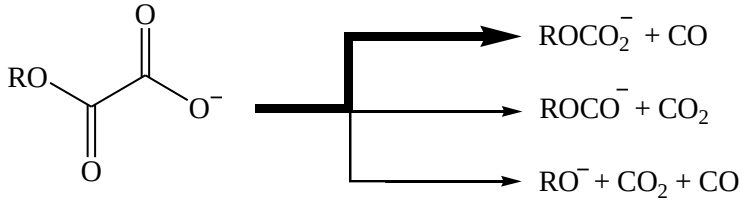

Scheme V.4-1: General dissociation scheme of alkyloxalates $ROCOCOO^-$ for R = H, CH_3, C_2H_5, *i*-C_3H_7, and *t*-C_4H_9. The bold arrow indicates the main dissociation pathway.

As far as the direct bond cleavages are concerned, the question of mechanisms is rather clear. In contrast, decarbonylation of alkyloxalates cannot be understood that easily because it requires a rearrangement of the anion; moreover, alkyloxylates possess two different carbonyl groups, which can potentially be eliminated. Two mechanisms appear most plausible (Scheme V.4-2). The first one, denoted as **A**, consists in the intermediary formation of an ion-neutral complex [$ROCO^-$ CO_2] from the alkyloxalate (for R = H to *t*-C_4H_9), followed by an intracomplex attack of carbon dioxide by the nucleophilic oxygen atom $O_{(4)}$ in the complex (INC_A).[27] This mechanism has been proposed by O'Hair and coworkers[23] in the study of the dissociation of the hydrogen oxalate ion, but has not been probed any further neither theoretically nor experimentally. The second variant, denoted as **B**, consists in a direct attack of the electrophilic atom $C_{(2)}$ by the oxygen atom $O_{(1)}$ carrying the negative charge in alkyloxalate with subsequent elimination of CO. For an example of an acid-catalyzed decarbonylation of α-keto carbonic acid involving the carboxyl CO group see Banholzer[28] and Elliott.[29] Experimentally, these two mechanisms could be probed by means of labeling experiments because the atoms involved are not the same;[30] however a selective synthesis of labeled ions such as $ROC^{18}OCOO^-$, $RO^{13}COCOO^-$, $ROCOCO^{18}O^-$ or $ROCO^{13}COO^-$ is far from being trivial and was hence not pursued any further.

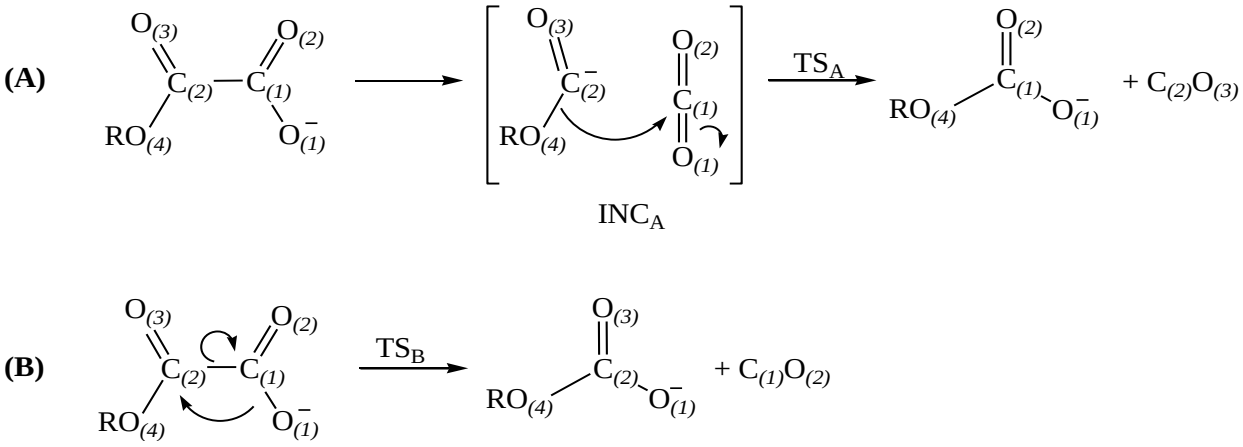

Scheme V.4-2: Two mechanistic variants for the decarbonylation of alkyloxalates $ROCOCOO^-$ (R = H, CH_3, C_3H_5, *i*-C_3H_7, and *t*-C_4H_9).

Instead, the two mechanisms have been studied computationally. Structures and energies of the transitions structures of variants **A** and **B** have been calculated at the MP2/6-311++G(3df,3pd)//MP2/6-311++G(d) level of theory, as well as the ion-neutral complex involved in mechanism **A** for the five alkyloxalates $\mathbf{6}^-$ to $\mathbf{10}^-$. The resulting energies are sum-

marized in Table V.4-4. Furthermore, a scan of the potential-energy surface revealed that the formation of INC_A proceeds without a barrier (Figure V.4-1).

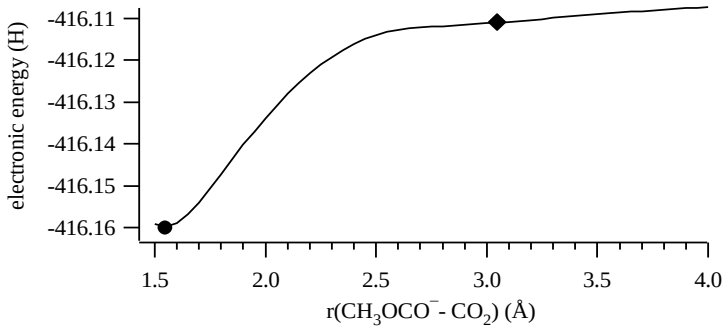

Figure V.4-1: Projection of the potential-energy surface of $CH_3OCOCOO^-$ on the r(CH_3OCO^-–CO_2) coordinate as determined by single point energy calculations (MP2/6-311++G(d). Here, the bond CH_3OCO^-–CO_2 was kept frozen, while all other parameters of the species were fully optimized. Further, the circle indicates the position of the equilibrium geometry of $CH_3OCOCOO^-$ and the diamond that of INC_A(**6**$^-$).

In general, the transition structures TS_A associated with mechanism **A** are by up to 20 kcal/mol lower in energy than the TS_B related to mechanism **B**. Formation of the ion-neutral complex INC_A costs on average 30 kcal/mol relative to the alkyloxalates, except for the hydrogen oxalate ion which is 38 kcal/mol less stable. From an energetic point of view, mechanism **A** is thus much more favorable than variant **B**. What can further help to exclude mechanism **B** is a consideration of the relative intensities of the fragment ions in the MI and CA experiments performed on alkyloxalates (Table V.4-2) as well as the energy demands of the various fragments (Table V.4-3). Decarbonylation dominates all spectra, which is partly explained by a most favorable thermochemistry of the products obtained as compared to those obtained from decarboxylation and simultaneous decarboxylation and decarbonylation. Nevertheless, this dissociation requires the passage through a transition structure, whereas the two other dissociations pathways are direct bond cleavages which, most likely, require no excess activation energies. If the transition structure associated with decarbonylation were energetically extremely demanding, the alkyloxalate ions would not be able to cross it particularly in the MI process and the other dissociation pathways would be accordingly more present. Hence, the transition structures TS_A which are similar in energy to the resulting products seems to be highly favored in the course of dissociation of alkyloxalates. By comparing the experimental results with the energies predicted for TS_A and TS_B, we conclude

that decarbonylation occurs through a mechanism of type **A**. The optimized structures of both INC_A and TS_A and of are presented in Chart V.4-2 for each alkylcarbonates **6**$^-$ to **10**$^-$.

Table V.4-4

Total and relatives energies (in Hartrees, H, and in kcal/mol, respectively) of the transition states TS_A[a] and TS_B[a] and of the ion-neutral complex, INC_A,[a] involved in the course of decarbonylation of alkyloxalates **6**$^-$ to **10**$^-$ at the MP2/6-311++G(3df,3pd)//MP2/6-311++G(d) level of theory.

		E_{tot}[b] (Hartree)	E_{rel}[c] (kcal/mol)
	TS_A	-377.1428343	43.7
6$^-$	INC_A	-377.1513545	38.3
	TS_B	-377.1044195	67.8
	TS_A	-416.3154505	36.3
7$^-$	INC_A	-416.3239468	30.9
	TS_B	-416.2786243	59.4
	TS_A	-455.5148716	36.1
8$^-$	INC_A	-455.5234566	30.7
	TS_B	-455.4771170	59.7
	TS_A	-494.716657	33.6
9$^-$	INC_A	-494.725741	27.9
	TS_B	-494.657488	70.7
	TS_A	-533.9136187	37.7
10$^-$	INC_A	-533.9236912	31.4
	TS_B	-533.8770840	60.6

[a] TS_A and TS_B correspond to the respective transition structures associated with the mechanistic variants **A** and **B** (Scheme V.4-2), and INC_A stands for the ion-neutral complex formed prior to decarbonylation.

[b] ZPE included and uniformly scaled (0.9496).

[c] Energies are given relative to those of the alkyloxalates in their most stable conformation (Table V.2-2).

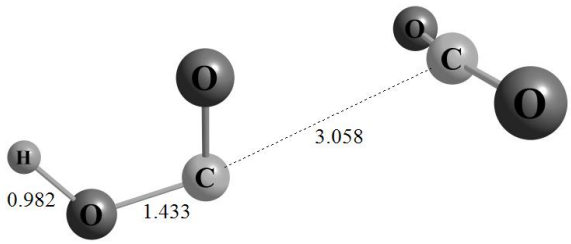

$INC_A(\mathbf{6}^-)$

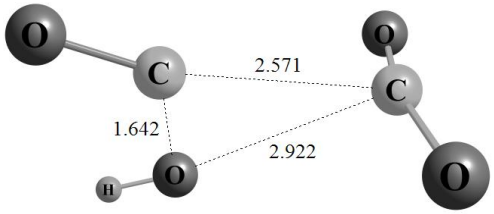

$TS_A(\mathbf{6}^-)$

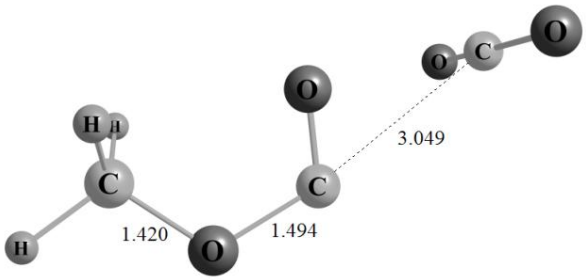

$INC_A(\mathbf{7}^-)$

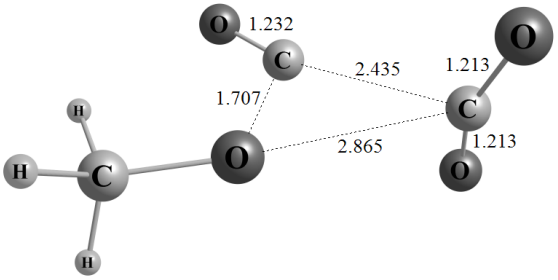

$TS_A(\mathbf{7}^-)$

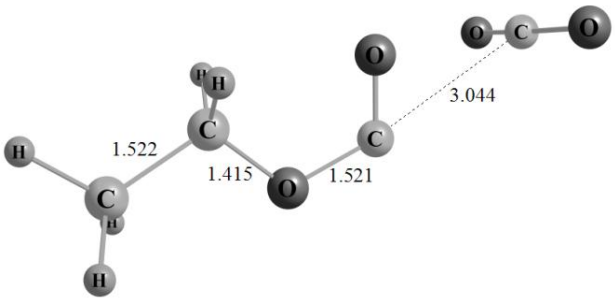

$INC_A(\mathbf{8}^-)$

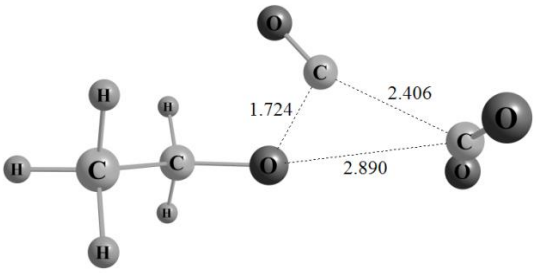

$TS_A(\mathbf{8}^-)$

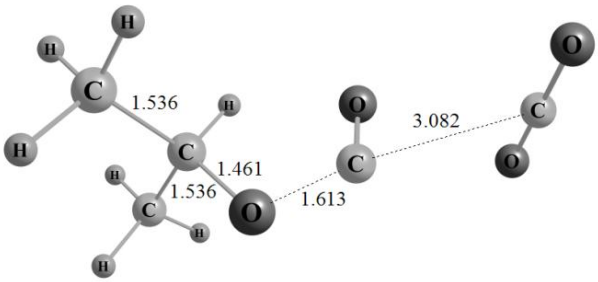

$INC_A(\mathbf{9}^-)$

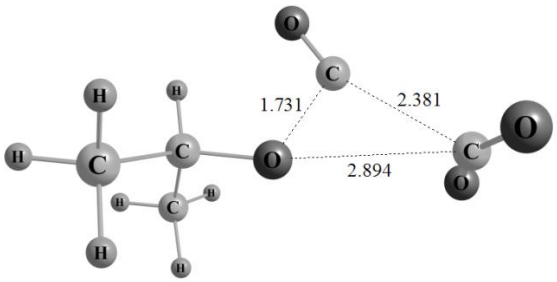

$TS_A(\mathbf{9}^-)$

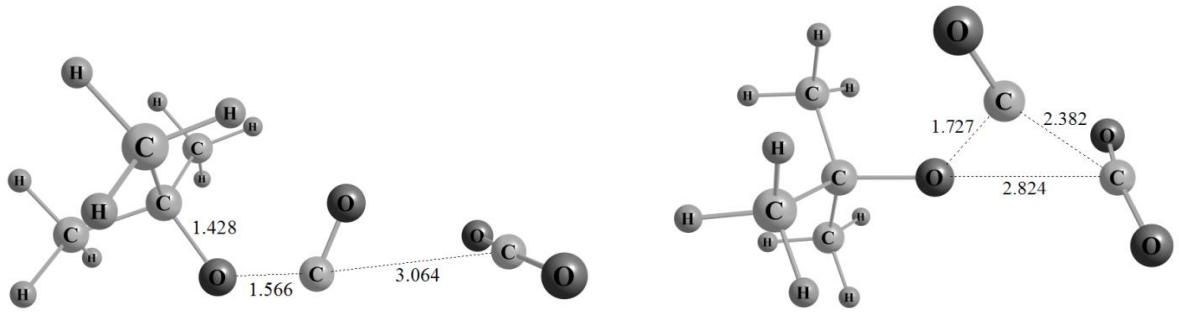

INC_A(**10**$^-$) TS_A(**10**$^-$)

Chart V.4-2: Optimized structures of the ion-neutral complexes INC_A and the transitions structures TS_A for the five alkyloxalates under study at the MP2/6-311++G(d) level of theory.

V.5. NIDD Study of Alkyloxalate Radicals

The gas-phase behavior of alkyloxalate radicals has been probed with the help of the NIDD method.[31] To this end, alkyloxalates $ROCOCOO^-$ have been submitted to charge-reversal and neutralization-reionization experiments. The resulting spectra are presented in Table V.5-1.

The CR and NR spectra of alkyloxalates differ mostly by the intensities of the ions observed, but some signals appear exclusively in either CR or NR spectra. Thus, for all alkyloxalates investigated, the *m/z* = 56 ion is present in the CR but not in the NR spectra (except for that of *t*-$C_4H_9OCOCOO^-$, see below). This ion most likely corresponds to ionized ethylene dione, $C_2O_2^{\bullet+}$ and is related to the ion chemistry.[32] In the $^-CR^+$ spectrum of methyloxalate, a weak signal at *m/z* = 88 is present, which does not appear in the corresponding $^-NR^+$ spectrum. This ion is attributed to the 1,2-dioxoethane-3,4-dione ion $C_2O_4^{\bullet+}$ and is associated with the cation chemistry.

The fragmentation is, in general, massive in the CR and NR spectra of alkyloxalates and many fragments with small *m/z* ratios are present, like $CO^{\bullet+}$ (*m/z* = 28), HCO^+ (*m/z* = 29), $CH_2O^{\bullet+}$ or $CHOH^{\bullet+}$ (*m/z* = 30). The CR and NR spectra of hydrogen-, methyl-, and ethyloxalates are dominated by the signal corresponding to $CO_2^{\bullet+}$ (*m/z* = 44) whereas those of *i*-propyl- and *t*-butyloxalates have the *m/z* = 43 ion and *m/z* = 57 (for NR of *t*-butyloxalate) ions as main signal. These two ions corresponds to $C_3H_7^+$ or CH_3CO^+ at *m/z* = 43 and to $C_4H_7^+$ or $C_2H_5CO^+$ or $C_2O_2H^+$ at *m/z* = 57. The assignment of these peaks will be discussed further.

Table V.5-1

Intensities[a] of selected[b] fragments in the $^{-}CR^{+c}$ and $^{-}NR^{+c}$ spectra of mass-selected[d] alkyloxalates RO-COCOO^{-} (**6**$^{-}$ to **10**$^{-}$ with R = H, CH_3, C_2H_5, *i*-C_3H_7, and *t*-C_4H_9).

R (*m/z*)[e]
H (89)
CR: 17 (1), 28 (64), 29 (45), 40 (2), 44 (100), 45 (97), 56 (9), 72 (5)
NR: 17 (12), 28 (80), 29 (24), 40 (1), 44 (100), 45 (79)
CH_3 (103)
CR: 28 (18), 29 (25), 30 (7), 40 (2), 44 (100), 45 (5), 56 (7), 59 (36), 72 (3), 88 (3)
NR: 28 (64), 29 (43), 30 (21), 40 (16), 44 (100), 45 (8), 59 (11), 103 (7)
C_2H_5 (117)
CR: 26 (7), 28 (20), 29 (59), 30 (10), 43 (16), 44 (100), 45 (3), 56 (5), 72 (1)
NR: 26 (15), 28 (84), 29 (44), 30 (14), 43 (25), 44 (100), 45 (2)
i-C_3H_7 (131)
CR: 28 (13), 29 (13), 40 (7), 42 (18), 43 (100), 44 (92), 45 (7), 56 (3)
NR: 28 (46), 29 (15), 40 (19), 42 (57), 43 (100), 44 (86), 45 (3), 58 (1)
t-C_4H_9 (145)
CR: 28 (13), 29 (13), 39 (40), 41 (46), 43 (100), 44 (74), 45 (7), 56 (15), 57 (36), 58 (52)
NR: 28 (39), 29 (17), 39 (94), 41 (95), 43 (69), 44 (71), 45 (4), 56 (63), 57 (100), 58 (12)

[a] Intensity relative to the base peak (= 100) into brackets.

[b] Due to the large number of fragments present in the $^{-}CR^{+}$ and $^{-}NR^{+}$ spectra of alkyloxalates, only the major signals and those considered the most relevant ones are presented.

[c] CR obtained with O_2 (80 % T) in C5 and NR with O_2 (80 % T) in C5 and C6.

[d] The mass selection was made with B1/E1 while B2 was scanned.

[e] Mass-to-charge ratio in amu.

Except for the $^{-}NR^{+}$ spectrum of $CH_3OCOCOO^{-}$, no recovery signal was observed in the CR and NR spectra of alkyloxalates (Table V.5-1). This result was somewhat expected in view of the computed geometries of $ROCOCOO^{-/\bullet/+}$ species (section V.1). Consistent differences in geometries and conformational minima between anions, radicals, and cations were indeed observed and have already been discussed. For hydrogen oxalate, comparison of the computed structures has even predicted that $HOCOCOO^{\bullet}$ is not reachable from the anions. Therefore, even though alkyloxalate neutrals may correspond to long-lived species, no reco-

very signal is present in the spectra. A necessary condition which needs to be fulfilled in order to apply the NIDD scheme concerns the existence of the neutrals of interest in the time scale of the experiment.[31] To probe their existence, when not established by the $^{-}NR^{+}$ experiments, $^{-}NR^{-}$ experiment can be utilized.[33] We have thus recorded the $^{-}NR^{-}$ spectra of alkyloxalates for all R substituents. An example of a spectrum obtained is given in Figure V.5-1 for methyloxalate.

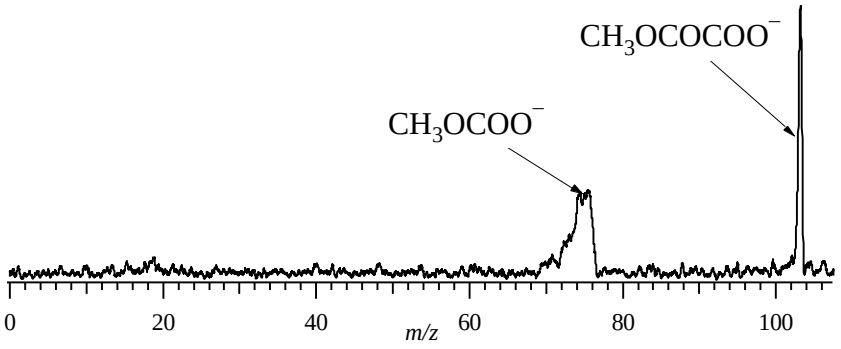

Figure V.5-1: $^{-}NR^{-}$ spectrum of B1-mass selected $CH_3OCOCOO^{-}$ **7**$^{-}$ (*m/z* = 103) using O_2 (C2, 80 % T) and Xe (C3, 80 % T).

The spectrum in Figure V.5-1 shows signals at *m/z* = 75 and *m/z* = 103, respectively. The former is attributed to methylcarbonate CH_3OCOO^{-}, formed from dissociation of methyloxalate referring to the investigation of the gas-phase behavior of alkyloxalate anions that has been treated in the previous section. The broadening of this signal is due to some kinetic energy released which originates from the associated reverse energy of the dissociation (see section V.4). Furthermore, the signal at *m/z* = 103 corresponds to $CH_3OCOCOO^{-}$. As all charged species are deflected before reionization, this signal originates unambiguously from the corresponding neutral. The existence of $CH_3OCOCOO^{\bullet}$ in the µs time scale of the experiment has thus been established. Similar spectra have been obtained for alkyloxylates with larger substituents R (R = C_2H_5 to *t*-C_4H_9), but not for hydrogen oxalate. The corresponding radical may nevertheless exist as a long-lived species but as it could not have been observed experimentally, the NIDD scheme cannot be applied to probe its reactivity.

As the existence of alkyloxalate radicals $ROCOCOO^{\bullet}$ (R = CH_3 to *t*-C_4H_9) has been established in the instrument time scale, the NIDD method can be applied to these neutrals in order to determine their gas-phase chemistry. The spectra obtained are given in Figure V.5-2. As defined in the NIDD method (Chapter II, section II.2.7), positive signals are related to the neutral chemistry and negative ones to the ion chemistry.[31]

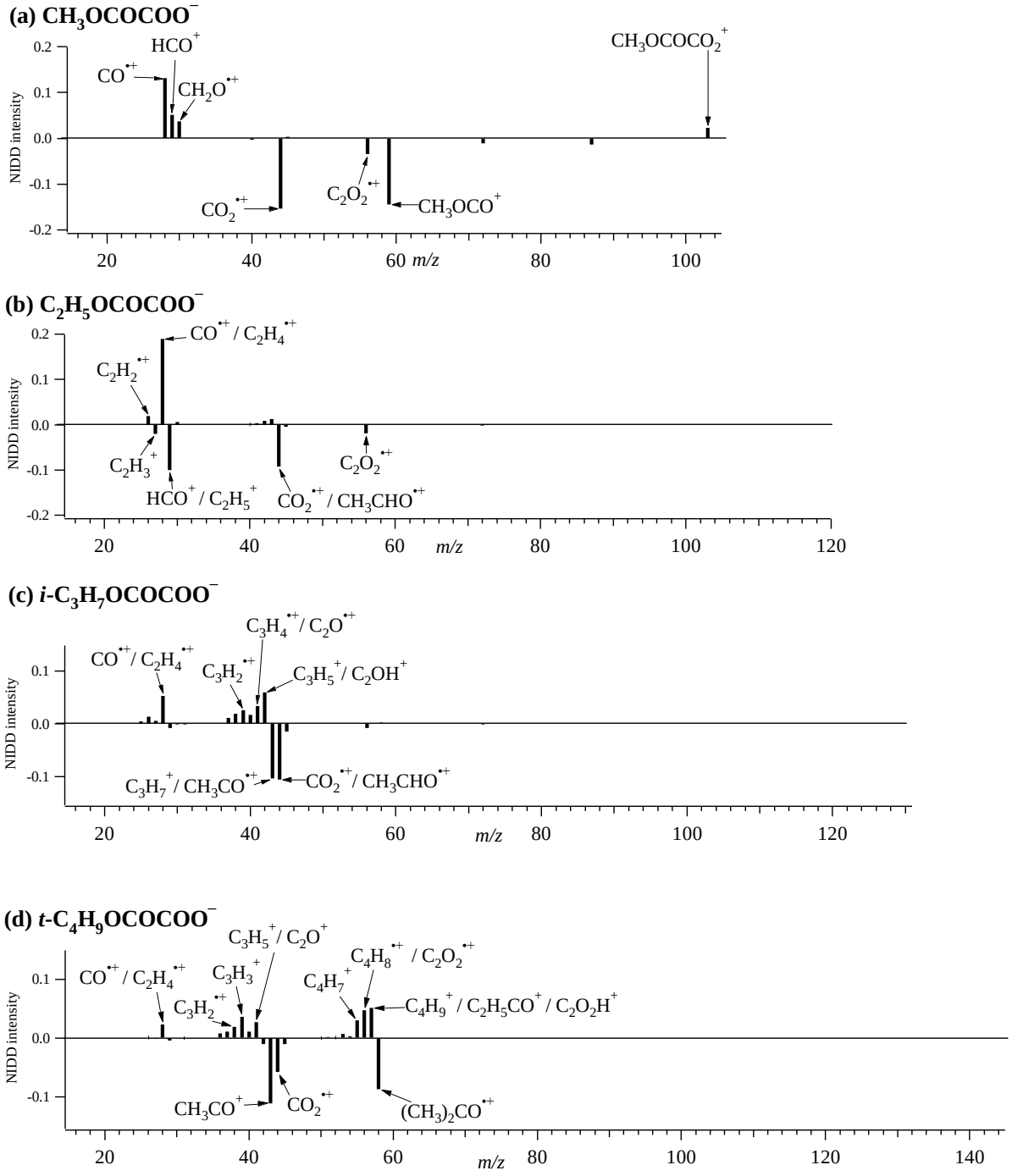

Figure V.5-2: $^{-}$NIDD^{+} spectra of the alkyloxalates under study. All signals with intensity higher than |0.02| are assigned.

The NIDD spectrum of $CH_3OCOCOO^-$ provides only little information concerning the neutral chemistry. Except the signal for $CH_3OCOO^{\bullet}$ which has survived the reionization into $CH_3OCOCOO^+$, three ions appear in the positive part of the spectrum (Figure V.5-2a): $CO^{\bullet+}$ (*m/z* = 28), HCO^+ (*m/z* = 29), and $CH_2O^{\bullet+}$ (*m/z* = 30). The ions $CO^{\bullet+}$ (in part), HCO^+, and $CH_2O^{\bullet+}$ most likely originates from dissociation of CH_3O^+ obtained by vertical ionization of

$CH_3O^{\bullet}$. Hornung *et al.*[34] have investigated the gas-phase behavior of alkoxide radicals $RO^{\bullet}$ (R = C_nH_{2n+1}, for n = 1 to 6) by means of the NIDD method. The authors have shown that the CH_3O^+ ion is unstable with respect to dissociation, when formed by vertical ionization from transient $CH_3O^{\bullet}$. The fragments formed therefrom are $CH_2O^{\bullet+}$, HCO^+, and $CO^{\bullet+}$, as observed in the positive part of the spectrum in Figure V.5-2a.

Table V.5-2

Calculated heats of reaction[a] at 298 K (in kcal/mol) of possible dissociation processes of alkyloxalates $ROCOCOO^-$ (R = H, CH_3, C_2H_5, *i*-C_3H_7, and *t*-C_4H_9) obtained at the MP2/6-311++G(3df,3pd)// MP2/6-311++G(d) level of theory.

R	$\Delta_r H°_{298K}$ (kcal/mol)[a]			
	$ROCO^{\bullet} + CO_2$	$ROCOO^{\bullet} + CO$	$RO^{\bullet} + CO + CO_2$	$R^{\bullet} + C_2O_4$
H	-39.5	-1.7	-10.3	79.5
CH_3	-36.6	-0.3	-16.2	62.6
C_2H_5	-36.6	-0.2	-13.8	66.4
i-C_3H_7	-36.7	-0.1	-13.1	67.8
t-C_4H_9	-37.8	-0.1	-12.9	69.5

[a] ZPE included and uniformly scaled.

[b] Total energies of alkyloxalates radicals are obtained from the most stable conformation and taken from Table V.2-5.

The fragment $CH_3O^{\bullet}$ may be obtained by dissociation of $CH_3OCO^{\bullet}$, formed itself by dissociation of $CH_3OCOCOO^{\bullet}$ into $CH_3OCO^{\bullet}$ and CO_2, or by direct dissociation of the radical into $CH_3O^{\bullet}$ and C_2O_3. As discussed in the previous section, Peppe and coworkers[15] have shown that the neutral C_2O_3 has a structure of a weakly-bound van der Waals complex (Scheme V.3-1) and is thus expected to undergo an immediate dissociation into CO_2 and CO. The two possibilities of formation of $CH_3O^{\bullet}$ from methyloxalate radical are thus the $CH_3O^{\bullet}$ – C_2O_3 bond cleavage or the fragmentation of the radical into $CH_3OCO^{\bullet}$ and CO_2 followed by dissociation of $CH_3OCO^{\bullet}$ into $CH_3O^{\bullet}$ and CO. The latter is favored by thermochemistry which predicts it to be more favorable than the former by about 20 kcal/mol (Table V.5-2). It implies nevertheless that the $CH_3OCO^{\bullet}$ radical dissociates preferentially into $CH_3O^{\bullet}$ and CO_2, which is not obvious. This radical has indeed been the subject of many controversies concerning its

gas-phase behavior. Two dissociation pathways exist, formation of $CH_3^{\bullet}$ and CO_2 or of $CH_3O^{\bullet}$ and CO, the former being favored by thermochemistry compared to the latter.[35] Some experimental and theoretical work nevertheless indicates that formation of $CH_3O^{\bullet}$ and CO is a dominant dissociation channel of $CH_3OCO^{\bullet}$ because a high barrier avoids the other channel to occur efficiently.[25,36-39] Moreover, if the radical $CH_3OCO^{\bullet}$ is formed, it does not survive reionization into CH_3OCO^+ as shown by Schröder and coworkers,[25] but lead to $CH_2O^{\bullet+}$ and $CO^{\bullet+}$,[25] which are fragments observed in the positive part of the NIDD spectrum (Figure V.5-2a).

A consideration thus the NIDD spectrum of $CH_3OCOCOO^{\bullet}$ thus reveals that the fragment $CH_3O^{\bullet}$ is formed, but its origin remains uncertain: it can either be obtained from the direct $CH_3O^{\bullet} - C_2O_3$ bond cleavage or from the dissociation of $CH_3OCO^{\bullet}$ formed by fragmentation of $CH_3OCOCOO^{\bullet}$. In both cases, its formation is coupled with the production of CO_2 and CO. Consequently, after reionization, the ions $CO^{\bullet+}$ and $CO_2^{\bullet+}$ should be obtained. While this is the case for the ion $CO^{\bullet+}$ which appears with a positive NIDD intensity, it does not hold true for the ion $CO_2^{\bullet+}$, which is related to the cation chemistry (negative NIDD signal, Figure V.5-2a). To understand this feature, the cation chemistry has to be considered.

Dissociation of the $CH_3OCOCOO^+$ ion formed from vertical charge transfer from the corresponding anion leads to the ions $CO_2^{\bullet+}$ (*m/z* = 44), $C_2O_2^{\bullet+}$ (*m/z* = 56), and CH_3OCO^+ (*m/z* = 59) (Figure V.5-2a). The ions $CO_2^{\bullet+}$ and CH_3OCO^+ most likely originate from the $[CH_3OCO - CO_2]^+$ bond cleavage. According to Stevenson's rule which stipulates that during the unimolecular dissociation of a cation, the positive charge remains on the fragment having the lowest ionization energy, only the CH_3OCO^+ fragment should be formed therefrom because $IE(CH_3OCO) < IE(CO_2)$ (8.9[25] and 13.8[40] eV respectively). Accordingly, the ions $CO_2^{\bullet+}$ should not appear with such a large intensity in the spectrum, but (i) as seen in Chapter III for alkylcarbonates, dissociation of excited species formed by vertical charge transfer from the anions, may not follow Stevenson's rule. (ii) $CO_2^{\bullet+}$ may be formed from dissociation of CH_3OCO^+, as observed by Bursey[41] and Schröder.[25] In this case, a competition between $CH_3OCOCOO^+$ and $CH_3OCOCOO^{\bullet}$ takes place for formation of $CO_2^{\bullet+}$, which may potentially explain the negative NIDD signal of this ion, even though it is also formed at the neutral stage. Another important point to consider concerns the method used itself: due to the fact that, in a NR process, two collision events take place, in contrast with a CR process for which only one collision occurs, the fragmentation is expected to be larger in the NR process than in the CR because species involved are more rovibrationally excited. Accordingly, $CO_2^{\bullet+}$ is expected to dissociate more when formed in a NR process than when it originates from CR, and

this could also explain the negative NIDD signal of $CO_2^{\bullet+}$ (because more remain intact in the CR process).

Another interesting point in the NIDD spectrum of methyloxalate (Figure V.5-2a) concerns the occurrence of a negative $C_2O_2^{\bullet+}$ signal. This ion, related to the cation chemistry, cannot be formed by means of simple bond cleavage from $CH_3OCOCOO^+$. Intramolecular rearrangement of ions, prior to fragmentation, is rather unlikely to happen in charge reversal processes due to the high rovibrational excitation of the ions formed therefrom. Instead, dissociation by means of direct bond cleavage processes is favored.[42,43] The fragment $C_2O_2^{\bullet+}$ is thus more plausibly formed as a secondary fragment, i.e. as the fragment of a fragment of $CH_3OCOCOO^+$. Two fragments precursor are conceivable: $C_2O_3^{\bullet+}$ or $C_2O_4^{+}$. Metastable dissociation of the latter has been studied by Stace[44], Futrell,[45] and Illies,[46,47] All the works have concluded that $C_2O_4^{+}$ fragmentation leads exclusively to $CO_2^{\bullet+}$ and CO_2. This ion can thus not be at the origin of the formation of $C_2O_2^{\bullet+}$ which is consequently created from dissociation of $C_2O_3^{\bullet+}$,[15] formed itself from $CH_3OCOCOO^+$ by the homolytic $CH_3O^{\bullet}$ – $C_2O_3^{\bullet+}$ bond cleavage. This process leads preferentially to the formation of $C_2O_3^{\bullet+}$ and $CH_3O^{\bullet}$ instead of CH_3O^+ and C_2O_3 according to Stevenson's rule[48] because *IE*(C_2O_3) < *IE*($CH_3O^{\bullet}$) (9.0 and 10.7 eV, respectively).[40,49] Overviews of dissociations of $CH_3OCOCOO^{\bullet}$ and $CH_3OCOCOO^+$ formed from vertical charge transfer of $CH_3OCOCOO^-$ are given in Scheme V.5-1a and V.5-1b.

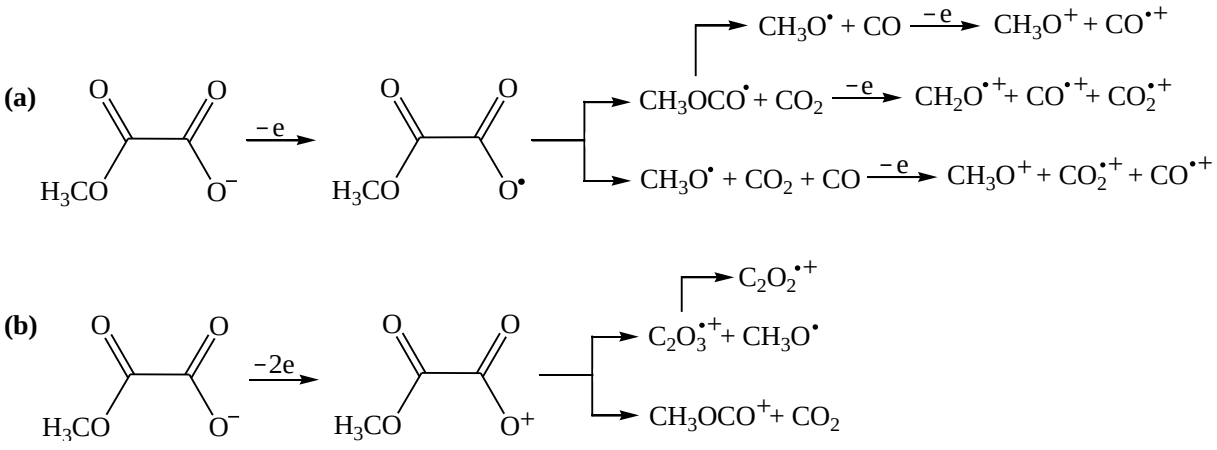

Scheme V.5-1: General scheme of dissociation of (a) methyloxalate radicals $CH_3OCOCOO^{\bullet}$ formed by vertical neutralization of methyloxalate anions, and (b) methoxycarbonyl carboxyl ions $CH_3OCOCOO^+$ obtained by double electron transfer from the corresponding anion.

In summary, the analysis of the NIDD spectrum of methyloxalate shows complex patterns. Formation of $CH_3O^{\bullet}$ in the course of the $CH_3OCOCOO^{\bullet}$ dissociation could have been

established, but no information concerning the associated mechanism is provided in the spectrum. Furthermore, the $CO_2^{\bullet+}$ signal, obtained from reionization of CO_2 formed during dissociation of $CH_3OCOCOO^{\bullet}$ is not present with a positive NIDD intensity, which is explained by a competition between $CH_3OCOCOO^{\bullet}$ and $CH_3OCOCOO^{+}$ for formation of this ion.

The NIDD spectra of ethyl-, *i*-propyl-, and *t*-butyloxalates provide much less information than the spectra of methyloxalate. Thus, in the positive part of the spectra in Figures V.5-2b, V.5-2c, and V.5-2d, only signals related to reionized alkyl group $R^{\bullet}$ (R = C_2H_5, *i*-C_3H_7, and *t*-C_4H_9) can be identified and are: $C_2H_2^{\bullet+}$ for ethyloxalate, $C_3H_2^{\bullet+}$ for *i*-propyloxalate, and $C_4H_7^{+}$, $C_3H_3^{+}$, $C_3H_2^{\bullet+}$ for *t*-butyloxalate (only signals unambiguously attributed (no mass overlap) are cited). The presence of signals related to $R^{\bullet}$ may be explained considering the dissociation of alkyloxalate neutrals into C_2O_4 and $R^{\bullet}$ or secondary fragmentations of the products $RO^{\bullet}$ or $ROCO^{\bullet}$. The $R^{\bullet}$ – C_2O_4 bond cleavage is disfavored from a thermodynamic point of view because it is found to be endothermic by almost 70 kcal/mol for the alkyloxalates considered (Table V.5-2). The radical $R^{\bullet}$ most likely originate from dissociation of $RO^{\bullet}$ or of $ROCO^{\bullet}$, formed themselves by fragmentation of transient $ROCOCOO^{\bullet}$ into $RO^{\bullet}$ and C_2O_3 or into $ROCO^{\bullet}$ and CO_2 respectively, for R = C_2H_5, *i*-C_3H_7, and *t*-C_4H_9 (as discussed in the case of methylcarbonate, the C_2O_3 fragment is expected to dissociate immediately into CO and CO_2). The $RO^{\bullet}$ – C_2O_3 bond cleavage seems, nevertheless, less plausible than the $ROCO^{\bullet}$ – CO_2 bond cleavage because Hornung *et al.*[34] have shown that alkoxide radicals $RO^{\bullet}$ produce ionized aldehydes and ketones when submitted to vertical charge transfer. In the NIDD spectra in Figures V.5-2b, V.5-2c, and V.5-2d, no positive signals related to such species appear. Moreover, thermochemistry shows also a clear preference for the $ROCO^{\bullet}$ – CO_2 bond cleavage, which costs in general 23 kcal/mol less than the RO – $C_2O_3^{\bullet}$ bond fragmentation (Table V.5-2). In contrast to methylcarbonyl $CH_3OCO^{\bullet}$, the alkylcarbonyl radicals $ROCO^{\bullet}$ (R = C_2H_5, *i*-C_3H_7, and *t*-C_4H_9) dissociate preferentially into $R^{\bullet}$ and CO_2 than into $RO^{\bullet}$ and CO, as shown by Morihovitis *et al.*[50] who found barriers relatively low (< 20 kcal/mol) for this exothermic bond cleavage.

Consequently, the $ROCO^{\bullet}$ – CO_2 bond cleavage seems the most likely dissociation process occurring for alkyloxalate radicals $ROCOCOO^{\bullet}$ (R = C_2H_5, *i*-C_3H_7, and *t*-C_4H_9) formed by vertical charge transfer from the corresponding anions (Scheme V.5-2a). The $CO_2^{\bullet+}$ ion appears with a negative NIDD intensity in the spectra (Figures V.5-2b, V.5-2c, and V.5-2d), even though it would be expected to be related to the neutrals chemistry. As for methyloxalate, we relate this feature to a competition for the formation of this ion between $ROCOCOO^{+}$ and $ROCOCOO^{\bullet}$. The negative part of the NIDD spectra shows signals indica-

ting decarboxylation of the (carboxyalkyl)carboxyl ions $ROCOCOO^+$ (R = C_2H_5, *i*-C_3H_7, and *t*-C_4H_9) because corresponding to the ions RO^+: $CH_3CHO^{\bullet+}$ for R = C_2H_5 and *i*-C_3H_7, and $(CH_3)_2CO^{\bullet+}$ for R = *t*-C_4H_9. The ion $CO_2^{\bullet+}$ is also present in these spectra even though it should not appear according to the Stevenson's rule,[48] but as discussed above, highly excited ions may have an unexpected dissociation behavior. Furthermore, the $C_2O_2^{\bullet+}$ ion is also present in the spectra with a negative intensity for ethyl- and *i*-propyloxalates. Its origin is attributed to $C_2O_3^{\bullet+}$ formed by a $RO^{\bullet} - C_2O_3^{\bullet+}$ bond cleavage. For *t*-butyloxalate, this ion appears with a positive NIDD intensity (Figure V.5-2d), but in this case, a mass overlap with the $C_4H_8^{\bullet+}$ ion exist, which very likely causes this feature. As all other cations investigated have shown this dissociation behavior, the *t*-butyloxycarbonyl carboxyl cation is indeed also expected to undergo a *t*-$C_4H_9O^{\bullet} - C_2O_3^{\bullet+}$ bond cleavage.

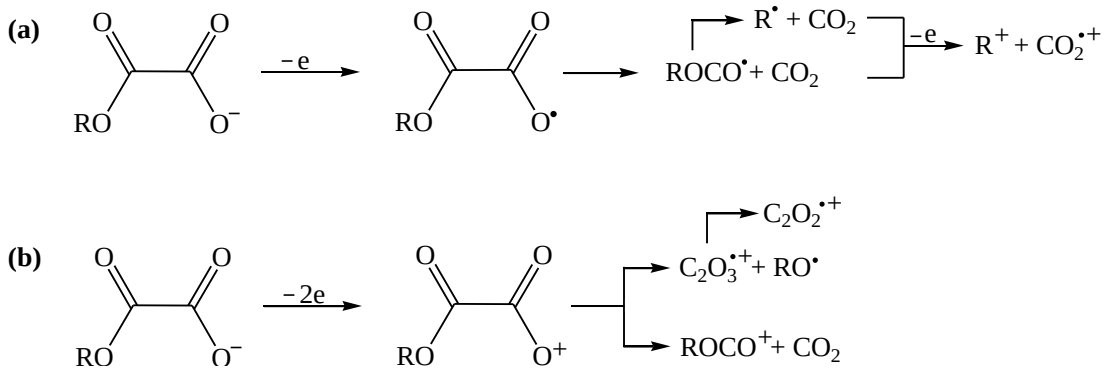

Scheme V.5-2: General scheme of dissociation of (a) alkyloxalate radicals $ROCOCOO^{\bullet}$ and (b) (carboxyalkyl)carboxyl ions $ROCOCOO^+$, both obtained by vertical electron transfer from the corresponding alkyloxalate anions (R = C_2H_5, *i*-C_3H_7, and *t*-C_4H_9).

The NIDD study of alkyloxalate radicals shows that the neutrals obtained by vertical charge transfer from the corresponding anions undergo a massive dissociation by bond cleavage leading to the fragments $R^{\bullet}$, CO, and CO_2. Two processes are possible, one corresponding to the $RO^{\bullet} - C_2O_3$ bond cleavage and one leading to the fragmentation into $ROCO^{\bullet}$ and CO_2. As the fragments C_2O_3 and $ROCO^{\bullet}$ do not appear in the spectra, it was not possible to distinguish these two mechanisms. The $ROCO^{\bullet} - CO_2$ bond cleavage is favored by thermochemistry, but both of the processes are exothermic and it seem more likely to consider that both occur. Other types of dissociation, like fragmentation into $ROCOO^{\bullet}$ and CO, have not been observed. This process is ca. 1 kcal/mol exothermic (Table V.5-2), but as it requires a

rearrangement of the radicals prior to fragmentation, it is not likely to occur, due to the conditions of the experiment.

V.6. Conclusions

Conformational structures of alkyloxalate anions and radicals $ROCOCOO^{-/\bullet}$ have been investigated computationally for R = H, CH_3, C_2H_5, *i*-C_3H_7, and *t*-C_4H_9. The results differ for the charge states considered and show that anions have different favored conformational structures according to the size of the substituent R whereas all alkyloxalate radicals investigated show a high preference for the planar *tC* conformation. Due to an intramolecular hydrogen bond, the hydrogen oxalate ion is particularly stabilized in a planar *cC* conformation, whereas a *trans* (*T*) conformation between the two carbonyl groups is preferred for the larger substituents. The favorable spatial position of the substituents also differs with R for the anions. The most stable conformation with respect to rotation around the $O_{(4)}$-$C_{(2)}$ bond is *cis* for R = H, CH_3, and C_2H_5, whereas the *trans* conformation is favored for R = *i*-C_3H_7 and *t*-C_4H_9. Comparison of the structures of the anions, radicals, and cations further show that not only the preferred conformational structures differ between the species, but also do the bond lengths and angles, particularly between the cations on the one and the anions and radicals on the other hand. These features are rather unfavorable for an experimental observation of the radicals because large difference in geometries may prevent the detection of the neutral molecules by vertical charge transfer. In the case of hydrogen oxalate, theory predicts that formation of the radical from the anion is not possible due to the absence of a conformational structure favorable for both of the species. This assumption is confirmed latter by experiment as no recovery signal for $HOCOCOO^{\bullet}$ could have been found.

Moreover, the standard heats of formation of alkyloxalate anions and neutrals have been determined via bond-separation reactions and atomization energies. The results agree well, with error in general < 0.6 kcal/mol. The formation enthalpies obtained are extremely low, ranging between -205 and -230 kcal/mol for anions and between -110 and -130 kcal/mol for radicals, showing thus a high intrinsic stability for these species.

Furthermore, the gas-phase behavior of alkyloxalates anions has been probed by means of MI and CA experiments. The results are similar for all substituents and three decomposition pathways are observed: decarbonylation, decarboxylation, and simultaneous decarboxylation and decarbonylation. The first pathway is by far the dominant decomposition process ob-

served in both MI and CA experiments, which is also confirmed from a thermochemical point of view. Loss of CO leads to the formation of alkylcarbonates $ROCOO^-$, whereas elimination of CO_2 leads to alkoxycarbonyl anions $ROCO^-$, and the combined production of CO and CO_2 affords the corresponding alkoxy anions RO^-. While the two latter decomposition paths correspond to direct bond cleavages, decarbonylation requires a rearrangement of the anions which is suggested to proceed via the formation of an intermediate ion-neutral complex.

The NIDD method has been applied to alkyloxalate radicals $ROCOCOO^\bullet$ for R = CH_3, C_2H_5, *i*-C_3H_7, and *t*-C_4H_9 because the existence of these neutrals during the time scale of the experiment has been established. The spectra obtained do not provide much information concerning the neutral's chemistry because they are dominated by massive fragmentations. This feature is in part explained by the difference found between the structures of anions, radicals, and cations which lead to highly rovibrationally excited species which do not survive vertical charge transfer. Dissociation of the radicals leading to the fragments $R^\bullet$, CO_2, and CO could have been deduced from the spectra, but the mechanisms associated with the formation of these compounds remain uncertain. For alkyloxalate radicals, thermochemistry predicts the $ROCO^\bullet - CO_2$ bond cleavage to be the most favorable, and this process appears to be the most likely for ethyl, *i*-propyl-, and *t*-butyloxalates, whereas a $CH_3O^\bullet - C_2O_3$ bond cleavage may also occur for methyloxalate.

V.7. References and Notes

1. Bock, C. W.; Redington, R. L., *J. Chem. Phys.* **1986**, *85*, 5391.
2. Higgins, J.; Zhou, X.; Liu, R.; Huang, T. T. S., *J. Phys. Chem. A* **1997**, *101*, 2702.
3. Mohajeri, A.; Shakerin, N., *J.Mol. Struct.: THEOCHEM* **2004**, *711*, 167.
4. Remko, M.; Liedl, K. R.; Rode, B. M., *J. Chem. Soc., Perkin Trans. 2* **1996**, 1743.
5. Tyrrell, J., *J.Mol. Struct.: THEOCHEM* **1992**, *258*, 389.
6. Van Alsenoy, C.; Klimkowski, V. J.; Schafer, L., *J.Mol. Struct.: THEOCHEM* **1984**, *109*, 321.
7. Cheng, C.; Shyu, S.-F., *Int. J. Quantum Chem.* **2000**, *76*, 541.
8. Exner, O.; Čársky, P., *J. Am. Chem. Soc.* **2001**, *123*, 9564.
9. Morton, T. H., *Org. Mass Spectrom.* **1992**, *27*, 353.
10. Whitmore, F., *J. Am. Chem. Soc.* **1932**, *54*, 3274.
11. Schröder, D.; Soldi-Lose, H.; Schwarz, H., *Aust. J. Chem.* **2003**, *56*, 443.
12. McMillen, D. F.; Golden, D. M., *Annu. Rev. Phys.* **1982**, *33* 493.
13. Benassi, R.; Taddei, F., *J.Mol. Struct.: THEOCHEM* **1994**, *303*, 101.
14. Levsen, K.; Schwarz, H., *Mass Spectrom. Rev.* **1983**, *2*, 77.
15. Peppe, S.; Dua, S.; Bowie, J. H., *J. Phys. Chem. A* **2001**, *105*, 10139.
16. Langlet, J.; Caillet, J.; Allavena, M.; Raducu, V.; Gauthier-Roy, B.; Dahoo, R.; Abouaf-Marguin, L., *J. Mol. Struct.* **1999**, *484*, 145.
17. Muenter, J. S.; Bhattacharjee, R., *J. Mol. Spectrosc.* **1998**, *190*, 290.
18. Raducu, V.; Gauthierroy, B.; Dahoo, R.; Abouafmarguin, L.; Langlet, J.; Caillet, J.; Allavena, M., *J. Chem. Phys.* **1995**, *102*, 9235.
19. Randall, R. W.; Summersgill, J. P. L.; Howard, B. J., *J. Chem. Soc., Faraday Trans.* **1990**, *86*, 1943.
20. Xu, Y.; McKellar, A. R. W.; Howard, B. J., *J. Mol. Spectrosc.* **1996**, *179*, 345.
21. Schröder, D.; Schwarz, H.; Dua, S.; Blanksby, S. J.; Bowie, J. H., *Int. J. Mass Spectrom.* **1999**, *188*, 17.
22. Hayes, R. N.; Waugh, R. J.; Bowie, J. H., *Rapid Commun. Mass Spectrom.* **1989**, *3*, 338.

23. O'Hair, R. A. J.; Bowie, J. H.; Hayes, R. N., *Rapid Commun. Mass Spectrom.* **1988**, *2*, 275.

24. Graul, S. T.; Squires, R. R., *J. Am. Chem. Soc.* **1988**, *110*, 607.

25. Schröder, D.; Semialjac, M.; Schwarz, H., *Eur. J. Mass Spectrom.* **2003**, *9*, 287.

26. Ramond, T. M.; Davico, G. E.; Schwartz, R. L.; Lineberger, W. C., *J. Chem. Phys.* **2000**, *112*, 1158.

27. Heinrich, N.; Schwarz, H. in *Ion and Cluster-Ion Spectroscopy and Structure*; Elsevier: Amsterdam, 1989, p. 329.

28. Banholzer, K.; Schmid, H., *Helv. Chim. Acta* **1956**, *39*, 548.

29. Elliott, W. W.; Hammick, D. L., *J. Chem. Soc.* **1951**, 3402.

30. Eichinger, P. C. H.; Hayes, R. N.; Bowie, J. H., *J. Chem. Soc., Perkin Trans. 2* **1991**, 1815.

31. Schalley, C. A.; Hornung, G.; Schröder, D.; Schwarz, H., *Int. J. Mass Spectrom. Ion Processes* **1998**, *172*, 181.

32. Schröder, D.; Heinemann, C.; Schwarz, H.; Harvey, J. N.; Dua, S.; Blanksby, S. J.; Bowie, J. H., *Chem. Eur. J.* **1998**, *4*, 2550.

33. McMahon, A. W.; Chowdhury, S. K.; Harrison, A. G., *Org. Mass Spectrom.* **1989**, *24*, 620.

34. Hornung, G.; Schalley, C. A.; Dieterle, M.; Schröder, D.; Schwarz, H., *Chem. Eur. J.* **1997**, *3*, 1866.

35. Wantuck, P. J.; Oldenborg; R. C.Baughcum, S. L.; Winn, K. R., *Chem. Phys. Lett.* **1987**, *138*, 548.

36. Kang, J. K.; Musgrave, C. B., *J. Chem. Phys.* **2001**, *115*, 11040.

37. Francisco, J. S., *Chem. Phys.* **1998**, *237*, 1.

38. Wang, B.; Hou, H.; Gu, Y., *J. Phys. Chem. A* **1999**, *103*, 8021.

39. Zhou, Z.; Cheng, X.; Zhou, X.; Fu, H., *Chem. Phys. Lett.* **2002**, *353*, 281.

40. Linstrom, P. J.; Mallard Eds., W. G., NIST Chemistry WebBook, NIST Standard Reference Database Number 69, National Institute of Standards and Technology, Gaithersburg MD, 20899, June 2005 (http://webbook.nist.gov).

41. Bursey, M. M.; Harvan, D. J.; Parker, C. E.; Pedersen, L. G.; Hass, J. R., *J. Am. Chem. Soc.* **1979**, *101*, 5489.

42. Bowie, J. H.; Blumenthal, T., *J. Am. Chem. Soc.* **1975**, *97*, 2959.

43. Cooks, R. G., *Collision Spectroscopy*; Plenum Press: New York, 1978.

44. Stace, A. J.; Shukla, A. K., *Int. J. Mass Spectrom. Ion Phys.* **1980**, *36*, 119.

45. Futrell, J. H.; Stephan, K.; Mark, T. D., *J. Chem. Phys.* **1982**, *76*, 5893.

46. Illies, A. J.; Jarrold, M. F.; Wagner-Redeker, W.; Bowers, M. T., *J. Phys. Chem. A* **1984**, *88*, 5204.

47. Illies, A. J.; McKee, M. L.; Schlegel, H. B., *J. Phys. Chem.* **1987**, *91*, 3489.

48. Stevenson, D. P., *Discuss. Faraday Soc.* **1951**, *10*, 35.

49. *IE*(C_2O_3) corresponds to a vertical ionization energy and has been deduced from the energies of C_2O_3 and $C_2O_3^{\bullet+}$ given by Peppe *et al.*.[17]

50. Morihovitis, T.; Schiesser, C. H.; Skidmore, M. A., *J. Chem. Soc., Perkin Trans. 2* **1999**, 2041.

VI. Conclusions and Perspectives

The present Thesis reports on the gas-phase chemistry of alkylcarbonates and alkyloxalates, which may play a role in the formation of complex molecules in the Mars atmosphere. The structures, stabilities and dissociation behavior of these compounds at different charge states have been investigated using experiment and theory. The results obtained are summarized at the end of the corresponding chapters, only some more general conclusions will thus be drawn here, concerning, firstly, the efficiency of the particular methods employed and, secondly, the implications of the results to the problematic presented in the introduction.

(i) Usually, theoretical predictions of thermochemical data are performed on closed-shell systems.[1] In this study, standard heats of formation were required for alkylcarbonate ions, but also for the corresponding radicals which are open-shell species. Among the different methods which can be applied to access thermochemical quantities, the bond-separation (BS) reactions method gives the most satisfying results for radicals.[2-4] In contrast, this method is rather rarely employed for ionic species for which atomization energies are preferred.[5] Therefore, these two methods have been used in this work in order to provide more information concerning enthalpies of formation obtained for ions with atomization energies and for radicals with BS reactions. For a good overview, all the results have been collected in Figure VI.1. The largest difference observed between the two methods is of 1.1 kcal/mol and is obtained for *t*-$C_4H_9OCOO^-$. For all series of data, the standard deviation is of 0.5 kcal/mol which is very satisfying, as they are within chemical accuracy (± 2.5 kcal/mol).[6] Furthermore, comparison of the results with previous studies was only possible for hydrogencarbonate. In this case, a difference of less than 1 kcal/mol between the values given here and in other studies was observed (section III.3). Consequently, thermochemical data evaluated in this work seem to have a rather reasonable accuracy. The similarity of the results obtained with atomization energies and BS reactions show also the good performance of these two methods for thermochemical predictions for anions and radicals; this was not obvious before.

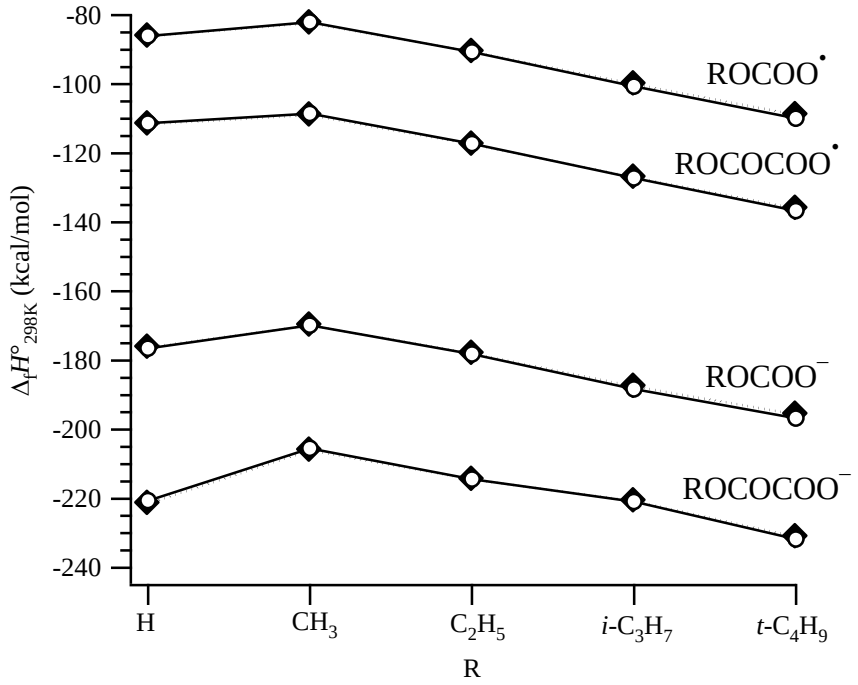

Figure VI.1: Standard heats of formation obtained for alkylcarbonate and alkyloxalate ions and radicals $ROCOO^{-/\bullet}$ and $ROCOCOO^{-/\bullet}$ (R = H, CH_3, C_2H_5, *i*-C_3H_7, and *t*-C_4H_9), using atomization energies (♦) and bond-separation reactions (○).

(ii) Energy resolved experiments have been employed in this study to gain more insights concerning dissociation energetics of methoxycarboxyl radical and cation formed by vertical charge transfer of methylcarbonate (Chapter IV). The results have been further compared to theoretical predictions performed at the MP2/6-311++G(3df,3pd)//MP2/6-311++G(d) level, and show, in this context, a difference of about 4 eV. This large deviation is attributed to experimental as well as theoretical errors including too simplifying assumptions made for the collisional electron transfer. Furthermore, these experiments have required the evaluation of the instrumental error associated with charge-transfer reactions. This was done using atomic gases and by comparing the results to well-known literature. The differences observed clearly vary according to the ions studied and to the processes considered (neutralization reionization and charge reversal). The difficulty of this evaluation thus arises from the determination of the parameters influencing the instrumental energies. Some linear relation has been found between the measured energy losses and some intrinsic parameters of the ions, but this effect remains by far not understood perfectly. Hence, the dissociation energetics extracted experimentally are given only with a rough estimation of the error, which may therefore explain the large differences observed between experiment and theory.

(iii) In contrast with previous work,[7] the results obtained here for the study of the gas-

phase chemistry of transient neutrals with the neutral and ion decomposition difference (NIDD) method are rather ambivalent. The use of this method has enabled us to show that the radicals under study are stable within the experimental time scale (except for $HOCOCOO^{\bullet}$), but the results obtained concerning the unimolecular dissociation of these species are rather disappointing. Indeed, only direct bond cleavages are observed consisting only in the loss of neutral carbon dioxide (Chapters III and V). These observations may, of course, depict the real dissociation behavior of these ions, but some features related to the experiment suggest that the method employed may not be the most adequate. Vertical charge transfers which are required to use the NIDD method (charge reversal and neutralization reionization), show the best efficiency when the geometries of the initial precursor, the possible intermediate and the final compound are similar. For the systems studied here, rather large differences between the structures of anions, cations, and radicals are predicted theoretically. Hence, the radicals and cations formed by vertical charge transfer are expected to be highly excited, and experimentally a massive dissociation is observed. The analysis of the NIDD spectra obtained is therefore quite complex, and results show that dissociation is following almost exclusively the thermodynamically most favorable pathway. With this method, insights about kinetically favored decomposition channels are thus not accessible, what would have been of considerable interest concerning the context of this study. Little energy is indeed available for chemical reactions to proceed in atmospheres because they generally occur at low temperature (very few collisions). The NIDD method consequently shows some limitations for the investigation of gas-phase chemistry of transient radicals and "softer" methods for generation of these species may be required in order to definitely establish their dissociation behavior.[8]

(iv) The unimolecular dissociation behavior of alkylcarbonate and alkyloxalate ions has been probed by means of metastable ion and collisional activation experiments. Interesting results have been obtained for methyl- and ethylcarbonate for which the favored decomposition pathway consists of a hydride-transfer reaction leading to the ion HCO_2^- and formaldehyde or acetaldehyde, respectively (Chapter III). The chemistry of the other alkylcarbonates is less original as they mostly favor direct bond-cleavage processes like decarboxylation. Concerning alkyloxalate ions, the first observation made is that the results do not vary with the size of the substituents. Thus, all the ions studied show a clear trend to eliminate carbon monoxide, leading then to the corresponding alkylcarbonate ions. This relation between alkyloxalates and alkylcarbonates is of particular interest for the methyl and ethyl substituents because it allows establishing a connection between a reaction potentially occurring in the Mars atmosphere and formaldehyde or acetaldehyde (Figure VI.2.). Association[9] of two

carbon dioxide units and a methyl or ethyl anion formed by photoionization seems conceivable with regard to the composition of the Martian atmosphere.[10,11] Through the different steps given in Figure VI.2, formaldehyde and acetaldehyde can finally be formed. These molecules are of particular interest because they are key starting components for the formation of complex molecules in atmospheres.[12] This study reveals therefore the potential important role of anions in the chemistry of atmospheres, even though in this context negative ions are quite often not considered as relevant as cations.[13]

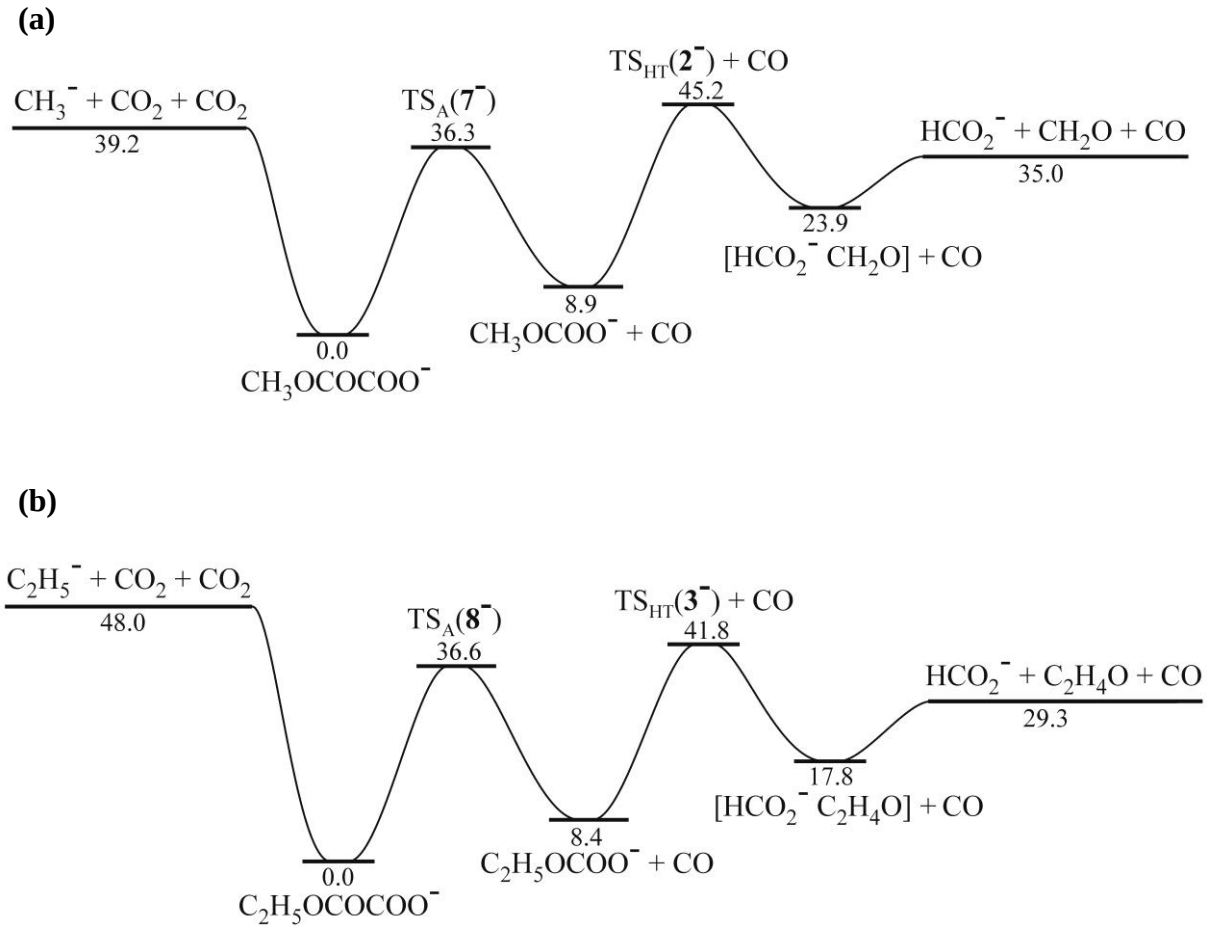

Figure VI.2: Schematic representation of the potential-energy surface of (a) methyloxalate and (b) ethyloxalate and some of their dissociation products obtained at the MP2/6-311++G(3df,3pd)//MP2/6-311++G(d) level of theory. Relative energies are given in kcal/mol. The transitions structures are denoted using the nomenclature employed in Chapters III and V.

References and Notes

1. Lewis, G. N.; Randall, M., *Thermodynamics*; Second Edition, revised by K. S. Pitzer and L. Brewer; Mc Graw-Hill: New York, 1961.

2. Henry, D. J.; Radom, L. in *Quantum-Mechanical Prediction of Thermochemical Data.*; Cioslowski, J., Ed.; Kluwer Academic: Dordrecht, 2001, p. 161.

3. Bally, T.; Borden, W. T. in *Reviews in Computational Chemistry*; Lipkowitz, K. B., Boyds, D. B., Eds.; Wiley-VCH: New York, 1999; Vol. 13, p. 1.

4. Simoes, J. A. M.; Greenberg, A.; Liebman, J. F., *Energetics of Organic Free Radicals*; Blackie Academic and Professional: London, 1996.

5. Harvey, Z., Ph. D. Thesis, La Trobe University, Bundoora (AU), 2006.

6. Cioslowski, J., *Quantum-Mechanical Prediction of Thermochemical Data.*; Kluwer: Dordrecht, 2001.

7. Schalley, C. A., Ph. D. Thesis, Technische Universität, Berlin, 1997.

8. Among various methods, one can cite flash pyrolysis[(a)] or laser induced photodissociation.[(b)]
(a) Kohn, D. W.; Clauberg, H.; Chen, P., *Rev. Sci. Instrum.* **1992**, *63*, 4003. (b) Nahon, L.; Tremblay, J.; Larzilliere, M.; Duffy, L.; Morin, P., *Nucl. Instrum. Methods Phys. Res., Sect. B* **1990**, *47*, 72.

9. Smith, D., *Int. J. Mass Spectrom. Ion Processes* **1993**, *129*, 1.

10. Atreya, S. K.; Gu, Z. G., *Adv. Space Res.* **1995**, *16*, 57.

11. Moroz, V. I., *Adv. Space Res.* **1998**, *22*, 449.

12. Brack, A., *Adv. Space Res.* **1999**, *24*, 417.

13. Eisele, F. L.; Lovejoy, E. R.; Kosciuch, E.; Moore, K. F.; Mauldin III, R. L.; Smith, J. N.; McMurry, P. H.; Iida, K., *J. Geophys. Res., D* **2006**, *111*, D04305.